Christopher C. Goodis

Professional Summary

Exceptional synthetic organic chemist with deep technical expertise on inhibiting oncoproteins via different molecular mechanisms including selective covalent inhibitors and protein degraders while avoiding off-target effects.

Extensive experience with a myriad of chemical reactions (e.g. nucleophilic substitution, redox, cyclization, halogenation, and electrophilic aromatic substitution chemistry), including air and moisture sensitive reactions (e.g. cross-coupling and working with pyrophorics).

First-hand experience with analytical instruments including NMR, intact mass spectrometry for analyzing adduct formation between covalent inhibitors and proteins, and HPLC to analyze compound purity.

Possesses excellent communication, writing, team collaboration, and presentation skills in addition to an outstanding mentorship style utilized to train six graduate students in the Fletcher laboratory.

Education

University of Maryland, School of Pharmacy Baltimore, MD
Ph.D., Pharmaceutical Sciences *Dec. 2024*

- Thesis topic: Molecular Strategies to Combat Acquired Resistance to the Anti-Leukemic Drug Venetoclax.
- Served as an elective board member for the diverse student government body and queer student alliance.

University of Michigan–Dearborn Dearborn, MI
BS., Biochemistry *April 2019*

- Graduate of the University of Michigan–Dearborn honors program.

Research Experience

University of Maryland, School of Pharmacy Baltimore, MD
Graduate Research Assistant in Fletcher Laboratory *Aug.2019 – Present*

- Synthesized over a thousand small molecules utilizing nucleophilic substitution, redox, cyclization, and cross-coupling reactions to create inhibitors targeting various oncoproteins and a collaborative project with the Pearson laboratory focused on drug-polymer conjugates to combat cancer and inflammation.
- Synthesized inhibitors employing multiple molecular strategies to inhibit oncoproteins including covalent inhibitors, protein degraders (e.g. PROTACs and hydrophobic degraders), and molecular glues

- Collaborated with the MacKerell lab to conduct Site Identification by Ligand Competitive Saturation (SILCS) simulations on lead compounds to predict binding favorability to target proteins and guide drug design.
- Cross-trained in the Deredge laboratory to prepare protein samples and conduct intact mass spectrometry experiments on protein samples with covalent small molecules to analyze adduct formation.

University of Michigan - Dearborn Dearborn, MI *Undergraduate Research Assistant* *Oct. 2017 – April 2019*

- Designed inductively coupled plasma mass spectrometry experiments to determine metal concentration in different natural environments.
- Deconstructed extended X-ray absorption fine structure experiments on riboflavin binding protein to examine the residues chelating a calcium cofactor.

Skills

- Structure-based drug design
- Multi-step small molecule synthesis
- Drug discovery
- mg to multi-gram scale synthesis
- Air sensitive chemistry
- Analytical chemistry
- Liquid–liquid extraction
- Lyophilization
- Column chromatography purification
- (Re)crystallization techniques
- Distillation purification
- Filtration techniques
- Proton nuclear magnetic resonance (1H NMR)
- Carbon nuclear magnetic resonance (13C NMR)
- Liquid chromatography mass spectrometry
- HPLC
- Computational chemistry
- Inductively coupled plasma mass spectrometry
- Database searching
- Academic writing
- Public communication
- Presenting summaries and reports
- Team coordination and project management
- Proficient with Microsoft Office suite, VnmrJ, ChemDraw suite, Pymol Scifinder , ChemSpide

Publications

Goodis, C.C.*, Chan, A.M.*, Eberley, C.*, Cooper, B., Lapidus, R., Civin, C.I., Fletcher, S. Transformation of the pan-CDK Inhibitor AT7519 into AMC-3-225, a CDK9-Selective Degrader., *manuscript in preparation*. (*co-first authors)

Chan, A.M., Eberley, C., Drennen, B., **Goodis, C.C.**, Wuyts, Z., Civin, C.I., Fletcher, S. Augmenting the Anti-leukemic Activity of the BCL-2 Inhibitor Venetoclax through its Transformation into Polypharmacologic Dual BCL-2/HDAC1 or Dual BCL-2/HDAC6 Inhibitors., *manuscript in preparation.*

Goodis, C.C., Eberly, C., Chan, A.M., Kim, M., Lowe, B.D., Civin, C.I., Fletcher, S. The polypharmacy combination of the BCL-2 inhibitor venetoclax (VEN) and the FLT3 inhibitor gilteritinib (GIL) is more active in acute myeloid leukemia cells than novel polypharmacologic BCL-2/FLT3 VEN–GIL hybrid single-molecule inhibitors. *EuroJMedChem* **2024**. *Accepted*

Truong, N., Cottingham, A.L., Dharmaraj, S., Shaw, J.R., Lasola, J., **Goodis, C.C.**, Fletcher, S., Pearson, R.M. Multimodal nanoparticle-containing modified suberoylanilide hydroxamic acid polymer conjugates to mitigate immune dysfunction in severe inflammation. *Journal of Controlled Release* **2024**, *9*, e10611.

Chen, L., Chauhan, J., Yap, J.L., **Goodis, C.C.**, Wilder, P.T., Fletcher, S. Discovery of N-sulfonylated aminosalicylic acids
as dual MCL-1/BCL-xL inhibitors. *RSC Medicinal Chemistry,* **2023**, *14*, 103-112.

Goodis, C.C.*, Drennen, B.*, Bowen, N., Yu, W., Vickers, G., Wilder, P., Mackerell, A.D., Fletcher, S. Scaffold Hopping from Indoles to Indazoles Yields Dual MCL-1 / BCL-2 Inhibitors from MCL-1 Selective Leads. *RSC Medicinal Chemistry,* **2022**, *13*, 963-969. (*co-first authors)

Goodis, C.C.*, Chan, A.M.*, Pommier, E., Fletcher, S. Recent Application of Covalent Chemistries in Protein-Protein Interaction Inhibitors. *RSC Medicinal Chemistry,* **2022**, *13*, 921-928. (*co-first authors)

Truong, N., **Goodis, C.C.**, Cottingham, A.L., Shaw, J.R., Fletcher, S., Pearson, R.M. Modified Suberoylanilide Hydroxamic Acid Reduced Drug Associated Immune Cell Death and Organ Damage under Lipopolysaccharide Inflammatory Challenge. *ACS Pharmacol. Transl. Sci.,* **2022**, *5*, 1128–1141.

Notable Achievements

- Converted the FLT3 inhibitor gilteritinib into a covalent inhibitor via deliberate positioning of electrophilic warheads.
- Optimized indazole N2 alkylation via Mitsunobu reaction conditions and directly compared yield vs traditional alkylation via alkyl bromide.

- Secured over $3,000 in total funding from the UMB student government association for multiple events focused on supporting LGBTQIA+ students on campus.

Awards

2024 – Awarded Chemistry and Biology Interface (CBI) NIH T32 training fellowship
2023 – Awarded CBI NIH T32 training fellowship totaling
2023 – Received Department of Pharmaceutical Sciences (PSC) merit award
2022 – Received PSC merit award
2022 – Awarded NIH sponsored CBI training fellowship
2021 – Awarded NIH sponsored CBI training fellowship
2020 – Awarded NIH sponsored CBI training fellowship
Fall 2020 – Awarded PSC dean's teaching fellowship
2019 – Recipient of biochemistry honors award from University of Michigan-Dearborn
2019 – Recipient of biochemistry research award from University of Michigan-Dearborn
2019 – Graduated with honors from University of Michigan-Dearborn

Presentations

Goodis, C.C., Fletcher, S. Molecular Strategies to Combat Acquired Resistance to the Anti-Leukemic Drug Venetoclax. Concordia University Wisconsin, Mequon, WI; Nov 2024. (seminar)

Goodis, C.C., Carlson, A.M., Eberly, C., Civin, C.I., Fletcher, S. Transformation of venetoclax (VEN) into PROTACs affords recovery of anti-leukemic activity in VEN-resistant AML cells. The 2024 Frontiers in Chemistry and Biology Interface Symposium, UMBC, Baltimore, MD; May 2024. (poster)

Goodis, C.C., Chan A.M., Eberly C., Civin C. Fletcher S. *Transformation of venetoclax (VEN) into PROTACs affords recovery of anti-leukemic activity in VEN-resistant AML cells.* ACS Spring 2024: Many Flavors of Chemistry, New Orleans Convention Center, New Orleans, LA; March 2024. (poster)

Goodis, C.C., Wenbo, Y., Lowe, B.D., MacKerell, A.D., Fletcher, S. *Discovery of novel BFL-1 inhibitors by CADD and screening an in-house library of synthetic BH3 mimetics.* Graduate Research Conference, University of Maryland, Baltimore, Baltimore, MD; March 2023. (oral)

Goodis, C.C., Wenbo, Y., Lowe, B.D., MacKerell, A.D., Fletcher, S. *Discovery of Novel BFL-1 Inhibitors by Computer-Aided Drug Design and Screening an In-House Library of Synthetic a-Helix Mimetics.* ACS Spring 2023: Crossroads of Chemistry, Indianapolis Convention Center, Indianapolis, IN; March 2023. (poster)

Goodis, C.C., Zhao, M., Conlon, I.L., Li, A., MacKerell, A.D., Fletcher, S. *Synthesizing a-helix mimetics with CADD-positioned electrophilic warheads to inhibit the BFL-1 anti-apoptotic protein.* ACS Spring 2022: Bonding Through Chemistry, San Diego Convention Center, San Diego, CA; March 2022. (poster)

Goodis, C.C., Conlon, I.L., Cottingham A., Fletcher, S. *Augmenting the efficacy of venetoclax in AML resistant cell lines via a PROTAC strategy.* ACS Fall 2021: Resilience of Chemistry, Georgia World Congress Center, Atlanta, GA; August 2021. (poster)

Goodis, C.C., Conlon, I.L., Cottingham A., Fletcher, S. *A PROTAC Strategy to Rescue Venetoclax Sensitivity in AML-Resistant Cells.* ACS 2021 Virtual Middle Atlantic Regional Meeting, virtual conference; June 2021. (poster)

Goodis, C.C., Li, A., Fletcher, S. *Synthetic a-helix mimetics as irreversible inhibitors of the BFL-1 anti-apoptotic protein.* 13th annual Frontiers in Chemistry and Biology Interface Symposium (FCBIS), virtual conference; May 2021. (poster)

Goodis, C.C., Conlon, I.L., Cottingham A., Fletcher, S. *A PROTAC Strategy to Rescue Venetoclax Sensitivity in AML-Resistant Cells.* ACS Spring 2021: Macromolecular Chemistry: The Second Century, virtual conference; April 2021. (poster)

Teaching Experience

2024 Research Rotation Mentor – Mentored Ruchira Basu in the Fletcher laboratory.
2023 Research Rotation Mentor – Mentored Logan Badeau in the Fletcher laboratory.
2022 Research Rotation Mentor – Mentored Sarah Pogash in the Fletcher laboratory.
2021 Research Rotation Mentor – Mentored Brandon Lowe in the Fletcher laboratory.
2020 Research Rotation Mentor – Mentored Andrea Cottingham and Angela Lee in the Fletcher laboratory.
2020 Grad Teaching Assistant – Conducted one lecture and held multiple review sessions for first year graduate students.

Abstract:

Title of Dissertation: Molecular Strategies to Combat Acquired Resistance to the Anti-Leukemic Drug Venetoclax

Christopher C. Goodis, Doctor of Philosophy, 2024

Dissertation Directed by: Dr. Steven Fletcher, Associate Professor and Director of MS in Pharmaceutical Sciences Program, Department of Pharmaceutical Sciences

A key hallmark of cancer is the ability to manipulate homeostatic pathways within cells to promote tumor growth. A significant example of this is intrinsic apoptotic pathway, which is regulated by members of the B-cell lymphoma 2 (BCL-2) protein family, that comprises two sub-populations of anti-apoptotic proteins (i.e. BCL-2, MCL-1, BCL-xL, BFL-1 and BCL-w) and pro-apoptotic proteins (which are further divided into BH3-only proteins, such as BIM and PUMA, and effector proteins, e.g. BAK and BAX). Under normal conditions, these proteins exist in similar ratios, interacting with one another via an a-helical BH3 “death” domain on the pro-apoptotic protein and a conserved BH3-binding groove on the surface of the anti-apoptotic proteins. In this state of affairs, homodimerization of the effector proteins is not possible, and apoptosis is prevented. However, when stress occurs in the cell, pro-apoptotic proteins are upregulated. This shift further activates BAK and BAX causing apoptosis. In BCL-2-dependent cancers, one or several of the anti-apoptotic BCL-2 proteins are overexpressed resulting in the sequestration and neutralization of pro-apoptotic proteins bound, disabling the ability to induce apoptosis. Inhibitors seeking to restore apoptotic function are designed to target the BH3 binding groove by mimicking the BH3 “death” domain.

These inhibitors, dubbed “BH3 mimetics”, function by masquerading as pro-apoptotic BCL-2 proteins, which themselves become bound by the anti-apoptotic proteins thereby releasing the *bona fide* pro-apoptotic proteins, and restoring apoptosis in cancerous cells. A breakthrough utilizing BH3 mimicry came with the development of the BCL-2 selective inhibitor venetoclax (VEN). Gaining FDA approval in 2016 for patients with chronic lymphocytic leukemia (CLL), and then later for acute myeloid leukemia (AML), VEN has cemented itself as the current standard-of-care drug for treating these diseases. Unfortunately, patients administered VEN develop resistance to the therapeutic after ~17 months of treatment. While these resistances can manifest in multiple ways, the focus of this dissertation was to tackle the compensatory upregulations of sister anti-apoptotic BCL-2 proteins, particularly BCL-xL, MCL-1, and BFL-1. However, targeting these sister anti-apoptotic proteins presents their own challenges. Direct inhibition of BCL-xL causes thrombocytopenia, while multiple clinical trials for MCL-1 inhibitors have been halted or terminated due to cardiotoxicity, leading to the deaths of at least two patients. It has been stated that BFL-1 is the underdog of the BCL-2 family, having received comparatively far less attention than its sister proteins towards the discovery of new anti-cancer drugs. Although herein we have not identified any potent BFL-1 inhibitors, we anticipate our foundational work will provide a springboard for future work.

Molecular Strategies to Combat Acquired Resistance to the Anti-Leukemic Drug Venetoclax

by
Christopher C. Goodis

Dissertation submitted to the Faculty of the Graduate School of the
University of Maryland, Baltimore in partial fulfillment
of the requirements for the degree of
Doctor of Philosophy
2024

Table of Contents .....

Chapter 1: Targeting BCL-2 Anti-apoptotic Proteins 1

1.1 Intrinsic Cellular Apoptosis Pathway and BCL-2 Apoptotic Protein Members 1

1.1.1 BCL-2 Protein Family: Members and Structures 1

1.1.2 BCL-2 Protein Family: Activating and Initiating Apoptosis 3

1.1.3 BCL-2 Protein Family: Manipulation by Cancer and Role in Tumorigenesis ... 4

1.2 Development of BCL-2 Anti-apoptotic Protein Inhibitors 6

1.2.1 Navitoclax: a Dual BCL-2/BCL-xL inhibitor 7

1.2.2 Venetoclax: a Selective BCL-2 inhibitor 8

1.3 Development of MCL-1 Anti-apoptotic Protein Inhibitors 9

1.3.1 Direct MCL-1 Inhibitors 10

1.3.2 Allosteric MCL-1 Inhibitors 14

1.4 Development of BFL-1 Anti-apoptotic Protein Inhibitors 15

1.4.1 Direct BFL-1 Inhibitors 15

Chapter 2: Targeting Non-BCL-2 Family Anti-Leukemic Targets 18

2.1 Alternative targets to combat hematological malignancies 18

2.2 Fms related receptor tyrosine kinase 3 (FLT3) 19

2.2.1 Mutations on the FLT3 gene are the most common cause of AML 19

2.2.2 Development of FLT3 Inhibitors 21

2.2.2.1 Midostaurin 21

2.2.2.2 Quizartinib 22

2.2.2.3 Gilteritinib 23

2.2.2.4 FF-10101 24

2.3 Cyclin-dependent kinase 9 (CDK9) 25

2.3.1 TP-1287 27

2.3.2 GFH009 27

2.3.3 SNS-032 28

2.3.4 AT7519 29

Chapter 3: Molecular Strategies to Combat Acquired Resistance 30

3.1 Multitargeted non-covalent inhibitors 30
3.1.1 Heterobifunctional drug design 30
3.1.2 Design of heterobifunctional compounds 31
3.1.3 Polypharmacological drug development 32
3.1.1.1 Design rational: linked polypharmacological agents 34
3.1.1.2 Design rational: merged polypharmacological agents 35
3.2 Covalent Based Inhibitors: A Renaissance for Drug Discovery 36
3.2.1 Mildly reactive electrophilic warheads 37
3.2.2 Advantages of covalent inhibitors 38
3.3 Heterobifunctional Targeted Protein Degradation 40
3.3.1 Hydrophobic Tagging Molecules 41
3.3.2 Proteolysis-Targeting Chimera (PROTAC) Protein Degraders 42
3.3.2.1 Craig Crews and the Invention of PROTACs 43
3.3.2.2 Ternary Complex and Hook Effect 44
3.3.2.3 Ubiquitin-proteasome system (UPS) 46
3.3.2.4 E3 Ligases 47
3.3.2.5 E3 Ligase Ligands 48
3.3.2.6 Linking Groups 49
3.3.2.7 Ibrutinib Recovery via Conversion into a Protein Degrader 49

Chapter 4: Scaffold hopping from indoles to indazoles yields dual MCL-1/BCL-2 inhibitors from MCL-1 selective leads 51

4.1 Introduction 51
4.2 Results and Discussion 52
4.3 Conclusions 62
4.4 Methods 63
4.5 Experimental Procedures 75

Chapter 5: Synthesis of FLT3 Inhibitors Through Multiple Molecular Strategies 97

5.1 The polypharmacy combination of the BCL-2 inhibitor venetoclax (VEN) and the FLT3 inhibitor gilteritinib (GIL) is more active in acute myeloid leukemia cells than novel polypharmacologic BCL-2/FLT3 VEN–GIL hybrid single-molecule inhibitors. 97
5.1.1 Introduction 97

5.1.2 Design Rationale 102
5.1.3 Results and Discussion 104
5.1.4 Conclusion 111
5.1.5 Methods 112
5.1.6 Experimental Procedures 116
5.2 Synthesis of FLT3 Covalent Inhibitors to Counter Gatekeeper Mutation 136
5.2.1 Introduction 136
5.2.2 Design Rationale 137
5.2.3 First Generation FLT3 Covalent Inhibitors 139
5.2.3.1 Synthesis of first generation FLT3 Covalent Inhibitors 140
5.2.3.2 Biological Evaluation of first generation FLT3 Covalent Inhibitors 141
5.2.4 Second Generation FLT3 Covalent Inhibitors 147
5.2.4.1 Synthesis of first generation FLT3 covalent Inhibitors 148
5.2.4.2 Biological Evaluation of second generation FLT3 Covalent Inhibitors .. 151
5.2.5 Third Generation FLT3 Covalent Inhibitor 155
5.2.5.1 Synthesis of Third Generation FLT3 Covalent Inhibitor 157
5.2.5.2 Biological Evaluation of 3rd generation FLT3 Covalent Inhibitors 157
5.2.6 Conclusions and Future Directions 158
5.2.7 Methods 158
5.2.8 Experimental Procedures 162

Chapter 6: Transformation of the pan-CDK Inhibitor AT7519 into AMC-3-221, a CDK9-Selective Degrader 193

6.1 Introduction 193
6.2 Design Rationale 194
6.3 First Generation AT7519 PROTACs 195
6.3.1: Synthesis of AT7519 195
6.3.2: Synthesis of Modified AT7519 196
6.3.3: Synthesis of Modified Thalidomide 197
6.3.4 Synthesis of First Generation CDK9 PROTACs 197
6.3.5 Biological Evaluation for First Generation CDK9 PROTACs 198
6.4 Second Generation AT7519 PROTACs 201

6.4.1 Synthesis of Second Generation CDK9 PROTACs 202
6.4.2 Biological Evaluation of Second Generation CDK9 PROTACs..... 203
6.5 Flow Cytometry..... 207
6.6 Degradation of CDK9 and Downregulation of MCL-1 208
6.7 CDK9 PROTACs in Additional Cancer Models..... 212
6.8 CDK9 PROTACs in Fibroblast Cells..... 213
6.9 In Vivo Evaluation of AMC-3-221 214
6.10 Conclusions and Future Directions 216
6.11 Methods..... 216
6.12 Experimental Procedures..... 221

Chapter 7: Appendix 253

7.1 BCL-2 G101V Confers Venetoclax resistance 253
7.1.1 BCL-2 Protein Degraders 253
7.1.2 Synthesis of BCL-2 Hydrophobic Degraders..... 254
7.1.3 Synthesis of First Generation BCL-2 PROTACs 255
7.1.4 Final Compound Structures of Hydrophobic Degraders and first Generation BCL-2 PROTACs..... 259
7.1.5 Nanosyn Testing of Hydrophobic Degraders and 1st Generation BCL-2 PROTACs..... 261
7.1.6 AlamarBlue testing of Hydrophobic Degraders and first Generation BCL-2 PROTACs..... 262
7.1.7 Synthesis of second generation BCL-2 PROTACs 265
7.1.8 Final Compound Structures of second generation BCL-2 PROTACs 269
7.1.9 AlamarBlue testing of second generation BCL-2 PROTACs 271
7.2.10 Conclusions and Future Directions..... 273
7.2 BFL-1 Upregulation Causes Tumorigenesis and Venetoclax Resistance..... 274
7.2.1 BFL-1 Covalent Inhibitors..... 274
7.2.2 Inhibitor Design..... 275
7.2.3 Synthesis of first generation BFL-1 inhibitors 275
7.2.4 Final Compound Structures of 1st generation BFL-1 inhibitors 278
7.2.5 Cell Free Testing of 1st generation BFL-1 inhibitors..... 279
7.2.6 Synthesis of CG-3-116 SAR Compounds 280

7.2.7 Final Compound Structures of CG-3-116 SAR Compounds 283
7.2.8 Cell Free Testing of CG-3-116 SAR Compounds..... 284
7.2.9 Synthesis of Non-Covalent BFL-1 Inhibitors..... 286
7.2.10 Final Compound Structures of Non-Covalent BFL-1 Inhibitors..... 287
7.2.11 Cell Free Testing of Non-Covalent BFL-1 Inhibitors 287
7.2.12 Synthesis of Indole-Based Covalent BFL-1 Inhibitors..... 288
7.2.13 Final Compound Structures of Indole-Based BFL-1 Covalent Inhibitors.... 291
7.2.14 Cell Free Testing of Indole-Based BFL-1 Covalent Inhibitors. 292
7.2.15 Conclusions and Future Directions..... 293

Chapter 8: Concluding Remarks 294

8.1 Future Directions..... 294

References:..... 296

List of Tables:

Table 4.2.1: 56

Table 4.2.2: 60

Table 4.4.1: 68

Table 4.4.2: 69

Table 4.4.3: 71

Table 4.4.4: 74

Table 4.4.5: 75

Table 5.1.3.1: 107

Table 5.1.3.2: 109

Table 5.2.3.1: 140

Table 5.2.3.2.1: 143

Table 5.2.3.2.2: 145

Table 5.2.3.2.3: 147

Table 5.2.4.1: 148

Table 5.2.4.2.1: 152

Table 5.2.4.2.2: 155

Table 5.2.5.2.1 158

Table 6.3.5.1: 199

Table 6.3.5.2: 201

Table 6.4.2.1: 204

Table 6.4.2.2: 207

Table 6.7.1: 213

Table 6.8.1: 213

Table 7.2.5.1: 280

Table 7.2.8.1: 285

Table 7.2.8.2: 286

Table 7.2.11.1: 288

Table 7.2.14.1: 292

List of Figures:

Figure 1.1.1.1: 2

Figure 1.1.2.1: 4

Figure 1.1.3.1: 6

Figure 1.2.1: 7

Figure 1.2.1.1: 8

Figure 1.2.2.1: 9

Figure 1.3.1.1: 11

Figure 1.3.1.2: 12

Figure 1.3.1.3: 12

Figure 1.3.1.4: 13

Figure 1.3.1.5: 13

Figure 1.3.1.6.: 14

Figure 1.3.2.1: 15

Figure 1.4.1.1: 16

Figure 1.4.1.2: 17

Figure 2.2.1.1: 20

Figure 2.2.2.1.1: 22

Figure 2.1.2.2.1: 23

Figure 2.2.2.3.1: 24

Figure 2.2.2.4.1: 25

Figure 2.3.1: 26

Figure 2.3.1.1: 27

Figure 2.3.2.1: 28

Figure 2.3.3.1: 29

Figure 2.3.4.1: 29

Figure 3.1.1: 30

Figure 3.1.1.1: 34

Figure 3.2.1: 37

Figure 3.2.2: 37

Figure 3.2.1.1: 38

Figure 3.2.1.2: 38

Figure 3.3.1.1: 42

Figure 3.3.2.1: 43

Figure 3.3.2.1.1: 44

Figure 3.3.2.2.1: 46

Figure 3.3.2.5.1: 49

Figure 3.3.2.7.1: 50

Figure 4.2.1:. 53

Figure 4.2.2: 58

Figure 4.2.3: 59

Figure 4.2.4: 62

Figure 4.4.1: 67

Figure 4.4.2: 72

Figure 5.1.1.1: 101

Figure 5.1.2.1: 104

Figure 5.1.3.1: 105

Figure 5.1.3.2: 106

Figure 5.1.3.3: 111

Figure 5.2.1.1: 137

Figure 5.2.1.2: 137

Figure 5.2.2.1: 139

Figure 5.2.2.2:. 139

Figure 5.2.3.1.1: 141

Figure 5.2.3.2.1: 143

Figure 5.2.3.2.2: 144

Figure 5.2.3.2.3: 146

Figure 5.2.3.2.4: 146

Figure 5.2.4.1.1: 149

Figure 5.2.4.1.2: 150

Figure 5.2.4.1.3: 150

Figure 5.2.4.1.4: 151

Figure 5.2.3.4.1: 153

Figure 5.2.3.4.2: 153

Figure 5.2.3.4.3: 154

Figure 5.2.3.4.4: 154

Figure 5.2.5.1: 156

Figure 5.2.5.2: 157

Figure 5.2.5.1.1: 157

Figure 6.3.1.1: 196

Figure 6.3.2.1: 197

Figure 6.3.3.1: 197

Figure 6.3.4.1: 198

Figure 6.3.5.1: 200

Figure 6.4.1.1: 203

Figure 6.4.2.1: 205

Figure 6.4.2.2: 206

Figure 6.5.1: 208

Figure 6.6.1: 210

Figure 6.6.2: 212

Figure 6.9.1: 215

Figure 6.9.2: 215

Figure 7.1.2.1: 255

Figure 7.1.3.1: 257

Figure 7.1.3.2: 258

Figure 7.1.3.3: 259

Figure 7.1.4.1: 261

Figure 7.1.5.1: 262

Figure 7.1.6.1: 263

Figure 7.1.6.2: 263

Figure 7.1.6.3: 264

Figure 7.1.6.4: 264

Figure 7.1.6.5: 265

Figure 7.1.7.1: 266

Figure 7.1.7.2: 266

Figure 7.1.7.3: 267

Figure 7.1.7.5: 268

Figure 7.1.7.7: 269

Figure 7.1.8.1: 270

Figure 7.1.9.1: 271

Figure 7.1.9.2: 271

Figure 7.1.9.3: 272

Figure 7.1.9.4: 272

Figure 7.1.9.5: 273

Figure 7.2.3.1: 278

Figure 7.2.4.1: 279

Figure 7.2.6.1: 283

Figure 7.2.7.1: 284

Figure 7.2.9.1: 287

Figure 7.2.10.1: 287

Figure 7.2.12.1: 291

Figure 7.2.13.1: 292

List of Abbreviations

ADME	Absorption, distribution, metabolism, and excretion
AKT	PI3K-Akt signaling pathway
AML	Acute myeloid leukemia
APAF-1	Apoptotic protease activating factor 1
ATP	Adenosine triphosphate
AXL	Tyrosine-protein kinase receptor UFO
BAD	Bcl-2-associated death promoter
BAK	Bcl-2 homologous antagonist killer
BAX	Bcl-2 Associated X-protein
BCL-2	B-cell lymphoma-2
BCL-xL	B-cell lymphoma-extra large
BCR	B-cell receptor
BFL-1	Bcl-2-related protein A1
BH	Bcl-2 homology
BIM	Bcl-2-like protein 11
BTK	Bruton's tyrosine kinase
cal	Calorie
CDK2	Cyclin-dependent kinase 2
CDK5	Cyclin-dependent kinase 5
CDK7	Cyclin-dependent kinase 7
CDK9	Cyclin-dependent kinase 9
CLL	Chronic lymphocytic leukemia
CRBN	Cereblon

Cytc	Cytochrome c
DIPEA	N,N-diisopropylethylamine
DMAP	4-Dimethylaminopyridine
DMF	Dimethylformamide
DMSO	Dimethyl sulfoxide
DTT	Dithiothreitol
EDCI	1-Ethyl-3-(3-dimethylaminopropyl)carbodiimide
EMSA	Electrophoretic mobility shift assay
ESI	electrospray ionization
FDA	Food and drug administration
FITC	Fluorescein isothiocyanate
FL	FLT3 ligand
FLT3	Fms-like tyrosine kinase 3
FLT3-ITD	FLT3 internal tandem duplication
FLT3-TKD	FMS-like tyrosine kinase-3 tyrosine kinase duplication
FPCA	Fluorescence polarization competition assay
GCMC-MD	Grand canonical Monte Carlo-molecular dynamics
GIL	Gilteritinib
HATU	Hexafluorophosphate azabenzotriazole tetramethyl uronium
HBTU	Hexafluorophosphate benzotriazole tetramethyl uronium
HRMS	High resolution mass spectrometry
HRMS-ESI	High resolution electrospray ionization mass spectrometry
IC_{50}	Half-maximal inhibitory concentration

JM	Juxtamembrane
K_d	Dissociation constant
K_i	Inhibitory constant
LGFE	Ligand grid free energy
LRMS	Low resolution mass spectrometry
MAPK	Mitogen-activated protein kinases
MCL-1	Myeloid cell leukemia-1
MetAP-2	Methionine aminopeptidase-2
mi-RNAs	MicroRNAs
MM	Multiple myeloma
MOMP	Mitochondrial outer membrane permeabilization
mRNA	Messenger RNA
MW	Molecular weight
MYC	Myelocytomatosis
NHL	Non-Hodgkin's lymphoma
NMP	N-Methylpyrrolidone
NMR	Nuclear magnetic resonance
NOXA	Phorbol-12-myristate-13-acetate-induced protein 1
NRG	NOD-Rag1^{null}IL2rg^{null}
OE	Overexpressing
PBP	penicillin-binding protein
PBS	Phosphate buffered saline
PDB	Protein data bank

PEG	Polyethylene glycol
POI	Protein of interest
PPI	Protein-protein interactions
PROTAC	Proteolysis-Targeting Chimera
PUMA	p53 upregulated modulator of apoptosis
Rf	Retention factor
RNAPII	RNA Polymerase II
RR	Relapsed refractory
RT	Room temperature
RTK	Receptor tyrosine kinase
$SCF^{\beta\text{-TRCP}}$	Skp1-Cullin-F box β-TRCP complex
SCLC	Small cell lung cancer
SILCS	Site identification by ligand competitive saturation
SILCS-MC	Site identification by ligand competitive saturation Monte-Carlo
tCDKs	Transcription-associated cyclin-dependent kinases
TEA	Triethylamine
TFA	Trifluoroacetic acid
THF	Tetrahydrofuran
TK	Tyrosine kinase
TKIs	Tyrosine kinase inhibitors
TLC	Thin Layer Chromatography
TR-FRET	Time-resolved fluorescence energy transfer
UPS	Ubiquitin-proteasome system

VEN	Venetoclax
VHL	Von Hippel-Lindau
WT	Wild type

Chapter 1: Targeting BCL-2 Anti-apoptotic Proteins

1.1 Intrinsic Cellular Apoptosis Pathway and BCL-2 Apoptotic Protein Members

Cells contain numerous systems and signaling cascades to maintain homeostasis. When that balance is severely disrupted, the cell must initiate apoptosis, or cell death, in order to maintain the overall balance within the biological system.[1,2] One key pathway to initiate apoptosis is the intrinsic mitochondrial-mediated apoptotic pathway governed by the BCL-2 family of proteins.[3,4,5,6]

1.1.1 BCL-2 Protein Family: Members and Structures

The BCL-2 protein family is divided between two members: pro-apoptotic proteins (e.g. BIM, BAD, PUMA, BAX, BAK) and anti-apoptotic proteins (e.g. BCL-2, MCL-1, BCL-xL, and BFL-1).[4,6] Pro-apoptotic proteins are further divided into two sub members: the effectors (e.g. BAX, BAK) and BH3-only proteins (e.g. BIM, BAD, PUMA).[4] This distinction is due to these proteins containing a certain number of BH domains.[3,4,5,6] The BH3-only proteins are classified because of their structure being comprised of only the BH3 homology domain. [4,6] Whereas the effector pro-apoptotic proteins contain the BH1-3 domains.[4,6] Anti-apoptotic proteins are defined by their conserved solvent-exposed binding groove which recognizes the BH3 domain of all pro-apoptotic proteins (**Figure 1.1.1.1**).[3,4,5,6] This conserved binding groove is comprised of multiple shallow hydrophobic pockets denoted as "p-pockets" and are labeled p1-p4.[3,4,5,6] The pro-apoptotic proteins recognize the binding groove by undergoing a conformational change of their BH3 domain into an α-helical conformation.[4,6] Once in this conformation, the BH3 domain protrudes multiple hydrophobic residues off one face of the protein in an R*i,*

R*i+3/4*, and R*i+7* orientation.[7] These hydrophobic residues then interact with the p-pockets on the anti-apoptotic protein and engage with the protein.[3,4,5,6] Additionally, an acidic residue on the opposite face of the helix forms a salt bridge with the anti-apoptotic protein conserved basic residue.[8]

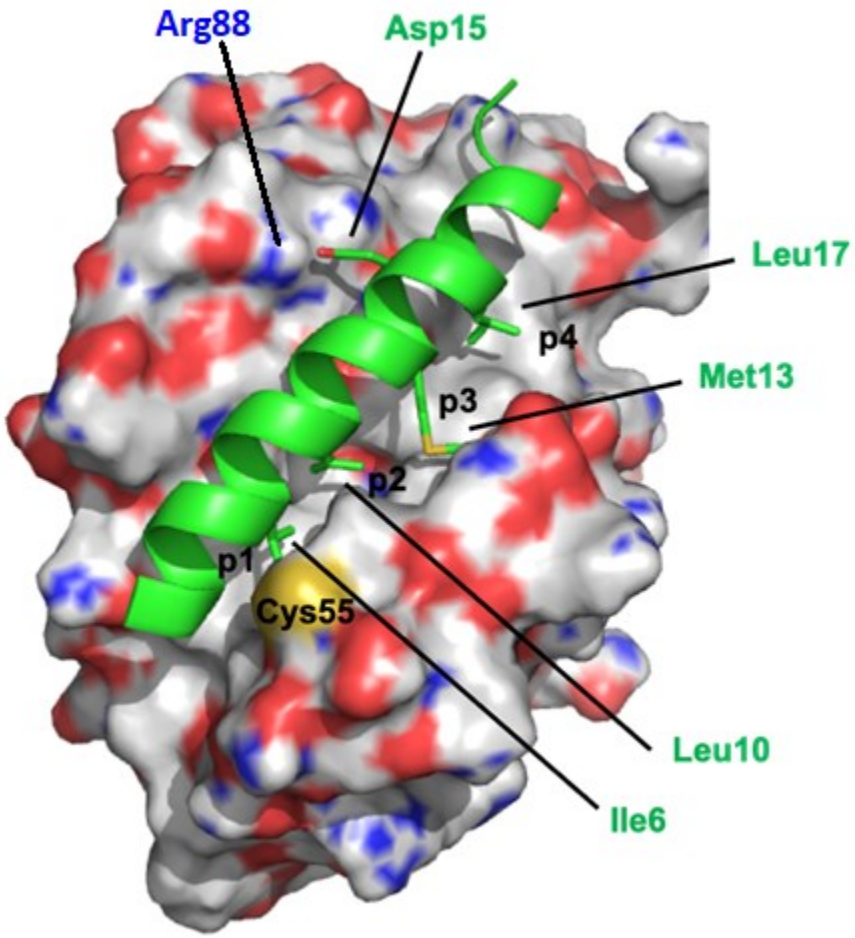

Figure 1.1.1.1: *Crystal structure of pro-apoptotic protein PUMA bound to anti-apoptotic protein BFL-1 (PDB ID: 5UUL). Hydrophobic residues and the aspartic acid residue are labeled on PUMA protein. Hydrophobic p-pockets, solvent exposed cysteine residue, and arginine residue on BFL-1 are labeled.*

1.1.2 BCL-2 Protein Family: Activating and Initiating Apoptosis

Within cells, anti-apoptotic proteins prevent apoptosis initiation by sequestering pro-apoptotic members via their conserved PPI site that recognizes the BH3 domain.[3,4,5,6] When a cellular stress occurs and the cell needs to undergo apoptosis, pro-apoptotic BH3-only proteins are upregulated (**Figure 1.1.2.1**).[3,4,5,6] There are two classes of BH3-only proteins with distinct functions.[3,4,5,6] De-repressor proteins have the sole function of preventing the anti-apoptotic proteins from sequestering any other pro-apoptotic proteins.[5,6] Activator proteins start the pathway towards apoptosis by activating the effector proteins via binding either to the N-terminus or a hydrophobic core formed by the BH1-3 domains.[5,6] Once activated, the effector proteins oligomerize and initiate MOMP.[9,10] After forming these pores, the mitochondria releases Cytc which interacts with APAF-1 to induce caspase activation which ultimately starts the controlled destruction of cellular components.[9,10]

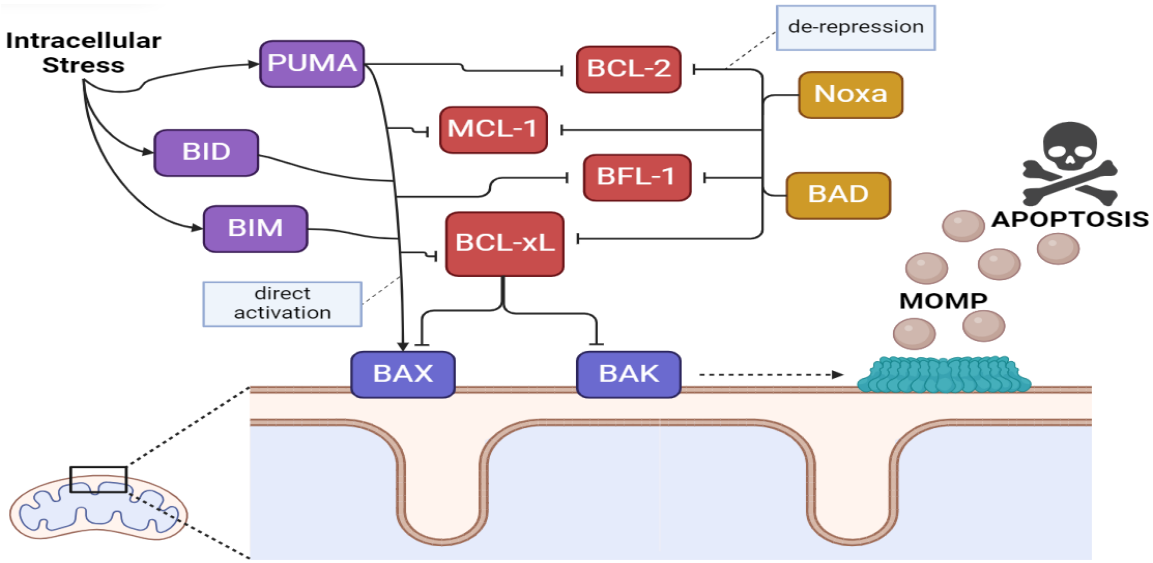

Figure 1.1.2.1: *Representation of BCL-2 family of proteins initiating intrinsic cellular apoptosis. Intracellular stress initiates the upregulation of activator & de-repressor proteins which ultimately activate the effector proteins BAX & BAK. BAX & BAK dimerize causing mitochondrial outer membrane permeabilization (MOMP) which releases cytochrome c starting the controlled destruction of the cell.*

Created in BioRender.com

1.1.3 BCL-2 Protein Family: Manipulation by Cancer and Role in Tumorigenesis

Multiple types of cancer manipulate the BCL-2 family of proteins to promote tumorigenesis.[5] Cancer has this ability because of the numerous cancer associated mi-RNAs that regulate the BCL-2 family.[11] The two primary cancer types that engage in this function are AML and CLL.[12,13] Both being leukemias, these cancers target the production of infant white blood cells which prevents the formation of mature white blood cells.[14,15] In healthy bone marrow, blood stem cells differentiate into myeloid stem cells, which further develop into red blood cells, granulocytes, and plasma cells, or they can differentiate into lymphoid stems cells that develop into multiple lymphocytic white blood cells.[14,15] AML overproduces damaged myeloblasts which are the precursor stem cells to granulocyte white blood cells.[14] CLL is defined as the overproduction of

abnormal lymphoblasts which are precursor stem cells of lymphocytic white blood cells.[15] In both cases, this overproduction causes multiple complications in patients due to the absence of mature white blood cells including fatigue, ease of bleeding or bruising, and will escalate to fatality of the patient.[14,15] These severe symptoms are reflected in the 5-year survival rate of AML being an abysmal 32% while the 10-year survival rate of CLL sits at 65%.[16,17] New cases of AML and CLL total roughly 40,000 per year in the United States and both are the cause of approximately 15,000 death in the U.S. as well.[16,18] Adding to this, AML accounts for approximately 15% of all childhood leukemia cases.[19]

Both leukemias frequently manipulate the BCL-2 family by upregulating the anti-apoptotic members within the family.[3,4,5,6] The BCL-2 anti-apoptotic protein specifically is upregulated commonly in these leukemias to such a degree that all pro-apoptotic are sequestered and the intrinsic apoptotic pathway is nullified (**Figure 1.1.3.1**).[3,4,5,6] Since all pro-apoptotic proteins contain a BH3 binding domain, this means that all effectors, activators, and de-repressor proteins have their function neutralized.[3,4,5,6] This allows the tumor blood cells to propagate within the bone marrow while also circulating throughout the body where tumor cells can coagulate and initiate tumorigenesis distal to the source.[3,4,5,6]

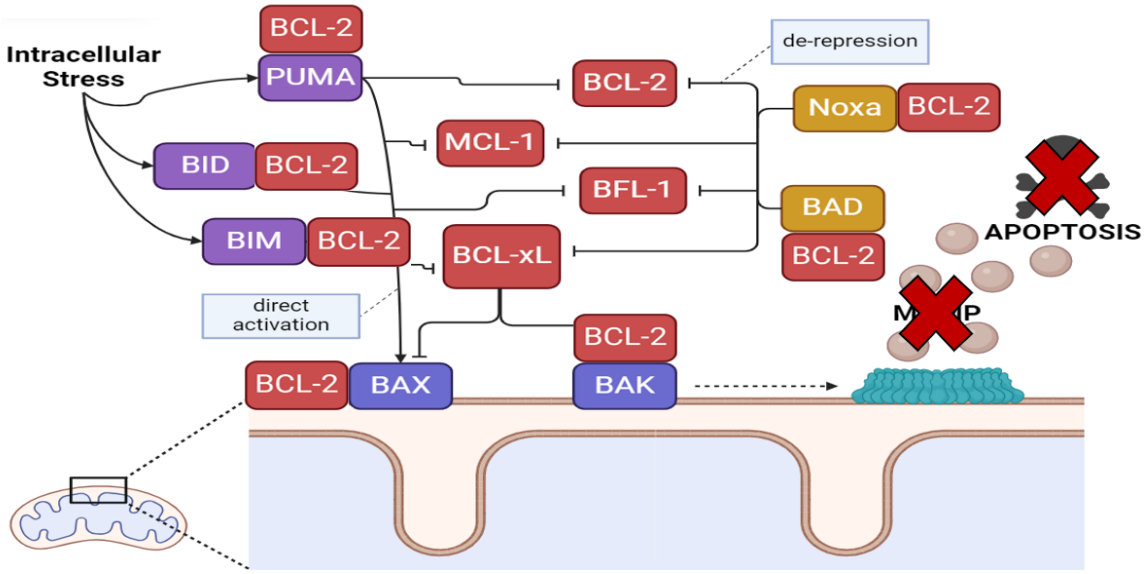

Figure 1.1.3.1: *Representation of BCL-2 anti-apoptotic protein being overexpressed in cancer cells. Overexpressed BCL-2 sequesters all pro-apoptotic proteins preventing MOMP and apoptosis from occurring.*

Created in BioRender.com

1.2 Development of BCL-2 Anti-apoptotic Protein Inhibitors

To counter the upregulation of BCL-2 protein, efforts have focused on developing competitive inhibitors for the protein to release the sequestered pro-apoptotic proteins and restore function to the apoptotic pathway.[20] However, the challenge with developing inhibitors for the anti-apoptotic proteins is due to the lack of any deep pockets or catalytic residues on the conserved BH3 binding groove.[21] Despite this, inhibitors have been created that utilize multiple hydrophobic motifs attached to a large connecting backbone to target the p-pockets within the BH3 binding groove (**Figure 1.2.1**).[22]

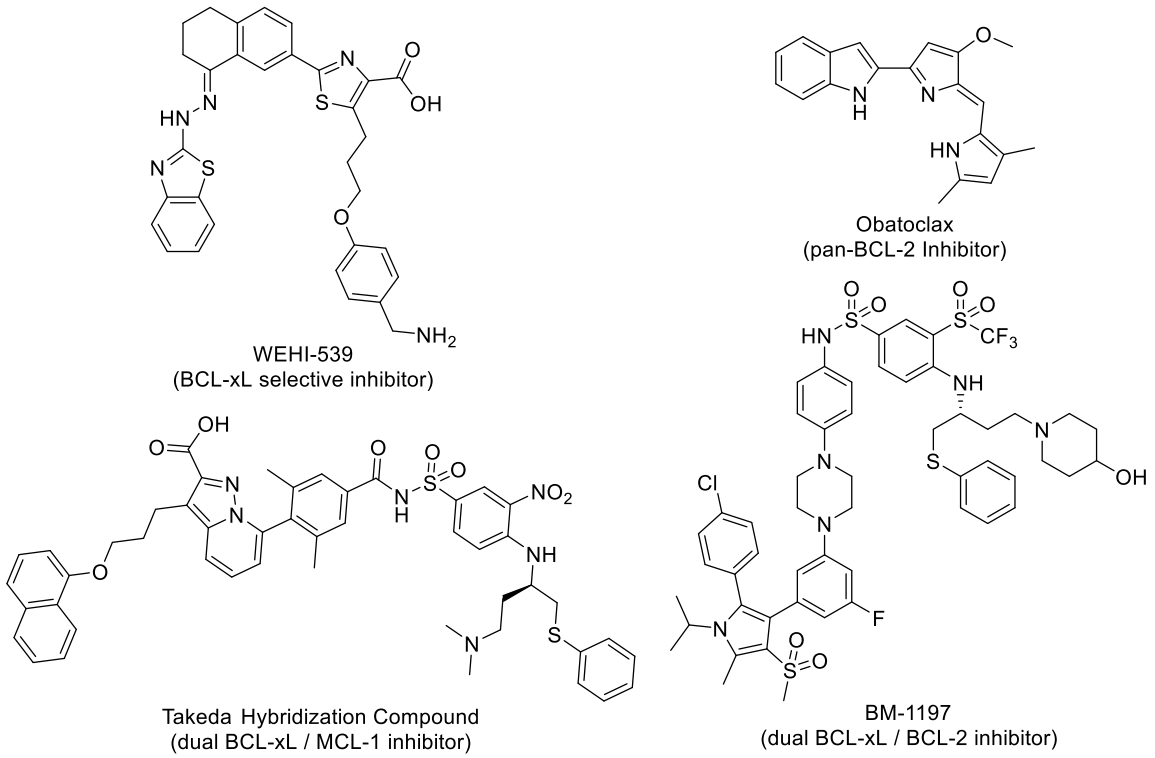

Figure 1.2.1: Structures of prominent BCL-2 / BCL-xL inhibitors

1.2.1 Navitoclax: a Dual BCL-2/BCL-xL inhibitor

Beginning in 2008, Abbott began publishing on a novel BCL-2 inhibitor named ABT-263, or navitoclax (**Figure 1.2.1.1**), which demonstrated an inhibitory effect on anti-apoptotic proteins.[23] This work revealed that the compound had a high affinity towards BCL-2 and BCL-xL while avoiding MCL-1 binding.[23] Navitoclax was then shown to weakly induce apoptosis in BCL-2-deficient cells via the reactivation of BAX and release of Cytc.[23] In addition, navitoclax was effective in SCLC xenograft models and found that daily oral treatment attenuated tumor growth.[23] However, clinical trials for the therapeutic have been unsuccessful due to the adverse side effects.[24] The most severe effect of the drug is thrombocytopenia which is a disease caused by a low number of platelet cells in the body.[24] This causes excessive bleeding from the gums, nose, and excretory tracts

while also causing blood vessels to leak blood underneath the skin causing purpura rashes.[25] These symptoms have been linked to BCL-xL inhibition as the function of the protein is essential for platelet health.[26] Because of these adverse effects, Navitoclax has yet to obtain FDA approval for treating AML and CLL. However, the development of this therapeutic is a milestone in BCL-2 inhibitor development, showcasing the ability to interact with the BH3 binding groove of anti-apoptotic proteins.

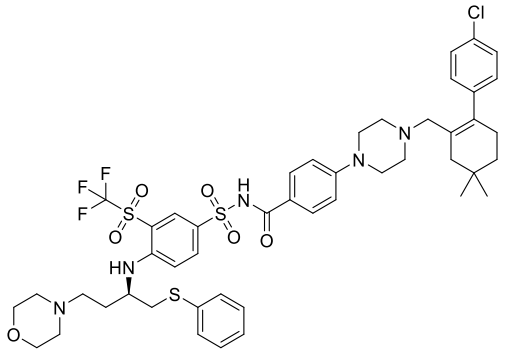

Navitoclax

Figure 1.2.1.1: *Structure of Navitoclax*

1.2.2 Venetoclax: a Selective BCL-2 inhibitor

Even after the adverse side effects of Navitoclax became well known, researchers were still focused on creating an inhibitor that can restore the intrinsic apoptotic pathway while avoiding BCL-xL inhibition and by extension thrombocytopenia. This culminated in 2013 with the development of ABT-199, or venetoclax (**Figure 1.2.2.1**), which utilized the same mechanism of binding as navitoclax wherein venetoclax bindings to the BH3 binding groove of BCL-2.[27] Venetoclax differs in that it contains an azaindole motif to form a salt bridge between the Asp103 residue on BCL-2 which corresponds to Glu96 in the BCL-xL offering a unique residue between the two proteins.[27] This additional

interactions pushed venetoclax towards being a selective picomolar inhibitor for BCL-2 protein over the other anti-apoptotic proteins.[27] Pre-clinical studies demonstrated venetoclax to have antitumor activity against CLL and AML *in vitro* as well as *in vivo* with mouse xenograft studies against AML.[27] Following this, venetoclax quickly gained approval for use in patients suffering from CLL in 2016 and additional approval was granted in 2018 for use in patients suffering from AML.[28,29]

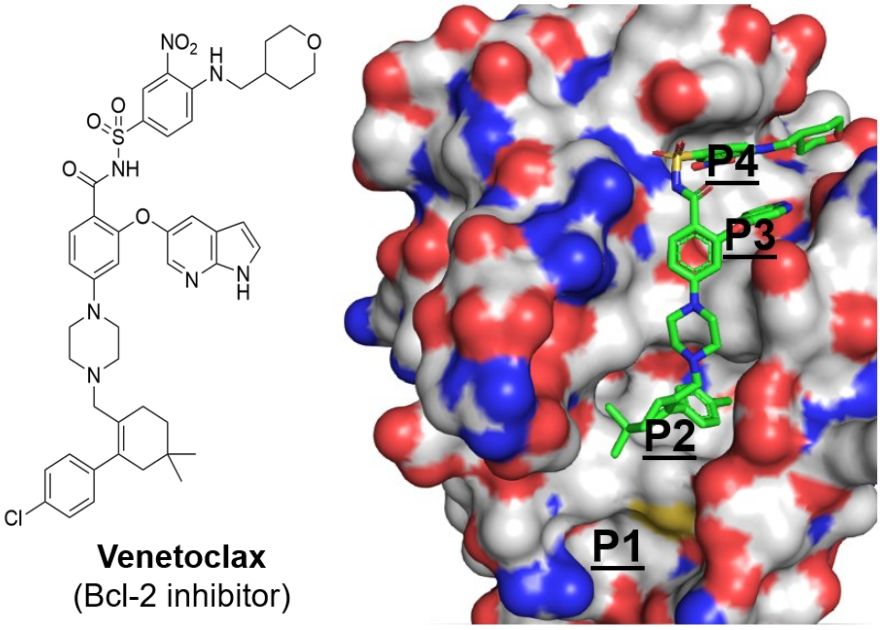

Figure 1.2.2.1: *Structure of venetoclax (left) and crystal structure of venetoclax bound to BCL-2 anti-apoptotic protein (PDB ID: 6O0O)*

1.3 Development of MCL-1 Anti-apoptotic Protein Inhibitors

Another key anti-apoptotic protein is the MCL-1 protein that functions similarly to BCL-2 and BCL-xL wherein the protein recognizes pro-apoptotic proteins to prevent apoptosis.[30] MCL-1 is also a highly oncogenic protein and has been shown to cause many types of solid tumor cancers and hematological malignancies due to the protein being

upregulated.[30,31] In addition to causing different types of cancer, MCL-1 has also been shown to cause resistance to certain therapeutics.[32,33] A notable case occurs in patients prescribed venetoclax for treatment of AML or CLL. [33] Patients given this treatment only see an effect for roughly 17 months, after which they develop resistance due to the upregulation of MCL-1.[33] There are currently no FDA-approved inhibitors for MCL-1, however research is still ongoing for an effective antileukemic therapy for MCL-1 upregulated cancers.

1.3.1 Direct MCL-1 Inhibitors

Multiple groups have attempted to create MCL-1 inhibitors by binding directly to the BH3 binding groove. One of the pioneering MCL-1 inhibitors, S63845 (**Figure 1.3.1.1**) was developed by Walter and Eliza Hall Institute of Medical Research in 2016 via an NMR-based fragment screen followed by SAR studies.[34] S63845 demonstrated a K_d of 0.19 nM against MCL-1 with no binding against BCL-2 or BCL-xL. S63845 performed well in killing MCL1-dependent cancer cells including multiple myeloma, leukemia and lymphoma cells by reinitiating the intracellular apoptotic pathway.[34] *In vivo* studies also showcased potent anti-tumour activity against multiple cancers.[34] In 2016, phase I clinical trials for S63845 both as a single agent and combination therapy were initiated, but since then these trials have been completed with no clear result posted.[35,36]

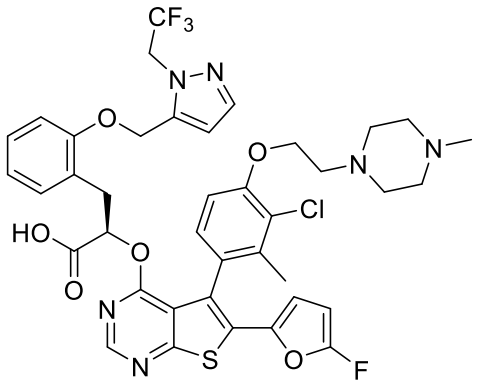

***Figure 1.3.1.1*:** Structure of S63845

During the development of S63845, the Fesik research group were also at work to synthesize MCL-1 inhibitors and identified a series of indole-based inhibitors.[37,38,39] This group initially performed a fragment-based chemical library screen using NMR to identify small molecules that interacted with the PPI site of MCL-1.[37] Two lead compounds were identified to be effective MCL-1 binders.[37] Class II fragments contained indole-, benzothiphene-, or benzofuran-based heterocycles that were substituted at the 3-, 4-, or 6- positions and contained a carboxylic acid motif at the 2- position of the ring.[37] Class II fragments contained various aromatic motifs linked to a carboxylic acid or aromatic bicycle via an alkyl chain (**Figure 1.3.1.2**).[37] Next, the Fesik group conducted NOE-guided fragment docking simulations between both compound classes and MCL which predicted that class I compounds bind to the p3 pocket with slight interactions with the p2 pocket while class II compounds were predicted to bind deep within the p2 pocket.[37] Combining these two class compounds resulted in their two potent MCL-1 inhibitors compounds **52** (K_i = 0.055 μM) and **60** (K_i = 0.32 μM) (**Figure 1.3.1.3**).[37]

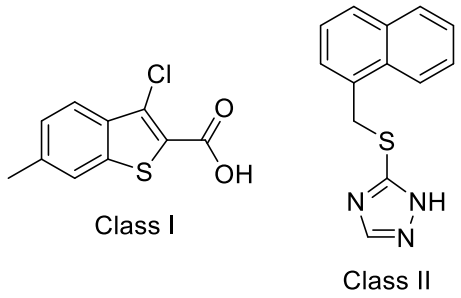

Figure 1.3.1.2: *Structures of Class I and Class II fragments*

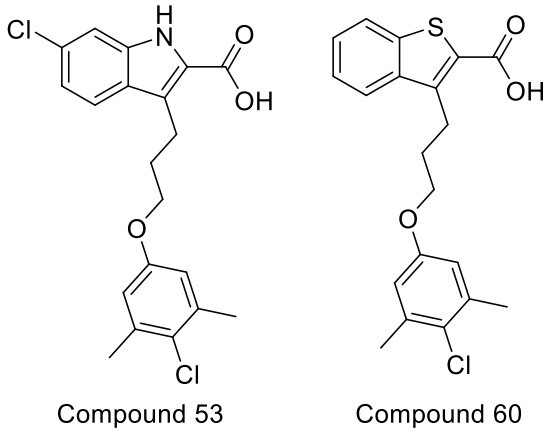

Figure 1.3.1.3**:** Structures of Compound 53 & 60

To optimize their previous compounds, the Fesik group expanded upon their indole-based MCL-1 inhibitor **53** by grafting on additional hydrophobic groups to engage with the p4 pocket on MCL-1.[39] Additional fragment-based NMR screens where conducted with the p2 pocket saturated with a reported indole and determined that various heterocycles weakly interacted with the p4 pocket.[39] The Fesik group utilized an acylsulfonamide bond to engage with the p4 pocket due to this motif being a bioisostere of carboxylic acids.[39] Compound **9** (**Figure 1.3.1.4**) was developed to test this theory that p4 binding can be achieved, which was confirmed via a crystal structure of **9** binding to MCL-1.[39]

Compound **9** was optimized via SAR studies to create compound **47** (Ki = 10 nM) (**Figure 1.3.1.5**) which contained an isobutyl group connected to an amide group.[39]

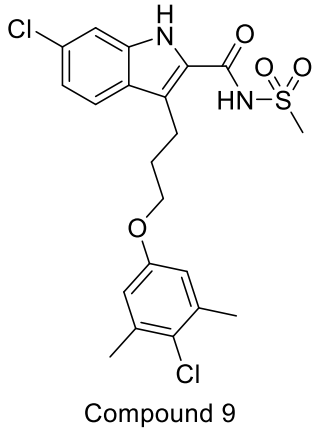

***Figure 1.3.1.4*:** Structure of Compound 9

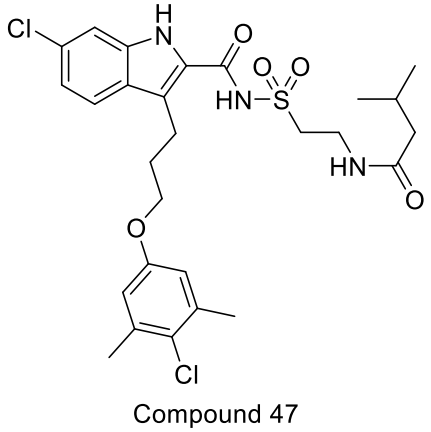

***Figure 1.3.1.5*:** Structure of Compound 47

Taking inspiration from the work in the Fesik lab, AstraZeneca developed the most selective MCL-1 inhibitor in AZD5991.[40] From a 2018 publication, AZD5991 (**Figure 1.3.1.6**) was shown to have a K_i = 0.2 nM to MCL-1 while only demonstrating mM affinity towards the other anti-apoptotic proteins.[40] AZD5991 showcased the ability to reinitiate apoptosis in MOLP-8 multiple myeloma cells, preferably killed hematological

cells over solid tumors, and drove tumor regression in AML models.[40] Despite this, a phase 1 clinical trial using AZD5991 was closed due to low overall response rate and a high rate of cardiotoxicity.[41] This has been attributed to MCL-1 function being crucial for the survival of cardiomyocytes.[41]

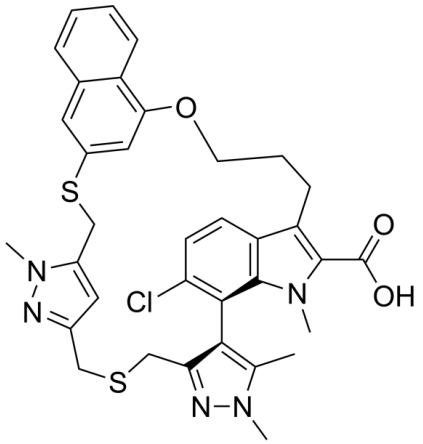

***Figure 1.3.1.6.*:** Structure of AZD5991

1.3.2 Allosteric MCL-1 Inhibitors

Another avenue for inhibiting MCL-1 has been targeting a distal binding site to confer a conformation change to the MCL-1 binding groove. In 2016, the Walensky group published their findings on the MAIM1 (**Figure 1.3.2.1**) compound and demonstrated that the compound was responsible for impairing the binding between MCL-1 and BAX both *in vitro* and in mouse cells.[42] MAIM1, which has a IC_{50} value of 450 nM to MCL-1, accomplishes this by binding to an allosteric site on the back side of the MCL-1 protein and forming a covalent bond with the Cys286 residue.[42] Once bound, MAIM1 influences the conformation of the BH3 binding groove on MCL-1 and this has an approximate 10-fold decrease in binding between MCL-1-MAIM1 and BID BH3 protein.[42]

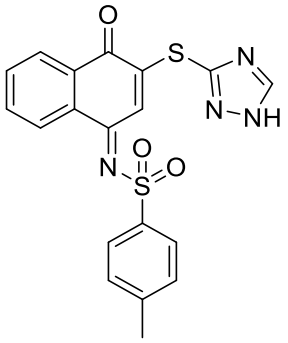

MAIM1

Figure 1.3.2.1: *Structure of MAIM1*

1.4 Development of BFL-1 Anti-apoptotic Protein Inhibitors

Similar to the other anti-apoptotic proteins, BFL-1 is responsible for preventing pro-apoptotic proteins from initiating cell death.[43,44] In addition, BFL-1 dependence has been shown in various leukemias, lymphomas, and melanomas.[43,44] Despite this fact, research geared towards creating a selective BFL-1 inhibitor has been sparce. BFL-1 has a hydrophobic groove like the sister proteins in the family, however BFL-1 contains a unique solvent exposed cysteine residue Cys55.[44] This cysteine is the focus of most of the BFL-1 inhibitor designs due to the reactivity demonstrated and the lack of any deep pockets within the binding groove.

1.4.1 Direct BFL-1 Inhibitors

In a similar manner to the other anti-apoptotic proteins, targeting the BH3 binding groove is a distinct challenge due to the lack of deep pockets or catalytic residues.[43] The Walensky group circumvented this challenge by creating a stapled peptide based of the NOXA BH3 protein that also contained an acrylamide motif to form an irreversible covalent bond with Cys55.[45,46]

Another group advancing the field of BFL-1 inhibitors is the Nikolovska-Coleska group who were responsible for publishing a dual MCL-1 / BFL-1 inhibitor.[47] From their starting point of 2,5-Substituted Benzoic Acid, multiple NMR and crystallography experiments culminated in compound **24** (**Figure 1.4.1.1**). This compound demonstrated a K_i = 100 nM for both MCL-1 and BFL-1.[47]

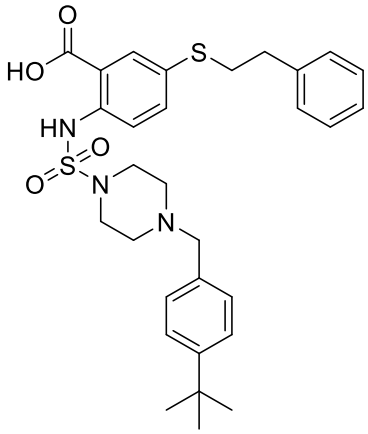

24

Figure 1.4.1.1: *Structure of Compound* ***24***

The next advancement came from the Zhao group, when they published their indole based covalent BFL-1 inhibitor compound **12** (**Figure 1.4.1.2**) which demonstrated a BFL-1 K_i of 410 nM.[48] The compound was also tested against the full gambit of anti-apoptotic proteins and was selective for BFL-1.[48] Additionally, covalent adduct formation was confirmed via intact mass spectrometry in which an adduct corresponding to BFL-1 + **12** was detected.[48] To further support the idea that compound **12** inhibited BFL-1 via covalent bond formation, a negative control compound of **12** was created that had the acrylamide double bond reduced and this compound **23** had a BFL-1 K_i of 24 mM.[48]

Finally, **12** initiated apoptosis in myeloid leukemia U937 cells which was confirmed by flow cytometry and annexin V staining.[48]

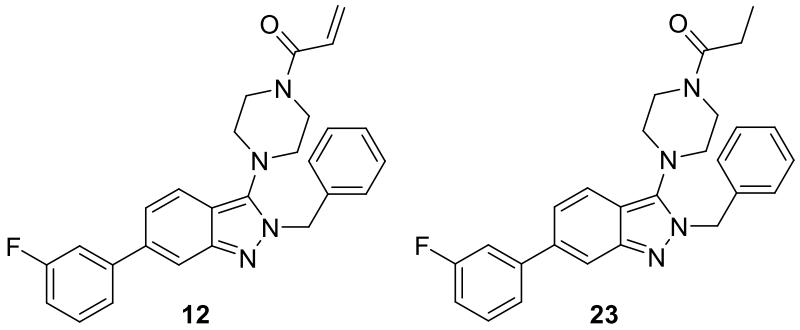

Figure 1.4.1.2: *Structure of Compound **12** and **23***

Chapter 2: Targeting Non-BCL-2 Family Anti-Leukemic Targets

2.1 Alternative targets to combat hematological malignancies

As was outlined earlier, BCL-2 anti-apoptotic proteins are upregulated in several hematological malignancies to promote tumorigenesis.[3,4,5,6] As discussed previously, multiple research groups have focused on creating inhibitors for these proteins that halt this tumor growth. However, several issues related to the direct inhibition of these anti-apoptotic proteins have been identified including resistance via counter upregulation of sister anti-apoptotic proteins, the development of thrombocytopenia due to BCL-xL inhibition, and cardiotoxicity due to MCL-1 inhibition.[24,33,41]

For MCL-1 inhibition specifically, there are two distinct challenges that could explain the absence of any clinically relevant MCL-1 inhibitors. Firstly, designing inhibitors for the BCL-2 anti-apoptotic proteins is a difficult task due to the lack of any deep pockets with catalytic residues to target, and because the affinity between the anti-apoptotic members and pro-apoptotic members is measured to be in the pM range.[49] Because most MCL-1 inhibitors are directly targeting the BH3 binding groove to outcompete the pro-apoptotic members, this pM limit restricts the chemical motifs med chemists can use since the barrier for biological inhibition is so high. In addition to this, it is unclear if the cardiotoxic side effects demonstrated in clinical trials for MCL-1 inhibitors are attributed to inhibiting the MCL-1 protein itself, or if this is due to the specific structures of the inhibitors.[50,51] While there is an increasing volume of studies focused on measuring the health of cardiomyocytes during MCL-1 deletion / inhibition, it remains unclear what exactly is causing the observed cardiotoxicity in clinical studies.[50,51]

Because of these issues, developing a single agent anti-apoptotic protein inhibitor might not be the most effective strategy to combat these hematological malignancies. Towards broadening our approach, we explored different oncogenes that are upregulated in hematological malignancies that also play a role in upregulating anti-apoptotic proteins. Two oncoproteins that fit this criteria are the tyrosine receptor kinase FLT3 and the cyclin-dependent kinase CDK9. Each of these proteins have been implicated in promoting hematological malignancies while also promoting the upregulation of MCL-1 anti-apoptotic protein.[52,53] Inhibiting these oncoproteins as an additional approach directly targets the cancers they promote while also offering an avenue to regulate the BCL-2 anti-apoptotic family of proteins to initiate apoptosis in cancerous cells.

2.2 Fms related receptor tyrosine kinase 3 (FLT3)

FLT3 is an important regulator of cell proliferation that is expressed in immature hematopoietic cells, the placenta, the gonads, and the brain.[54] The protein is a transmembrane protein that comprises a C-terminal domain, a JM domain, a TK domain in the intracellular region, and five immunoglobulin-like domains in the extracellular region.[54] Activation is initiated by binding FL that is expressed in a membrane-bound form or as a soluble form by bone marrow stoma cells.[54] Once the FL is bound the FLT3, the kinase undergoes a conformational change to a dimer state.[54] FLT3 in this state initiates multiple intracellular signaling pathways, mainly MAPK and AKT signals, promoting hematopoietic cell proliferation.[54]

2.2.1 Mutations on the FLT3 gene are the most common cause of AML

In the late 90s, scientists discovered an internal tandem duplication within the JM domain of FLT3 that was being expressed in AML cells.[55] This mutation, dubbed FLT3-ITD,

caused the FLT3 protein to become constitutive activity ultimately causing the upregulation of cancerous myeloid cells.[54,55] In addition to this mutation, multiple point mutations were later discovered on the D835 residue of FLT3s TK domain.[56] This mutation was later classified as FLT3-TKD and produced the same effect as FLT3-ITD wherein the protein was stabilized in the dimer state and cell proliferation signaling was upregulated causing AML (**Figure 2.2.1.1**). Both mutations account for directly causing ~30% of all AML cases.[54,55,56]

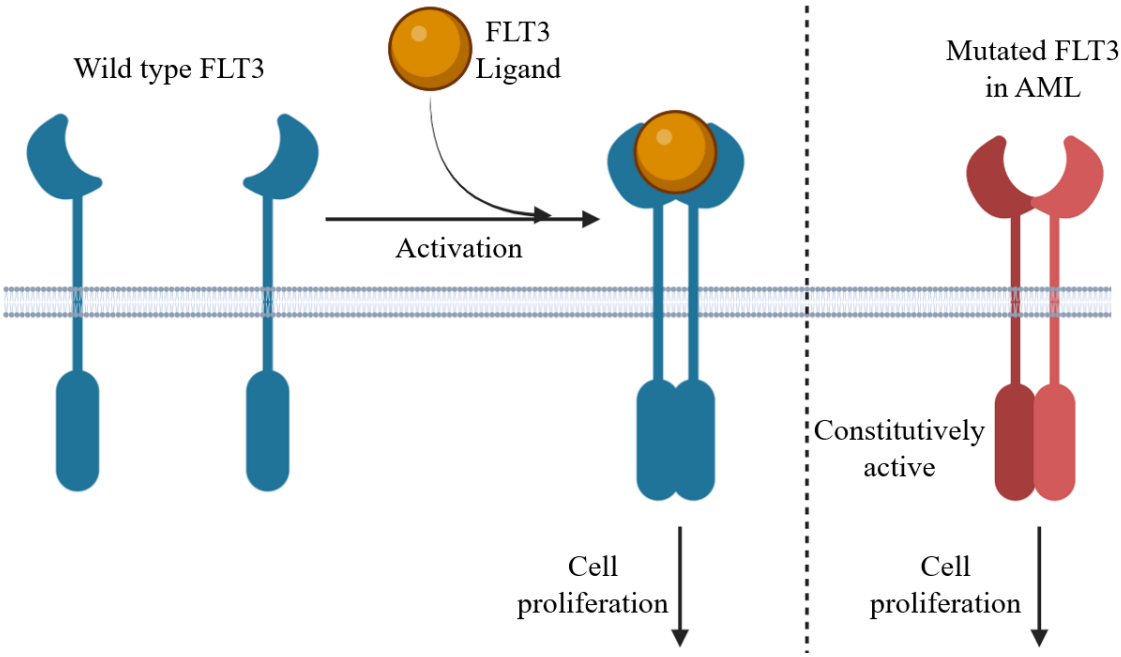

Figure 2.2.1.1: *Representation of Wild Type FLT3 dimerizing after binding to FLT3 ligand and initiating cell proliferation (left) and mutated FLT3 dimerizing in the absence of FLT3 ligand and still initiating cell proliferation in tumor cells (right)*

Created in Biorender.com

2.2.2 Development of FLT3 Inhibitors

Due to the abundance of patients suffering from AML caused by mutated FLT3 with poor prognosis, development of a FLT3 inhibitor has garnered a lot of attention.[57] Early stages of FLT3 inhibitor design focused on classes of TKIs that did not consider selectively targeting FLT3 and instead focused on creating a high affinity therapeutic for mutated FLT3.[52,57] Soon it was discovered that these therapeutics could be classified into two types of inhibition and these types target different conformations of FLT3.[52,57] Depending on the orientation of three key residues (Asp-Phe-Gly) within the activation loop, FLT3 will be in an active or inactive conformation.[52,57] Type 1 inhibitors are designed to bind to the ATP-binding region at a high affinity meaning they can bind to either conformation of FLT3.[52,57] This allows type 1 inhibitors to be designed to target both FLT3-ITD and FLT-TKD mutations.[52,57] Contrasting this, type 2 inhibitors can only bind to the back pocket of the ATP-binding region only when FLT3 is in the inactive conformation.[52,57] This allows type 2 inhibitors to be designed to better target FLT3 selectively over other kinases, however this means that type 2 inhibitors cannot inhibit FLT3-TKD.[52,57]

2.2.2.1 Midostaurin

The earliest FLT3 inhibitor to gain FDA approval is the first generation type I inhibitor midostaurin (**Figure 2.2.2.1.1**).[58,59] Originally midostaurin was designed to improve the efficacy of staurosporine, a pan-kinase inhibitor, but it was later found that midostaurin was an effective inhibitor of multiple TKDs including PKC-α, FLT3, c-KIT, VEGFR, and PDGFR.[59] Midostaurin would go on to gain FDA approval in 2017 as a combination treatment for patients with AML.[58] However, multiple complications were discovered when patients were administered midostaurin with the most severe adverse effect being

cytopenias (destruction of blood cells by the immune system).[60] Because of these complications, further development was done to create a second generation of FLT3 inhibitors.

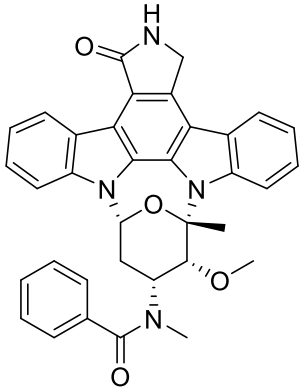

***Figure 2.2.2.1.1*:** Structure of Midostaurin

2.2.2.2 Quizartinib

In 2009, Ambit scientists reported that they created an effective type II FLT3 inhibitor targeting FLT3-ITD mutated AML cell lines.[61] Quizartinib (**Figure 2.2.2.2.1**) was notable in that it was more selective for FLT3 over other kinases while still being potent *in vivo*.[61] Quizartinib would gain FDA approval in 2023 for use in RR AML, however since gaining approval numerous resistance mechanisms including the upregulation of FLT3-TKD, which nullifies Quizartinib affinity, have been demonstrated clinically.[62,63]

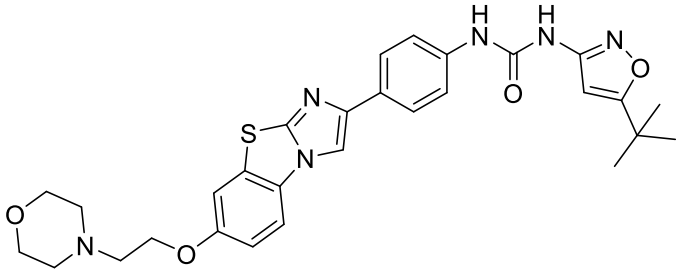

Quizartinib

***Figure 2.1.2.2.1*:** Structure of Quizartinib

2.2.2.3 Gilteritinib

After the marginal success of previous FLT3 inhibitors, efforts grew to synthesize a new type II FLT3 inhibitor that would be selective for FLT3, while also combating AML caused by FLT3-ITD and FLT3-TKD mutations. Gilteritinib (**Figure 2.2.2.3.1**) is a type 1 FLT3 inhibitor which means it has an effect on both FLT3-ITD and FLT3-TKD.[64] Additionally, FLT3 demonstrates better selectivity for FLT3 over other kinases while also having a higher affinity than first-generation inhibitors.[64] Another key function of gilteritinib is the inhibition of AXL.[64] Previous clinical studies have shown AXL to be upregulated as a resistance mechanism to FLT3 inhibitors.[65] It has also been validated that AXL inhibition slows the growth of FLT3-ITD AML tumors.[65] A crystal structure of gilteritinib bound to FLT3 was published showcasing H-bond interactions between the carbamoyl group of gilteritinib and the backbone of Glu692 and Cys694 as well as slight π–π stacking interactions between the phenyl ring of gilteritinib and Tyr693.[66] Clinical trials for gilteritinib showcased an increased response rate in patients with an acceptable safety profile.[67] Gilteritinib gained FDA approval in 2018 for the treatment of RR FLT3-mutated AML and has been the standard of care therapeutic for FLT3-mutated AML.[68]

However, after ~7 months of gilteritinib treatment patients developed resistance to the therapeutic through a F691L point mutation on FLT3-ITD.[69] This point mutation, dubbed the "gatekeeper mutation", imparts a 20-fold decrease in K_d against FLT3-ITD F691L and an 11-fold decrease in IC_{50} against cells expressing FLT3-ITD F691L.[69]

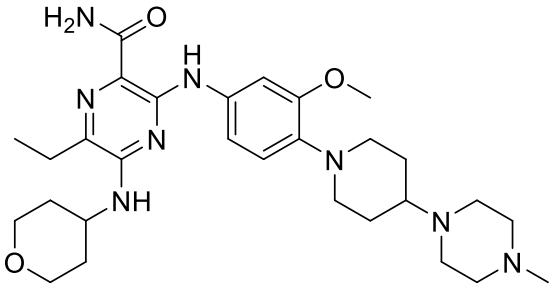

Gilteritinib

Figure 2.2.2.3.1: *Structure of Gilteritinib*

2.2.2.4 FF-10101

After the gatekeeper mutation was well established, research shifted towards creating an effective inhibitor that could combat FLT3-ITD F691L. The most promising compound currently is the covalent type 1 inhibitor FF-10101 (**Figure 2.2.2.4.1**).[70] Present on the compound is a phenyl group connected to a pyrimidine ring which binds within the active site of FLT3.[70] Unique to FF-10101 compared to the previously discussed inhibitors is a reactive acrylamide motif.[70] This motif allows FF-10101 to form an irreversible covalent bond with FLT3 protein utilizing a solvent exposed cysteine residue (Cys695).[70] FF-10101 works first by non-covalently binding into the active site of FLT3, after which the acrylamide motif interacts with Cys695 to create an irreversible covalent bond locking the drug into a bound state.[70] This mechanism of action wherein the non-covalent portion of the drug directs the covalent portion to react is favorable when creating covalent drugs

due to the lower toxicity when using milder reacting groups.[70] Both portions contribute to the high affinity between FF-10101 and different isoforms of FLT3 that normally cause type 1 and type 2 inhibitor resistance.[70] Recently a phase 1 clinical trial of FF-10101 was concluded that demonstrated the therapeutic to be a well-tolerated oral treatment for AML patients who were previously given gilteritinib.[71] Issues still exist however, within the same phase 1 study the drug only managed an overall response rate of 10%.[71]

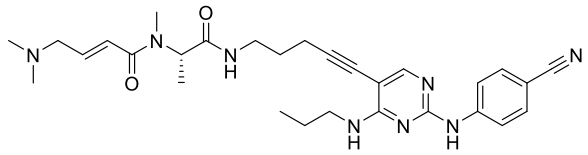

***Figure 2.2.2.4.1*:** Structure of FF-10101

2.3 Cyclin-dependent kinase 9 (CDK9)

Transcription is regulated by different signaling events within cells to produce RNA.[72] An important class of proteins that governs this process are the tCDKs and they are activated at different stages of the cell cycle to facilitate cell proliferation, transcription, differentiation, metabolism, and apoptosis.[72,73] tCDKs are further divided into two classes that perform different functions within the cell. CDK 1, 2, 4, and 6 are the regulators of the cell cycle while CDK 7, 8, 9, 12, and 13 regulate transcription.[72,73] CDK 7, 8, 9, 12, and 13 regulate transcription via the phosphorylation of residues at the C-terminus of RNAPII which activates the protein to drive the fundamental steps of transcription.[72,73] In addition to phosphorylating RNAPII, CDK9 is one of the stabilizing factors of the P-TEFb complex, which includes cyclin T1 and BRD4, which engages RNAPII and initiates transcription elongation.[72,73] CDK9 is a transcription kinase that has garnered a

lot of attention due to it being widely and abnormally expressed in various tumors, including hematological malignancies, wherein CDK9 plays a role in upregulating various oncoproteins.[74] Two proteins of note that CDK9 upregulates is the MCL-1 anti-apoptotic protein and the MYC protein (**Figure 2.3.1**).[72,73,74] As discussed earlier, MCL-1 is commonly upregulated as a resistance mechanism for therapeutics targeting the BCL-2 anti-apoptotic protein.[30,31] MYC is one of the most amplified oncogenes in human cancers, and the disordered nature of the protein makes inhibitor design for the protein a substantial challenge.[75] Previous studies looking at mRNA levels of various AML cell types have characterized an increase in CDK9 mRNA expression.[72,73] In addition to overexpression of CDK9, CDK9 pathway activity is also dysregulated in hematologic malignancies further promoting the transcription of MCL-1 and MYC.[72,73] Due to this relationship, CDK9 has become a popular target for inhibitor design to combat hematologic malignancies.

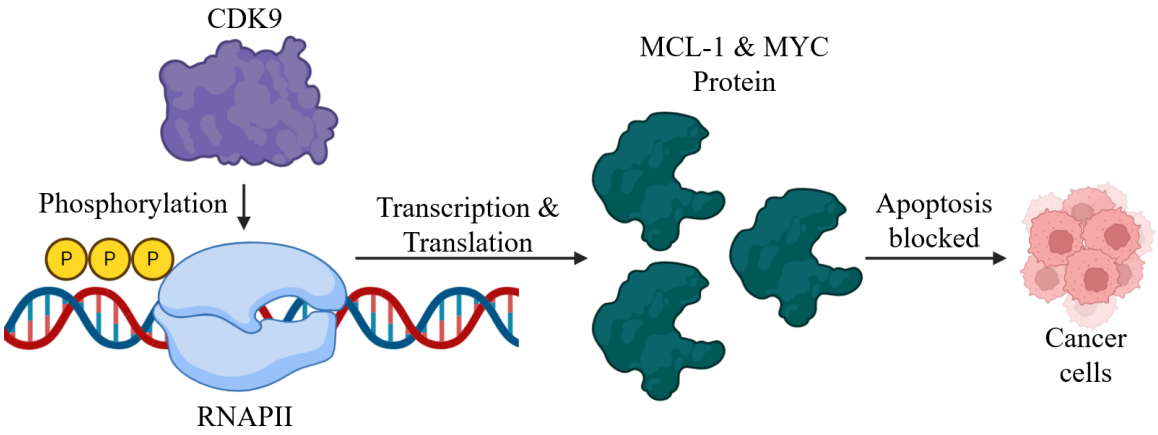

Figure 2.3.1: *Representation of CDK9 activating RNAPII via phosphorylation which initiates the downstream transcription and translation of MCL-1 & MYC proteins ultimately causing cancer cells to proliferate.*

Created in Biorender.com

2.3.1 TP-1287

A major success in the field of CDK9 inhibitors is the compound TP-1287 (**Figure 2.3.1.1**) which demonstrates potency against CDK 1, 2, & 9 (IC50 = 5-15 nM) as well as CDK4 & 6 (IC50 = 40-300 nM).[76] In early 2023, the FDA granted TP-1287 a rare pediatric disease designation to treat patients suffering from Ewing sarcoma.[77] Despite this, the compound's safety characteristics have not been fully assessed, meaning server adverse side effects could be associated with the compound. These concerns stem from the fact that TP-1287 is a pan-CDK inhibitor and compounds previously tested that that target multiple CDKs are associated with adverse effects.[78]

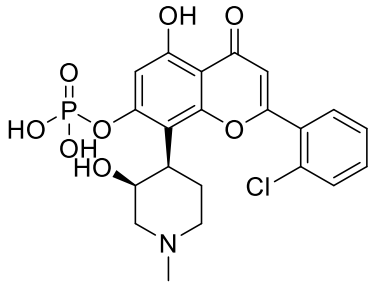

TP-1287

***Figure 2.3.1.1*:** Structure of TP-1287

2.3.2 GFH009

The next substantial development in CDK9 inhibition came in 2022 with the creation of GFH009 (**Figure 2.3.2.1**) which is a potent cyclin T1/CDK9 (IC_{50} = 9 nM) inhibitor while containing negligible interactions with the other CDKs.[79] The FDA then approved GFH009 with an orphan drug designation to treat patients experiencing RR AML.[80]

Phase 2a clinical trials were then completed in June 2024 with the inhibitor increasing median overall survival by ~5 months.[81] While these results are promising, CDK9 dysregulation causes multiple hematological and solid malignancies creating the possibility that GFH009 is not effective in combatting multiple cancer types.

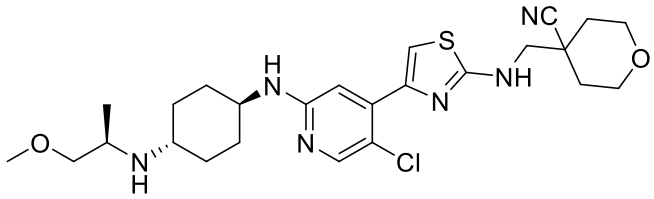

GFH009

***Figure 2.3.2.1*:** Structure of GFH009

2.3.3 SNS-032

Another possible breakthrough in CDK9 inhibition came with the creation of SNS-032. Originally designed to selectively inhibit CDK2, SNS-032 (**Figure 2.3.3.1**) emerged after it was well tolerated in clinical trials.[82] Further studies on the compound revealed that it had a high affinity for CDK2 (IC_{50} = 38 nM), CDK7 (IC_{50} = 62 nM), and CDK9 (IC_{50} = 4 nM).[83] Once this was discovered, SNS-032 use shifted in patients who were diagnosed with CLL. However, a 2010 phase 1 clinical trial using SNS-032 for patients diagnosed with CLL and MM showcased that the inhibitor had a limited clinical efficacy.[84] Since then, SNS-032 testing against CLL and MM has decreased substantially with groups testing the inhibitor against different cancers.

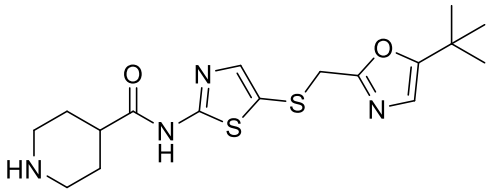

SNS-032

***Figure 2.3.3.1*:** Structure of SNS-032

2.3.4 AT7519

Another promising CDK9 inhibitor is AT7519 (**Figure 2.3.4.1**) which was developed using a fragment-based x-ray crystallography method.[85] AT7519 has exceptional potency for CDK9 (IC50 < 10nM), while also being potent against CDK2 and CDK5 (IC50 = 47nM and 13nM, respectively).[85] AT7519 has been tested in multiple human cancer cell lines and xenograft animal models and has demonstrated anti-leukemic effect in all of these.[86,87] AT7519 has since moved to clinical trials targeting solid and hematological tumors as a single agent while also being used in combination treatment.[88,89] These trials showcased AT7519s ability to downregulate MCL-1 and MYC expression through the deactivation of RNAPII.

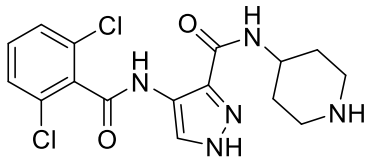

AT7519

Figure 2.3.4.1: *Structure of AT7519*

Chapter 3: Molecular Strategies to Combat Acquired Resistance

3.1 Multitargeted non-covalent inhibitors

Traditional drug design follows the approach of creating one therapeutic to target one specific protein. If multiple proteins need to be targeted, another therapeutic is combined with the original treatment to make a "drug cocktail" (**Figure 3.1.1**). While this has been the standard approach of drug development, the reality is that therapies that target multiple targets, but to not cause severe adverse effects, are attributed with high clinical efficacy.[90,91] Because of this, there has been a shift in drug development to intentionally create multitarget therapeutics.

Figure 3.1.1: *Representation of drug cocktail therapy wherein one shape corresponds to a therapeutic for one target.*

3.1.1 Heterobifunctional drug design

Heterobifunctional compounds are comprised of ligands for two or more biological targets such that one compound can inhibit multiple POI.[92] Because of this added complexity, heterobifunctional compounds can work via multiple mechanisms (which we explore further within this chapter) to inhibit their POI.[92,93] Indeed, this expansion of drug design gives scientists the ability to target troublesome targets including the previously discussed oncoproteins. Additionally, the approach of heterobifunctional drug design

offers the possibility to create compounds that have increased therapeutic efficacy with a lower required dosage that can also overcome various mutations.[92,93] This added complexity of heterobifunctional compounds does raise the workload needed to create these compounds, however, similarities between heterobifunctional compounds do exist that can help guide the development of such therapeutics.

3.1.2 Design of heterobifunctional compounds

At their core, heterobifunctional compounds are comprised of chemical motifs from multiple therapeutics. Typically, the design of heterobifunctional compounds starts from previously developed and well characterized inhibitors to alleviate the workload.[94] However, multiple aspects need to be considered before changing the structure of previously characterized compounds. First, a compounds binding to its original POI needs to be considered carefully before accommodating a second ligand. Compounds that bind deep within protein pockets for example are not ideal candidates for heterobifunctional drug design as additional ligands being grafted on could cause steric clash between the new compound and the POI. Knowing this, the best candidate drug to convert into a heterobifunctional compound is one that binds in a relatively shallow pocket with a solvent exposed group present.[95] These solvent exposed groups, also termed an “exit vector”, are commonly included to increase the compounds solubility while not interfering with the binding mode of the compound.[95] Exit vectors can range from easily modifiable secondary amines to ring systems like morpholine that need to be removed and replaced to accommodate the additional ligand.[95]

Another key characteristic to consider when designing a heterobifunctional compound is the end compound’s “drug-likeness”. It is agreed upon that final candidate

compounds that have too high of molecular weights, poor solubility, large areas of lipophilicity, and low cell permeability will not be successful therapeutics.[92-95] Lipinski's Rules of 5 is a helpful guide to avoid creating a useless drug candidate which states that to create a orally bioavailable drug it should have a molecular weight less than 500 g/mol, have no more than five hydrogen bon donors and 10 hydrogen bond acceptors, and the clogP should be no greater than 5.[96] While there exist contradictions to these rules, they serve as a guide for drug development that can aid in creating effective heterobifunctional compounds. For examples of how these rules guide design, the use of shorter linking groups can control the molecular weight, solubility can be improved by incorporating tertiary amines, and cell permeability can be increased by removing amide bonds and including fluorine.[97,98]

Using these two strategies, medicinal chemists have been able to synthesize heterobifunctional compounds that have reached clinical trials as orally bioavailable treatments. We will incorporate these strategies in our heterobifunctional approach when possible to increase the chance of our final compounds being successful therapeutics.

3.1.3 Polypharmacological drug development

One avenue for developing a heterobifunctional therapeutic that inhibits multiple targets is by combining bioactive portions of multiple therapeutics into one compound.[95] This approach dubbed "polypharmacology" aims to take two or more compounds that are commonly administered together and by combining the bioactive pharmacophores, one compound can be administered that inhibits multiple proteins of interest (**Figure 3.1.1**

.1).[94,95] This approach of drug development is rapidly growing in fields such as oncology wherein multiple targets or pathways need to be interrupted to obtain a therapeutic effect. Importantly, these polypharmacological agents do not need to simultaneously bind to all targets to obtain this therapeutic effect but by dissociating from one target, the compound is able to bind to its other designed targets.[95]

Groups that aim to create polypharmacological therapeutics typically identify previously characterized inhibitors that are already used in combination treatments that showcase synergistic or increased therapeutic efficacy when administered together. However, target selectivity is still important when designing polypharmacological inhibitors to avoid unwanted side effects. Additionally, when selecting biological targets it is important to account for the location of each target. For example, creating a polypharmacological inhibitor for an intracellular protein and an extracellular protein is not the best avenue as the compound would need to cross the cellular membrane rapidly to produce a therapeutic effect.[94,95] Finally, when creating polypharmacological inhibitors it is best to use two or more therapeutics that have similar potencies to their intended targets as this allows for easier dosing with the lowest risk of toxicities.[94,95]

Advantages of this approach include simplified ADME properties, increased efficacy through synergistic effects, the ability to fine tune affinity for different targets, and an increase in patient compliance.[92,93] Since one therapeutic is being administered, the ADME properties are easier to determine compared to multiple compounds in a drug cocktail.[92,93] Additionally, with one compound we can be confident that an increase in efficacy due to synergistic effects will occur because of the presence of all bioactive portions of our polypharmacological drug always being present.[92-95] This design approach

also allows us to fine tune affinity for one or more targets since we can better control the bioactive portions that target one protein over another.[94,95] Finally, due to only one therapy having to be administered, patient compliance should increase due to the reduction in the overall number of drugs.[95]

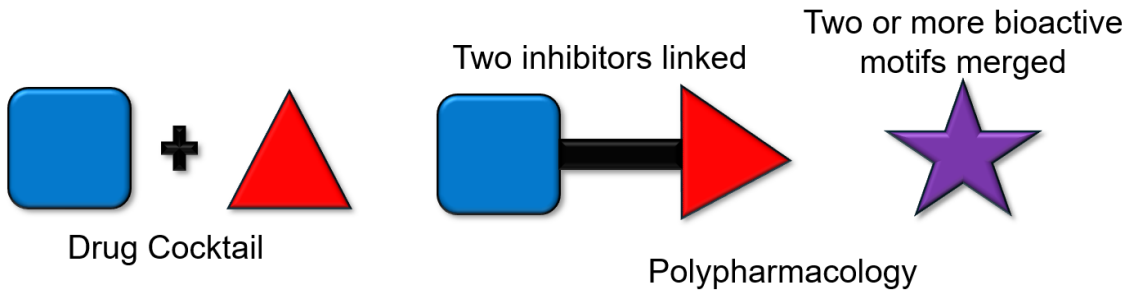

Figure 3.1.1.1: *Schematic depiction of two polypharmacological approaches to drug design. Linked polypharmacology involves two bioactive molecules that are linked together (middle) while merged polypharmacology involves the merging of two bioactive pharmacophores into a novel inhibitor (right).*

3.1.1.1 Design rational: linked polypharmacological agents

A straightforward approach for creating a polypharmacological drug is by linking two bioactive molecules together to create a new therapy.[95] While straightforward, multiple things need to be considered when creating a linker inhibitor. The first thing to consider is the size of the final molecule being synthesized. Compounds that exceed 1 kDa in size could face issues with penetrating the cell wall.[95,96] Additionally, the grafting point of the new linker needs to be established that allows for two or more compounds to be linked without interfering with the original compound's affinities.[94,95] Compounds that contain a solubilizing group or an "exit vector" that is pointing away from the target and into the solvent are ideal grafting points for various linkers.[95] While exit vectors make ideal

grafting points, removing solubilizing groups could cause extensive lipophilicity and cause issues with the compound not being able to enter biological systems.[96]

Another factor to consider is the design of the linking group itself. Initially groups utilized alkyl chain or PEG linkers for their ease of synthesis, lack of toxicity, high commercial availability, and low toxicity.[94] These flexible linkers offer the highest variability when it comes to testing optimal linker lengths for polypharmacological inhibitors.[94] Additionally, "spacers" are groups that can be added to prevent unfavorable interactions between one pharmacophore and another POI when the polypharmacological inhibitor is bound.[94,95] However, it has been demonstrated that these flexible linkers raise concerns about metabolic stability and solubility within biological environments.[92,93] Recently it has been demonstrated that polypharmacological compounds contain more ridged linkers such as piperidines and piperazines have had more success with producing a therapeutic effect.[95] This increase in therapeutic effect has been attributed to these linkers being more energetically favorable due to a lower entropic loss when bound as well as having favorable interactions with protein surfaces.[94,95]

3.1.1.2 Design rational: merged polypharmacological agents

Another method employed is by incorporating bioactive pharmacophores for different targets into a dual-active single pharmacophore.[91] This is a more involved approach since it involves a strategic incorporation of two distinct bioactive portions, however, there exist advantages for this method. Compared to linked agents, merged agents tend to have a smaller molecular weight and can avoid high lipophilicity.[91,96] The lack of a linker group also increases the metabolic stability of these merged polypharmacological compound's.[91] Merged polypharmacological inhibitors are commonly created when two

or more therapeutics share a similar scaffold such as a heterocycle or bicycle that can be differentiated easily to target multiple POI.[91]

3.2 Covalent Based Inhibitors: A Renaissance for Drug Discovery

Covalent drugs operate by forming an irreversible covalent bond with a POI which confers additional affinity towards the POI beyond non-covalent interactions (**Figure 3.2.1**).[99] This covalent bond, once formed, means the inhibitor cannot be displaced and the POI must recycle to regain its unbound form.[99] Historically, development of covalent inhibitors were held back due to concerns of the reactive molecules interfering with biological assays and a potential lack of selectivity.[99,100] Early examples of successful covalent drugs date back to the early 1900s with the discovery of aspirin and penicillin (**Figure 3.2.2**) in which they were discovered serendipitously.[99] It took until 1971 for scientists to discover that aspirin created its therapeutic effect by acetylating Ser529 in the substrate-binding channel of cyclooxygenase 1, which prevents the protein from converting arachidonic acid into prostaglandins.[99] Likewise with penicillin, scientists later discovered that the compound binds to PBPs, which maintain the bacterial cell wall structure, and acylates the active-site serine residues which inhibits PBP activity and leads to cell membrane destruction.[99] Even after these molecules were fully characterized, the stigma of covalent drugs being too promiscuous and causing off-target effects persisted. This thinking started to shift when the covalent 26S proteasome inhibitor Bortezomib (**Figure 3.2.2**) was approved in 2003 for the treatment of MM.[101] Bortezomib contains a boronic acid that covalently binds to a catalytic threonine residue in the 26S proteasome which prevents tumorigenesis.[101] Recently, the field of rationally designed covalent inhibitors is experiencing a resurgence in popularity.

Figure 3.2.1: *Representation of covalent inhibitors and their mechanism of binding. First, non-covalent interactions drive the inhibitor to bind to the enzyme. Once bound, an electrophilic warhead reacts with a readily reactive residue on the protein and forms an irreversible covalent bond between the inhibitor and enzyme.*

Created in Biorender.com

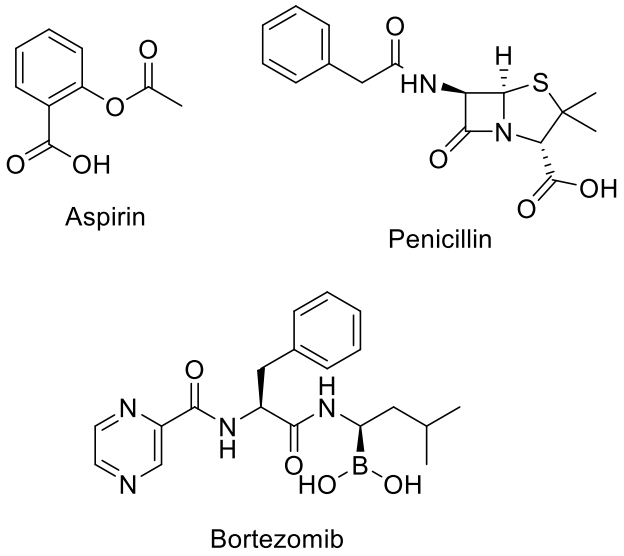

Figure 3.2.2: *Structures of aspirin, penicillin, and bortezomib*

3.2.1 Mildly reactive electrophilic warheads

Part of this resurgence in covalent inhibitor design is due to the study of different covalent motifs and the identification of mildly reactive electrophilic warheads.[102] One such warhead is the acrylamide motif which can react with cysteine residues via the Michael addition (**Figure 3.2.1.1**).[103] The thiol of the cysteine residue attacks the double bond of the acrylamide which forms the enol intermediate and is eventually pushed to the

final carbonyl adduct.[103] One of most prominent inhibitors to be fashioned with the acrylamide motif is the BTK covalent inhibitor ibrutinib (**Figure 3.2.1.2**).[104] Approved in 2013, ibrutinib inhibits BTK by covalently reacting with Cys481 located in the hinge region.[105] Since the approval of ibrutinib, the field of covalent inhibitors has exploded with three additional FDA-approved covalent drugs containing the acrylamide motif as an electrophilic warhead.[99]

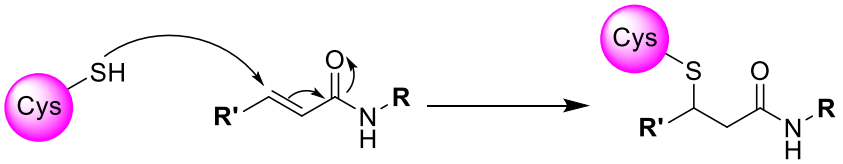

Figure 3.2.1.1: *Mechanism of cysteine residue reacting with an acrylamide electrophilic warhead through Michael addition.*

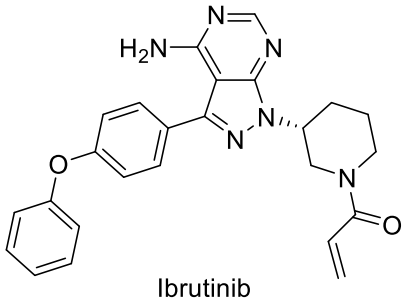

Figure 3.2.1.2: *Structure of Ibrutinib*

3.2.2 Advantages of covalent inhibitors

Covalent inhibitors offer a plethora of advantages over conventional drug inhibition via non-covalent interactions.[99] The main mechanism of action of covalent inhibitors is forming an irreversible covalent bond to increase potency for a target, meaning without the presence of a reactive residue on the protein a covalent inhibitor can be designed to be

selective for one protein that contains a reactive residue.[99] POI that are a part of a family of proteins that contain similar structure and function are one such example where covalent inhibitors can be used to obtain selectivity because one protein could carry an unconcerned reactive residue.[106] BFL-1 is one such protein that was discussed earlier in which it contains a unique solvent-exposed surface cysteine residue proximal to the conserved BH3 binding groove.[44]

Covalent inhibitors are also an effective strategy for overcoming point mutations that occur as a resistance to different therapeutics. Like we discussed before, oncoproteins are notorious for forming point mutations as a response to certain treatments. Gilteritinib discussed earlier is only effective for ~7 months before patients develop the F691L point mutation.[69] Scientists were then able to develop FF-10101 as a response which reacts with Cys695 while still occupying the active site of FLT3 to inhibit the F691L mutated version.[70]

An important issue facing medicinal chemists when it comes to designing inhibitors is the fact that target proteins don't always contain well defined or deep pockets that can be targeted with a traditional therapeutic.[106] The BCL-2 anti-apoptotic proteins contain a PPI site that is devoid of deep pockets and reactive residues making these proteins a challenge to design inhibitors for.[106] Additionally, certain proteins like the proteosome were thought to be undruggable before the invention of bortezomib due to

the size of the POI.[101] In total, covalent inhibitors give medicinal chemists a wide range of targets because of the ability to target previously "undruggable" targets.

Finally, covalent inhibitors grant medicinal chemist flexibility when designing covalent inhibitors due to the increase in affinity from the formation of a covalent bond. This increase in affinity means that more drugs can be created with heightened "drug-likeness" because affinity is no longer dependent on big lipophilic motifs to interact with troublesome POI.[96,106] Properties like molecular weight can be lowered without sacrificing affinity to the POI, solubility can also be increased due to this reduction in size, and metabolic stability can be increased without the need of linking groups.

3.3 Heterobifunctional Targeted Protein Degradation

An emerging strategy for protein inhibition is the invention of compound's that degrade a POI rather than simply inhibiting via non-covalent interactions.[107] Protein degradation is heterobifunctional in design wherein a POI ligand is grafted to another ligand that triggers the degradation of the protein.[107] This approach has been implemented in targeting proteins that are difficult to inhibit via small molecule therapeutics.[108] Proteins that have large and smooth binding sites, such as the BCL-2 anti-apoptotic proteins discussed earlier, are one case in which protein degraders could be effective. This is because protein degraders inhibit targets via "event-driven pharmacology" which is the concept that an inhibitor only has to interact with a protein for a certain amount of time before the degradation process can occur.[109] This means that a POI ligand with a lower affinity to the target can be utilized and the degradation process can still occur.[109] Another advantage of this design is the catalytic mechanism of action with these compounds.[107-109] Once the POI is fully degraded, the protein degrader is free to bind to other copies of the

POI which initiates a cascade of degradation.[107-109] This means that less overall drug load can be administered compared to traditional non-covalent inhibitors which could lower adverse side effects and increase patient compliance.[107]

3.3.1 Hydrophobic Tagging Molecules

One design for targeted protein degraders is the synthesis of small-molecule hydrophobic tagging degraders (**Figure 3.3.1.1**).[110] These consist of a POI ligand linked to a hydrophobic fragment, which could range in size from a single substituted hexane ring up to multiple aromatic rings.[110] Once the POI ligand interacts with the POI, two mechanisms can occur that lead to protein degradation. One mechanism is the recruitment of Hsp70 or the 20S proteasome directly to the POI which initiates protein degradation.[110] The other mechanism involves the hydrophobic fragment destabilizing the POI due to the large lipophilic interactions present in the degrader.[110] Once destabilized, chaperone proteins are recruited that shuttle the damaged protein to the proteasome for degradation.[110]

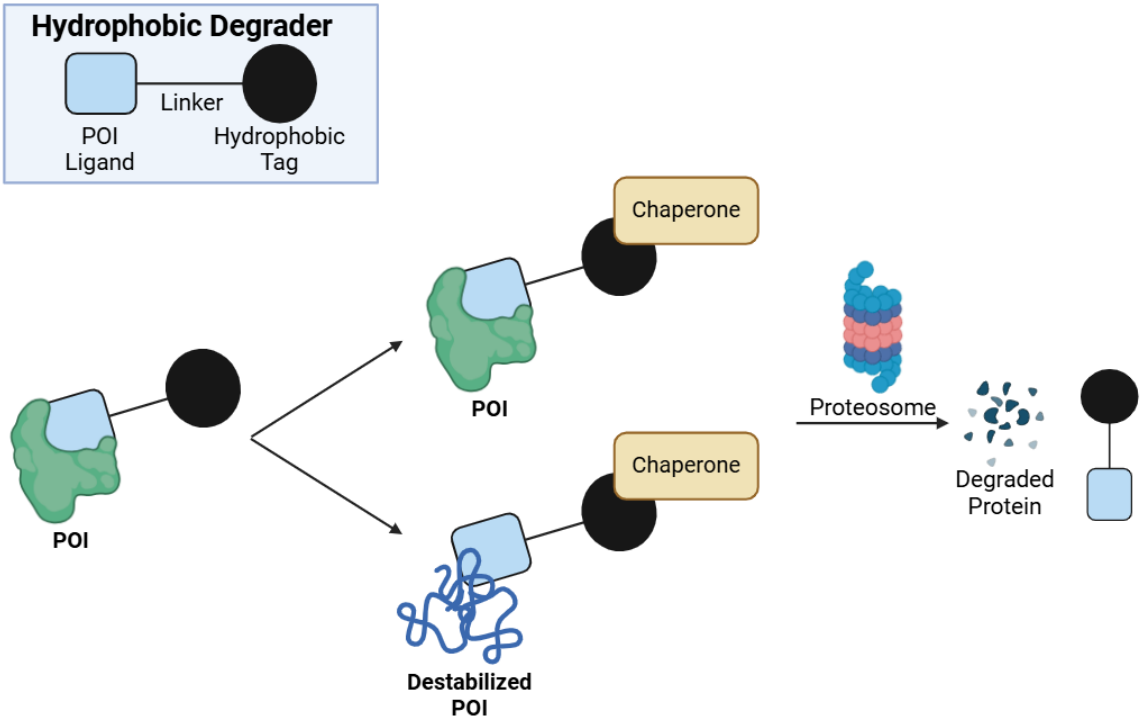

Figure 3.3.1.1: *Mechanism of hydrophobic tagging molecules. POI ligand is linked to a hydrophobic tag and two distinct events can occur that lead to protein degradation. One scenario involves the hydrophobic tag recruiting chaperone proteins that shuttle the POI to the proteasome for degradation. The hydrophobic tag can also destabilize the POI, which also recruits chaperone proteins and leads to proteasome mediated degradation. After both cases, the hydrophobic degrader is free to bind to more POI.*

Created in Biorender.com

3.3.2 Proteolysis-Targeting Chimera (PROTAC) Protein Degraders

Another design for protein degraders is the synthesis of PROTACs which are comprised of a POI ligand linked to a E3 ligase ligand (**Figure 3.3.2.1**).[111] PROTACs work by exploiting the ubiquitin-proteasome system of the cell in which simultaneous binding to a POI interest and an E3 ligase ligand will initiate polyubiquitination and protein degradation.[111] This initiation occurs when a ternary complex between the POI, PROTAC, and E3 ligase is formed after which solvent exposed lysine residues are

polyubiquitinated. Once the POI is tagged, chaperone proteins guide the tagged protein to the proteasome where the protein is degraded.[111]

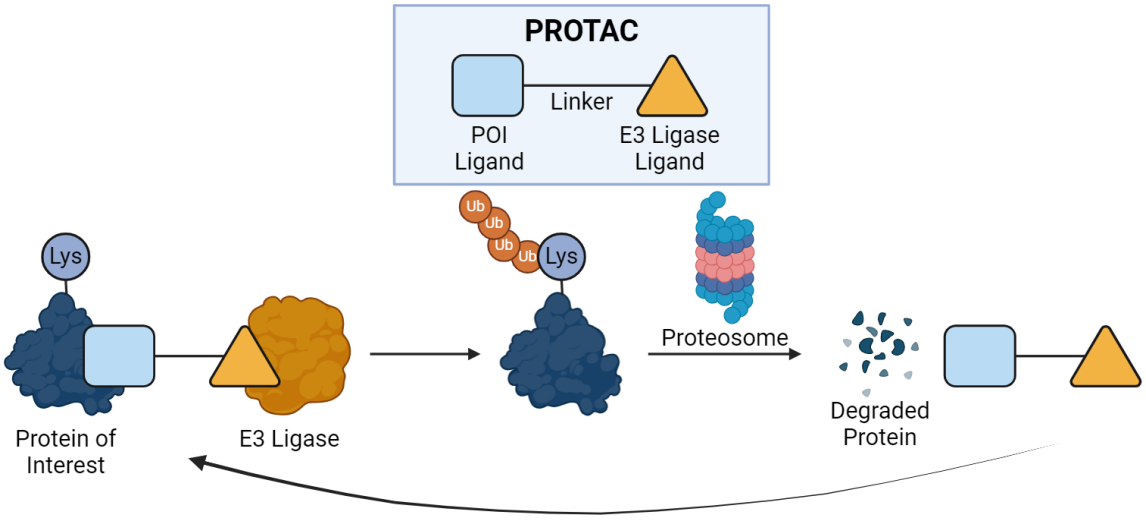

Figure 3.3.2.1: *Mechanism of PROTAC protein degraders. PROTACs bind simultaneously to a POI and E3 Ligase protein to form a ternary complex. Once this complex is formed, the POI surface lysine residues are polyubiquitinated and shuttled to the proteasome for degradation. PROTACs are catalytic during this process and are free to bind to additional POI.*

Created in Biorender.com

3.3.2.1 Craig Crews and the Invention of PROTACs

Over 20 years ago, the Crews lab demonstrated that they could utilize the ubiquitin–proteasome system to target MetAP-2.[112] They chose MetAP-2 because high expression of the proteins has been linked to tumorigenesis in human colorectal cancer tissues and colon cancer.[112] For the E3 ligase, Crews decided to utilize the $SCF^{\beta\text{-TRCP}}$ because MetAP-2 is not known to be ubiquitinated by any SCF complex.[112] Crews decided to use IκBα phosphopeptide as their POI ligand and ovalicin as the E3 ligase ligand due to both being potent recruiters and inhibitors respectively.[112] Their final PROTAC-1 (**Figure**

3.3.2.1.1) demonstrated the ability to form a ternary complex with $SCF^{\beta\text{-}TRCP}$ and MetAP-2 which ultimately resulted in MetAP-2 degradation in a PROTAC-1 dependent manner.[112]

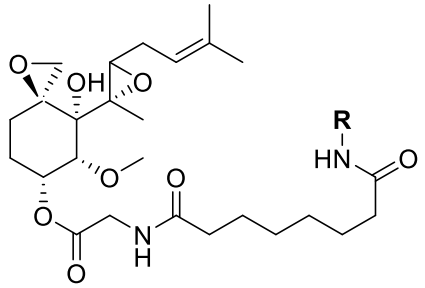

R = GGGGGGRAEDSGNESEGE-COOH
or GGGGGGDRIISGLDSM-COOH

PROTAC-1

Figure 3.3.2.1.1: *Structure of PROTAC-1*

3.3.2.2 Ternary Complex and Hook Effect

An important step for the event driven pharmacology that governs protein degraders activity is the formation of a ternary complex.[113] This complex is formed when the heterobifunctional protein degrader engages with the POI and the secondary degrader protein simultaneously to initiate protein destruction.[113] Studies focused on evaluating the ternary complex are increasing and what has been discovered is that formation is highly dependent on the two targets, their overall abundance, and their wildtype function within the cell.[114] One topic that is not fully understood with this technology is related to the cooperative effect between the two POI.[113] Different proteins can either have a cooperative effect that stabilizes the overall ternary complex, but there are cases where the two proteins repel each other when they are forced to interact.[113] While there have

been examples of increased cooperation leading to a decrease in the efficiency of event occurrence, the prevailing thought is that increasing cooperativity between the two proteins leads to an increase in therapeutic efficacy.[113]

Another important concept to consider when designing and testing PROTACs is the hook effect (**Figure 3.3.2.2.1**).[115] When an inhibitor works via an event-driven pharmacology that requires the compound to be bound to two independent proteins and form a ternary complex, the concentration of said inhibitor can impact testing.[115] Plotting the concentration of compound versus ternary complex formation produces a bell curve, with the highest concentration of compound resulting in a scenario where all targets are saturated with compound via monovalent inhibition. This effect has been observed in multiple in vitro testing experiments with PROTACs and has resulted in lower efficacy at high dosing.[116,117] Ultimately this means that clinical parameters of novel PROTACs, such as dosing, require additional studies to avoid safety concerns and progress these compounds through clinical trials.

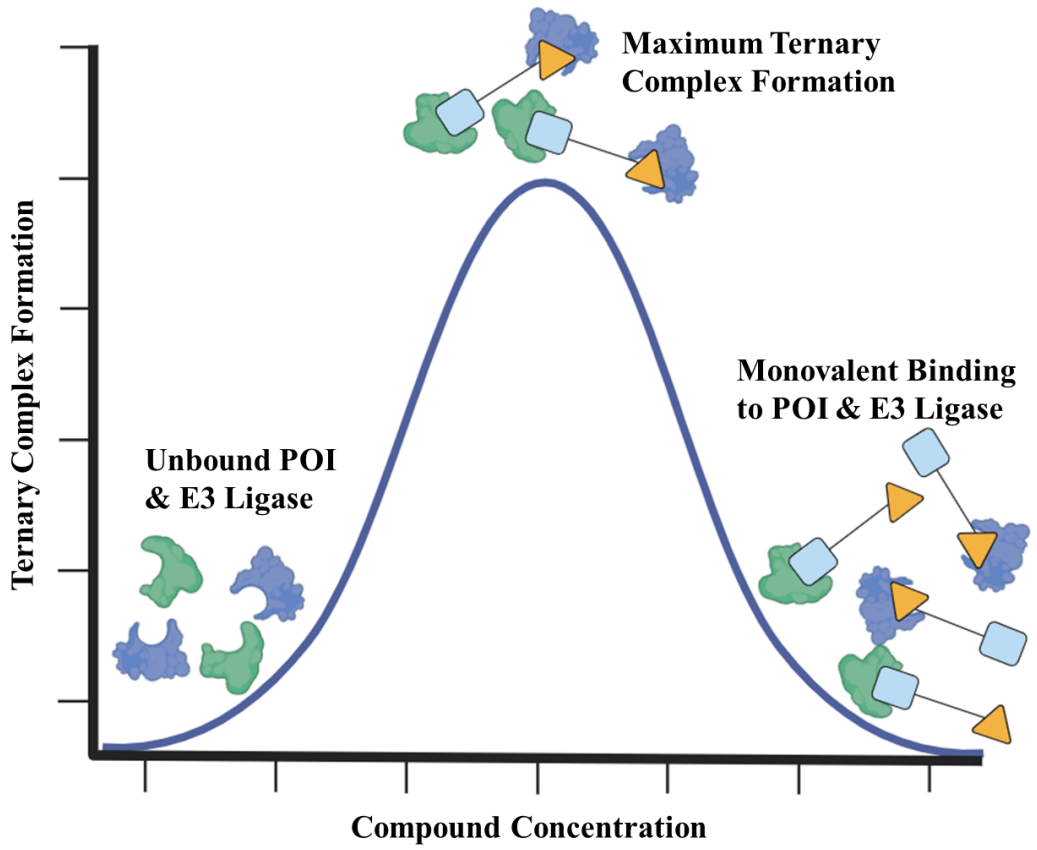

Figure 3.3.2.2.1: *Graphical depiction of the Hook Effect. A compound concentration of zero results in no POI or E3 Ligase being bound (bottom left). Fully saturated compound concentration results in monovalent binding of POI and E3 Ligases preventing ternary complex formation and no POI is degraded (bottom right). At an ideal concentration of PROTAC molecules, ternary complex formation is maximized, and POI degradation occurs more favorably (top of bell curve).*

Created in Biorender.com

3.3.2.3 Ubiquitin-proteasome system (UPS)

The UPS system withing cells is the main method of protein degradation in which multiple proteins and complex work together to clear the cell of undesirable proteins to maintain cellular homeostasis.[118] When a protein is unfolded or damaged, it is polyubiquitinated by the E1, E2, and E3 proteins which are responsible for the activation,

conjugation, and ligation of the ubiquitin chain to the desired protein.[118] This polyubiquitin chain is recognized by the 26S proteasome, which is a large protein complex of about 2.5 MDa.[118] When a protein bearing the polyubiquitin chain is brought near the proteasome, the macromolecule cleaves peptide bonds that hold the protein together and results in oligopeptides ranging from 3-15 amino acids after which these oligopeptides strands are further hydrolyzed into amino acids (**Figure 3.3.2.3.1**).[118]

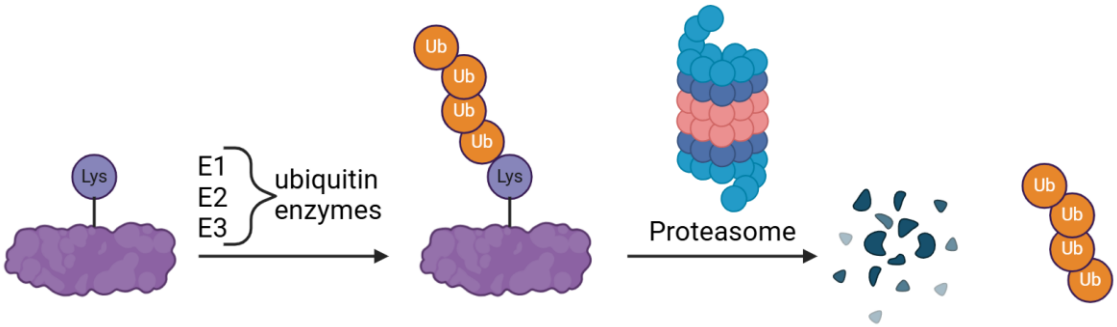

Figure 3.3.2.3.1: *Protein degradation via the UPS. A protein is ubiquitinated by the E1, E2, and E3 ubiquitin proteins. The ubiquitin chain acts as a tag for degradation by the proteasome, resulting in breakdown of the protein into amino acids and recycling of the ubiquitin chain.*

Created in Biorender.com

3.3.2.4 E3 Ligases

A critical part of the protein degradation mechanism are the E3 ligases which are responsible for polyubiquitinating proteins.[119,120] E3 proteins are the most diverse of the ubiquitinating proteins with over 500 known E3 ligases.[119,120] However, only a handful of E3 ligases are utilized when creating protein degraders which include CRBN and VHL due to the previous knowledge on their structural information, cellular abundance, and natural cooperation with other proteins.[121] Additionally, most of the well-known E3 ligase ligands developed target these E3 ligases.[121] For example, CRBN is often recruited

because it is recognized as being able to degrade a large number of proteins and the amount of ligands that target CRBN are numerous.[121] In a similar manner VHL is commonly targeted and has demonstrated the ability to degrade a wide range of proteins.[121] However, VHL is essential for survival in multiple cell lines tested, unlike CRBN.[122] Currently, there is a push to develop more E3 ligase ligands to increase the variety that medicinal chemists can utilize.

3.3.2.5 E3 Ligase Ligands

As stated before, E3 ligase ligands are responsible for binding to the E3 ligase proteins and can be linked to POI ligands thereby forming a ternary complex and ultimately polyubiquitinating the POI which leads to degradation. Of the E3 ligase ligands currently used, the two most popular ligands are thalidomide and VHL-1 ligand (**Figure 3.3.2.5.1**).[123,124] Both thalidomide and VHL-1 ligand are strong, specific binders that have been validated for their intended targets and have well-characterized binding modes.[123,124] Additionally, these compounds have favorable drug-likeness stemming from their low molecular weights, high solubility, and low reactivity. Both thalidomide and VHL-1 contain grafting sites or can be easily modified to graft on linkers for the conversion into a protein degrader.[123,124] The prominent concern with using these compounds is due to an increased resistance observed as these compounds become more commonly used.[123,124] Towards combatting this, novel E3 ligase ligand development is a growing field to diversity protein degradation design.

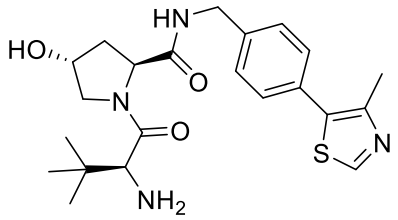

VHL-1 Ligand

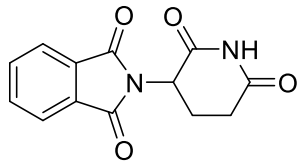

Thalidomide

***Figure 3.3.2.5.1*:** Structures of VHL-1 Ligand and Thalidomide

3.3.2.6 Linking Groups

As with polypharmacological drug design, linker design is important for the creation of a successful protein degrader. Like polypharmacological inhibitors, early designs of protein degraders relied on linkers comprised of alkyl chains or PEG linkers due to their malleable nature which offered an avenue to test optimal linker lengths.[125] However, these flexible chains raise concerns related to overall solubility and metabolic stability of the final protein degrader.[125] Recently there has been a shift towards using more rigid linkers using piperidine and piperazine motifs as these have demonstrated their ability to stabilize ternary complex formation.[125] While more work has gone into predicting optimal linker lengths, this area of protein degradation design has remained empirical in nature.

3.3.2.7 Ibrutinib Recovery via Conversion into a Protein Degrader

Another advantage of PROTAC design is the ability to be robust against point mutations that are a common resistance mechanism employed by cancers. One key example comes from the FDA-approved BTK inhibitor ibrutinib to treat resistant NHL.[126] NHL develops from BTK overactivation that promotes BCR malignancies.[127] In response to this,

ibrutinib was developed as a potent inhibitor for BTK with an IC50 of 0.5 nM and was approved in 2013.[104] However, multiple lymphomas develop resistance to the inhibitor via a C481S point mutation in BTK which increases the IC_{50} of ibrutinib to ~1 mM.[127] To combat this, the Crews lab converted ibrutinib into a PROTAC, compound P13I (**Figure 3.3.2.7.1**), by grafting off a secondary amine to attach the linker which was further modified to include thalidomide which is a well characterized E3 ligase ligand against cereblon.[127] The authors demonstrated that their PROTAC was able to degrade both WT BTK as well as C491S BTK with high efficacy.[127]

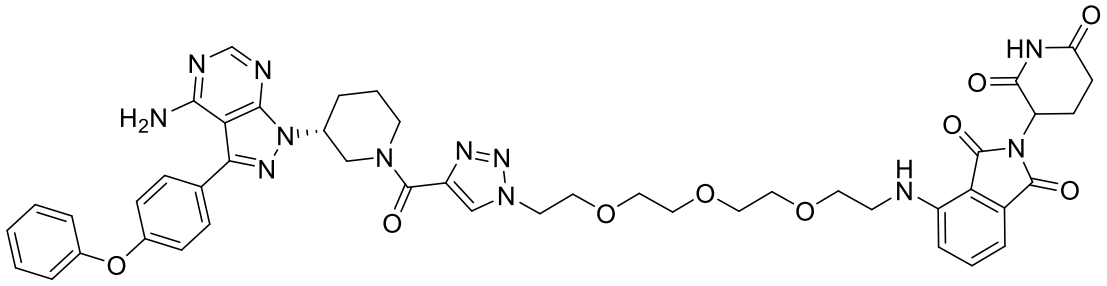

Figure 3.3.2.7.1: *Structure of P13I*

Chapter 4: Scaffold hopping from indoles to indazoles yields dual MCL-1/BCL-2 inhibitors from MCL-1 selective leads

4.1 Introduction

The BCL-2 family of proteins comprises pro-apoptotic members and anti-apoptotic counterparts that interact together to regulate apoptosis.[21] In a plethora of cancers, the anti-apoptotic proteins, which include BCL-2, BCL-xL and MCL-1, are upregulated, and directly contribute to the development and progression of the cancer.[128,131] In addition, MCL-1 overexpression has been associated with resistance to conventional chemotherapies.[31] The primary interaction between the pro- and anti-apoptotic members is described by an α-helical BH3 "death" domain on the former that is sequestered by a hydrophobic BH3-binding groove on the latter. Key contacts within this protein–protein interaction are hydrophobic side chains projected from one face of the α-helix that nestle into sub-pockets labelled p1 through p4 in the hydrophobic groove, as well as a salt bridge through a conserved aspartate on the opposing face of the helix.[21,4] The development of small-molecules that mimic the BH3 α-helix as a strategy to re-activate apoptosis has been an active area of research for over 20 years.[4,133]

Several of the earlier small-molecule BCL-2 antagonists, such as TW-37, are pan-BCL-2 inhibitors, binding BCL-2, BCL-xL and MCL-1 with similar affinities, a consequence of the highly conserved BH3-binding grooves on their surfaces.[4] However, in the last decade or so, selective inhibitors have emerged, such as the BCL-2 inhibitor venetoclax (VEN).[7] In fact, VEN has received FDA approval for acute myeloid leukemia (as well as chronic lymphocytic leukemia and small lymphocytic leukemia) in combination with a

hypomethylating agent, such as azacytidine, or low-dose cytarable,[134], [135] although resistance to these treatments soon emerges,[136] commonly due to to MCL-1 (or BCL-xL) upregulation[129], [137–140] (as well as to mutations in BCL-2 (in CLL)[141]).

Accordingly, this has fuelled research into the development of MCL-1 inhibitors,[30142] and, in the last few years, multiple academic laboratories and pharmaceutical companies have achieved subnanomolar, selective inhibitors of MCL-1,[132], [40], [34], [143] culminating in clinical trials for several chemotypes. Alarmingly, however, at least three of these trials have been suspended or terminated for safety reasons.[144] There is a double-edged sword here because MCL-1 upregulation is the most common mechanism of resistance to VEN,[129], [137–140] several cell types depend on MCL-1 function for survival, including hematopoietic stem cells,[145] cardiomyoctes[50] and hepatocytes;[146] MCL-1 knockout in mice is embryonic lethal.[147] Inspired by the synergism observed in combination studies with a BCL-2 inhibitor and an MCL-1 inhibitor,[148] we hypothesize that (less potent) inhibitors of MCL-1 that are equipped to also recognize BCL-2 but not BCL-xL (to avoid thrombocytopenia) may provide the balanced platform needed

4.2 Results and Discussion

The discovery of novel chemotypes in drug discovery is crucial to increasing the probability of a drug successfully advancing through clinical trials.[149] An expedited strategy towards this goal is "scaffold hopping" in which the scaffold of an existing inhibitor is modified to generate a new chemotype.[150] Fesik's laboratory, Abbvie and AstraZeneca have all experienced much success with the indole-2-carboxylic acid scaffold, in which the critical p2-binding moiety is grafted adjacent to the carboxylic acid that forms an essential salt bridge with Arg263.[10, p. 59], [143], [37] One of Fesik's earliest

lead compounds (1) demonstrates nanomolar inhibition of MCL-1 (Ki = 55 nM), sub-micromolar inhibition of BCL-2 (Ki = 0.87 μM) and is inactive against BCL-xL (Ki > 15 μM).[37] We, therefore, considered this was a promising starting point towards the discovery of dual MCL-1/BCL-2 inhibitors. The benzimidazole and indazole scaffolds provide excellent alternative scaffolds to the benchmark indole core and permit the preservation of the 1,2 relationship of the p2-binding group and the carboxylic acid (**Figure 4.2.1**), although it is acknowledged that the proposed indazole core itself may bind differently given the displaced benzene ring component of the bicycle.

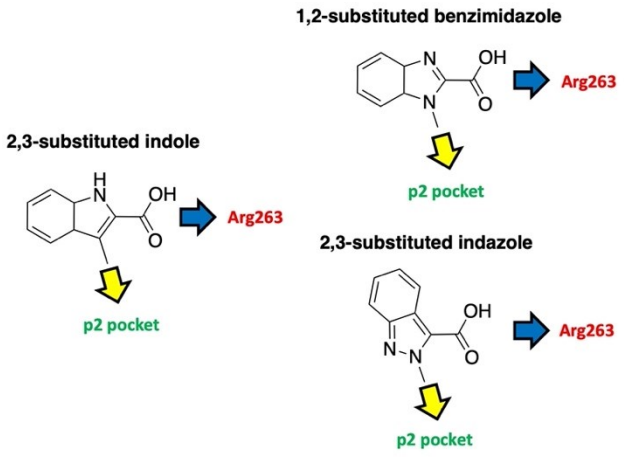

Figure 4.2.1: *Scaffold hopping from indoles to benzimidazoles and indazoles.*

We prepared the indole-based MCL-1 inhibitor 1,[37] as a positive control, and the corresponding benzimidazole 2 and 2,3-substituted indazole 3. (Full synthetic procedures for the syntheses of 2 and 3 are provided in the Supporting Information.) The non-chlorinated benzimidazole was used to avoid ambiguity in the position of the chlorine atom upon alkylation of the benzimidazole nucleus. The control indole 1 performed as expected, confirming the functionality of our fluorescence polarization competition assay (FPCA).[151–157] Unfortunately, the benzimidazole and the indazole elicited negligible

inhibition of MCL-1. At this stage, we elected to pursue only the indazole scaffold, since the benzimidazole scaffold exhibited significant polarity (TLC) which may compromise binding in the hydrophobic cleft, although this may be further investigated in the future. First, we shortened the three-carbon linker between the indazole core and the p2-binding 3,5-dimethyl-4-chlorophenyl moiety (4), but this also did not restore binding affinity. Next, we used a more rigid benzyl linker (5), which provided some recovery in inhibition of MCL-1 (Ki = 2.36 μM) relative to the parent indole 1. Since the synthesis of N2-substituted indazole 5 also yielded the corresponding N1 isomer in the same pot, we evaluated compound 6 as well, which performed comparably to 5. Lastly, shifting the chlorine from the 5- to the 6-position (7) resulted in a marginal increase in binding affinity (Ki = 1.76 μM).

Since the synthesis of 5 was much higher yielding than that of 6 and 7, we decided to move forward with compound 5. With a new chemotype confirmed for MCL-1 inhibition, we also evaluated 5 against BCL-2 and BCL-xL. Pleasingly, 5 inhibited BCL-2 in the single-digit micromolar range (Ki = 1.48 μM) yet was inactive against BCL-xL (Ki > 10 μM), reflecting the relative BCL-2/BCL-xL affinities of the original lead 1.[37] In a follow-up publication to their seminal work on the discovery of MCL-1 inhibitors, Fesik's laboratory elaborated their indole-2-carboxylic acids by converting the acid functional group into acylsulfonamides that retains the acidity of the parent group but also enables the inhibitors to occupy more of the hydrophobic BH3-binding groove by probing into the p4 pocket.[39] In this way, they were able to substantially improve MCL-1 binding affinities while simultaneously preserving selectivity for MCL-1 over BCL-xL. No binding data for BCL-2 was provided. We were curious to learn if the likewise

transformation of our indazole acids into indazole acylsulfonamides would also improve MCL-1 binding affinities and retain selectivity for MCL-1 over BCL-xL but also improve, or at the very least retain, binding affinities to BCL-2.

Compound Number	Structure	K_i, μM (MCL-1)
1	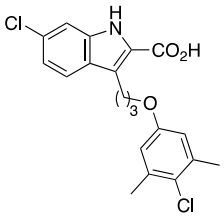	0.247 ± 0.03
2	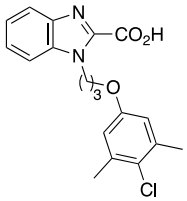	> 10
3	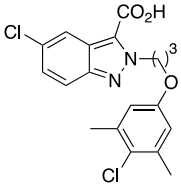	> 10
4	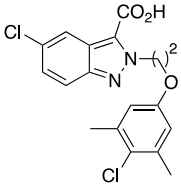	> 10
5	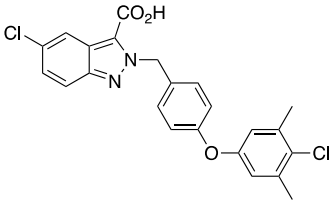	2.36 ± 0.29
6	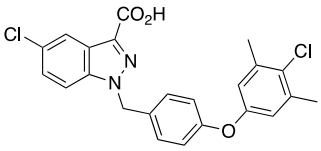	2.28 ± 0.34
7	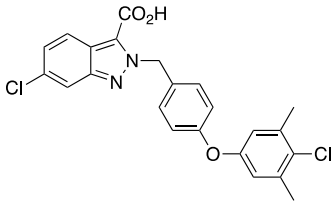	1.76 ± 0.55

Table 4.2.1: *Binding affinities of initial "scaffold-hopping" MCL-1 inhibitors.*

Accordingly, we prepared acylsulfonamide analogues of acid 5 (Scheme 1) in which the sulfonamide fragment was inspired by the corresponding fragment in VEN. Briefly, 5-chloroisatin (8) was transformed into 5-chloroindazole-3-carboxylic acid (9) as described previously,[158] and was advanced to the next step without purification: thionyl chloride-mediated esterification of crude acid 9 yielded methyl ester 10. Alkylation of the indazole functional group can produce differing amounts of the N1- and the N2-alkylated products depending on the reaction conditions.[159] We employed direct alkylation conditions of the benzylic bromide 5-(4-(bromomethyl)phenoxy)-2-chloro-1,3-dimethylbenzene with K_2CO_3 in DMF at RT, which produced an approximate 1:1 separable mixture of the N1 and N2 products. The distribution of products could be tipped in favour of N2 (in a 2:1) ratio by adjusting the conditions to a Mitsunobu reaction with the corresponding alcohol (see Experimental Section for full details), and it is known that direct alkylation with an alkyl halide versus alkylation by the Mitsunobu reaction can afford different product distributions with tautomeric heterocycles.[160-163]

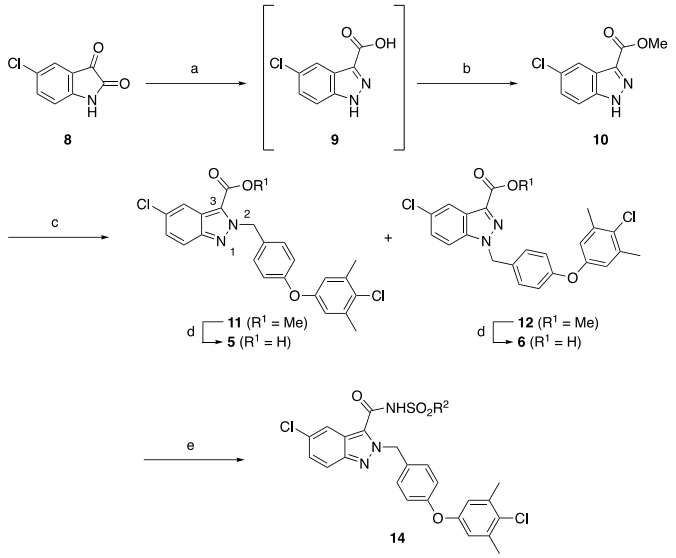

Figure 4.2.2: *(a) NaOH(aq), 45 °C, 30 min; (ii) $NaNO_2$(aq), 10 min, 0 °C H_2SO_4, 30 min; (iii) $SnCl_2$, c.HCl, 0 °C → RT, 16 h; (b) $SOCl_2$, MeOH, reflux; (c) $HOCH_2C_6H_4O$-(4-Cl-3,5-diMe)-Ph, DIAD, PPh_3, THF, RT (yields a 2:1 ratio of 11:12); (d) LiOH·H_2O, THF/MeOH/H_2O, 3:1:1, rt; (e) $R^2SO_2NH_2$ (13), EDCI, DIPEA, DMAP, CH_2Cl_2, rt.*

Previously, N1- and N2-substituted methyl indazole-3-carboxylates were distinguished based on their polarities and NMR spectra: the N2 isomers are less polar and the protons on the carbon directly attached to the indazole nitrogen are more downfield by around 0.5ppm, presumably due to the deshielding effect of the adjacent ester functional group. We also observed clear differences in polarity for the two isomers 11 and 12. In **Figure 4.2.3**, the less polar isomer (Rf = 0.59 (hexanes/ethyl acetate, 2:1, versus Rf = 0.43 for the more polar product) whose NMR spectrum is shown in panel A, also exhibited a more deshielded benzylic CH_2 group by 0.39ppm (as did the ortho-phenyl protons). Thus, we assigned the less polar product as the N2-alkylated isomer 11 and the more polar product as the N1-alkylated isomer 12. Saponifications of 11 and 12 yielded carboxylic acids 5 and 6, respectively. Subsequently, acylation of sulfonamides 13a-13r with acid 5 furnished the target N2-substituted indazole-3-acylsulfonamides 14a-14r.

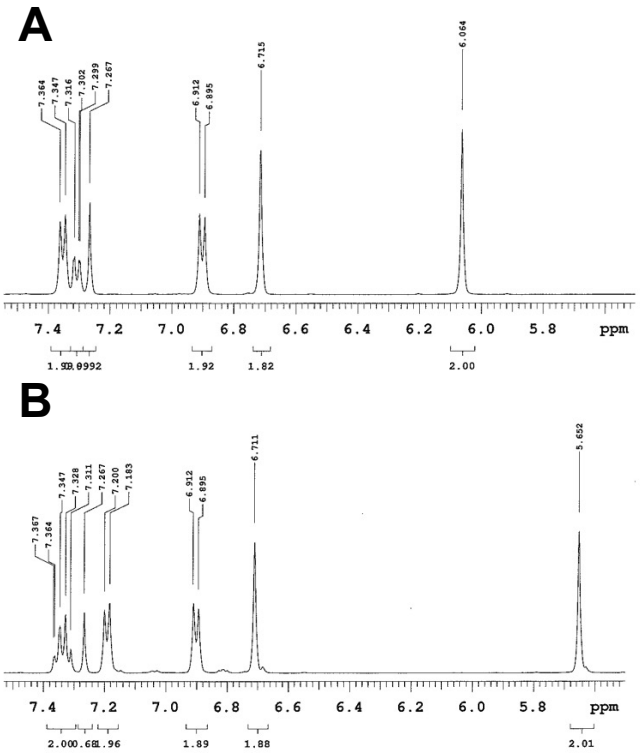

Figure 4.2.3: *1H NMR spectra of the isomers (A) 11 and (B) 12. Structures assigned based on TLC polarities (11: Rf = 0.59; 12: Rf = 0.43 (hexanes/ethyl acetate, 2:1)) and* δ_H *values of the benzylic methylenes.*

Once again, we employed the established FPCA to determine inhibitory activities of our acylsulfonamides, and the data are shown in **Table 4.2.2** (ABT-737 and S63845 are dual BCL-2/BCL-xL and selective MCL-1 inhibitors, respectively). Pleasingly, we observed an improvement in MCL-1 inhibition over parent acid 5 by up to 2-fold with acylsulfonamide 14g proving the most potent MCL-1 inhibitor (K_i = 1.12 μM vs 2.36 μM) for the corresponding carboxylic acid), although with such a small improvement in affinity, it is difficult to draw any specific conclusions about the contributions of the functionalized amino group on the nitroarene ring. More interestingly, these acylsulfonamides also proved effective inhibitors of BCL-2 with 14h the best compound

(K_i = 0.46 μM). Generally, the acylsulfonamides were more potent inhibitors of BCL-2 than MCL-1 by up to 3-fold. In every case, the binding affinities to BCL-xL were several-fold worse, and often >10 μM. The most potent dual MCL-1/BCL-2 inhibitor was 14a with Ki values of 1.20 μM and 0.51 μM for MCL-1 and BCL-2, respectively, and a Ki >10μM for BCL-xL. Switching the relative positions of the nitro and amino-substituents had little impact on binding affinities.

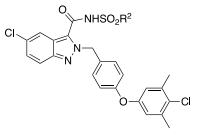

Compound Number	R^2	K_i (μM) MCL-1	BCL-2	BCL-xL
14a		1.20 ± 0.17	0.51 ± 0.10	>10
14b	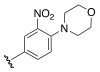	1.32 ± 0.16	0.53 ± 0.09	7.99 ± 2.43
14c	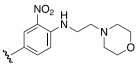	1.61 ± 0.10	0.42 ± 0.16	NA
14d	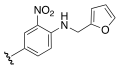	1.30 ± 0.11	0.57 ± 0.09	>10
14e	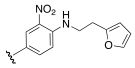	1.28 ± 0.15	0.62 ± 0.14	3.40 ± 1.19
14f	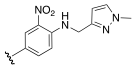	1.57 ± 0.14	0.60 ± 0.11	3.85 ± 0.73
14g	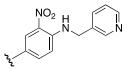	1.12 ± 0.07	1.18 ± 0.14	4.42 ± 0.53
14h	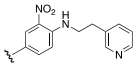	1.46 ± 0.13	0.46 ± 0.05	>10
14i	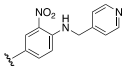	1.65 ± 0.18	1.52 ± 0.31	>10
14j	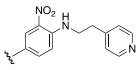	1.77 ± 0.29	0.66 ± 0.18	>10
14k	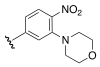	2.30 ± 0.17	0.90 ± 0.25	6.66 ± 3.14
14l	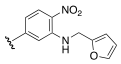	1.68 ± 0.33	0.96 ± 0.08	>10
14m	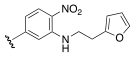	2.16 ± 0.61	0.84 ± 0.23	>10
14n	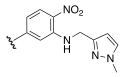	1.95 ± 0.18	0.71 ± 0.11	7.41 ± 2.56
14o	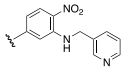	1.00 ± 0.10	1.22 ± 0.50	>10
14p	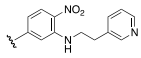	1.46 ± 0.13	0.46 ± 0.05	>10
14q	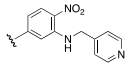	1.36 ± 0.21	0.71 ± 0.25	>10
14r	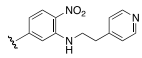	1.42 ± 0.11	0.77 ± 0.18	NA
1	-	0.247 ± 0.03	1.20 ± 0.16	>10
ABT-737	-	NA	< 0.04	< 0.04
S63845	-	0.039 ± 0.01	NA	NA

Table 4.2.2: *Binding affinities of N2-substituted-indazole-3-acylsulfonamides to MCL-1, BCL-2 and BCL-xL. NA = no activity.*

Molecular modelling of compound 14c using SILCS methodology[157] (see Supporting Information) was conducted by Dr. Wenbo Yu and provided predicted binding modes with MCL-1 and BCL-2, and reported LGFEs of -8.5 and -9.3 kcal/mol, respectively, which is in agreement with the relative experimental binding affinities. As shown in **Figure 4.2.4A**, 14c binds somewhat similarly to acylsulfonamide 49 from reference [39], with the 3,5-dichloro-4-methylphenyl substituents probing deep into the p2 pockets, the acylsulfonamide substituents being projected into the p4 pockets, and the acidic acylsulfonamide itself binding Arg263. However, in stark contrast, the indazole core of 14c is forced out of the binding pocket adopted by the indole core of 49, and this may account for the reduced binding affinity of 14c to MCL-1 (Kd: 1.61 μM vs 361 nM). **Figure 4.2.4B** illustrates the binding mode of 14c in BCL-2 overlaid with that of VEN. While the larger molecule VEN clearly makes greater interactions and extends deeper into the p4 pocket, 14c appears to engage the p2 and p4 pockets, like VEN, as well as form a salt bridge between its acylsulfonamide and Arg146. In both proteins, 14c is predicted to make contacts with both the p2 and p4 pockets, but with MCL-1, the indazole core is forced away from the protein surface, while with BCL-2, the indazole core binds towards the p1 pocket. Given the predicted binding modes are significantly different, concomitant optimization of binding to both MCL-1 and BCL-2 may prove challenging, therefore It is crucial that co-crystal structures are solved to determine the specific binding modes of our lead compounds, and this information will aid in the design of next generation dual MCL-1/BCL-2 inhibitors.

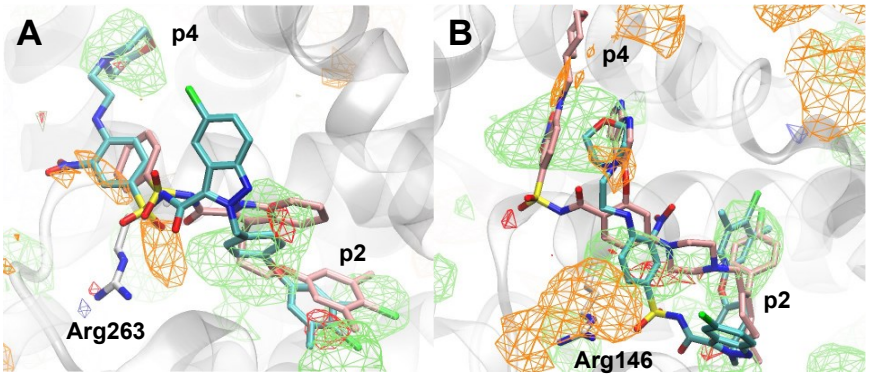

Figure 4.2.4: *SILCS-MC predicted binding poses (carbons in cyan) of compound 14c with (A) MCL-1 and (B) BCL-2. Crystal orientations (carbons in pink) of compound MCL-1 inhibitor 49 from Ref[39] (PDB:5FDO) and BCL-2 inhibitor VEN (PDB:6O0K) are overlaid in (A) and (B), respectively. SILCS FragMaps for apolar, H-bond acceptor and negatively charged types are shown in green, red, and orange meshes, respectively, and rendered at a LGFE level of -1.2 kcal/mol.*

4.3 Conclusions

While this work was in progress, 1-substituted 3-acylsulfonamide indazoles were reported as selective MCL-1 inhibitors (although there was no discussion of regioselectivities, we have analyzed their NMR data and we believe these are consistent with their reported identities as the N1-regioisomers).[164] It will be important to ascertain if the ability of our analogous 2-substituted 3-acylsulfonamide indazoles to recognize both MCL-1 and BCL-2 is due to the different substitution pattern, the p2-binding groups or a combination of both. In this regard, we are engaged in further exploring different p2-binding groups (including from the N1 position) as well as substitutions off the benzene ring component of the indazole scaffold. Additional future work will focus on attempts to solve crystal structures of our best compounds with both proteins to help drive the design of next generation compounds. In conclusion, by scaffold hopping from an indole core to an indazole we have transformed MCL-1 selective inhibitors into dual MCL-1/BCL-2

inhibitors. This finding is significant because the BCL-2 selective inhibitor VEN provides a median survival of about only 18 months primarily due to the upregulation of MCL-1.[129], [131], [136] A dual MCL-1/BCL-2 inhibitor may prove an essential weapon in the anti-cancer artillery.

4.4 Methods

Fluorescence Polarization Competition Assay

The fluorescence polarization assays were performed in 96 well polypropylene F-bottom black microplates (Greiner Bio-One) with a final volume of 100 µL. During the competition assay, a fluorescently labeled Bak-BH3 peptide (FITC-Ahx GQVGRQLAIIGDDINR-$CONH_2$, hereafter "FITC-Bak", where FITC = fluorescein isocyanate; Ahx = 6-aminohexanoyl linker) was competed off of either MCL-1172-327, BCL-X 1-212 or BCL-21-211 with the synthesized inhibitors. The binding affinities of FITC-Bak to MCL-1, BCL-X_L and BCL-2 were determined via a fluorescence polarization assay where various concentrations of the selected proteins were titrated into solutions of 10nM FITC-Bak in 20 mM HEPES, pH 6.8, 50 mM NaCl, 3 mM DTT, 0.01% Triton X-100 and 5% DMSO at room temperature. The changes in the fluorescence polarization were then measured using a BMG PHERAstar FS multimode microplate reader equipped with two PMTs for simultaneous measurements of both the perpendicular and parallel fluorescence emission at a 485 nm excitation and 520 nm emission filter. Regression analysis was then performed on the polarization data using Origin (OriginLab, Northampton, MA) and the data was fitted to the Hill equation, thus producing binding curves for FITC-Bak with MCL-1, BCL-X_L and BCL-2. FITC-Bak's

K_d's were then determined to be 42 nM for MCL-1, 6 nM for BCL-X_L and 33 nM for BCL-2.

The fluorescence polarization competition assays were setup using a Biomek FXP Automated Liquid Handling System. Protein concentrations of either 100nM of MCL-1, 15 nM of BCL-X_L or 75 nM of BCL-2 with 10 nM of FITC-Bak (in 20 mM HEPES, pH 6.8, 50 mM NaCl, 3 mM DTT, 0.01% Triton X-100 and 1% DMSO) were chosen and various concentrations of the inhibitors were titrated into the solutions. Wells possessing only the peptide, only the desired protein and both the peptide plus the desired protein without inhibitor were used as controls. Changes in fluorescence polarization were measured after 4 hours of incubation at room temperature using the BMG PHERAstar FS multimode plate reader previously mentioned and regression analysis was performed using Prism 8 (Graphpad) with the data fitted to a sigmoidal curve to determine inhibitor IC_{50} values. The IC_{50} values were then converted to K_i values using an equation derived by Nikolovska-Coleska *et al*. All inhibitors were tested in triplicate.

SILCS-Molecular Simulations

The Site-Identification by Ligand Competitive Saturation (SILCS) approach, as used in our previous MCL-1 study[21], was conducted by Dr. Wenbo Yu and was used to predict docking poses and contributions to the binding affinities of the synthesized compounds for MCL-1. The SILCS FragMaps were previously generated from SILCS GCMC-MD simulations [128] conducted using the crystal structure of MCL- 1 (PDB entry 4HW3)[129]. SILCS simulations for BCL-2 were performed using the crystal structure PDB entry 6O0K. For MCL-1, the molecular structures of all compounds were prepared using MOE (Chemical Computing Group) and aligned with the crystal binding mode of compound **1**

(PDB: 4HW2) for compounds **5** and **6** and with the crystal binding mode of compound **49** from Fesik's work on a series of **14** compounds (PDB ID: 5FDO)[130]. For BCL-2, molecular structures of all compounds were aligned with the crystal binding mode of compound Venetoclax (PDB:6O0K). Exhaustive SILCS-MC docking studies were performed from the aligned compound structures using SILCS FragMaps. The computational details about SILCS and SILCS-MC setups can be found in our previous work [128].

Figure 4.4.1A shows the predicted binding mode of compound **5** aligned with the crystal binding mode of Fesik's compound **1**. The SILCS FragMaps capture important functional group contributions to the binding of compound 1 including the hydrophobic moieties as indicated by the apolar green meshes and the carboxylate group as shown by the negative orange meshes, as described previously [21]. Compound **5**, with the indole in **1** being replaced by indazole, is predicted to adopt a similar binding orientation as **1**, with the 4-Cl-3,5-diMe-phenyl being deeply inserted into the P2 pocket. The linker between the bi-cyclic ring and halogenated phenyl is changed from a propyl in **1** to a phenyl ring in compound 5, but still presents a very similar binding orientation. The carboxylate groups in both **1** and **5** occupy the P2 pocket entrance and form ionic interactions with near-by R263 residue. However, since the carboxylate group in compound **5** is at the 3 position of indazole while is at the 2 position of the indole in **1**, the binding orientation of the indazole ring in compound **5** is turned away from that of the compound 1 indole ring. This is suggested to explain why Fesik's compound **1** has higher affinity than our compound **5**.

The arrangement of the carboxylate (2 position) and (4-Cl-3,5-diMe-phenoxy)propyl (3 position) groups around the indole ring (**Figure 4.4.1A**) allows the indole ring to be fully accommodated by the hydrophobic environment at P2 pocket as indicated by the favorable apolar FragMaps (green meshes). However, for compound **5**, the arrangement of carboxylate (3 position) and the (4-Cl- 3,5-diMe-phenoxy)-phenyl (2 position) on the indazole ring, though still allowing the carboxylate and (4-Cl-3,5-diMe-phenoxy)phenyl groups to fully occupy the desired regions, lead to the indazole ring being rotated 90˚ from the indole binding mode, and thus is less favorably accommodated by the pocket (off the favorable region as indicated by the apolar FragMaps.

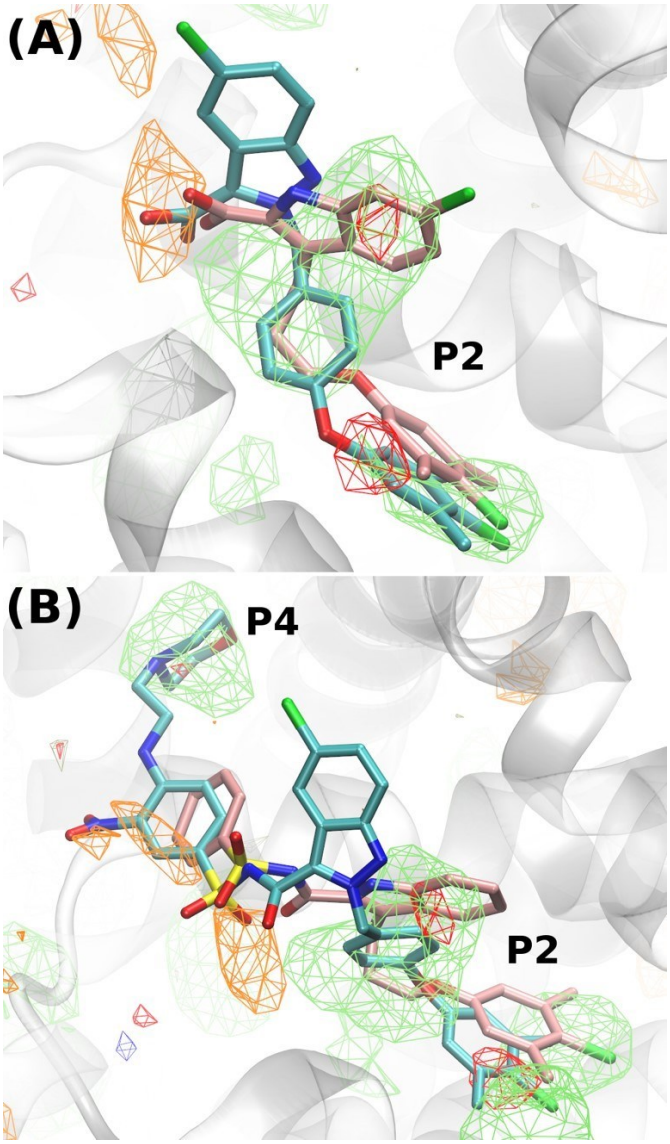

Figure 4.4.1: *Predicted MCL-1 binding poses (carbons in cyan) of compound* ***5*** *(A) and* ***14c*** *(B) by SILCS-MC. Crystal orientation (carbons in pink) of compound* ***1*** *(PDB ID:4HW2) and compound* ***49*** *from Ref*[129] *(PDB:5FDO) are overlaid on* ***5*** *and* ***14c****, respectively. SILCS FragMaps for apolar, H- bond acceptor and negatively charged types are shown in green, red, and orange meshes, respectively, and rendered at a GFE level of -1.2 kcal/mol.*

To quantitatively describe the differences between Fesik compound **1** and **5**, the LGFE scores and the GFE contributions for different functional groups to the total LGFE of the compounds are shown in **Table 4.4.1**. The predicted binding affinities based on the LGFE

scores captures the more favorable binding of compound **1** (Ki = 0.25 μM) as compared to compound **5** (Ki = 2.36 μM). GFE contributions from the di-Me-4-Cl-phenyl, the ester oxygen, the linker and the carboxylate groups are very similar for both **1** and **5**. The difference in binding is due to the GFE contribution from the bi-cyclic ring with the indole ring in compound **1** making a more favorable contribution than the indazole ring in **5**. Such analyses will facilitate future design of MCL-1 compounds. For example, swapping the substituent positions of carboxylate and (4-Cl-3,5-diMe-phenoxy) phenyl groups on the indazole ring might allow the resulting benzimidazole ring to bind in a similar way as the indole ring in compound **1** and let the entire compound benefit from this orientation for binding.

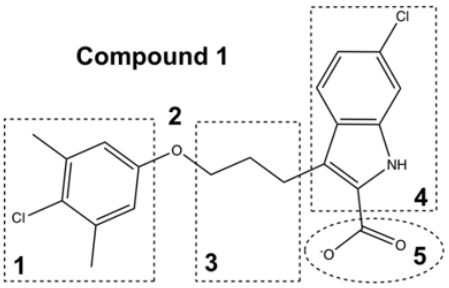

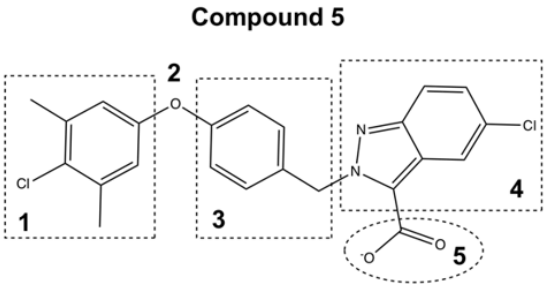

Compound	LGFE	GFE				
		1	2	3	4	5
		4-Cl-3,5-diMe-phenyl	Ester O	Propyl / phenyl	Indole / indazole	carboxylate
1	-7.8	-2.0	-0.1	-1.8	-1.8	-2.1
5	-7.4	-2.4	-0.4	-2.1	-0.4	-2.1

Table 4.4.1: *LGFE scores and GFE contributions (kcal/mol) from different functional groups to the overall predicted binding affinities of compound 1 and 5 to MCL-1.*

The predicted binding mode of one of our acylsulfonamides compound, **14c**, aligned with the crystal binding mode of one Fesik's acylsulfonamide compound **49** is shown in **Figure 4.4.1B** [130]. The overall similar binding orientations are evident. The core part of compound **14c** retains a similar binding orientation as with compound **5** with the acyl-sulfonamide group of **14c** occupying the position of the acid group in compound **5** as designed. The morpholine group occupies the MCL-1 P4 pocket as indicated by the apolar FragMaps. Such an additional occupancy of P4 pocket helps to improve the binding of the **14** series of compounds over compound **5**. However, the binding improvement (Ki is 1.61 μM for compound **14c** compared to 2.32 μM for **5**) is not that promising given the number of additional functional groups being added.

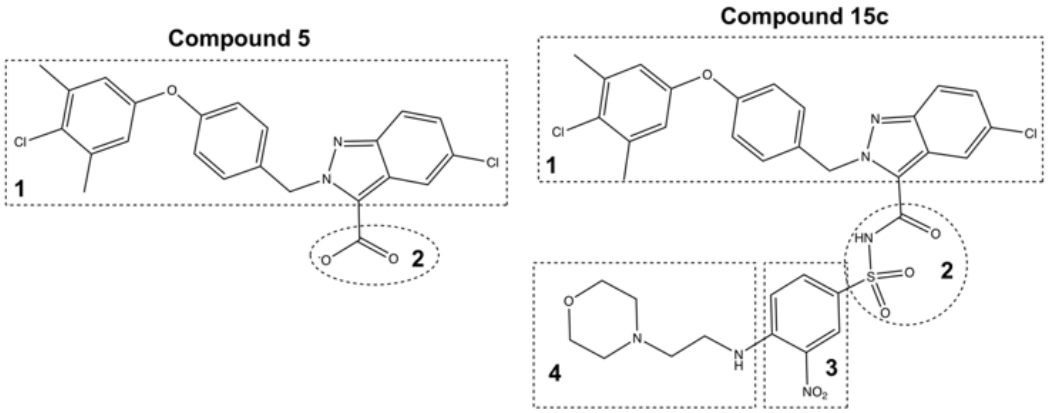

Compound	LGFE	GFE			
		1	2	3	4
		P2 pocket	carboxylate/ acyl-sulfonamide	nitrophenyl	P4 pocket
5	-7.4	-5.3	-2.1	-	-
14c	-8.5	-4.4	-1.5	-0.5	-2.1

Table 4.4.2: *LGFE scores and GFE contributions (kcal/mol) from different functional groups to the overall predicted binding affinities of compound **5** and **14c** to MCL-1.*

To understand the relatively small change in the overall binding functional group GFE analysis was performed (**Table 4.4.2**). The overall predicted binding affinity based on LGFE captures the favored binding of compound **14c** compared to 5. The GFE contribution from the additional functional groups in compound **14c** targeting the P4 pocket do yield very favorable binding contributions (group 3 and 4 together). However, the acyl-sulfonamide group in compound **14c** which replaces the acid group in compound 5, contributes a slightly smaller binding benefit as compared to the acid group, and the P2 pocket core part (group 1) in compound **14c** also offsets the contribution from the additional functional groups designed to target the P4 pocket. Clearly, acyl-sulfonamide group designed to retain the acceptor role of the acid group in compound 5 while enabling linking to additional groups to access the P4 pocket binding, does not fully maximize the benefits from the additional groups to the binding. Similar data are observed for other **14** series compounds as listed in the Supplementary Information **Table 4.4.1**. This observationon our designed compounds is consistent with Fesik's acyl-sulfonamide designs. One acyl-sulfonamide design from their study [130], compound **50**, which has exactly the same P2 pocket part with the original acid compound 1, but with acyl-sulfonamide-phenyl group to replace the acid group, has a measured Ki of 91 nM, compared to the 55 nM measured Ki for compound **1**, which indicates the acyl-sulfonamide group does not retain the same level of affinity benefit as the acid group. Thus, based on the SILCS GFE analyses, this suggests that to further efficiently extend the scaffold to utilize the P4 pocket, additional functional groups that extend from the acyl- sulfonamide group need to be carefully optimized to maintain the binding

contribution of the P2 pocket core part as well as the acyl-sulfonamide group. An alternative is to keep the carboxylate group while extending the molecule from other positions in the current scaffold. This approach actually was explored in work from Souers et al [131]. In that work, compound 5 is similar to the Fesik's compound 1 with the di-Me-4-Cl-phenyl ring replaced by naphthalene and the 6-Cl being absent. And to further utilize the P4 pocket, instead of altering the carboxylate group, they introduced substituent at the 1 and 7 positions on the indole ring and extend the scaffold from there to design a series of compounds to utilize the P4 pocket. One compound **30b** (Ki = 0.43 nM) showed a thousand-fold binding affinity increase compared to the compound **5** (Ki = 0.34 μM).

Target	LGFE	GFE			
		1	2	3	4
		P2 pocket	carboxylate/ acyl-sulfonamide	nitrophenyl	P4 pocket
MCL-1	-8.5	-4.4	-1.5	-0.5	-2.1
BCL-2	-9.3	-4.3	-1.0	-1.0	-3.0

Table 4.4.3: *LGFE scores and GFE contributions (kcal/mol) from different functional groups to the overall predicted binding affinities of compound* ***14c*** *to MCL-1 and BCL-2.*

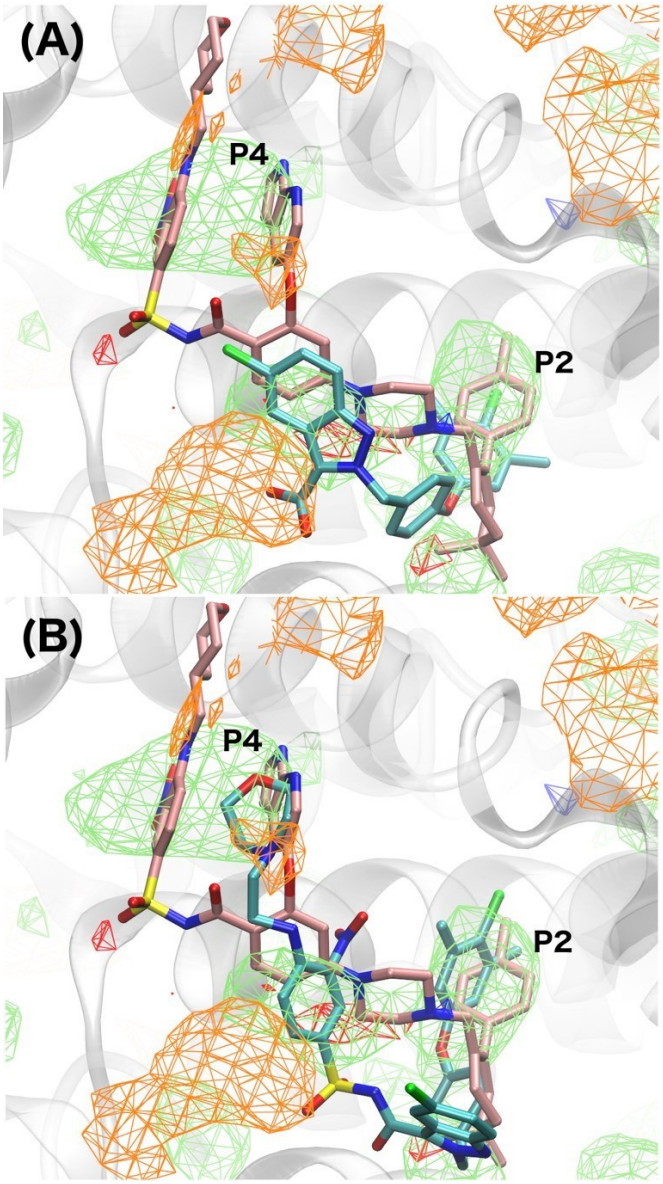

Figure 4.4.2: *Predicted binding poses (carbons in cyan) of compound* ***5*** *(A) and* ***14c*** *(B) by SILCS- MC targeting BCL-2. Crystal orientation (carbons in pink) of compound venetoclax (PDB:6O0K) is overlaid on* ***5*** *and* ***14c****. SILCS FragMaps for apolar, H-bond acceptor and negatively charged types are shown in green, red, and orange meshes, respectively, and rendered at a GFE level of -1.2 kcal/mol.*

The designed compounds were also found to be active toward BCL-2. **Figure 4.4.2** shows the predicted binding modes of compound **5** and **14c** to BCL-2. The binding orientations of both compound **5** and **14c** are similar to the crystal binding mode of

venetoclax with the di-Me-4-Cl- phenyl bound in the BCL-2 P2 pocket, carboxylate or acyl-sulfonamide bound near residue R105 and morpholine group in compound **14c** bound to the P4 pocket. **Table 4.4.3** lists the LGFE and GFE contributions for compound **14c** targeting MCL-1 and BCL-2. Data for other synthesized compounds are listed in **Table 4.4.4** and **Table 4.4.5**. Predicted binding affinities in terms of LGFE capture the favorable binding to BCL-2 over MCL-1 for studied compounds. For compound **14c**, the GFE contributions indicate the more affinity gain on BCL-2 over MCL-1 was brought by the nitrophenyl and morphiline groups. And for other compounds as shown in **Table 4.4.4** and **Table 4.4.5**, binding of the nitrophenyl group is more favorable targeting BCL-2 than MCL-1 in general. This is consistent with the observed apolar FragMaps overlaid on the nitrophenyl group as shown in **Figure 4.4.2** for BCL-2, while MCL-1 lack of such binding patterns at this position as shown in **Figure 4.4.1**.

As a conclusion, the predicted docking poses using the SILCS FragMaps along with the GFE analyses helps to explain the experimental binding observations on MCL-1 and BCL-2 and shed insights on how to further optimize our scaffold to maximize its binding to MCL-1.

Compound	LGFE	GFE			
		1	2	3	4
14a	-7.0	-5.1	-1.3	-0.6	-
14b	-7.6	-3.4	-1.6	-0.5	-2.1
14c	-8.5	-4.4	-1.5	-0.5	-2.1
14d	-7.2	-4.0	-1.6	-0.7	-0.9
14e	-7.5	-4.2	-1.6	-0.5	-1.2
14f	-7.4	-4.3	-1.6	-0.6	-0.9
14g	-8.0	-4.4	-1.5	-0.5	-1.6
14h	-8.2	-4.5	-1.6	-0.5	-1.6
14i	-7.4	-3.9	-1.6	-0.8	-1.1
14j	-7.9	-4.1	-1.6	-0.6	-1.6
14k	-7.4	-4.0	-1.6	-0.6	-1.2
14l	-7.0	-4.0	-1.7	-0.6	-0.7
14m	-7.1	-3.8	-1.5	-0.7	-1.1
14n	-7.6	-4.0	-1.6	-0.7	-1.3
14o	-7.8	-4.0	-1.6	-0.7	-1.5
14p	-8.2	-3.8	-1.6	-0.7	-2.1
14q	-8.1	-4.6	-1.6	-0.5	-1.4
14r	-8.2	-3.9	-1.7	-0.4	-2.2

Table 4.4.4: *GFE contributions (kcal/mol) from different functional groups in 14 series of compounds to the predicted LGFE scores for MCL-1.*

Compound	LGFE	GFE			
		1	2	3	4
14a	-7.7	-4.7	-1.8	-1.2	-
14b	-8.3	-4.4	-1.2	-1.3	-1.4
14c	-9.3	-4.3	-1.0	-1.0	-3.0
14d	-8.2	-4.1	-1.6	-1.2	-1.3
14e	-8.9	-4.5	-0.8	-1.8	-1.8
14f	-9.0	-3.6	-1.4	-1.6	-2.4
14g	-8.8	-3.0	-1.4	-1.5	-2.9
14h	-9.0	-4.6	-0.8	-1.5	-2.1
14i	-8.5	-3.5	-1.0	-2.0	-2.0
14j	-9.1	-3.9	-1.6	-1.3	-2.3
14k	-8.9	-4.3	-2.1	-1.9	-0.6
14l	-8.2	-4.6	-2.1	-0.5	-1.1
14m	-8.3	-4.3	-1.9	-0.6	-1.5
14n	-8.4	-4.2	-1.8	-0.7	-1.7
14o	-8.3	-4.3	-1.8	-1.1	-1.1
14p	-8.7	-3.6	-2.3	-1.1	-1.7
14q	-8.1	-4.1	-2.1	-0.5	-1.4
14r	-8.7	-4.1	-2.3	-0.9	-1.4

Table 4.4.5: *GFE contributions (kcal/mol) from different functional groups in* ***14*** *series of compounds to the predicted LGFE scores for BCL-2.*

4.5 Experimental Procedures

General Procedure 1: Synthesis of functionalized sulfonamides (**13a**–**13r**): Either 4-fluoro-3- nitrobenzenesulfonamide or 3-fluoro-4-nitrobenzenesulfonamide (1 eq.) was placed in a reaction flask and solubilized in DMF (0.1 M). Selected amines (1.1 eq.) and

K_2CO_3 (2.0 eq.) were added to the reaction mixture. The reaction was stirred at RT for 16 h. Reaction completion was monitored via TLC (CH_2Cl_2/MeOH/NH_4OH, 92:7:1). Upon completion, the reaction was partitioned between EtOAc and brine. The organic layer was washed five times with brine to remove the DMF and excess amine. The organic layer was then collected, dried with Na_2SO_4, filtered and concentrated to produce the desired functionalized sulfonamides that needed no further purification.

General Procedure 2: Sulfonamide coupling of N-alkylated indazole carboxylic acids: An N- alkylated indazole (1 eq.) was dissolved in anhydrous DMF (0.1 M). DIPEA (1 eq.), DMAP (0.5 eq.) and EDCI (1.2 eq.) were then added. The reaction was stirred at RT for 10 min before the addition of the appropriate sulfonamide (**13a**–**13r**; 1.1 eq.). The reaction was stirred at RT for 16

h. Completion of the reaction was monitored via TLC (CH_2Cl_2/MeOH/NH_4OH, 92:7:1). The reaction was partitioned between EtOAc and brine, then the organic layer was washed 5 times with brine, collected, dried with Na_2SO_4, filtered and concentrated. The crude material was adsorbed onto silica gel, then purified by flash column chromatography eluting with CH_2Cl_2/MeOH/NH_4OH, 92:7:1.

General Procedure 3: Esterfication of carboxylic acids: The carboxylic acid (1 eq.) was dissolved in MeOH (0.1 M) at 0 ºC. $SOCl_2$ (3 eq.) was slowly added to the reaction, and then it was stirred at 65°C for 16 h. Completion of the reaction was monitored via TLC (CH_2Cl_2/MeOH/CH_3COOH, 92:7:1). The reaction was concentrated, then partitioned between EtOAc and sat. $NaHCO_3$. The organic layer was collected, dried with Na_2SO_4, filtered and concentrated to yield the target methyl ester.

General Procedure 4: N-Alkylation of the heterocyclic cores: A heterocyclic core (1 eq.) was added to a reaction flask, followed by the addition of DMF (0.1 M). The desired alkyl bromide (1.1 eq.) and K_2CO_3 (2 eq.) were then added to the reaction mixture. The reaction was stirred for at a given temperature for 16 h. Completion of the reaction was monitored via TLC (hexanes/EtOAc, 2:1). The reaction mixture was partitioned between EtOAc and brine. The organic layer was washed 5 times with brine, collected, dried with Na_2SO_4, filtered and concentrated. The crude material was adsorbed onto silica gel and purified via flash column chromatography eluting with a gradient of EtOAc in hexanes.

General Procedure 5: Saponification of methyl esters: A methyl ester (1 eq.) was dissolved in a 3:1 mixture of THF/MeOH (0.1 M). H_2O was then added (0.2 M) followed by the addition of NaOH (3.0 eq). The reaction was stirred at RT for 16h. Completion of the reaction was monitored via TLC (CH_2Cl_2/MeOH/CH_3COOH, 92:7:1). The reaction mixture was partitioned between EtOAc and 1 M HCl. The organic layer was collected, dried with Na_2SO_4, filtered and concentrated to yield the target acid that did not require further purification.

1-(3-(4-Chloro-3,5-dimethylphenoxy)propyl)-1H-benzo[d]imidazole-2-carboxylic acid (2). 1H- Benzo[d]imidazole-2-carboxylic acid was esterified on a 3.08 mmol scale according to General Procedure 3 to deliver methyl 1H-benzo[d]imidazole-2-carboxylate as a viscous oil (521 mg, 96%): 1H NMR (400 MHz, d6-DMSO) δ = 13.55 (s, 1H), 7.79 (d, J = 7.6 Hz, 1H), 7.59 (d, J = 8.0 Hz, 1H), 7.40 (t, J = 7.8 Hz, 1H), 7.32 (t, J = 7.8 Hz, 1H), 3.97 (s, 3H). Subsequently, this ester (2.04 mmol scale) was treated with 5-(3-bromopropoxy)-2-chloro-1,3-dimethylbenzene according to General Procedure 4, heating the reaction at 45 ºC for 16 h. After flash column chromatography, methyl 1-(3-(4-chloro-

3,5-dimethylphenoxy)propyl)-1H-benzo[d]imidazole-2- carboxylate (the less polar of the two products) was yielded as a viscous oil (530 mg, 70%): 1H NMR (400 MHz, CDCl3) δ = 7.90 (d, J = 7.2 Hz, 1H), 7.47 (d, J = 7.6 Hz, 1H), 7.36-7.34 (m, 2H), 6.58 (s, 2H), 4.85 (t, J = 7.0 Hz, 4.00 (s, 3H), 3.91 (t, J = 5.6, 2H), 2.35-2.33 (m, 8H). 13C NMR (400 MHz, CDCl3) δ = 158.7, 154.6, 140.0, 138.7, 135.5, 134.6, 124.8, 124.1, 122.2, 120.3, 112.8, 109.0, 63.0, 51.2, 40.8, 28.4, 19.3. Methyl 1-(3-(4-chloro-3,5-dimethylphenoxy)propyl)- 1H-benzo[d]imidazole-2-carboxylate was saponified on a 1.29 mmol scale according to General Procedure 5 to deliver 1-(3-(4-chloro-3,5-dimethylphenoxy)propyl)-1H-benzo[d]imidazole-2- carboxylic acid (3) as an off-white solid (439 mg, 95%): 1H NMR (400 MHz, d6-DMSO) δ = 9.61 (s, 1H), 8.02 (m, 1H), 7.90 (m, 1H), 7.60 (m, 2H), 6.67 (s, 2H), 4.67 (t, J = 6.6 Hz, 2H), 4.05 (t, J = 5.6 Hz, 2H), 2.38 (t, J = 5.8 Hz, 2H), 2.28 (s, 6H); 13C NMR (400 MHz, CDCl3) δ = 161.3, 147.1, 141.6, 137.2, 136.6, 131.1, 130.8, 130.3, 120.5, 119.8 (2), 118.2, 70.1, 48.9, 33.4, 25.6.

5-Chloro-2-(3-(4-chloro-3,5-dimethylphenoxy)propyl)-2H-indazole-3-carboxylic acid (3). A solution of methyl 5-chloroindazole-3-carboxylate (10; 400 mg, 2.27 mmol, 1 eq) in anhydrous THF (15 mL) was treated with 3-(4-chloro-3,5-dimethylphenoxy)propan-1-ol (487 mg, 2.27 mmol, 1 eq), PPh3 (715 mg, 2.72 mmol, 1.2 eq) and DIAD (540 mL, 2.72 mmol, 1.2 eq). The reaction was stirred at RT for 16 h. Flash column chromatography was performed using a gradient hexanes/ethyl acetate to yield methyl 5-chloro-2-(3-(4-chloro-3,5- dimethylphenoxy)propyl)-2H-indazole-3-carboxylate as the major product: (570 mg, 67%): 1H NMR (400 MHz, CDCl3) δ = 7.95 (s, 1H), 7.66 (d, J = 9.2 Hz, 1H), 7.25 (d, J = 8.4 Hz, 1H), 6.51 (s, 2H), 5.06 (t, J = 7.2 Hz, 2H), 3.95 (m, 5H), 2.45-2.40 (m, 2H), 2.28 (s, 6H). Subsequently, the material was subjected to General

Procedure 5 on a 1.35 mmol scale to deliver the title carboxylic acid (3) as a white solid (469 mg, 88%): 1H NMR (400 MHz, d6-DMSO) δ = 13.2 (s, 1H), 8.02 (s, 1H), 7.82 (d, J = 8.4 Hz, 1H), 7.44 (d, J = 8.8 Hz, 1H), 6.62 (s, 2H), 4.64 (t, J = 6.8 Hz, 2H), 3.92 (t, J = 5.6 Hz, 2H), 2.29-2.22 (m, 8H); 13C NMR (400 MHz, DMSO) δ = 163.0, 156.2, 139.2, 136.4, 134.5, 127.6, 126.9, 125.1, 123.8, 120.2, 114.7, 112.6, 64.8, 46.2, 28.8, 20.4.

5-Chloro-2-(2-(4-chloro-3,5-dimethylphenoxy)ethyl)-2H-indazole-3-carboxylic acid (4): Methyl 5- chloroindazole-3-carboxylate (10; 2.37 mmol) and 5-(2-bromoethoxy)-2-chloro-1,3- dimethylbenzene were reacted together according to General Procedure 4 at RT. Flash column chromatography was performed using a gradient hexanes/ethyl acetate to yield methyl 5-chloro- 2-(3-(4-chloro-3,5-dimethylphenoxy)ethyl)-2H-indazole-3-carboxylate (the less polar of the two products) as a viscous oil (367 mg, 39%): 1H NMR (400 MHz, CDCl3) δ = 7.96 (s, 1H), 7.70 (d, J = 8.4 Hz, 1H), 7.27 (d, J = 8.8 Hz, 1H), 6.55 (s, 2H), 5.26 (t, J = 5.8 Hz, 2H), 4.43 (t, J = 6.0 Hz, 2H), 4.03 (s, 3H), 2.26 (s, 6H). Subsequently, the material was subjected to General Procedure 5 on a 0.559 mmol scale to deliver the title carboxylic acid (4) as a white solid (188 mg, 89%): 1H NMR (400 MHz, d6-DMSO) δ = 7.99 (s, 1H), 7.84 (d, J = 9.2 Hz, 1H), 7.38 (d, J = 9.2 Hz, 1H), 6.73 (s, 2H), 5.25 (t, J = 5.2 Hz, 2H), 4.50 (t, J = 5.4 Hz, 2H), 2.24 (s, 6H); 13C NMR (400 MHz, CDCl3) δ = 165.8, 161.1, 150.3, 141.7 (2), 134.4, 132.4 (2), 130.5, 128.6, 125.3, 119.9, 71.8, 57.1, 25.5.

5-Chloro-2-(4-(4-chloro-3,5-dimethylphenoxy)benzyl)-2H-indazole-3-carboxylic acid (5): Methyl 5-chloroindazole-3-carboxylate (2.09 g, 7.95 mmol, 1 eq) in anhydrous THF (40 mL) was treated with 4-(4-chloro-3,5-dimethylphenoxy)phenyl)methanol (1.40 g, 7.95 mmol, 1 eq), PPh3 (2.50 g, 9.55 mmol, 1.2 eq) and DIAD (1.88 mL, 9.55 mmol, 1.2

eq). The reaction was stirred at RT for 16 h. Flash column chromatography was performed using a gradient hexanes/ethyl acetate to yield methyl 5-chloro-2-(4-(4-chloro-3,5-dimethylphenoxy)benzyl)-2H-indazole-3-carboxylate (11) as a viscous oil (2.18 g, 65%): Rf 0.59 (Hex/EtOAc, 2:1); 1H NMR (400 MHz, CDCl3) δ = 8.00 (s, 1H), 7.74 (d, J = 8.8 Hz, 1H), 7.36 (d, J = 8.8 Hz, 2H), 7.30-7.26 (m, 1H), 6.90 (d, J = 8.8 Hz, 2H), 6.70 (s, 2H), 6.05 (s, 2H), 4.03 (s, 3H), 2.31 (s, 6H); 13C NMR (400 MHz, CDCl3) δ = 160.3, 157.3, 154.4, 145.9, 137.7, 131.2, 130.7, 129.7, 127.9, 124.0, 120.4, 119.9, 119.0, 118.5 (2), 56.1, 52.2, 21.7, 20.8. Isomer 12 (methyl 5-chloro-1-(4-(4-chloro-3,5-dimethylphenoxy)benzyl)-1H-indazole-3-carboxylate) was also isolated during this purification: Rf 0.43 (Hex/EtOAc, 2:1): 1H NMR (400 MHz, CDCl3) δ = 8.24 (s, 1H), 7.34 (d, J = 2.8 Hz, 2H), 7.20 (d, J = 8.4, 2H), 6.91 (d, J = 8.8 Hz, 2H), 6.72 (s, 1H), 5.67 (s, 2H), 4.07 (s, 3H), 2.33 (s, 6H);13C NMR (400 MHz, CDCl3) δ = 162.6, 157.5, 154.2, 138.9, 137.8, 134.5, 129.8, 129.4, 128.9 (2), 127.9, 124.9, 121.6, 119.1, 118.7, 111.2, 53.8, 52.3, 20.9. Subsequently, ester 11 was subjected to General Procedure 5 to deliver the title carboxylic acid (5) as a white solid (yield = 92%): 1H NMR (400 MHz, d6-DMSO) δ = 7.96 (s, 1H), 7.82 (d, J = 8.4 Hz, 1H), 7.35 (d, J = 7.2 Hz, 1H), 7.26 (d, J = 8.8 Hz, 2H), 6.92 (d, J = 8.8 Hz, 2H), 6.83 (s, 2H), 6.02 (s, 2H), 2.24 (s, 6H);13C NMR (400 MHz, CDCl3) δ = 165.7, 161.6, 159.4, 150.5, 142.6, 136.7, 134.8 (2), 133.5, 132.5, 129.5, 128.7, 125.4, 124.2, 123.5 (2), 60.3, 25.5. Finally, ester 12 was likewise saponified to deliver 5-chloro-1-(4-(4-chloro-3,5-dimethylphenoxy)benzyl)-1H-indazole-3-carboxylic acid (6) as a white solid: 1H NMR (400 MHz, DMSO) δ = 13.3 (s, 1H), 8.08 (s, 1H), 7.98 (d, J = 8.4 Hz, 1H), 7.54 (d, J = 9.6 Hz, 1H), 7.33 (d, J = 8.4 Hz, 2H), 6.98 (d, J = 7.6 Hz, 2H), 6.87 (s, 2H), 5.78 (s, 2H), 2.29 (s, 6H); 13C NMR (400 MHz,

CDCl3) δ = 168.2, 161.6, 159.4, 144.2, 142.6, 140.0, 136.5, 134.7, 133.5, 133.0, 132.4, 129.2, 125.6, 124.2, 123.7, 118.0, 57.3, 25.5; HRMS-ESI: m/z found 439.0609 [M+H]+, $C_{23}H_{17}Cl_2N_2O_3$ requires 439.0622.

6-Chloro-2-(4-(4-chloro-3,5-dimethylphenoxy)benzyl)-2H-indazole-3-carboxylic acid (7): 6- Chloro-1H-indazole-3-carboxylic acid (1.02 mmol) underwent General Procedure 3, followed by General Procedure 4 (0.266 mmol scale) with 5-(4-(bromomethyl)phenoxy)-2-chloro-1,3- dimethylbenzene at RT, and then the less polar product was subjected to General Procedure 5 (0.197 mmol scale) to yield the title compound (7) as a white solid (77 mg, 92%): 1H NMR (400 MHz, d6-DMSO) δ = 8.07 (d, J = 9.2 Hz, 1H), 7.91 (s, 1H), 7.34 (d, J = 8.8 Hz, 3H), 6.98 (d, J = 8.4 Hz, 2H), 6.88 (s, 2H), 6.09 (s, 2H), 2.30 (6H); 13C NMR (400 MHz, DMSO) δ = 161.1, 156.8, 154.7, 147.4, 137.9, 132.2, 131.5, 130.0, 128.7, 126.2, 125.7, 124.1, 121.9, 119.4, 118.8, 117.2, 55.4, 20.7.

Methyl 5-chloroindazole-3-carboxylate (10): 5-chloroisatin (8; 1.0 mmol) was added to a reaction flask, followed by the addition of H2O (0.1 M) and NaOH (1.1 mmol). The reaction was heated to 45°C and stirred for 30 minutes or until all the starting material was solubilized. The reaction mixture was then cooled to 0 ºC. NaNO2 (1.0 mmol) was dissolved in H2O and slowly added to the reaction. The reaction stirred for 10 minutes and then H2SO4 (2.5 mmol) was added to the reaction. After 30 minutes of stirring, SnCl2 was dissolved in concentrated HCl and slowly added to the reaction mixture. The reaction was stirred at 0 ºC for 16 h. The resulting precipitate was filtered from the reaction mixture to deliver crude 5-chloroindazole-3-carboxylic acid (9), which was carried forwarded to the next reaction. Subsequently, this crude material was dissolved in

MeOH (0.1 M), and SOCl2 (3.0 mmol) was slowly added to the reaction. The reaction was stirred at 65°C for 16 h. Completion of the reaction was monitored via TLC. The reaction was concentrated down and then partitioned between brine and ethyl acetate. The organic layer was collected, dried with Na2SO4, filtered and concentrated. The crude material was redistributed in CH_2Cl_2 and adsorbed to silica gel. Flash column chromatography was then performed to purify the desired product using a gradient of hexanes/ethyl acetate to yield methyl 5-chloroindazole- 3-carboxylate (10): 1H NMR (400 MHz, d6-DMSO) δ = 8.02 (s, 1H), 7.69 (d, J = 8.4 Hz, 1H), 7.46 (d, J = 9.2 Hz, 1H), 3.91 (s, 3H); 13C NMR (400 MHz, CDCl3) δ = 162.8, 139.9, 135.1, 128.0, 127.6, 123.4, 120.3, 113.5, 52.2.

Synthesis of 4-chlorobenzenesulfonamide (13a): 4-chlorobenzenesufonyl chloride (1.0 mmol) was dissolved in dioxane (0.1 M), and cooled to 0 °C. NH4OH (5.0 mmol) was added dropwise to the reaction. The reaction was stirred at 0 °C for 30 minutes. Completion of the reaction was monitored via TLC (hexanes/EtOAc). The reaction was partitioned between ethyl acetate and brine. The organic layer was collected, dried with Na2SO4, filtered, concentrated to deliver the title compound as a white solid (yield = 88%). 1H and 13C spectra were consistent with the literature.25

Synthesis of 4-morpholino-3-nitrobenzenesulfonamide (13b): Follow General Procedure 1 using 4-fluoro-3-nitrobenzenesulfonamide and morpholine (yield = 77%): yellow solid; 1H (400 MHz, d6-DMSO) δ 8.22 (s, 1H), 7.92 (d, J = 7.4Hz, 1H), 7.46 (d, J = 8Hz, 2H), 3.72 (t, J = 6.8Hz, 4H), 3.14 (t, J = 6.8Hz, 4H), 2.00 (s, 1H); 13C NMR (400 MHz, d6-DMSO) δ= 152.3, 144.1, 140.2, 136.1, 129.5, 126.2, 71.0, 55.8, 51.0.

Synthesis of 4-((2-morpholinoethyl)amino)-3-nitrobenzenesulfonamide (13c): Follow General Procedure 1 using 4-fluoro-3-nitrobenzenesulfonamide and 2-morpholinoethan-1-amine (yield = 65%): yellow solid; 1H (400 MHz, d6-DMSO) δ 8.78 (t, J = 7Hz, 1H), 8.48 (s, 1H), 7.85 (d, J = 7.4Hz, 1H), 7.35 (s, 2H), 7.23 (d, J = 7.4Hz, 1H), 3.61 (m, 4H), 3.50 (q, J = 6.8Hz, 2H), 2.64 (t, J = 6.8Hz, 2H), 2.46 (s, 4H); 13C NMR (400 MHz, d6-DMSO) δ 151.6, 138.0, 135.3, 134.6, 129.8, 121.1, 71.5, 60.5, 58.0, 45.3.

Synthesis of 4-((furan-2-ylmethyl)amino)-3-nitrobenzenesulfonamide (13d): Follow General Procedure 1 using 4-fluoro-3-nitrobenzenesulfonamide and furan-2-ylmethanamine (yield = 73%): yellow solid; 1H (400 MHz, d6-DMSO) δ 8.89 (t, J = 7.4 Hz, 1H), 8.49 (s, 1H), 7.83 (d, J = 7 Hz, 1H), 7.62 (s, 1H), 7.31-7.33 (m, 2H), 6.41 (s, 2H), 4.71 (d, J = 6.8 Hz, 2H); 13C NMR (400 MHz, d6-DMSO) δ 156.1, 151.3, 147.9, 137.8, 135.8, 129.8, 121.0, 115.7, 113.1, 45.1.

Synthesis of 4-((2-(furan-2-yl)ethyl)amino)-3-nitrobenzenesulfonamide (13e): Follow General Procedure 1 using 4-fluoro-3-nitrobenzenesulfonamide and 2-(furan-2-yl)ethan-1-amine (yield = 74%): yellow solid; 1H NMR (400 MHz, d6-DMSO) δ 8.58 (t, J = 5.4 Hz, 1H), 8.50 (d, J = 2.4 Hz, 2H), 7.86 (d, J = 9.6 Hz, 1H), 7.59 (s, 1H), 7.38 (s, 2H), 7.25 (d, J = 9.2 Hz, 1H), 6.41 (s, 1H), 6.28 (d, J = 2.8 Hz, 1H), 3.72 (q, J = 6.4 Hz, 2H), 3.03 (t, J = 7.0 Hz, 2H); 13C NMR (400 MHz, d6-DMSO) δ 157.5, 151.5, 147.2, 138.0, 135.5, 134.7, 129.9, 120.6, 115.8, 111.9, 46.5, 32.1.

Synthesis of 4-(((1-methyl-1H-pyrazol-3-yl)methyl)amino)-3-nitrobenzenesulfonamide (13f): Follow General Procedure 1 using 4-fluoro-3-nitrobenzenesulfonamide and (1-methyl-1H- pyrazol-3-yl)methanamine (yield = 63%): yellow solid; 1H NMR (400 MHz, d6-DMSO) δ= 8.83 (t, J = 5.6 Hz, 1H), 8.51 (s, 1H), 7.84 (d, J = 8.4 Hz, 1H), 7.71 (s,

1H), 7.48 (s, 1H), 7.36 (s, 2H), 7.28 (d, J = 9.6 Hz, 1H), 4.53 (d, J = 6 Hz, 2H), 3.80 (s, 3H); 13C NMR (400 MHz, d6-DMSO) δ 149.6, 141.5, 136.2, 133.7, 133.1, 128.2, 120.9, 119.3 (2), 40.6 (2).

Synthesis of 3-nitro-4-((pyridin-3-ylmethyl)amino)benzenesulfonamide (13g): Follow General Procedure 1 using 4-fluoro-3-nitrobenzenesulfonamide and pyridin-3-ylmethanamine (yield = 69%): yellow solid; 1H (400M Hz, d6-DMSO) δ= 9.11 (t, J = 7.8 Hz, 1H), 8.64 (s, 1H), 8.47-8.50 (m, 2H), 7.77 (m, 2H), 7.35-7.38 (m, 1H), 7.31 (s, 2H), 7.11 (d, J = 8.4 Hz, 1H), 4.75 (d, J = 8.4 Hz, 2H); 13C NMR (400 MHz, d6-DMSO) δ 149.0, 148.8, 146.5, 135.3, 134.1, 133.2, 131.0, 130.6, 125.2, 124.1, 116.1, 43.8.

Synthesis of 3-nitro-4-((2-(pyridin-3-yl)ethyl)amino)benzenesulfonamide (13h): Follow General Procedure 1 using 4-fluoro-3-nitrobenzenesulfonamide and 2-(pyridin-3-yl)ethan-1-amine (yield = 64%): yellow solid; 1H NMR (400 MHz, d6-DMSO) δ = 8.56 (d, J = 7.2 Hz, 2H), 8.50 (s, 1H), 8.47 (d, J = 4.0 Hz, 1H), 7.87 (d, J = 8.8 Hz, 1H), 7.76 (d, J = 7.6 Hz, 1H), 7.37 (d, J = 12.0 Hz, 4H), 3.74 (q, J = 6.4 Hz, 2H), 3.00 (t, J = 7.2 Hz, 2H); 13C NMR (400 MHz, d6-DMSO) δ 150.4, 148.1, 146.7, 136.9, 134.6, 133.3, 130.7, 129.9, 125.2, 123.9, 116.0, 43.9, 31.8.

Synthesis of 3-nitro-4-((pyridin-4-ylmethyl)amino)benzenesulfonamide (13i): Follow General Procedure 1 using 4-fluoro-3-nitrobenzenesulfonamide and pyridin-4-ylmethanamine (yield = 58%): yellow solid; 1H NMR (400 MHz, d6-DMSO) δ = 9.13 (t, J = 6.2 Hz, 1H), 8.52 (d, J = 2.4 Hz, 3H), 7.75 (d, J = 7.6 Hz, 1H), 7.35-7.33 (m, 4H), 6.97 (d, J = 8.4 Hz, 1H), 4.77 (d, J = 6.0 Hz, 2H); 13C NMR (400 MHz, d6-DMSO) δ 155.0, 154.9, 152.2, 151.7, 148.2, 135.8, 130.0, 129.9, 127.1, 127.0, 120.8, 49.9.

Synthesis of 3-nitro-4-((2-(pyridin-4-yl)ethyl)amino)benzenesulfonamide (13j): Follow General Procedure 1 using 4-fluoro-3-nitrobenzenesulfonamide and 2-(pyridin-4-yl)ethan-1-amine (yield = 55%): yellow solid; 1H NMR (400 MHz, d6-DMSO) δ 8.54 (bs, 2H), 8.26 (d, J = 8.4 Hz, 2H), 7.67 (s, 2H), 7.51 (s, 1H), 7.37 (bs, 2H), 7.08 (d, J = 8.8 Hz, 1H), 3.69 (t, J = 5.8 Hz, 2H), 3.03 (t, J = 6.6 Hz, 2H); 13C NMR (400 MHz, d6-DMSO) δ 155.7, 154.8, 153.0, 149.6, 137.5, 133.1, 129.5, 116.9, 116.7, 48.0, 38.5.

Synthesis of 3-morpholino-4-nitrobenzenesulfonamide (13k): Follow General Procedure 1 using 3-fluoro-4-nitrobenzenesulfonamide and morpholine (yield = 75%): yellow solid; 1H NMR (400 MHz, d6-DMSO) δ= 8.02 (d, J = 8.8 Hz, 1H), 7.68 (s, 1H), 7.62 (s, 2H), 7.51 (d, J = 8.8 Hz), 3.72 (t, J = 4.4 Hz, 4H), 3.05 (t, J = 4.4 Hz, 4H); 13C NMR (400 MHz, d6-DMSO) δ 148.7, 145.5, 144.0, 127.1, 118.9, 118.6, 66.4, 51.5.

Synthesis of 3-((furan-2-ylmethyl)amino)-4-nitrobenzenesulfonamide (13l): Follow General Procedure 1 using 3-fluoro-4-nitrobenzenesulfonamide and furan-2-ylmethanamine (yield = 70%): yellow solid; 1H NMR (400 MHz, d6-DMSO) δ 8.64 (t, J = 5.8 Hz, 1H), 8.26 (d, J = 8.4 Hz, 1H), 7.64 (s, 3H), 7.54 (s, 1H), 7.09 (d, J = 8.8 Hz, 1H), 6.41 (d, J = 16.4 Hz, 2H), 4.66 (d, J = 6.4 Hz, 2H); 13C NMR (400 MHz, d6-DMSO) δ = 151.4, 150.7, 144.7, 143.2, 133.0, 128.2, 112.4, 112.3, 111.1, 108.3.

Synthesis of 3-((2-(furan-2-yl)ethyl)amino)-4-nitrobenzenesulfonamide (13m): Follow General Procedure 1 using 3-fluoro-4-nitrobenzenesulfonamide and 2-(furan-2-yl)ethan-1-amine (yield = 78%): yellow solid; 1H NMR (400 MHz, d6-DMSO) δ 8.30 (t, J = 5.4 Hz, 1H), 8.26 (d, J = 8.4 Hz, 1H), 7.65 (s, 2H), 7.59 (s, 1H), 7.47 (s, 1H), 7.08 (d, 9.6 Hz, 1H), 6.41 (t, J = 2.4 Hz, 1H), 6.28 (d, J = 2.8 Hz, 1H), 3.68 (q, J = 6.4 Hz, 2H), 3.05 (t, J

= 7.0 Hz, 2H); 13C NMR (400 MHz, d6- DMSO) δ 157.5, 155.7, 149.6, 147.2, 137.4, 133.0, 116.8, 116.7, 115.7, 111.8, 46.4, 32.0.

Synthesis of 3-(((1-methyl-1H-pyrazol-3-yl)methyl)amino)-4-nitrobenzenesulfonamide (13n): Follow General Procedure 1 using 3-fluoro-4-nitrobenzenesulfonamide and (1-methyl-1H- pyrazol-3-yl)methanamine (yield = 68%): yellow solid; 1H NMR (400 MHz, d6-DMSO) δ 8.54 (t, J = 5.4 Hz, 1H), 8.27 (d, J = 9.2 Hz, 1H), 7.71 (s, 1H), 7.68 (s, 2H), 7.52 (s, 1H), 7.47 (s, 1H), 7.07 (d, J = 9.2 Hz, 1H), 4.48 (d, J = 5.6 Hz, 2H), 3.81 (s, 3H); 13C NMR (400 MHz, d6-DMSO) δ 153.8, 147.9, 141.5, 135.8, 133.2, 120.9, 115.5, 114.9, 43.7, 40.6.

Synthesis of 4-nitro-3-((pyridin-3-ylmethyl)amino)benzenesulfonamide (13o): Follow General Procedure 1 using 3-fluoro-4-nitrobenzenesulfonamide and pyridin-3-ylmethanamine (yield = 60%): yellow solid; 1H NMR (400 MHz, DMSO) δ 8.84 (t, J = 6.2 Hz, 1H), 8.63 (s, 1H), 8.49 (d, J = 3.6 Hz, 1H), 8.28 (d, J = 8.8 Hz, 1H), 7.79 (d, J = 7.6 Hz, 1H), 7.61 (s, 2H), 7.40-7.37 (m, 1H), 7.33 (s, 1H), 7.07 (d, J = 8.4 Hz, 1H), 4.70 (d, J = 6.4 Hz, 2H); 13C NMR (400 MHz, d6-DMSO) δ 150.7, 149.0, 144.7, 135.3, 134.1, 133.1, 128.3, 124.2, 112.21, 112.16, 44.0.

Synthesis of 4-nitro-3-((2-(pyridin-3-yl)ethyl)amino)benzenesulfonamide (13p): Follow General Procedure 1 using 3-fluoro-4-nitrobenzenesulfonamide and 2-(pyridin-3-yl)ethan-1-amine (yield = 64%): yellow solid; 1H NMR (400 MHz, d6-DMSO) δ 8.56 (s, 1H), 8.48 (s, 1H), 8.27 (d, J = 8.4 Hz, 2H), 7.77 (d, J = 8.0 Hz, 1H), 7.67 (s, 2H), 7.51 (s, 1H), 7.40 (t, J = 6.2 Hz, 1H), 7.08 (d, J = 9.6 Hz, 1H), 3.68 (q, J = 6.8 Hz, 2H), 3.03 (t, J = 7.0 Hz, 2H); 13C NMR (400 MHz, d6-DMSO) δ 150.9, 150.2, 148.1, 144.8, 137.0, 134.7, 132.7, 128.3, 124.1, 112.2, 111.9, 44.0, 31.6.

Synthesis of 4-nitro-3-((pyridin-4-ylmethyl)amino)benzenesulfonamide (13q): Follow General Procedure 1 using 3-fluoro-4-nitrobenzenesulfonamide and pyridin-4-ylmethanamine (yield = 55%): yellow solid; 1H NMR (400 MHz, d6-DMSO) δ 8.89 (t, J = 5.8 Hz, 1H), 8.55 (d, J = 5.6 Hz, 2H), 8.31 (d, J = 9.2 Hz, 1H), 7.60 (s, 1H), 7.39 (d, J = 4.4 Hz, 2H), 7.22 (s, 1H), 7.09 (d, J = 9.6 Hz, 1H), 4.73 (d, J = 6.4 Hz, 2H); 13C NMR (400 MHz, d6-DMSO) δ 155.5, 155.0, 152.5, 149.5, 137.9, 133.1, 127.1, 125.7, 117.0, 116.9, 50.1.

Synthesis of 4-nitro-3-((2-(pyridin-4-yl)ethyl)amino)benzenesulfonamide (13r): Follow General Procedure 1 using 3-fluoro-4-nitrobenzenesulfonamide and 2-(pyridin-4-yl)ethan-1-amine (yield = 58%): yellow solid; 1H NMR (400 MHz, d6-DMSO) δ 8.57-8.50 (m, 4H), 7.88 (d, J = 8.8 Hz, 1H), 7.39-7.36 (m, 5H), 3.78-3.73 (m, 2H), 3.00 (t, J = 7.4 Hz, 2H); 13C NMR (400 MHz, d6- DMSO) δ 154.8, 152.9, 151.4, 138.1, 135.5, 134.7, 129.9, 129.6, 120.8, 47.9, 38.6.

Synthesis of 5-chloro-2-(4-(4-chloro-3,5-dimethylphenoxy)benzyl)-N-((4-chlorophenyl)sulfonyl)- 2H-indazole-3-carboxamide (14a): Follow General Procedure 2 with 5 and 13a. The product was purified via flash column chromatography, eluting with CH_2Cl_2/MeOH/NH_4OH, 92:7:1 (yield = 55%); white solid; 1H NMR (400 MHz, d6-DMSO) δ 8.21 (s, 1H), 7.89 (d, J = 8.4, 2H), 7.69 (d, J = 9.6, 1H), 7.51 (d, J = 8.4, 2H), 7.27 (dd, J = 9.6, 1.6, 1H), 7.19 (d, J = 8.8, 2H), 6.86-6.82 (m, 4H), 6.03 (s, 2H), 2.29 (s, 6H); 13C NMR (400 MHz, d6-DMSO) δ 156.7, 154.7, 145.5, 137.9, 136.2, 132.7, 130.3 (2), 129.6 (2), 128.5 (2), 127.7, 127.1, 122.9, 122.1, 119.8, 119.5, 118.4, 109.5, 54.7, 20.8; HRMS-ESI: m/z found 612.0293 [M+H]+, $C_{29}H_{21}Cl_3N_3O_4S$ requires 612.0324.

Synthesis of 5-chloro-2-(4-(4-chloro-3,5-dimethylphenoxy)benzyl)-N-((4-morpholino-3-nitrophenyl)sulfonyl)-2H-indazole-3-carboxamide (14b): Follow General Procedure 2 with 5 and 13b. The product was purified via flash column chromatography, eluting with CH_2Cl_2/MeOH/NH_4OH, 92:7:1 (yield = 42%): yellow solid; 1H NMR (400 MHz, DMSO) δ 8.27 (d, J = 8.0, 2H), 8.00 (d, J = 8.8, 1H), 7.67 (d, J = 9.2, 1H), 7.31 (d, J = 8.8, 1H), 7.26-7.23 (m, 3H), 6.85-6.84 (m, 4H), 6.08 (s, 2H), 3.66 (s, 4H), 3.03 (s, 4H), 2.29 (s, 6H); 13C NMR (400 MHz, DMSO) δ 156.5, 154.8, 146.8, 145.5, 139.5, 139.8, 137.8, 132.9 (2), 130.4, 128.6, 127.5, 126.9, 125.8, 123.0, 122.4, 120.4, 119.7, 119.3 (2), 118.6 (2), 66.3 (2), 51.3, 20.7; HRMS-ESI: m/z found 708.1098 [M+H]+, $C_{33}H_{28}Cl_2N_5O_7S$ requires 708.1092.

Synthesis of 5-chloro-2-(4-(4-chloro-3,5-dimethylphenoxy)benzyl)-N-((4-((morpholinoethyl)amino)-3-nitrophenyl)sulfonyl)-2H-indazole-3-carboxamide (14c): Follow General Procedure 2 with 5 and 13c. The product was purified via flash column chromatography, eluting with CH_2Cl_2/MeOH/NH_4OH, 92:7:1 (yield = 44%): yellow solid; 1H NMR (400 MHz, DMSO) δ 8.64 (s, br, 1H), 8.58 (s, 1H), 8.29 (s, 1H), 8.97 (d, J = 8.0, 1H), 7.64 (d, J = 9.6, 1H), 7.27-7.22 (m, 3H), 7.07 (d, J = 7.6, 1H), 6.85-6.83 (m, 4H), 6.11 (s, 2H), 3.58 (s, br, 4H), 3.42 (s, br, 2H), 2.60 (s, br, 2H), 2.42 (s, br, 4H), 2.28 (s, 6H); 13C NMR (400 MHz, DMSO) δ = 163.7, 156.4, 154.8, 146.2, 145.5, 137.8, 135.3, 133.1, 132.7, 132.0, 130.4 (2), 128.6, 127.3, 126.9, 126.1, 123.0 (2), 122.6, 119.6, 119.2, 118.6, 114.6, 66.5, 55.6, 54.6, 53.0, 20.7; HRMS-ESI: m/z found 751.1571 [M+H]+, $C_{35}H_{33}Cl_2N_6O_7S$ requires 751.1514.

Synthesis of 5-chloro-2-(4-(4-chloro-3,5-dimethylphenoxy)benzyl)-N-((4-((furan-2-ylmethyl)amino)-3-nitrophenyl)sulfonyl)-2H-indazole-3-carboxamide (14d): Follow

General Procedure 2 with 5 and 13d. The product was purified via flash column chromatography, eluting with CH_2Cl_2/MeOH/NH_4OH, 92:7:1 (yield = 56%): yellow solid; 1H NMR (400 MHz, DMSO) δ 8.73 (m, 1H), 8.58 (s, 1H), 8.25 (s, 1H), 7.94 (d, J = 8.4, 1H), 7.66 (d, J = 8.4, 1H), 7.58 (s, 1H), 7.26-7.24 (m, 3H), 7.19 (d, J = 9.6, 1H), 6.84-6.83 (m, 4H), 6.38 (s, 2H), 6.08 (s, 2H), 4.65 (d, J = 6.4, 2H), 2.28 (s, 6H); 13C NMR (400 MHz, DMSO) δ 163.3, 156.5, 154.8, 151.5, 146.0, 145.5, 143.1, 137.8, 135.0, 133.0, 132.5, 130.3, 128.6, 127.5, 127.0, 126.2, 124.8, 123.7, 123.0, 122.4, 119.7, 119.3, 118.6, 118.2, 114.7, 110.9, 108.2, 54.6, 20.7; HRMS-ESI: m/z found 718.0912 [M- H]-, $C_{34}H_{26}Cl_2N_5O_7S$ requires 718.0935.

Synthesis of 5-chloro-2-(4-(4-chloro-3,5-dimethylphenoxy)benzyl)-N-((4-((2-(furan-2-yl)ethyl)amino)-3-nitrophenyl)sulfonyl)-2H-indazole-3-carboxamide (14e): Follow General Procedure 2 with 5 and 13e. The product was purified via flash column chromatography, eluting with CH_2Cl_2/MeOH/NH_4OH, 92:7:1 (yield = 54%): yellow solid; 1H NMR (400 MHz, d6-DMSO) δ 8.64 (s, 1H), 8.61 (br, 1H), 8.03 (s, 1H), 7.98 (d, J = 9.2 Hz, 1H), 7.79 (d, J = 8.4 Hz, 1H), 7.56 (s, 1H), 7.36 (d, J = 9.6 Hz, 1H), 7.21 (d, J = 9.2 Hz, 1H), 7.15 (d, J = 8.4 Hz, 2H), 6.81 (d, J = 8.0 Hz, 5H), 6.37 (s, 1H), 6.24 (d, J = 3.2 Hz, 1H), 5.93 (s, 2H), 3.68 (q, J = 6.4 Hz, 2H), 2.99 (t, J = 7.2 Hz, 2H), 2.29 (s, 6H); 13C NMR (400 MHz, d6-DMSO) δ 161.2, 156.6, 154.7, 152.7, 146.9, 145.5, 142.4 (2), 137.8, 135.0, 133.5, 132.4, 130.2, 127.4, 127.2, 122.7, 121.3, 120.1, 119.2, 118.6, 114.8, 112.0, 111.0 (2), 107.1 (2), 55.0, 41.7, 27.3, 20.7; HRMS-ESI: m/z found 732.1071 [M+H]+, $C_{35}H_{28}Cl_2N_5O_7S$ requires 732.1092.

Synthesis of 5-chloro-2-(4-(4-chloro-3,5-dimethylphenoxy)benzyl)-N-((4-(((1-methyl-1H-pyrazol- 3-yl)methyl)amino)-3-nitrophenyl)sulfonyl)-2H-indazole-3-carboxamide

(14f): Follow General Procedure 2 with 5 and 13f. The product was purified via flash column chromatography, eluting with CH_2Cl_2/MeOH/NH_4OH, 92:7:1 (yield = 44%): yellow solid; 1H NMR (400 MHz, d6-DMSO) δ 8.69 (t, J = 5.6 Hz, 1H), 8.61 (s, 1H), 8.21 (s, 1H), 7.97 (d, J = 9.6 Hz, 1H), 7.71 (s, 1H), 7.69 (s, 1H), 7.45 (s, 1H), 7.31 (s, 2H), 7.24 (d, J = 8.4 Hz, 2H), 7.18 (t, J = 4.0 Hz, 2H), 7.05 (s, 1H), 6.84 (d, J = 7.2 Hz, 4H), 6.06 (s, 2H), 4.46 (d, J = 5.6 Hz, 2H), 3.78 (s, 3H), 2.29 (s, 6H); 13C NMR (400 MHz, d6-DMSO) δ 156.5, 154.8, 146.2, 145.5, 138.4, 137.8, 135.1, 132.8, 130.3 (2), 130.0, 128.6, 127.7, 127.1, 126.5, 122.9, 122.1, 119.8, 119.3, 118.6, 117.8, 114.8, 54.7, 46.2, 41.8, 40.6, 38.9, 37.4, 20.7; HRMS-ESI: m/z found 732.1189 [M+H]+, $C_{34}H_{28}Cl_2N_7O_6S$ requires 732.1204.

Synthesis of 5-chloro-2-(4-(4-chloro-3,5-dimethylphenoxy)benzyl)-N-((3-nitro-4-((pyridin-3- ylmethyl)amino)phenyl)sulfonyl)-2H-indazole-3-carboxamide (14g): Follow General Procedure 2 with 5 and 13g. The product was purified via flash column chromatography, eluting with CH_2Cl_2/MeOH/NH_4OH, 92:7:1 (yield = 39%): yellow solid; 1H NMR (400 MHz, DMSO) δ 8.94 (t, J = 6.2, 1H), 8.64 (s, br, 1H), 8.59 (s, 1H), 8.45 (s, br, 1H), 8.23 (s, 1H), 7.89 (d, J = 8.4 Hz, 1H), 7.78 (d, J = 8.0 Hz, 1H), 7.64 (d, J = 9.6 Hz, 1H), 7.34 (m, 1H), 7.26-7.22 (m, 3H), 7.00 (d, J = 9.6 Hz, 1H), 6.85-6.83 (m, 4H), 6.09 (s, 2H), 4.69 (d, J = 6.4 Hz, 2H), 2.28 (s, 6H); 13C NMR (400 MHz, d6-DMSO) δ = 163.7, 156.5, 154.8, 148.8, 148.5, 145.9, 145.5, 137.8, 135.6, 135.1 (2), 133.1, 133.0, 131.9, 130.4, 128.6, 127.3, 126.9, 126.1, 123.0, 122.6, 119.6, 119.3, 118.6 (2), 114.6 (2), 54.5, 43.8, 20.7; HRMS-ESI: m/z found 731.1294 [M+H]+, $C_{35}H_{29}Cl_2N_6O_6S$ requires 731.1241.

Synthesis of 5-chloro-2-(4-(4-chloro-3,5-dimethylphenoxy)benzyl)-N-((3-nitro-4-((2-(pyridin-3- yl)ethyl)amino)phenyl)sulfonyl)-2H-indazole-3-carboxamide (14h): Follow General Procedure 2 with 5 and 13h. The product was purified via flash column chromatography, eluting with CH_2Cl_2/MeOH/NH_4OH, 50:7:1 (yield = 35%): yellow solid; 1H NMR (400 MHz, d6-DMSO) δ 8.63 (s, 1H), 8.60 (s, 1H), 8.55 (d, J = 4.0 Hz, 1H), 8.44 (t, J = 5.8 Hz, 1H), 8.29 (s, 1H), 7.99 (d, J = 8.4 Hz, 1H), 7.93 (d, J = 7.6 Hz, 1H), 7.67 (d, J = 8.4 Hz, 1H), 7.52 (t, J = 6.2 Hz, 1H), 7.37 (1H), 7.29-7.23 (m, 4H), 7.12 (s, 1H), 6.86 (d, J = 8.8 Hz, 2H), 6.82 (s, 2H), 6.11 (s, 2H), 3.69 (q, J = 6.4 Hz, 2H), 3.01 (t, J = 7.4 Hz, 2H), 2.27 (s, 6H); 13C NMR (400 MHz, d6-DMSO) δ 168.1, 161.2, 159.6, 153.0, 150.9, 150.8, 150.2, 144.2, 142.5 (2), 140.7, 140.1, 137.8, 137.2, 136.5, 135.1 (2), 132.1, 131.7, 131.1, 129.5, 127.7, 127.2, 124.4, 123.9, 123.4, 119.2, 59.3, 48.4, 36.5, 25.5; HRMS-ESI: m/z found 745.14.14 [M+H]+, $C_{36}H_{31}Cl_2N_6O_6S$ requires 745.1397.

Synthesis of 5-chloro-2-(4-(4-chloro-3,5-dimethylphenoxy)benzyl)-N-((3-nitro-4-((pyridin-4- ylmethyl)amino)phenyl)sulfonyl)-2H-indazole-3-carboxamide (14i): Follow General Procedure 2 with 5 and 13i. The product was purified via flash column chromatography, eluting with CH_2Cl_2/MeOH/NH_4OH, 75:14:2 (yield = 37%): yellow solid; 1H NMR (400 MHz, d6-DMSO) δ 9.06 (bs, 1H), 8.70 (bs, 1H), 8.67 (d, J = 18.0 Hz, 2H), 8.22 (s, 1H), 7.89 (d, J = 9.2 Hz, 1H), 7.74 (bs, 2H), 7.68 (d, J = 8.8 Hz, 1H), 7.26 (d, J = 8.8 Hz, 3H), 6.86 (d, J = 3.2 Hz, 5H), 6.08 (s, 2H), 4.89 (d, J = 4.8 Hz, 2H), 2.30 (s, 6H); 13C NMR (400 MHz, d6-DMSO) δ 163.0, 156.5, 155.9, 154.8, 145.9, 145.5, 144.9, 137.8, 135.1, 132.9, 132.5, 131.1, 130.9, 130.3, 128.6, 127.6, 127.0, 126.5, 124.3, 122.9, 122.2, 119.8, 119.3, 118.6, 114.6, 71.5, 45.6, 20.8; HRMS-ESI: m/z found 729.1091 [M+H]+, $C_{35}H_{27}Cl_2N_6O_6S$ requires 729.1095.

Synthesis of 5-chloro-2-(4-(4-chloro-3,5-dimethylphenoxy)benzyl)-N-((3-nitro-4-((2-(pyridin-4- yl)ethyl)amino)phenyl)sulfonyl)-2H-indazole-3-carboxamide (14j): Follow General Procedure 2 with 5 and 13j. The product was purified via flash column chromatography, eluting with CH_2Cl_2/MeOH/NH_4OH, 50:7:1 (yield = 39%): yellow solid; 1H NMR (400 MHz, d6-DMSO) δ 8.66 (d, J = 4.8 Hz, 2H), 8.30 (s, 1H), 8.24 (t, J = 6.0 Hz, 1H), 8.12 (d, J = 8.4 Hz, 1H), 7.73 (d, J = 5.6 Hz, 2H), 7.68 (d, J = 9.6 Hz, 2H), 7.31-7.23 (m, 4H), 7.11 (d, J = 8.4 Hz, 1H), 6.84 (t, J = 3.8 Hz, 4H), 6.11 (s, 2H), 3.75 (q, J = 6.0 Hz, 2H), 3.20 (t, J = 7.0 Hz, 2H), 2.29 (s, 6H); 13C NMR (400 MHz, d6-DMSO) δ 168.6, 161.2, 160.4, 159.5, 157.3, 150.3, 149.7, 149.1, 142.6, 137.7, 136.8, 136.5, 134.9 (2), 132.2, 131.8, 131.7, 131.3, 127.8, 127.3, 124.5, 124.1, 123.3 (2), 118.5, 59.4, 47.7, 39.0, 25.5; HRMS-ESI: m/z found 743.1244 [M+H]+, $C_{36}H_{29}Cl_2N_6O_6S$ requires 743.1252.

Synthesis of 5-chloro-2-(4-(4-chloro-3,5-dimethylphenoxy)benzyl)-N-((3-morpholino-4-nitrophenyl)sulfonyl)-2H-indazole-3-carboxamide (14k): Follow General Procedure 2 with 5 and 13k. The product was purified via flash column chromatography, eluting with CH_2Cl_2/MeOH/NH_4OH, 92:7:1 (yield = 57%): yellow solid; 1H NMR (400 MHz, d6-DMSO) δ 8.29 (s, 1H), 7.86 (d, J = 8.8 Hz, 1H), 7.76 (s, 1H), 7.67 (d, J = 9.2 Hz, 1H), 7.57 (d, J = 9.2 Hz, 1H), 7.25 (d, J = 9.2 Hz, 3H), 6.87 (d, J = 11.2 Hz, 4H), 6.09 (s, 2H), 3.66 (bs, 4H), 2.98 (bs, 4H), 2.28 (s, 6H); 13C NMR (400 MHz, d6-DMSO) δ 168.0, 163.9, 156.6, 154.7, 150.5, 145.6, 144.9, 143.7, 137.9, 133.0, 131.6, 130.3, 128.7, 127.5, 127.0, 125.9, 123.0, 122.5, 120.7 (2), 119.7, 119.4, 118.5, 66.4, 51.8, 20.7; HRMS-ESI: m/z found 708.1098 [M+H]+, $C_{33}H_{28}Cl_2N_5O_7S$ requires 708.1092.

Synthesis of 5-chloro-2-(4-(4-chloro-3,5-dimethylphenoxy)benzyl)-N-((3-((furan-2-ylmethyl)amino)-4-nitrophenyl)sulfonyl)-2H-indazole-3-carboxamide (14l): Follow General Procedure 2 with 5 and 13l. The product was purified via flash column chromatography, eluting with CH_2Cl_2/MeOH/NH_4OH, 92:7:1 (yield = 50%): yellow solid; 1H NMR (400 MHz, d6-DMSO) δ 8.53 (t, J = 5.8 Hz, 1H), 8.31 (s, 1H), 8.10 (d, J = 8.8 Hz, 1H), 7.67 (d, J = 9.2 Hz, 1H), 7.61 (s, 1H), 7.48 (s, 1H), 7.27 (d, J = 8.0 Hz, 3H), 7.11 (d, J = 9.2 Hz, 1H), 6.86 (t, J = 8.0 Hz, 4H), 6.29 (d, J = 2.4 Hz, 1H), 6.19 (s, 1H), 6.10 (s, 2H), 4.60 (d, J = 5.6 Hz, 2H), 2.28 (s, 6H); 13C NMR (400 MHz, d6-DMSO) δ 163.8, 156.5, 154.8, 152.9, 151.5, 145.5, 144.6, 142.9 (2), 137.8, 133.1, 132.2, 131.7, 130.2, 128.6, 127.4, 126.94, 126.9, 123.1, 122.6, 119.7, 119.3, 118.6, 114.1, 113.3, 110.8, 108.2, 40.6, 20.7; HRMS-ESI: m/z found 720.1048 [M+H]+, $C_{34}H_{28}Cl_2N_5O_7S$ requires 720.1081.

Synthesis of 5-chloro-2-(4-(4-chloro-3,5-dimethylphenoxy)benzyl)-N-((3-((2-(furan-2-yl)ethyl)amino)-4-nitrophenyl)sulfonyl)-2H-indazole-3-carboxamide (14m): Follow General Procedure 2 with 5 and 13m. The product was purified via flash column chromatography, eluting with CH_2Cl_2/MeOH/NH_4OH, 92:7:1 (yield = 52%): yellow solid; 1H NMR (400 MHz, d6-DMSO) δ 8.27 (br, 1H), 8.24 (s, 1H), 8.14 (d, J = 9.6 Hz, 1H), 7.72 (d, J = 8.8 Hz, 1H), 7.62 (s, 1H), 7.51 (s, 1H), 7.30 (d, J = 10.0 Hz, 1H), 7.27 (s, 1H), 7.23 (d, J = 8.8 Hz, 2H), 7.10 (d, J = 9.2 Hz, 1H), 6.84 (d, J = 6.0 Hz, 4H), 6.34 (s, 1H), 6.21 (d, J = 3.2 Hz, 1H), 6.05 (s, 2H), 3.66 (q, J = 4.4 Hz, 2H), 3.05 (t, J = 6.6 Hz, 2H), 2.23 (s, 6H); 13C NMR (400 MHz, d6-DMSO) δ 187.3, 162.9, 156.6, 154.7, 152.8, 145.5, 144.6, 142.3 (2), 137.8, 132.7, 132.2, 130.2, 128.6, 127.9, 127.2, 127.1,

122.9, 122.1, 119.9, 119.3, 118.5, 113.6 (2), 110.9, 106.9, 54.8, 41.7, 27.2, 20.7; HRMS-ESI: m/z found 732.1071 [M+H]+, $C_{35}H_{28}Cl_2N_5O_7S$ requires 732.1092.

Synthesis of 5-chloro-2-(4-(4-chloro-3,5-dimethylphenoxy)benzyl)-N-((3-(((1-methyl-1H-pyrazol- 3-yl)methyl)amino)-4-nitrophenyl)sulfonyl)-2H-indazole-3-carboxamide (14n): Follow General Procedure 2 with 5 and 13n. The product was purified via flash column chromatography, eluting with CH_2Cl_2/MeOH/NH_4OH, 92:7:1 (yield = 47%): yellow solid; 1H NMR (400 MHz, d6-DMSO) δ 8.42 (t, J = 5.6 Hz, 1H), 8.33 (s, 1H), 8.11 (d, J = 9.6 Hz, 1H), 7.67 (t, J = 11.8 Hz, 3H), 7.45 (s, 1H), 7.28 (t, J = 7.0 Hz, 3H), 7.08 (d, J = 8.8 Hz, 1H), 6.88 (d, J = 8.4 Hz, 2H), 6.85 (s, 2H), 6.14 (s, 2H), 4.44 (d, J = 4.4 Hz, 2H), 3.71 (s, 3H), 2.29 (s, 6H); 13C NMR (400 MHz, d6-DMSO) δ 163.8, 156.5, 152.9, 145.5, 144.6, 138.5 (2), 137.8 (2), 133.1, 131.8, 130.2, 130.0, 128.6, 127.4, 126.9 (2), 123.1, 122.6, 119.7, 119.3, 118.6, 118.0, 113.7, 113.5, 54.6, 38.8, 37.4, 20.7; HRMS-ESI: m/z found 732.1189 [M+H]+, $C_{34}H_{28}Cl_2N_7O_6S$ requires 732.1204.

Synthesis of 5-chloro-2-(4-(4-chloro-3,5-dimethylphenoxy)benzyl)-N-((4-nitro-3-((pyridin-3- ylmethyl)amino)phenyl)sulfonyl)-2H-indazole-3-carboxamide (14o): Follow General Procedure 2 with 5 and 13o. The product was purified via flash column chromatography, eluting with CH_2Cl_2/MeOH/NH_4OH, 92:7:1 (yield = 40%): yellow solid; 1H NMR (400 MHz, d6-DMSO) δ 8.72 (s, 1H), 8.25 (s, 1H), 8.11 (d, J = 8.4 Hz, 1H), 7.74 (bs, 2H), 7.68 (d, J = 8.4 Hz, 1H), 7.45 (s, 1H), 7.25 (d, J = 7.6 Hz, 4H), 7.08 (d, J = 8.8 Hz, 1H), 6.85 (t, J = 7.2 Hz, 4H), 6.07 (s, 2H), 4.66 (s, 2H), 2.27 (s, 6H); 13C NMR (400 MHz, CDCl3) δ = 168.5, 161.2, 159.5, 157.7, 153.6, 153.2, 150.3, 149.3, 142.6, 140.3 (2), 139.2, 137.8, 137.1, 136.4, 135.0, 132.2, 131.7, 128.8, 128.4, 127.8,

127.4, 124.4, 124.1, 123.3, 118.7, 118.1, 59.4, 48.8, 25.5; HRMS-ESI: m/z found 731.1176 [M+H]+, $C_{35}H_{29}Cl_2N_6O_6S$ requires 731.1241.

Synthesis of 5-chloro-2-(4-(4-chloro-3,5-dimethylphenoxy)benzyl)-N-((4-nitro-3-((2-(pyridin-3- yl)ethyl)amino)phenyl)sulfonyl)-2H-indazole-3-carboxamide (14p): Follow General Procedure 2 with 5 and 13p. The product was purified via flash column chromatography, eluting with CH_2Cl_2/MeOH/NH_4OH, 50:7:1 (yield = 38%): yellow solid; 1H NMR (400 MHz, d6-DMSO) δ 8.31 (s, 1H), 8.23 (t, J = 5.6 Hz, 1H), 8.11 (d, J = 8.4 Hz, 1H), 7.88 (d, J = 8.0 Hz, 1H), 7.72 (s, 1H), 7.67 (d, J = 9.2 Hz, 1H), 7.46 (s, 1H), 7.33 (s, 1H), 7.25 (d, J = 10.8 Hz, 3H), 7.21 (s, 1H), 7.11 (d, J = 9.2 Hz, 1H), 6.83 (d, J = 8.4 Hz, 4H), 6.10 (s, 2H), 3.68 (q, J = 7.2 Hz, 2H), 3.07 (t, J = 7.0 Hz, 2H), 2.29 (s, 6H); 13C NMR (400 MHz, d6-DMSO) δ 168.6, 161.2, 159.5, 157.4, 153.0, 150.8, 150.3, 149.3, 143.9, 142.6, 137.7, 136.7, 136.5, 134.9, 133.4, 132.2, 131.8, 131.7, 129.6, 127.8, 127.3, 124.5, 124.1, 123.2, 118.5, 118.4, 76.1, 59.4, 48.5, 36.3, 25.5; HRMS-ESI: m/z found 745.1414 [M+H]+, $C_{36}H_{31}Cl_2N_6O_6S$ requires 745.1397.

Synthesis of 5-chloro-2-(4-(4-chloro-3,5-dimethylphenoxy)benzyl)-N-((4-nitro-3-((pyridin-4- ylmethyl)amino)phenyl)sulfonyl)-2H-indazole-3-carboxamide (14q): Follow General Procedure 2 with 5 and 13q. The product was purified via flash column chromatography, eluting with CH_2Cl_2/MeOH/NH_4OH, 75:14:2 (yield = 35%): yellow solid; 1H NMR (400 MHz, d6-DMSO) δ 8.83 (t, J = 6.2 Hz, 1H), 8.63 (d, J = 5.2 Hz, 2H), 8.24 (s, 1H), 8.17 (d, J = 8.4 Hz, 1H), 7.77 (d, J = 5.6 Hz, 2H), 7.69 (d, J = 8.8 Hz, 1H), 7.30-7.23 (m, 4H), 7.14 (d, J = 8.0 Hz, 1H), 6.90-6.86 (m, 4H), 6.04 (s, 2H), 4.88 (d, J = 6.4 Hz, 2H), 2.30 (s, 6H); 13C NMR (400 MHz, d6-DMSO) δ 168.4, 161.3, 159.5, 157. 6, 150.2, 149.8, 148.9, 142.6 (2), 137.8, 136.3, 134.9, 132.2, 131.9, 131.7, 128.9 (2),

127.7, 127.3, 124.5, 124.1, 123.6, 123.4, 119.1, 118.0, 59.3, 50.4, 25.5; HRMS-ESI: m/z found 729.1091 [M+H]+, $C_{35}H_{27}Cl_2N_6O_6S$ requires 729.1095.

Synthesis of 5-chloro-2-(4-(4-chloro-3,5-dimethylphenoxy)benzyl)-N-((4-nitro-3-((2-(pyridin-4- yl)ethyl)amino)phenyl)sulfonyl)-2H-indazole-3-carboxamide (14r): Follow General Procedure 2 with 5 and 13r. The product was purified via flash column chromatography, eluting with CH_2Cl_2/MeOH/NH_4OH, 50:7:1 (yield = 36%): yellow solid; 1H NMR (400 MHz, d6-DMSO) δ 8.65 (d, J = 4.0 Hz, 2H), 8.61 (s, 1H), 8.43 (t, J = 5.4 Hz, 1H), 8.29 (s, 1H), 8.02 (d, J =9.6 Hz, 1H), 7.67 (d, J = 8.8 Hz, 1H), 7.64 (d, J = 4.8 Hz, 2H), 7.30-7.24 (m, 5H), 6.73 (d, J = 8.8 Hz, 2H), 6.82 (s, 2H), 6.12 (s, 2H), 3.73 (q, J = 6.4 Hz, 2H), 3.09 (t, J = 7.2 Hz, 2H), 2.27 (s, 6H); 13C NMR (400 MHz, d6-DMSO) δ 168.1, 161.2, 159.6, 158.3, 151.1, 150.8, 150.2, 142.6 (2), 140.1, 137.8, 137.2, 136.4, 135.1, 134.8, 132.1, 131.7, 131.1, 130.9, 127.7, 127.3, 124.4, 123.9, 123.4, 119.2, 59.3, 47.6, 39.0, 25.5; HRMS-ESI: m/z found 745.1414 [M+H]+, $C_{36}H_{31}Cl_2N_6O_6S$ requires 745.1397.

Chapter 5: Synthesis of FLT3 Inhibitors Through Multiple Molecular Strategies

5.1 The polypharmacy combination of the BCL-2 inhibitor venetoclax (VEN) and the FLT3 inhibitor gilteritinib (GIL) is more active in acute myeloid leukemia cells than novel polypharmacologic BCL-2/FLT3 VEN–GIL hybrid single-molecule inhibitors.

5.1.1 Introduction

Presently, most patients with acute myeloid leukemias (AMLs) are not cured, due at least in part to the varied molecular mechanisms and cellular heterogeneity of AML cases.[165] Further, current AML treatment regimens have unacceptable short- and long-term toxicities/side effects.[166] Thus, it is widely held that new drugs, with greater efficacies but less toxicities, are urgently needed, and that targeted inhibitors may provide selective antileukemic efficacy with less off-target toxicity than traditional antineoplastic drugs.[165,166] To address the multiple mechanisms of AMLs with targeted drugs, two prominent AML "driver" oncogenes – *e.g.*, B-cell lymphoma (BCL-2) and FMS-like tyrosine kinase 3 (FLT3) – are being targeted together in patients (*e.g.* NCT03625505). BCL-2 is one of five anti-apoptotic proteins, also including BCL-x_L and MCL-1, within the "BCL-2 family" that also contains multiple pro-apoptotic proteins, such as BAK, BAX, BIM and PUMA.[3] These opposing sub-families antagonize each others' effects through an intermolecular protein–protein interaction (PPI) between a BH3 "death domain" on a pro-apoptotic BCL-2 family member and the BH3-binding groove on the surface of an anti-apoptotic BCL-2 family member. Near the turn of the last century, the development of inhibitors of PPIs, such as BCL-2/BAK, was unchartered territory

compared with the more traditional drug discovery of targeting enzyme active sites, such as the ATP-binding site of the FLT3 receptor tyrosine kinase (RTK).[179] Devoid of any well-defined pockets that could be exploited by small-molecules, there was much doubt about whether such a feat could be accomplished by low molecular weight ligands, given the large, solvent-exposed and often featureless interfaces found between BCL-2/BAK and other PPIs.[152,168] Despite this skepticism, in the early 2000s, there was intense research into the development of BCL-2 (and BCL-x_L) inhibitors, pioneered largely by Stephen Fesik and colleagues at Abbvie. In an impressive feat of molecular engineering coupled with NMR-guided fragment screening, they first discovered the dual BCL-2/BCL-x_L inhibitor ABT-737, and its clinical counterpart ABT-263, later known as navitoclax, in the mid-2000s[152] shortly followed by its BCL-2-selective congener ABT-199, later known as venetoclax (VEN, **1**).[157] A picomolar BCL-2 inhibitor (K_i < 0.01 nM), VEN displaces sequestered pro-apoptotic BCL-2 proteins, including BH3-only proteins such as BIM and PUMA, and also the multi-domain BH1-3 pro-apoptotic BCL-2 proteins BAK and BAX, which (a) themselves are activated by BH3-only proteins, and (b) once freed, may oligomerize to cause mitochondrial outer membrane permeabilization, then a caspase cascade and cell death.[152]

FLT3 mutations are observed in about one-third of AML cases.[168] Most of these (~25% of all AML cases) are internal tandem duplication (ITD) mutations that promote dimerization of FLT3 monomers, resulting in constitutive activation of the FLT3 RTK, downstream cellular signaling via multiple molecular pathways, and switching on survival, proliferation and differentiation of cells, among other biological effects.[169] In addition, constitutively activating tyrosine kinase domain (TKD) mutations are also

observed, but less commonly (~7% of all AML cases).[168,169] Together, these FLT3 ITD and TKD mutations stimulated research into the discovery and development of FLT3 inhibitors, which presented a different obstacle to surmount than that of BCL-2 inhibitor design: that is, how to *selectively* target the ATP-binding pocket of FLT3, which is highly conserved across the hundreds of kinases.[170] Nevertheless, fierce medicinal chemistry research programs produced several potent and highly selective FLT3 inhibitors.[171,52] Type I FLT3 inhibitors bind the ATP-binding site of both the active and inactive conformations of FLT3, and are effective against both FLT3-ITD and FLT3-TKD mutations. Type II inhibitors bind a hydrophobic region adjacent to the ATP-binding site that is accessible only in the monomeric form of FLT3; consequently Type II inhibitors stabilize the protein in this inactive form. Since many TKD mutations favour the active form, this imparts resistance to Type II inhibitors, with the result that Type II inhibitors are effective against only FLT3-ITD mutations.[168,171,52] Since the majority of RTK inhibitors (RTKi's) are competitive with ATP, absolute selectivity is highly challenging, and most RTKi's bind strongly to one or more tyrosine kinase (TK) in addition to the desired target. Gilteritinib (GIL, **2**) is a highly potent Type I FLT3 inhibitor (IC_{50} = 0.29 nM), which also potently inhibits the TK AXL (IC_{50} = 0.73 nM). GIL has received FDA approval for AML as part of a "7 + 3" induction regimen (i.e. in combination with the standard AML regimen of cytarabine plus an anthracycline) or in combination with high-dose cytarabine (another standard AML treatment).[64] Other FLT3i's that have been approved for clinical treatment of AML include midostaurin (Type I) and quizartinib (Type II).[171,52]

VEN, in combination with decitabine, azacitidine, or low-dose cytarabine, has been approved for the treatment of adults with newly diagnosed AML who are ineligible for intensive standard chemotherapy regimens based on age >75 years or other clinical features predicting severe toxic side effects with standard AML chemotherapy regimens.[172] VEN is also being investigated in hundreds of clinical trials for leukemias and other cancers, especially in combinations.[173] A primary mechanism of resistance to VEN is via cellular overexpression of the anti-apoptotic BCL-2 family protein MCL-1, which, functionally similarly to BCL-2's mechanism of action in cancers, sequesters pro-death BCL-2 proteins, such as BIM and BAX. Zhu *et al.* demonstrated synergy between VEN and GIL in FLT3-ITD AML cells.[174] Similar findings have been reported by Brinton and colleagues,[175] and this phenomenon is due, in part, to FLT3i-induced downregulation of MCL-1 via the ERK pathway, which bolsters the antileukemic effect of VEN. Further, a recently-completed phase 1b clinical trial (NCT03625505) of VEN + GIL in patients with relapsed/refractory AML reported impressive response rates.

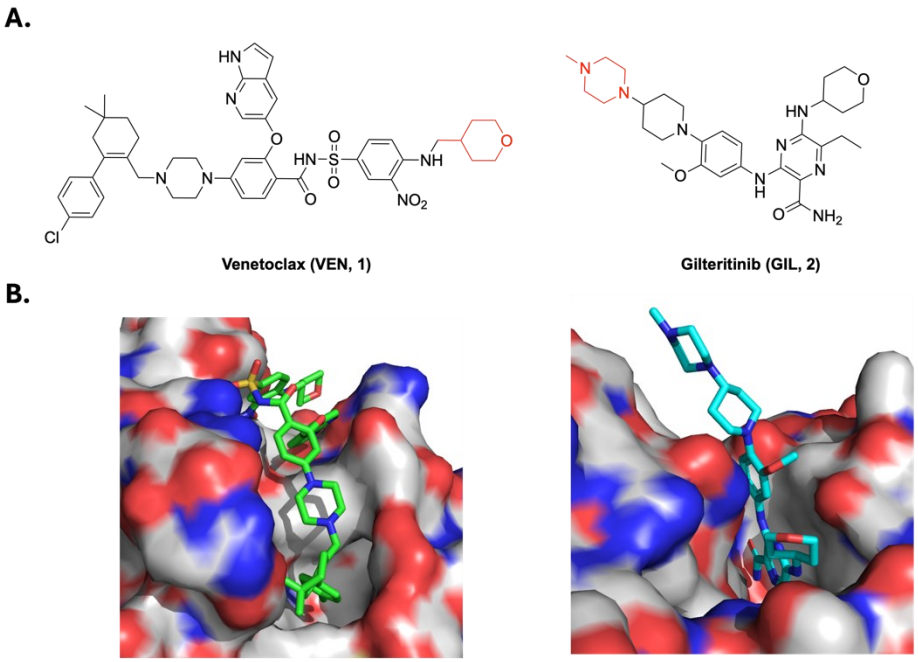

Figure 5.1.1.1: A. *Structures of the BCL-2 inhibitor VEN (**1**) and the FLT3 inhibitor GIL (**2**), solvent-exposed tetrahydropyran and piperazine motifs, respectively, highlighted in red;* ***B.*** *Co-crystal structures of (left)* ***1*** *(green) bound to BCL-2 (PDB ID: 6O0p[189]) and (right)* ***2*** *(cyan) bound to FLT3 (PDB ID: 6jqr), Connolly-surfaces coloured by atom type), rendered in PyMOL.*

As previously indicated, given the disparate molecular mechanisms of AML cases, clinical treatment regimens comprise combinations of drugs, or "drug cocktails," also called "polypharmacy." Polypharmacology instead involves the development of single drugs designed to inhibit two or more target proteins, which may be accomplished by linking together ligands for multiple protein targets, or by merging several ligands together, and has been promoted as hypothetically superior to the corresponding combination of drugs from which the polypharmacological agent was derived. Potential benefits of polypharmacology are the guaranteed (barring destructive metabolism) co-delivery of both ligands to a specific cell, which might maximize synergies of inhibiting both targets, and increased patient compliance due to simplified dosing regimens.[176] On

the other hand, advantages of polypharmacy include the ability to manipulate patient dosing of each drug individually, that the single-target inhibitors are generally smaller molecules with superior bioavailabilities, and that polypharmacy may be preferred when the two biological targets are localized to different cellular compartments. Herein, we describe our discovery of polypharmacologic VEN–GIL hybrid molecules, and explore their inhibition of AML cell lines, as compared to to the combination of VEN + GIL.

5.1.2 Design Rationale

As part of our long-standing interest in targeting the BCL-2 family of proteins,[152,183] coupled with potential advantages of polypharmacology,[184,187] we hypothesized that dual BCL-2/FLT3 inhibitors created by tethering VEN to GIL would be more potent in vitro than either of the parent drugs alone. However, since FLT3 is located on the extracellular surface of the cell, whilst BCL-2 is located within the cell, we did not anticipate that our dual inhibitors would outperform the combination of the parent drugs in vitro, since simultaneous occupation of both these targets by a single molecule is not feasible, unless transient inhibition of FLT3 extracellularly by the polypharmacologic agent *en route* to BCL-2 within the cell is adequate to downregulate MCL-1 and/or activate BIM.[174,175] Rather, the greatest benefit of a polypharmacology strategy in this particular context, may not be observed until clinical evaluation, to assess factors such as potential improved patient compliance with the polypharmacology approach. Although there is precedent for dual FLT3 inhibitors,[188] those molecules encompass a single ligand that recognizes both targets, whereas our strategy involves the linking of two individual ligands into a single molecule. Moreoever, to the best of our knowledge, there are no known dual BCL-2/FLT3 inhibitors reported in the literature. Inspection of the co-crystal structures of (a)

VEN with BCL-2 (PDB ID: 6O0p[189]), and (b) GIL with FLT3 (PDB ID: 6jqr) revealed in both cases that there are solvent-exposed domains of each inhibitor (VEN: tetrahydropyran; GIL: piperazine; highlighted in red) that might provide grafting points where the tethered molecule might have a minimally deleterious impact on target protein binding affinity (**Figure 5.1.1.1**). To our knowledge, there is no co-crystal structure of GIL bound to AXL, but we reasoned that, given its highly polar nature, GIL's piperazine motif is likely solvent-exposed in the AXL-GIL binary complex. Accordingly, we designed the potential polypharmacological compounds **3**–**5** (**Figure 5.1.2.1**). While it is recognized that the solvent-exposed piperazine of GIL likely promotes GIL's solubility, given the high molecular weights (MWs) of these hybrid molecules, *e.g.*, MW of **4** = 1418 Da, in parallel, we deleted the piperazinyl motif completely in our dual inhibitors, to produce hybrid molecules **6**–**8** (**Figure 5.1.2.1**) with lower MWs [*e.g.*, **7** = 1334 Da]. The syntheses of VEN and GIL have been reported elsewhere[190,191] and we needed to make only minor adjustments to those synthetic protocols to synthesize appropriate starting compounds for synthesis of our polypharmacologic hybrid compounds.

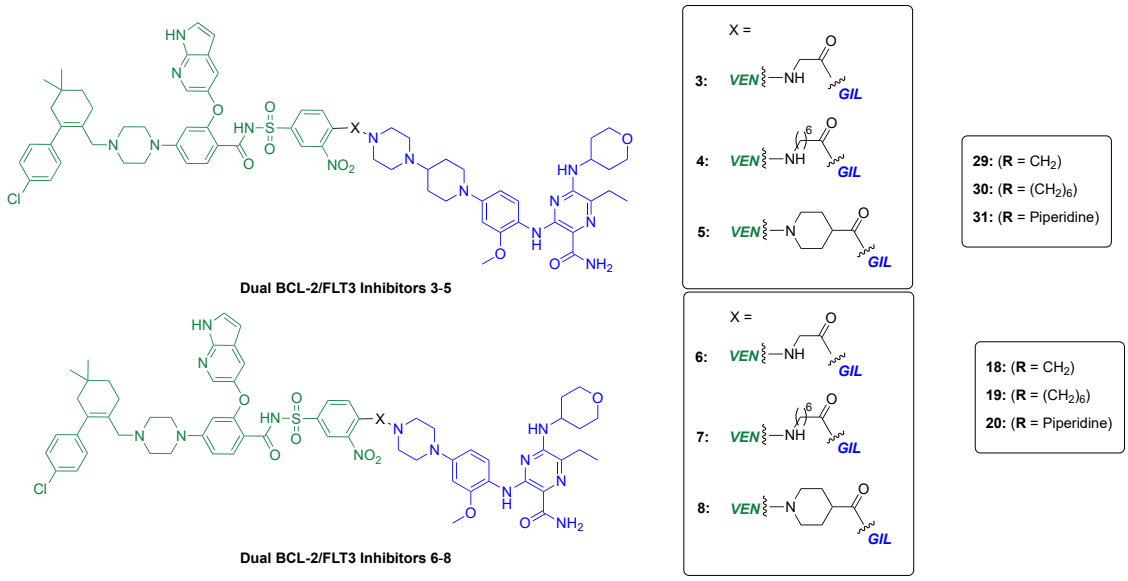

Figure 5.1.2.1: *Dual BCL-2/FLT3 target molecules* ***3-8****, designed through tethering the BCL-2 inhibitor VEN (****1****) and the FLT3 inhibitor GIL (****2****) through their solvent-exposed tetrahydropyran and piperazine motifs, respectively.*

5.1.3 Results and Discussion

Briefly, our synthetic strategy involved substituting the tetrahydropyranyl motif of the sulfonamide portion of VEN with various linkers, using modifications of the chemistry previously reported for the synthesis of VEN[190] to arrive at compounds **11a-11c**, which were subsequently coupled to the commercially available acid RCO_2H (**12**) and then deprotected to deliver compounds **13a**–**13c**, respectively, which were thus primed for coupling to modified GIL.[191]

Separately, in order to pepare dual inhibitors **3**–**5**, we needed to modify the structure of GIL by replacing the terminal 4-methylpiperazine with 4-Boc-protected piperazine. This modified GIL deritvative was largely synthesized following the reported protocol for GIL synthesis,[191] beginning with an S_NAr reaction with fluoronitroarene **14**; the only way our synthetic chemistry differed from the published route is that this particular step was conducted with 1-Boc-4-(piperidin-4-yl)piperazine instead of 1-methyl-4-(piperidin-4-

yl)piperazine to yield, after multiple subsequent standard maipulations, piperazine-terminated GIL **18**, which was subsequently coupled to acids **13a**–**13c**, to furnish the target dual BCL-2/FLT3 polypharmacological inhibitors **3**-**5**, respectively. Dual inhibitors **6**-**8** were synthesized analogously (**Figure 5.1.3.2**).

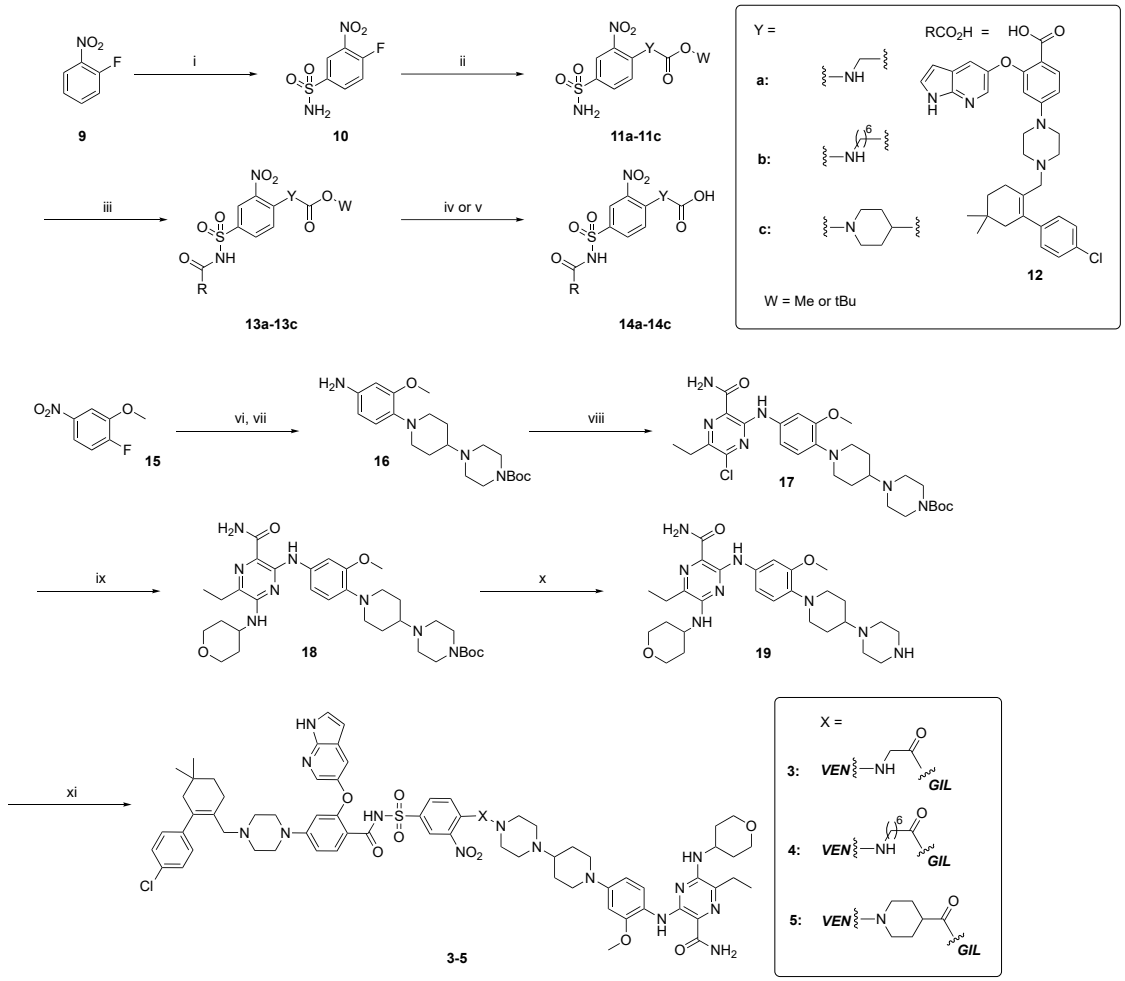

Figure 5.1.3.1: *(i) 1. HSO_3Cl, 95 °C, 16 h; 2. c.NH_4OH, 2-propanol, -10 °C, 30 min; 3. c.HCl, 85%; (ii) $NHYCO_2W$, K_2CO_3, DMF, RT, 16 h, 26-70%; (iii) RCO_2H, DMAP, EDCI, DIPEA, RT,16 h, 71-85%; (iv) 4M HCl / Dioxane, CH_2Cl_2, RT, 6 h, 86%; (v) LiOH·H_2O, THF:H_2O (3:1), RT, 6 h; (vi) tert-butyl 4-(piperidin-4-yl)piperazine-1-carboxylate, K_2CO_3, DMF, 50 °C, 16 h, 70%; (vii) H_2, 10% Pd/C, MeOH, RT, 16 h, 90%; (viii) 3,5-Dichloro-6-ethylpyrazine-2-carboxamide, DIPEA, Dioxane, 110 °C, 16 h, 86%; (ix) 4-aminotetrahydropyran, DIPEA, NMP, 150°C, 16 h, 61; (x) TFA, CH_2Cl_2, RT, 2 h; (xi)* ***13a-13c****, DIPEA, HATU, DMF, RT, 16 h, 41-63%.*

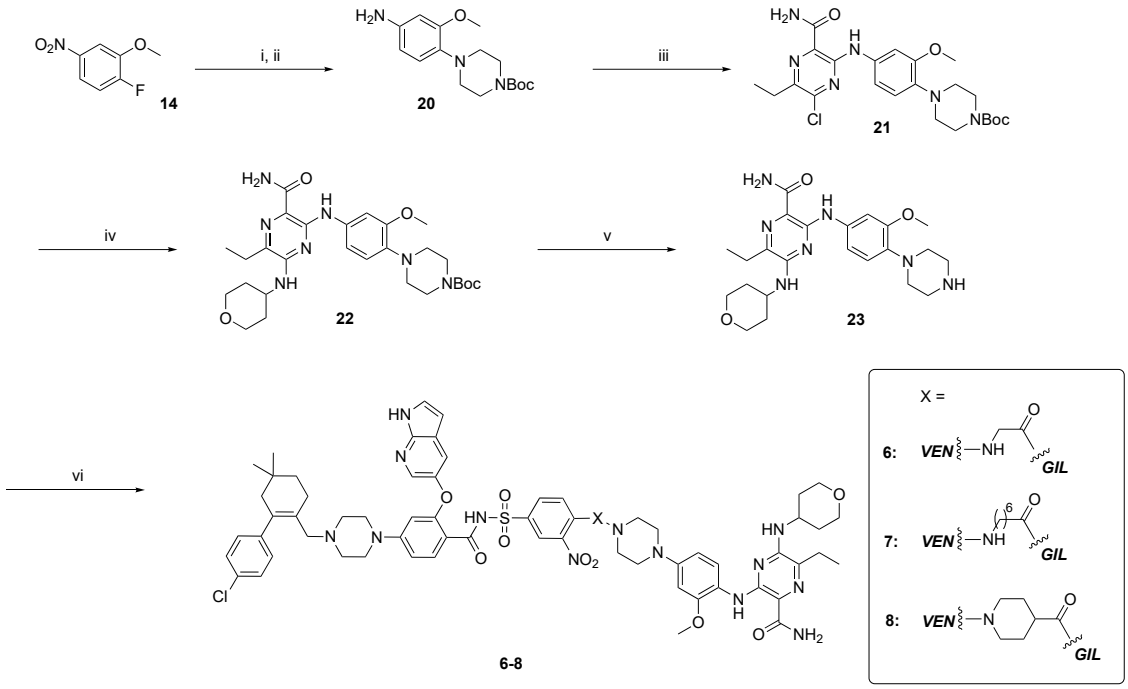

Figure 5.1.3.2: *(i) 4-Boc-Piperazine, K_2CO_3, DMF, 50 °C, 16 h, 95%; (ii) H_2, 10% Pd/C, MeOH, RT, 16 h, 74%; (iii) 3,5-Dichloro-6-ethylpyrazine-2-carboxamide, DIPEA, Dioxane, 110 °C, 16 h, 80%; (iv) 4-aminotetrahydropyran, DIPEA, NMP, 150 °C, 16 h, 60%; (v) TFA, CH_2Cl_2, RT, 2 h, 90%; (vi)* ***13a-13c****, DIPEA, HATU, DMF, RT, 16 h, 68-70%.*

We evaluated a representative compound from each of the above two sets of polypharmacological inhibitors in a cell-free competitive kinase binding assay (DiscoveRX's proprietary KINOME*scan*™ assay) (**Table 5.1.3.1**). In this assay, K_d values of 0.39 nM for VEN-BCL-2 and 1.5 nM for GIL-FLT3 were observed, comparable with literature values.[157,64] Novel hybrid compounds **3** (CG-4-210) and **6** (CG-3-246) also bound BCL-2 potently, with K_d's of 0.91 and 4.25 nM, respectively, confirming our choice of an appropriate grafting site on VEN. However, these novel hybrid compounds bound FLT3 much less strongly than GIL, with K_d's of 205 and 63 nM, respectively. Notably, truncated **6** (CG-3-246) bound 3-fold tighter than the larger **3**, although the trend for BCL-2 binding was in the reverse direction; therefore, we do not believe that the weaker FLT3-binding affinities are related to poorer solubility of the larger hybrid

molecules (furthermore, no precipitation was detected). Surprisingly, it appears that the solvent-exposed 1-methylpiperazine of GIL was not an optimal grafting point for preparing hybrid polypharmcologic inhibitors.

Compound number	K_d (nM) BCL-2	FLT3
3 (CG-4-210)	0.91 ± 0.19	205 ± 5
6 (CG-3-246)	4.25 ± 0.75	63 ± 3
1 (VEN)	0.39 ± 0.03	NT
2 (GIL)	NT	1.5 ± 0.4

Table 5.1.3.1: *Binding of novel hybrid compounds 3 and 6 to BCL-2 and FLT3 under cell-free conditions, using DiscoveRx's KINOMEscan™ assay. NB: For further information, see Experimental Section; NT = not tested.*

Next, our polypharmacologic hybrid VEN-GIL compounds were tested using a cell metabolic/viability assay (ThermoFisher's alamarBlue™) against the MV4;11 and MOLM14 human AML cell lines, which each express high levels of both BCL-2 and FLT3 proteins (**Table 5.1.3.2**).[192,193] Additionally, we evaluated our compounds against VEN-resistant MV4;11 BCL-2 over-expressing (OE) cells, a cell line that we engineered to force elevated levels of BCL-2 protein (see Experimental Section), and the published GIL-resistant mutant cell line MOLM14 F691L.[193] As anticipated, VEN or GIL (alone) each potently inhibited wild type (WT) MV4;11 and MOLM14 cells, consistent with the literature.[192,193] In comparison, VEN alone was over 25-fold less effective against the VEN-resistant MV4;11 BCL-2 OE cells, and GIL alone was 5-fold less effective against the GIL-resistant MOLM14 F691L cells.[193] The "cocktail" polypharmacy of VEN + GIL

(1:1 molar ratio) was more cytotoxic than either drug alone in all four cell lines, as expected.

Consistent with our above rationale that polypharmacy would be superior to polypharmacology in this context, each of our novel hybrid compounds was less active than the cocktail of the 2 parent drugs in WT MV4;11 or WT MOLM14 cells, although compounds **3** and **6** were almost equipotent with VEN alone, confirming, now in cells, that we have identified a desirable grafting point on the VEN molecule. Hybrid compounds **3** (CG-4-210), **6** (CG-3-246) and **7** (CG-3-242) were more active than VEN in the VEN-resistant MV4;11 BCL-2 OE cells. This highlights the contribution of the GIL moiety in these novel hybrids, and may be due, in part, to activation of the pro-apoptotic BH3-only proteins BIM and/or PUMA, or downregulation of MCL-1, all of which have been reported previously in the presence of FLT3i's.[174,175,194] The limited activity of these novel VEN-GIL hybrid compounds in the WT MOLM14 cell line may be due to weaker binding to FLT3 (evaluated only for **3** and **6**) and possibly to reduced cell penetration owing to their comparatively large molecular weights. Further, our hybrid compounds were less potent than GIL in the GIL-resistant MOLM14 F691L cells, although this was not unexpected since our strategy did not address GIL resistance due to the gatekeeper residue mutation F691L.

Compound number	IC_{50} (nM)			
	MV4;11	MV4;11 BCL2 OE	MOLM14	MOLM14 F691L
3 (CG-4-210)	33.7 ± 16.7	209 ± 84	1069 ± 393	>10,000
4 (CG-4-209)	94.0 ± 49.8	907 ± 397	3333 ± 800	>10,000
5 (CG-4-208)	1167 ± 692	>10,000	>10,000	>10,000
6 (CG-3-246)	54.7 ± 4.1	161.7 ± 7.8	265.2 ±13.3	1699 ± 100
7 (CG-3-242)	107.4 ± 7.9	280 ± 26.1	531.4 ± 75.1	3284 ± 501
8 (CG-3-245)	968 ± 109	3224 ± 135	>10,000	>10,000
1 (VEN)	28.7 ± 5.3	756 ± 269	1700 ± 142	2008 ± 69
2 (GIL)	14.7 ± 2.7	53.7 ± 12.6	25.7 ± 7.3	128 ± 22
1 (VEN) + 2 (GIL)[1]	2.6 ± 0.4	8.7 ± 0.0	16.4 ± 0.8	63.2 ± 0.9

Table 5.1.3.2: *Inhibitory activities (IC_{50}) of novel VEN-GIL hybrid compounds against wild-type (WT) and resistant mutant AML cell lines. NB [1]The combination of VEN + GIL was a 1:1 molar ratio, where each drug was made up to the same concentration of the VEN-GIL hybrid compounds.*

To verify that the observed drug-induced reductions in cell metabolism/viability resulted from apoptotic cell death, the established cellular mechanism of action of both VEN and GIL, flow cytometric analyses of of cell apoptosis/death were conducted for VEN-GIL hybrid compounds **3** (CG-4-210) and **6** (CG-3-246) in each of the above 4 AML cell lines. As a positive control, MV4;11 WT cells were treated with VEN + GIL (200nM each), which induced a potent (95.8%) decrease in % viability (defined as % AnnV-/7AAD- cells), revealing that essentially all of these cells had entered into early

(AnnV+/7AAD-) or late (AnnV+/7AAD+) stages of apoptotic cell death. Treatment with 200nM of either compound **3** (CG-4-210) or **6** (CG-3-246) alone mirrored this induction of apoptosis, albeit to a lesser extent (**Figure 5.1.3.3A**). Induction of apoptotic cell death by our novel VEN-GIL hybrid compounds confirms that the hybrid compounds inhibit AML cell lines via the established cellular mechanism of action of VEN and GIL. Consistent with this apoptotic mechanism of action, activity of these novel hybrid compounds was reduced in the VEN-resistant MV4;11 BCL-2 OE cells and the GIL-resistant MOLM14 F691L cells (**Figure 5.1.3.3B**).

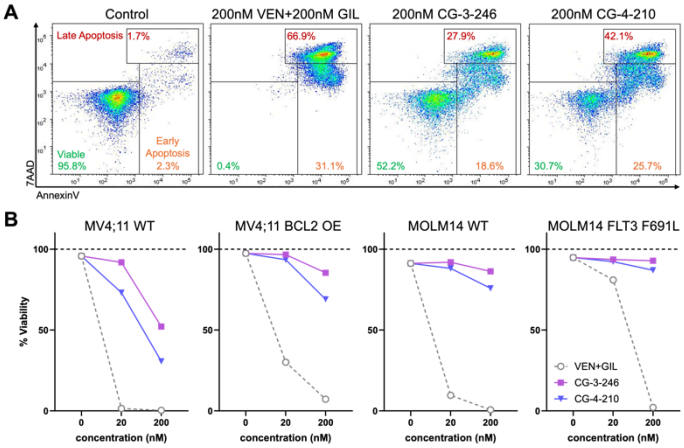

Figure 5.1.3.3:A. *Apoptosic cell death of WT and resistant AML cell lines. Cells were incubated with either 20nM or 200nM VEN + GIL, CG-3-246, or CG-4-210 in culture for 48 hours prior to AnnV/7AAD staining. An equi-volume DMSO-treated sample was plated for each cell line and used as a control to document baseline viability. (A) Flow cytometric dot plots of 200nM-treated WT MV4;11 cells stained with Annexin-V and 7AAD depict the gating strategy used to delineate viable cells (green values, AnnV-/7AAD-), early apoptotic cells (orange values, AnnV+/7AAD-), and late apoptotic cells (red values, AnnV+/7AAD+). Results of treatment with 20nM of each compound confirmed the same pattern of induction of apoptotic cell death, but in a concentration-dependent fashion (dot plots not shown).* ***B.*** *Summarized % viability (i.e., % AnnV-/7AAD- cells) of WT MV4;11, MV4;11 BCL-2 OE, WT MOLM14, and FLT3 F691L MOLM14 cells treated with 0, 20 or 200nM VEN.*

5.1.4 Conclusion

In summary, we compared the inhibitory potencies of the polypharmacy combination of the BCL-2 inhibitor VEN plus the FLT3 inhibitor GIL against AML cell lines versus several novel synthesized polypharmacologic tethered VEN–GIL hybrid compounds. While these hybrid compounds retained the potent BCL-2-binding affinity of the parent compound VEN, their FLT3-binding affinities were decreased relative to GIL. As an alternative grafting point, tethering of VEN via GIL's methoxy group, which resides at the entrance to FLT3's active site, may prove more fruitful. Nevertheless, hybrid compounds **3** (CG-4-210) and **6** (CG-3-246) represent potent novel antileukemic compounds, with an the expected apoptotic mechanism of antileukemic action, that

warrant further investigation towards the discovery of hybrid molecules that potently inhibit FLT3 as well as BCL-2. Finally, it should be reiterated that the potential benefit of a polypharmacological strategy wherein the grafted ligands have targets that are located in separate cellular compartments (or in this case, intracellularly and extracellularly), may be realized only in a clinical setting.

5.1.5 Methods

Chemistry

All reactions were performed in oven-dried glassware under non-inert atmosphere, unless otherwise stated. Chemicals and solvents were used as supplied without further purification. ^{1}H and ^{13}C NMR spectra were obtained on a Varian 400 MHz or 500 MHz spectrometer at 298K. Chemical shifts are reported in parts per million (ppm) and are referenced to residual non-deuterated solvent peak ($CHCl_3$: δ_H 7.26, δ_C 77.0; DMSO: δ_H 2.50, δ_C 39.5). Low resolution mass spectra (LRMS) were obtained on an Advion CMS-L mass spectrometer using electrospray ionization. High resolution mass spectra (HRMS) were obtained on an Aglient 6560 mass spectrometer using electrospray ionization. All final compounds were lyophilized before biological evaluation.

Cell-free binding assays

DiscoveRx's proprietary KINOMEscan™ is based on a competition binding assay that quantitatively measures the ability of a compound to compete with an immobilized, active-site directed ligand. The assay is performed by combining three components: DNA-tagged kinase; immobilized ligand; and a test compound. The ability of the test compound to compete with the immobilized ligand is measured via quantitative PCR of

the DNA tag. For most assays, kinase-tagged T7 phage strains were prepared in an E. coli host derived from the BL21 strain. E. coli were grown to log-phase and infected with T7 phage and incubated with shaking at 32°C until lysis. The lysates were centrifuged and filtered to remove cell debris. The remaining kinases were produced in HEK-293 cells and subsequently tagged with DNA for qPCR detection. Streptavidin-coated magnetic beads were treated with biotinylated small molecule ligands for 30 minutes at room temperature to generate affinity resins for kinase assays. The liganded beads were blocked with excess biotin and washed with blocking buffer (SeaBlock (Pierce), 1% BSA, 0.05% Tween 20, 1 mM DTT) to remove unbound ligand and to reduce non-specific binding. Binding reactions were assembled by combining kinases, liganded affinity beads, and test compounds in 1x binding buffer (20% SeaBlock, 0.17x PBS, 0.05% Tween 20, 6 mM DTT). Test compounds were prepared as 111X stocks in 100% DMSO. K_ds were determined using an 11-point 3-fold compound dilution series with three DMSO control points. All compounds for K_d measurements are distributed by acoustic transfer (non-contact dispensing) in 100% DMSO. The compounds were then diluted directly into the assays such that the final concentration of DMSO was 0.9%. All reactions performed in polypropylene 384-well plate. Each was a final volume of 0.02 ml. The assay plates were incubated at room temperature with shaking for 1 hour and the affinity beads were washed with wash buffer (1x PBS, 0.05% Tween 20). The beads were then re-suspended in elution buffer (1x PBS, 0.05% Tween 20, 0.5 μM nonbiotinylated affinity ligand) and incubated at room temperature with shaking for 30 minutes. The kinase concentration in the eluates was measured by qPCR.

Cell cultures

Pediatric acute myeloid leukemia cell lines harboring mixed-lineage-leukemia rearrangements were obtained from either ATCC (Manassas, VA) or DSMZ (Branschweig, DEU) (MOLM14, #ACC-777 DSMZ; MV4;11, #CRL-9591, ATCC). MOLM14 FLT3 F691L cells were a gift from Dr. Shah (UCSF). MV4;11 BCL-2 OE cells were generated via lentiviral transduction using a Transdux MAX kit (SBI, Cat# LV860A-1) following manufacturer's guidelines. The human BCL-2a open reading frame (ORF; 720bp) was amplified with gene-specific primers (BCL2aOE-2243-F: 5'-CTGAGAATTCATGGCGCACGCTGGGAGAACAG-3' and BCL2aOE-2243-R: 5'-CTGAGGTACCTCACTTGTGGCCCAGATAGGCAC-3') from NB4 human leukemia cell cDNA by PCR, and then cloned into pMJK2243 (our control empty lentivector) using EcoRI and KpnI restriction enzyme sites. pMJK2243 is a bidirectional dual promoter lentivector including the EF1a and hUbC promoters. In the BCL-2a expression lentivector, the EF1a promoter drives expression of the BCL-2a ORF, whereas the hUbC promoter drives expression of the green fluorescence protein (GFP) and puromycin resistance ($Puro^R$) genes. Lentiviruses (LVs) were generated in HEK293T cells as described previously.[195] The BCL-2 OE LV was validated in MOLM14 cells (>95% GFP^+ by the puromycin selection) with a 5-fold increase in BCL-2 protein levels compared to WT MOLM14 cells. Before proceeding with cell metabolic/viability and apoptosis/death assays, MV4;11 BCL-2 OE cells were cultured in puromycin-containing media until >95% GFP^+.

Cell lines were cultured in RPMI1640 media (Cellgro, # MDT-10-040-CV) containing 10% fetal bovine serum (Gemini BioProducts #100-106) and passaged twice per week to maintain cultures in log-phase-growth. Upon receipt, cell lines were expanded and

multiple aliquots cryopreserved in DMSO-containing medium in the vapor phase of liquid nitrogen. Cryopreserved cells were genetically authenticated and confirmed to be mycoplasma-negative prior to cryopreservation. Cells from a given cryopreserved aliquot were cultured for no more than 3-4 months.

Cell metabolic/viability assays

Cell metabolism/viability was assessed by alamarBlue assays (Thermo Fisher, cat# DAL1100) according to manufacturer's guidelines. Cells and concentrations of each compound were combined in culture for 48h. Cells were then incubated with alamarBlue reagent for a minimum of 5hr before absorbance was read using a Perkin Elmer Victor X3. Reads were normalized to the corresponding equimolar DMSO (vehicle) controls. IC_{50}s were generated in Prism's GraphPad by modeling a non-linear fit (4-parameter, variable Hill-slope) against log(inhibitor) vs relative absorbance values. Top and bottom constraints were set to 1 and 0, respectively.

Cell apoptosis/death assays

$2.5x10^5$ cells were stained with Annexin V/7-aminoactinomycin D (AnnV/7AAD) (BioLegend, San Diego, CA # BLD-640930) per manufacturer's guidelines, then assessed using either a Becton Dickinson Canto II flow cytometer. Compensation and gating were performed using FlowLogic cytometry analysis software v8.7.

Viable cell counts

Viable cells counted using a Nexcelcom K2 cell counter (#CS2-0106) after manufacturer's recommended staining protocol with acridine orange and propidium iodide.

5.1.6 Experimental Procedures

*General Procedure A: Nucleophilic aromatic substitution of Sulfonamides (**11a-11c**)*

To a stirring solution of 4-fluoro-3-nitrobenzenesulfonamide (1.1 eq) in DMF (0.1M), K_2CO_3 (3.0 eq) and the selected amines (1.0 eq) were added. The reaction was stirred at RT for 16 h. Reaction completion was monitored via TLC (CH_2Cl_2/MeOH/NH_4OH, 92:7:1). Upon completion, the reaction mixture was dissolved in EtOAc and partitioned with water and the product was extracted with EtOAc (3x). The organic layers were combined and washed with 0.1M HCl, saturated $NaHCO_3$, water (3x), and saturated NaCl, then dried over Na_2SO_4 and concentrated to dryness. The crude material was adsorbed onto silica gel, then purified by flash column chromatography eluting with CH_2Cl_2/MeOH/NH_4OH, 92:7:1.

*General Procedure B: Sulfonamide coupling to acid **12** (**13a-13c**)*

To a stirring solution of the sulfonamide (**11a**, **11b** or **11c**; 1.0 eq) in CH_2Cl_2 (0.1M), acid **12** (1.0 eq), DMAP (1.0 eq), EDCI (1.3 eq), and DIPEA (2.0 eq) were added. The reaction was stirred at RT for 16 hrs. Reaction completion was monitored via TLC (CH_2Cl_2/MeOH/AcOH, 92:7:1). Upon completion, 2.5 eq of N,N-dimethylethylenediamine was added and the reaction was left at RT for 1 h. the reaction mixture was then dissolved in CH_2Cl_2 and partitioned with 10% aq AcOH and the product was extracted with CH_2Cl_2 (3x). The organic layers were combined and washed with 10% aq AcOH, 5% aq saturated $NaHCO_3$, then dried over Na_2SO_4 and concentrated to dryness. The crude material was adsorbed onto silica gel, then purified by flash column chromatography eluting with CH_2Cl_2/MeOH/H_2O, 79:9:1 to deliver **13a**, **13b** or 1**3c**.

*General Procedure C: HATU-mediated coupling reactions (**3-8**)*

To a solution of the carboxylic acid (1.0 eq) in DMF (0.1M) was added DIPEA (1.1 eq) and HATU (1.2 eq) and stirred for 15 min. After this time, the corresponding amine (1.0 eq) and additional 1.0 eq DIPEA per HCl / TFA salt was added, and the reaction mixture was stirred at RT for 16 h. Upon completion, the reaction mixture was dissolved in EtOAc and partitioned with saturated $NaHCO_3$ and the product was extracted with EtOAc (3x). The organic layers were combined and washed with 0.1M HCl, saturated $NaHCO_3$, water (3x), and saturated NaCl, then dried over Na_2SO_4 and concentrated to dryness. The crude material was adsorbed onto silica gel, then purified by flash column chromatography eluting with CH_2Cl_2/MeOH/NH_4OH, 58:7:1.

4-fluoro-3-nitrobenzenesulfonamide (**10**). 2-fluoronitrobenzene (3.73 mL, 35.4 mmol, 1.0 eq) was added to a flask to which chlorosulfonic acid (11 mL, 3.2M) was added dropwise. The flask was heated at 95°C, and stirred for 16 h. Then, the reaction mixture was allowed to return to room temperature. A mixture of conc. NH_4OH (30 mL, 1.2M) to isopropanol (115 mL, 0.37M) was cooled to -10°C. The reaction mixture was added slowly to the -10°C flask after which the final mixture was stirred for an additional 30 mins. Conc. HCl (10 mL, 3.5M) was added dropwise to re-acidify the solution which caused a yellow precipitate to form. The resulting slurry was vacuum filtered and washed with cold 1M HCl solution after which the solid was dried at 50°C in a vacuum oven without further purification to yield the title compound. (yellow solid, yield = 85%): ^{1}H NMR (500 MHz, DMSO) δ = 8.53 (d, J = 7 Hz, 1H), 8.20 (d, J = 9 Hz, 1H), 7.81 (t, J = 10 Hz, 1H), 7.72 (s, 2H); ^{13}C NMR (400 MHz, DMSO) δ = 146.3, 138.8, 138.7, 129.4, 125.4, 125.2.

tert-butyl (2-nitro-4-sulfamoylphenyl)glycinate (**11a**). Glycine tert-butyl ester hydrochloride was reacted on a 4.13 mmol scale according to General Procedure A to deliver the title compound. (yellow solid, yield = 26%): ^{1}H NMR (400 MHz, DMSO) δ = 8.71 (s, 1H), 8.52 (s, 1H), 7.87 (d, J = 9.6 Hz, 1H), 7.37 (s, 2H), 7.11 (d, J = 9.2 Hz, 1H), 4.26 (d, J = 5.2 Hz, 2H), 1.48 (s, 9H); ^{13}C NMR (400 MHz, DMSO) δ = 168.8, 146.5, 133.1, 131.3, 130.3, 124.9, 116.5, 82.3, 45.4, 28.2.

methyl 7-((2-nitro-4-sulfamoylphenyl)amino)heptanoate (**11b**). 7-amino-heptanoic acid methyl ester hydrochloride was reacted on a 2.73 mmol scale according to General Procedure A to deliver the title compound. (yellow solid, yield = 63%): ^{1}H NMR (400 MHz, $CDCl_3$) δ = 8.72 (s, 1H), 8.38 (s, 1H), 7.91 (d, J = 8.8 Hz, 1H), 6.92 (d, J = 8.8 Hz, 1H), 5.16 (s, 2H), 3.68 (s, 3H), 3.38 (q, J = 6.53 Hz, 2H), 2.34 (t, J = 7.6 Hz, 2H), 1.78 (t, J = 7 Hz, 2H), 1.67 (t, J = 7.4 Hz, 2H), 1.51-1.42 (m, 4H); ^{13}C NMR (400 MHz, $CDCl_3$) δ = 169.4, 142.6, 128.4, 125.6, 123.3, 122.0, 109.9, 46.8, 38.5, 29.1, 23.9, 23.8, 21.8, 19.9.

tert-butyl 1-(2-nitro-4-sulfamoylphenyl)piperidine-4-carboxylate (**11c**). Tert-butyl piperidine-4-carboxylate hydrochloride was reacted on a 2.06 mmol scale according to General Procedure A to deliver the title compound. (yellow solid, yield = 70%): ^{1}H NMR (400 MHz, DMSO) δ = 8.17 (s, 1H), 7.85 (d, J = 8.8 Hz, 1H), 7.41-7.38 (m, 3H), 3.26 (s, 2H), 2.98 (t, J = 11.4 Hz, 2H), 2.48-2.43 (m, 1H), 1.86 (d, J = 11.2 Hz, 2H), 1.62 (q, J = 10.7 Hz, 2H), 1.39 (s, 9H); ^{13}C NMR (400 MHz, DMSO) δ = 173.7, 147.9, 138.9, 134.7, 131.2, 124.8, 121.6, 80.3, 50.3, 40.7, 38.1, 28.1.

tert-butyl (4-(N-(2-((1H-pyrrolo[2,3-b]pyridin-5-yl)oxy)-4-(4-((4'-chloro-5,5-dimethyl-3,4,5,6-tetrahydro-[1,1'-biphenyl]-2-yl)methyl)piperazin-1-yl)benzoyl)sulfamoyl)-2-nitrophenyl)glycinate (**12a**). **11a** was reacted on a 0.272 mmol scale according to General

Procedure B to deliver the title compound. (yellow solid, yield = 83%): ^{1}H NMR (400 MHz, DMSO) δ = 11.72 (s, 1H), 11.39 (s, 1H), 8.77 (t, J = 5 Hz, 1H), 8.62 (s, 1H), 8.06 (s, 1H), 7.88 (d, J = 9.6 Hz, 1H), 7.58 (s, 1H), 7.52-7.50 (m, 2H), 7.36 (d, J = 8 Hz, 2H), 7.06 (d, J = 8.4 Hz, 2H), 6.98 (d, J = 9.2 Hz, 1H), 6.69 (d, J = 8.4 Hz, 1H), 6.42 (s, 1H), 6.20 (s, 1H), 4.23 (d, J = 5.6 Hz, 2H), 3.10 (s, 4H), 2.79 (s, 2H), 2.23 (s, 4H), 2.16 (s, 2H), 1.97 (s, 2H), 1.47 (s, 9H), 1.40 (t, J = 5.8 Hz, 2H), 0.94 (s, 6H); ^{13}C NMR (400 MHz, DMSO) δ = 168.7, 164.3, 158.4, 155.0, 147.1, 146.9, 145.9, 142.4, 135.8, 134.4, 132.6, 131.3, 130.5 (2), 128.5 (2), 128.1, 127.8, 120.2, 118.4, 115.9, 109.1, 100.4, 82.3, 60.1 (2), 52.4 (2), 46.9 (3), 45.4, 35.2, 29.3, 28.4, 28.1 (2), 25.6.

methyl 7-((4-(N-(2-((1H-pyrrolo[2,3-b]pyridin-5-yl)oxy)-4-(4-((4'-chloro-5,5-dimethyl-3,4,5,6-tetrahydro-[1,1'-biphenyl]-2-yl)methyl)piperazin-1-yl)benzoyl)sulfamoyl)-2-nitrophenyl)amino)heptanoate (**12b**). **11b** was reacted on a 0.525 mmol scale according to General Procedure B to deliver the title compound. (yellow solid, yield = 71%): ^{1}H NMR (400 MHz, DMSO) δ = 11.67 (s, 1H), 11.39 (s, 1H), 8.53-8.50 (m, 2H), 8.01 (s, 1H), 7.78 (d, J = 9.2 Hz, 1H), 7.50-7.45 (m, 3H), 7.32 (d, J = 7.6 Hz, 2H), 7.02 (d, J = 8.8 Hz, 3H), 6.65 (d, J = 9.6 Hz, 1H), 6.36 (s, 1H), 6.17 (s, 1H), 3.55 (s, 3H), 3.36-3.30 (m, 4H), 3.05 (s, 4H), 2.72 (s, 2H), 2.28 (t, J = 7.6 Hz, 2H), 2.17-2.12 (m, 6H), 1.93 (s, 2H), 1.59-1.49 (m, 4H), 1.39-1.30 (m, 4H), 0.90 (s, 6H); ^{13}C NMR (400 MHz, DMSO) δ = 173.8, 158.2, 155.0, 147.6, 147.1, 145.8, 142.4, 135.7, 134.4, 132.5, 131.3 (2), 130.5, 129.9, 128.5 (2), 128.1(2), 126.3, 120.2, 118.2, 115.2, 109.2, 100.4 (2), 60.1, 52.5 (2), 51.6, 47.0 (2), 46.8, 42.9, 40.6, 35.3, 33.6, 29.3, 28.5, 28.4, 26.4, 25.6, 24.8.

tert-butyl 1-(4-(N-(2-((1H-pyrrolo[2,3-b]pyridin-5-yl)oxy)-4-(4-((4'-chloro-5,5-dimethyl-3,4,5,6-tetrahydro-[1,1'-biphenyl]-2-yl)methyl)piperazin-1-yl)benzoyl)sulfamoyl)-2-

nitrophenyl)piperidine-4-carboxylate (**12c**). **11c** was reacted on a 0.525 mmol scale according to General Procedure B to deliver the title compound. (yellow solid, yield = 85%): ^{1}H NMR (400 MHz, DMSO) δ = 11.69 (s, 1H), 11.26 (s, 1H), 8.24 (s, 1H), 8.02 (s, 1H), 7.80 (d, J = 8.8 Hz, 1H), 7.50 (t, J = 9 Hz, 3H), 7.32 (d, J = 8.4 Hz, 2H), 7.2 (d, J = 9.6 Hz, 1H), 7.02 (d, J = 8.8 Hz, 2H), 6.65 (d, J = 8.8 Hz, 1H), 6.39 (s, 1H), 6.17 (s, 1H), 3.31-3.23 (m, 4H), 3.06 (s, 4H), 2.97 (t, J = 11.2 Hz, 2H), 2.76 (s, 2H), 2.48-2.43 (m, 1H), 2.21 (s, 4H), 2.12 (s, 2H), 1.93 (s, 2H), 1.84 (d, J = 10.8 Hz, 2H), 1.60 (q, J = 11.1 Hz, 2H), 1.39 (s, 9H), 0.90 (s, 6H); ^{13}C NMR (400 MHz, DMSO) δ = 173.7, 164.6, 158.2, 154.9, 148.5, 147.1, 145.9, 142.3, 138.0, 135.8, 132.8, 132.6, 131.3, 130.4 (2), 128.6 (2), 128.2, 127.4, 120.8, 120.3, 118.3, 109.2, 103.0, 100.5, 80.3, 60.0, 52.4, 50.3 (2), 46.9 (2), 40.4, 35.2 (2), 29.3, 28.4, 28.1, 28.0, 25.6.

(4-(N-(2-((1H-pyrrolo[2,3-b]pyridin-5-yl)oxy)-4-(4-((4'-chloro-5,5-dimethyl-3,4,5,6-tetrahydro-[1,1'-biphenyl]-2-yl)methyl)piperazin-1-yl)benzoyl)sulfamoyl)-2-nitrophenyl)glycine (**14a**). **13a** (574 mg, 0.623 mmol, 1.0 eq) was dissolved in CH_2Cl_2 (0.1M). 4M HCl / Dioxane (0.1M) was added to the reaction and left stirring at RT for 6 h. Reaction completion was monitored via TLC (CH_2Cl_2/MeOH/AcOH, 92:7:1). Upon completion, the solvent was removed under vacuum and $CHCl_3$ was added and removed under vacuum to drive off Dioxane without further purification to yield the title compound. (yellow solid, yield = 86%): ^{1}H NMR (400 MHz, DMSO) δ = 11.83 (s, 1H), 11.69 (s, 1H), 10.79 (s, 1H), 8.78 (s, 1H), 8.57 (s, 1H), 8.06 (s, 1H), 7.83 (d, J = 9.2 Hz, 1H), 7.61 (s, 1H), 7.51-7.48 (m, 2H), 7.37 (d, J = 7.6 Hz, 2H), 7.07 (d, J = 8.8 Hz, 2H), 6.98 (t, J = 10.2 Hz, 1H), 6.69 (d, J = 8.8 Hz, 1H), 6.41 (s, 1H), 6.24 (s, 1H), 3.60 (d, J = 12.8 Hz, 2H), 3.50 (s, 4H), 3.25 (t, J = 11 Hz, 4H), 2.66 (d, J = 9.2 Hz, 2H), 2.33 (s, 2H),

1.98 (s, 2H), 1.43-1.41 (m, 2H), 0.91 (s, 6H); ^{13}C NMR (400 MHz, DMSO) δ = 170.9, 164.0, 158.2, 154.1, 147.2, 146.7, 145.1, 141.9, 140.9, 134.8, 134.3, 132.6, 132.1, 130.2, 128.1, 128.6, 128.0, 122.5, 120.8, 119.3, 116.1, 113.8, 109.6, 103.3, 100.7, 66.8, 58.2, 52.7, 50.8, 47.1, 44.8, 44.7, 43.8, 34.8, 29.1, 28.3, 26.1.

7-((4-(N-(2-((1H-pyrrolo[2,3-b]pyridin-5-yl)oxy)-4-(4-((4'-chloro-5,5-dimethyl-3,4,5,6-tetrahydro-[1,1'-biphenyl]-2-yl)methyl)piperazin-1-yl)benzoyl)sulfamoyl)-2-nitrophenyl)amino)heptanoic acid (**14b**). **13b** (341 mg, 0.374 mmol, 1.0 eq) was dissolved in 3:1 THF:H_2O (0.1M). Lithium hydroxide monohydrate (57 mg, 1.34 mmol, 6.6 eq) was added and left stirring at RT for 6 h. Reaction completion was monitored via TLC CH_2Cl_2/MeOH/H_2O, 79:9:1. Upon completion, stoichiometric amounts of 1M HCl was added to neutralize the reaction mixture while stirring. The reaction mixture was dissolved in EtOAc and partitioned with water and the product was extracted with ethyl acetate (3x). The organic layers were combined and washed with saturated NaH_2PO_4 (2x), then dried over Na_2SO_4 and concentrated to dryness without further purification to yield the title compound. (yellow solid, yield = 95%): ^{1}H NMR (400 MHz, DMSO) δ = 11.89 (s, 1H), 11.66 (s, 1H), 11.39 (s, 1H), 8.53 (s, 1H), 8.01 (s, 1H), 7.78 (d, J = 8.4 Hz, 1H), 7.50-7.47 (m, 3H), 7.32 (d, J = 7.6 Hz, 2H), 7.01 (d, J = 7.2 Hz, 3H), 6.65 (d, J = 8.8 Hz, 1H), 6.36 (s, 1H), 6.17 (s, 1H), 3.31 (s, 4H), 3.04 (s, 4H), 2.72 (s, 2H), 2.18-2.12 (m, 8H), 1.93 (s, 2H), 1.57 (s, 2H), 1.49 (s, 2H), 1.35-1.31 (m, 4H), 0.90 (s, 6H); ^{13}C NMR (400 MHz, DMSO) δ = 174.9, 158.2, 155.0, 147.6, 147.1, 145.8, 142.4, 135.7, 134.4, 132.5, 131.3, 130.5, 129.7, 128.5 (2), 128.1 (2), 120.2, 118.2, 115.2, 109.2, 102.9, 100.4 (2), 60.1, 52.5 (2), 47.0 (2), 46.8, 42.9, 40.6, 35.3, 34.0, 29.3, 28.6, 28.4 (2), 26.5, 25.6, 24.8.

1-(4-(N-(2-((1H-pyrrolo[2,3-b]pyridin-5-yl)oxy)-4-(4-((4'-chloro-5,5-dimethyl-3,4,5,6-tetrahydro-[1,1'-biphenyl]-2-yl)methyl)piperazin-1-yl)benzoyl)sulfamoyl)-2-nitrophenyl)piperidine-4-carboxylic acid (**14c**). **13c** (500 mg, 0.532 mmol, 1.0 eq) was dissolved in CH_2Cl_2 (0.1M). Trifluoroacetic acid (0.1M) was added to the reaction and left stirring at RT for 2 h. Reaction completion was monitored via TLC (CH_2Cl_2/MeOH/AcOH, 92:7:1). Upon completion, the solvent was removed under vacuum and $CHCl_3$ was added and removed under vacuum to drive off Dioxane without further purification to yield the title compound. (yellow solid, yield = 95%): ^{1}H NMR (400 MHz, DMSO) δ = 11.78-11.73 (m, 2H), 9.34 (s, 1H), 8.30 (s, 1H), 8.08 (s, 1H), 7.87 (d, J = 8.8 Hz, 1H), 7.60-7.54 (m, 3H), 7.42 (d, J = 8 Hz, 2H), 7.29 (d, J = 8.4 Hz, 1H), 7.11 (d, J = 7.6 Hz, 2H), 6.74 (d, J = 7.6 Hz, 1H), 6.45 (s, 1H), 6.27 (s, 1H), 3.68 (s, 2H), 3.60 (s, 2H), 3.31 (s, 4H), 3.04 (t, J = 10.6 Hz, 4H), 2.77 (s, 2H), 2.52 (s, 1H), 2.22 (s, 2H), 2.04 (s, 2H), 1.92 (d, J = 11.6 Hz, 2H), 1.67 (q, J = 10.4 Hz, 2H), 1.47 (s, 2H), 0.96 (s, 6H); ^{13}C NMR (400 MHz, DMSO) δ = 176.0 (2), 164.0, 158.3, 155.8, 154.0, 148.8, 146.7, 146.0, 137.7, 135.7 ,132.8 (2), 132.2, 130.2, 129.1, 128.3 (2), 127.8, 122.1, 120.9, 118.6, 109.6, 103.2, 100.5, 58.4, 50.9 (2), 50.0, 47.0, 44.2, 40.6, 34.7, 29.1, 28.3, 28.0, 25.2.

tert-butyl 4-(1-(4-amino-2-methoxyphenyl)piperidin-4-yl)piperazine-1-carboxylate (**15**). To a stirring solution of N-Boc-piperazine (1 g, 5.37 mmol, 1.0 eq) in anhydrous THF (0.2M) under nitrogen gas, was added DIPEA (983 mL, 5.37 mmol, 1.0 eq), N-benzyloxycarbonyl-4-piperidone (2.51 g, 10.7 mmol, 2eq), and $NaBH(OAc)_3$ (3.41 g, 16.1 mmol, 3.0 eq). The reaction was stirred at RT for 16 h. Reaction completion was monitored via TLC (CH_2Cl_2/MeOH/NH_4OH, 92:7:1). Upon completion, the reaction

mixture was then dissolved in CH_2Cl_2 and partitioned with saturated $NaHCO_3$ and the product was extracted with CH_2Cl_2 (3x). The organic layers were combined and washed with saturated $NaHCO_3$, water (3x), and saturated NaCl, then dried over Na_2SO_4 and concentrated to dryness. The crude material was adsorbed onto silica gel, then purified by flash column chromatography eluting with CH_2Cl_2/MeOH/NH_4OH, 192:7:1 to yield tert-butyl 4-(1-((benzyloxy)carbonyl)piperidin-4-yl)piperazine-1-carboxylate. (light yellow oil, yield = 48%): ^{1}H NMR (500 MHz, $CDCl_3$) δ = 7.38-7.31 (m, 5H), 5.12 (s, 2H), 4.23 (s, 2H), 3.42 (s, 4H), 2.79 (s, 2H), 2.49-2.40 (m, 5H), 1.86-1.79 (m, 4H), 1.46 (s, 9H); ^{13}C NMR (500 MHz, $CDCl_3$) δ = 155.3, 154.9, 137.0, 128.6, 128.1, 128.0, 79.8, 67.2, 62.0, 49.1 (2), 43.6, 28.6, 28.2. LRMS (ESI) m/z [M+H]+ calcd for $C_{22}H_{33}N_3O_4$ = 403.25; found = . Tert-butyl 4-(1-((benzyloxy)carbonyl)piperidin-4-yl)piperazine-1-carboxylate (1 g, 2.48 mmol, 1.0 eq) was dissolved in MeOH (30 mL, 0.75M), after which Pd(C) (100 mg, 10%wt) was added. The stirring solution was flushed through with hydrogen gas for 10 min and the reaction was stirred at RT for 16 h. Reaction completion was monitored via TLC (CH_2Cl_2/MeOH/NH_4OH, 92:7:1). Upon completion, the reaction was vacuum filtered through celite and washed with MeOH to separate Pd and crude product without further purification to yield tert-butyl 4-(piperidin-4-yl)piperazine-1-carboxylate. (light yellow oil, yield = 94%): ^{1}H NMR (400 MHz, $CDCl_3$) δ = 3.43 (s, 4H), 3.21 (d, J = 12.4 Hz, 2H), 2.64 (t, J = 10.2 Hz, 2H), 2.50 (s, 4H), 2.39 (t, J = 11.4 Hz, 1H), 1.84 (d, J = 12 Hz, 2H), 1.55-1.46 (m, 11H); ^{13}C NMR (400 MHz, $CDCl_3$) δ = 150.0, 74.8, 56.9, 46.8, 44.0, 40.9, 24.0, 23.7. To a stirring solution of 2-Fluoro-5-nitroanisole (347 mg, 2.02 mmol, 1.0 eq) in DMF (15 mL, 0.14M), K_2CO_3 (336 mg, 2.43 mmol, 1.2 eq) and tert-butyl 4-(piperidin-4-yl)piperazine-1-carboxylate (600 mg, 2.23 mmol, 1.1 eq) were

added. The reaction was stirred at 50°C for 16 h. Reaction completion was monitored via TLC (hexanes/EtOAc). Upon completion, the reaction mixture was dissolved in EtOAc and partitioned with water and the product was extracted with EtOAc (3x). The organic layers were combined and washed with saturated $NaHCO_3$, water (3x), and saturated NaCl, then dried over Na_2SO_4 and concentrated to dryness without further purification to yield tert-butyl 4-(1-(2-methoxy-4-nitrophenyl)piperidin-4-yl)piperazine-1-carboxylate. (yellow solid, yield = 70%): ^{1}H NMR (500 MHz, $CDCl_3$) δ = 7.84 (dd, J = 2.5, 8.5 Hz, 1H), 7.69 (s, 1H), 6.88 (d, J = 9 Hz, 1H), 3.94 (s, 3H), 3.75 (d, J = 12 Hz, 2H), 3.44 (s, 4H), 2.72 (t, J = 11.8 Hz, 2H), 2.54 (s, 4H), 2.47 (t, J = 11.8 Hz, 1H), 1.90 (d, J = 12.5 Hz, 2H), 1.74 (q, J = 12.7 Hz, 2H), 1.46 (s, 9H); ^{13}C NMR (500 MHz, $CDCl_3$) δ = 154.9, 151.3, 147.8, 142.0, 117.9, 117.0, 106.7, 79.8, 61.9, 56.1, 50.1, 49.1 (2), 28.6, 28.3. *tert*-Butyl 4-(1-(2-methoxy-4-nitrophenyl)piperidin-4-yl)piperazine-1-carboxylate (600 mg, 1.43 mmol, 1.0 eq) was dissolved in MeOH (30 mL, 0.05M), after which Pd(C) (60 mg, 10%wt) was added. The stirring solution was flushed through with hydrogen gas for 10 min and the reaction was stirred at RT for 16 h under a balloon of H_2. Reaction completion was monitored via TLC (CH_2Cl_2/MeOH/NH_4OH, 92:7:1). Upon completion, the reaction was vacuum filtered through celite and washed with MeOH to separate Pd and crude product without further purification to yield the title compound. (light yellow oil, yield = 90%): ^{1}H NMR (400 MHz, $CDCl_3$) δ = 6.78 (d, J = 8.8 Hz, 1H), 6.27-6.24 (m, 2H), 3.82 (s, 3H), 3.46-3.40 (m, 8H), 2.56-2.40 (m, 7H), 1.84-1.79 (m, 6H), 1.48 (s, 9H); ^{13}C NMR (400 MHz, $CDCl_3$) δ = 150.0, 148.5, 137.7, 129.2, 114.5, 102.0, 95.2, 74.8, 57.5, 50.6, 46.9, 44.1 (2), 23.7, 23.5.

tert-butyl 4-(1-(4-((3-carbamoyl-6-chloro-5-ethylpyrazin-2-yl)amino)-2-methoxyphenyl)piperidin-4-yl)piperazine-1-carboxylate (**16**). To a stirring solution of 3,5-Dichloro-6-ethylpyrazine-2-carboxamide (175 mg, 0.793 mmol, 1.0 eq) in Dioxane (5 mL, 0.16M), **15** (310 mg, 0.793 mmol, 1.0 eq) and DIPEA (277 mL, 1.59 mmol, 2.0 eq) were added. The reaction was stirred at 110°C for 16 h. Reaction completion was monitored via TLC (CH_2Cl_2/MeOH/NH_4OH, 192:7:1). Upon completion, the reaction mixture was dissolved in EtOAc and partitioned with saturated $NaHCO_3$ and the product was extracted with EtOAc (3x). The organic layers were combined and washed with saturated $NaHCO_3$, water (3x), and saturated NaCl, then dried over Na_2SO_4 and concentrated to dryness. The crude material was adsorbed onto silica gel, then purified by flash column chromatography eluting with CH_2Cl_2/MeOH/NH_4OH, 142:7:1 to yield the title compound. (yellow solid, yield = 86%): ^{1}H NMR (400 MHz, d_6-DMSO) δ = 11.00 (s, 1H), 8.20 (s, 1H), 8.00 (s, 1H), 7.25 (s, 1H), 7.06 (d, J = 7.2 Hz, 1H), 6.84 (d, J = 8.8 Hz, 1H), 3.77 (s, 3H), 3.35-3.30 (m, 6H), 2.78 (q, J = 7.5 Hz, 2H), 2.48-2.44 (m, 6H), 2.31 (s, 1H), 1.76 (d, J = 11.2 Hz, 2H), 1.53 (q, J = 10.7, 2H), 1.34 (s, 9H), 1.23 (t, J = 7.4 Hz, 3H); ^{13}C NMR (400 MHz, d_6-DMSO) δ = 168.5, 154.2, 152.5, 149.7, 147.2, 141.6, 137.8, 134.1, 125.1, 118.8, 112.3, 105.1, 79.1, 61.7, 55.8, 50.8, 49.0 (2), 28.5, 27.2, 26.6, 12.4.

tert-butyl 4-(1-(4-((3-carbamoyl-5-ethyl-6-((tetrahydro-2H-pyran-4-yl)amino)pyrazin-2-yl)amino)-2-methoxyphenyl)piperidin-4-yl)piperazine-1-carboxylate (**17**). To a stirring solution of **16** (350 mg, 0.609 mmol, 1.0 eq) in NMP (5 mL, 0.12M), was added 4-aminotetrahydropyran (252 mL, 2.44 mmol, 4.0 eq) and DIPEA (425 mL, 2.44 mmol. 4.0 eq). The reaction was stirred at 150°C for 16 h. Reaction completion was monitored via

TLC (CH_2Cl_2/MeOH/NH_4OH, 92:7:1). Upon completion, the reaction mixture was dissolved in EtOAc and partitioned with saturated $NaHCO_3$ and the product was extracted with EtOAc (3x). The organic layers were combined and washed with saturated $NaHCO_3$, water (3x), and saturated NaCl, then dried over Na_2SO_4 and concentrated to dryness. The crude material was adsorbed onto silica gel, then purified by flash column chromatography eluting with CH_2Cl_2/MeOH/NH_4OH, 192:7:1 to yield the title compound. (yellow solid, yield = 61%): ^{1}H NMR (400 MHz, d_6-DMSO) δ = 11.00 (s, 1H), 7.50 (s, 1H), 7.25-7.20 (m, 2H), 7.00 (s, 1H), 6.82-6.75 (m, 2H), 4.10 (s, 1H), 3.90 (d, J = 9.2 Hz, 2H), 3.79 (s, 3H), 3.37-3.28 (m, 6H), 2.56 (q, J = 7.3 Hz, 2H), 2.48-2.43 (m, 6H), 2.29 (s, 1H), 1.92-1.75 (m, 6H), 1.65-1.49 (m, 4H), 1.38 (s, 9H), 1.17 (t, J = 7.6 Hz, 3H); ^{13}C NMR (400 MHz, d_6-DMSO) δ = 170.1, 154.2, 152.7, 152.2, 150.6, 136.9, 135.8, 131.9, 118.7, 112.0, 105.2, 79.1, 66.9, 61.7, 56.1, 51.0, 49.0 (2), 48.0, 32.6, 28.5 (2), 24.6, 17.7, 11.4.

6-ethyl-3-((3-methoxy-4-(4-(piperazin-1-yl)piperidin-1-yl)phenyl)amino)-5-((tetrahydro-2H-pyran-4-yl)amino)pyrazine-2-carboxamide (**18**). **17** (170 mg, 0.305 mmol, 1.0 eq) was dissolved in CH_2Cl_2 (0.1M). Trifluoroacetic acid (0.1M) was added to the reaction and left stirring at RT for 2 h. Reaction completion was monitored via TLC (CH_2Cl_2/MeOH/NH_4OH, 92:7:1). Upon completion, the solvent was removed under vacuum without further purification to afford the title compound. (yellow oil, yield = 94%): ^{1}H NMR (400 MHz, d_6-DMSO) δ = 11.25 (s, 1H), 7.57 (s, 1H), 7.46 (d, J = 7.6 Hz, 1H), 7.28 (s, 1H), 7.15-7.13 (m, 2H), 6.86 (d, J = 6.8 Hz, 1H), 4.10 (s, 1H), 3.93-3.85 (m, 5H), 3.54 (d, J = 10.8 Hz, 2H), 3.39-3.32 (m, 10H), 3.06 (s, 2H), 2.58 (q, J = 7.3 Hz, 2H), 2.15 (d, J = 10.4 Hz, 2H), 1.93-1.82 (m, 5H), 1.64 (q, J = 11.7 Hz, 2H), 1.18 (t, J = 7

Hz, 3H); ^{13}C NMR (400 MHz, d_6-DMSO) δ = 170.0, 159.2, 158.8, 152.6, 152.1, 150.2, 132.8, 120.6, 117.7, 114.8, 112.4, 111.6, 104.6, 66.9, 56.6, 51.3, 48.1, 45.8, 41.4, 32.6, 25.9, 24.7, 11.3.

3-((4-(4-(4-((4-(N-(2-((1H-pyrrolo[2,3-b]pyridin-5-yl)oxy)-4-(4-((4'-chloro-5,5-dimethyl-3,4,5,6-tetrahydro-[1,1'-biphenyl]-2-yl)methyl)piperazin-1-yl)benzoyl)sulfamoyl)-2-nitrophenyl)glycyl)piperazin-1-yl)piperidin-1-yl)-3-methoxyphenyl)amino)-6-ethyl-5-((tetrahydro-2H-pyran-4-yl)amino)pyrazine-2-carboxamide (**3**, CG-4-210). **13a** and **18** were reacted on a 0.0803 mmol scale according to General Procedure C to deliver the title compound. (yellow solid, yield = 41%): ^{1}H NMR (400 MHz, d_6-DMSO) δ = 11.63 (s, 1H), 11.21 (s, 1H), 11.00 (s, 1H), 9.04 (s, 1H), 8.55 (s, 1H), 7.99 (s, 1H), 7.83 (d, J = 7.6 Hz, 1H), 7.50-7.45 (m, 4H), 7.31 (d, J = 7.6 Hz, 2H), 7.25 (d, J = 8.8 Hz, 1H), 7.20 (s, 1H), 7.02-7.00 (m, 4H), 6.81 (d, J = 7.6 Hz, 1H), 6.76 (d, J = 7.6 Hz, 1H), 6.64 (d, J = 8.8 Hz, 1H), 6.35 (s, 1H), 6.17 (s, 1H), 4.26 (s, 2H), 4.10 (s, 1H), 3.90 (d, J = 8.4 Hz, 2H), 3.79 (s, 3H), 3.56-3.52 (m, 4H), 3.03 (s, 6H), 2.91-2.53 (m, 10H), 2.15-2.12 (m, 8H), 1.92 (s, 2H), 1.84-1.82 (m, 4H), 1.62-1.60 (m, 4H), 1.35 (s, 2H), 1.21-1.15 (m, 4H), 0.90 (s, 6H); ^{13}C NMR (400 MHz, d_6-DMSO) δ = 170.1, 165.9, 158.1, 154.7, 152.7, 152.2, 150.6, 146.3, 145.7, 142.5 (2), 136.7, 135.9, 135.6, 134.6 (2), 132.6, 132.0, 131.3, 130.5, 129.7, 129.3, 128.5, 128.0, 127.5, 120.2, 118.8, 118.0, 116.3, 112.0, 109.3 (2), 105.2, 100.4 (2), 66.9 (2), 61.8, 60.1, 56.1, 52.5, 50.9 (2), 49.0 (2), 48.0, 47.2, 46.8, 44.9, 44.4, 35.3, 32.6, 29.3, 28.4 (2), 25.6, 24.6, 11.4; HRMS (ESI) m/z [M+H]+ calcd for $C_{68}H_{79}ClN_{14}O_{10}S$ = 1348.5851; found = 1348.5840.

3-((4-(4-(4-(7-((4-(N-(2-((1H-pyrrolo[2,3-b]pyridin-5-yl)oxy)-4-(4-((4'-chloro-5,5-dimethyl-3,4,5,6-tetrahydro-[1,1'-biphenyl]-2-yl)methyl)piperazin-1-

yl)benzoyl)sulfamoyl)-2-nitrophenyl)amino)heptanoyl)piperazin-1-yl)piperidin-1-yl)-3-methoxyphenyl)amino)-6-ethyl-5-((tetrahydro-2H-pyran-4-yl)amino)pyrazine-2-carboxamide (**4**, CG-4-209). **13b** and **18** were reacted on a 0.0803 mmol scale according to General Procedure C to deliver the title compound. (yellow solid, yield = 58%): ^{1}H NMR (400 MHz, d_6-DMSO) δ = 11.63 (s, 1H), 11.01 (s, 1H), 8.50-8.47 (m, 2H), 7.99 (s, 1H) 7.74 (d, J = 8.8 Hz, 1H), 7.50-7.45 (m, 4H), 7.31 (d, J = 7.6 Hz, 2H), 7.24 (d, J = 8 Hz, 1H), 7.20 (s, 1H), 7.01-6.95 (m, 4H), 6.80-6.75 (m, 2H), 6.64 (d, J = 8.4 Hz, 1H), 6.34 (s, 1H), 6.18 (s, 1H), 4.10 (s, 1H), 3.89 (d, J = 9.6 Hz, 2H), 3.78 (s, 3H), 3.43 (s, 8H), 3.02 (s, 4H), 2.69 (s, 2H), 2.60-2.44 (m, 10H), 2.27 (t, J = 7 Hz, 2H), 2.14-2.10 (m, 6H), 1.91 (s, 2H), 1.84-1.78 (m, 4H), 1.65-1.45 (m, 8H), 1.34-1.30 (m, 6H), 1.20-1.15 (m, 4H), 0.89 (s, 6H); ^{13}C NMR (400 MHz, d_6-DMSO) δ = 170.9, 170.1, 157.9, 152.7, 152.2, 150.6, 147.3, 145.7, 142.5, 136.7, 135.9, 135.6, 134.6 (2), 132.5, 131.9, 131.3, 130.5, 129.8, 129.4, 128.5 (2), 128.0, 127.7, 120.2, 118.8 (2), 117.8, 115.0, 112.0 (2), 109.3, 105.2, 100.3, 66.9, 61.8, 60.1, 56.1, 52.6 (2), 50.8 (2), 49.4, 49.0, 48.0, 47.2 (2), 46.8, 45.3, 42.9, 41.3, 35.3, 32.6, 32.5, 29.3, 28.8, 28.4 (2), 26.6, 25.6, 25.1, 24.6, 11.4; HRMS (ESI) m/z [M+H]+ calcd for $C_{74}H_{92}ClN_{15}O_{10}S$ = 1418.6634; found = 1418.6616.

3-((4-(4-(4-(1-(4-(N-(2-((1H-pyrrolo[2,3-b]pyridin-5-yl)oxy)-4-(4-((4'-chloro-5,5-dimethyl-3,4,5,6-tetrahydro-[1,1'-biphenyl]-2-yl)methyl)piperazin-1-yl)benzoyl)sulfamoyl)-2-nitrophenyl)piperidine-4-carbonyl)piperazin-1-yl)piperidin-1-yl)-3-methoxyphenyl)amino)-6-ethyl-5-((tetrahydro-2H-pyran-4-yl)amino)pyrazine-2-carboxamide (**5**, CG-4-208). **13c** and **18** were reacted on a 0.0803 mmol scale according to General Procedure C to deliver the title compound. (yellow solid, yield = 63%): ^{1}H NMR (400 MHz, d_6-DMSO) δ = 11.65 (s, 1H), 11.01 (s, 1H), 8.20 (s, 1H), 8.00 (1H),

7.75 (d, J = 8.8 Hz, 1H), 7.53-7.47 (m, 4H), 7.31 (d, J = 7.6 Hz, 2H), 7.25 (d, J = 8.8 Hz, 1H), 7.20 (s, 1H), 7.14 (d, J = 9.2 Hz, 1H), 7.02-6.99 (m, 3H), 6.80 (d, J = 8.4 Hz, 1H), 6.76 (d, J = 6.8 Hz, 1H), 6.64 (d, J = 8.4 Hz, 1H), 6.37 (s, 1H), 6.18 (s, 1H), 4.10 (s, 1H), 3.9 (d, J = 8 Hz, 2H), 3.79 (s, 3H), 3.57-3.51 (m, 4H), 3.37-3.26 (m, 8H), 3.02 (s, 7H), 2.87 (s, 1H), 2.71-2.48 (m, 7H), 2.17-2.12 (m, 6H), 1.92 (s, 2H), 1.85-1.82 (m, 4H), 1.67-1.61 (m, 8H), 1.35 (t, J = 5.6 Hz, 2H), 1.20-1.15 (m, 4H), 0.89 (s, 6H); ^{13}C NMR (400 MHz, d_6-DMSO) δ = 172.9, 170.1, 157.9, 154.5, 152.7, 152.2, 150.6, 148.1, 145.7, 142.4, 136.6, 135.9, 135.6, 134.8, 132.7 (2), 132.0, 131.3, 130.5 (2), 129.2, 128.5 (2), 128.0, 127.0, 120.5, 120.2, 118.8, 117.9, 112.1, 112.0, 109.3, 105.2, 103.8, 100.4, 66.9, 61.9, 60.1, 56.1, 52.5 (2), 50.7, 50.3, 49.6, 49.0, 48.0, 47.2 (2), 46.8, 44.9, 36.5, 35.3, 32.6, 29.3, 28.4 (2), 25.6, 24.6, 11.4; HRMS (ESI) m/z [M+H]+ calcd for $C_{73}H_{88}ClN_{15}O_{10}S$ = 1402.6321; found = 1402.6308.

tert-butyl 4-(4-amino-2-methoxyphenyl)piperazine-1-carboxylate (**19**). To a stirring solution of 2-Fluoro-5-nitroanisole (1.5 g, 8.77 mmol, 1.0 eq) in DMF (30 mL, 0.3M), K_2CO_3 (1.45 g, 10.52 mmol, 1.2 eq) and N-Boc piperazine (1.80 g, 9.64 mmol, 1.1 eq) were added. The reaction was stirred at 50°C for 16 h. Reaction completion was monitored via TLC (hexanes/EtOAc). Upon completion, the reaction mixture was dissolved in EtOAc and partitioned with water and the product was extracted with EtOAc (3x). The organic layers were combined and washed with 0.1M HCl, saturated $NaHCO_3$, water (3x), and saturated NaCl, then dried over Na_2SO_4 and concentrated to dryness without further purification to yield tert-butyl 4-(2-methoxy-4-nitrophenyl)piperazine-1-carboxylate. (yellow solid, yield = 95%): ^{1}H NMR (500 MHz, d_6-DMSO) δ = 7.83 (dd, J = 2.5, 8.5 Hz, 1H), 7.69 (s, 1H), 7.02 (d, J = 8.5 Hz, 1H), 3.91 (s, 3H), 3.46 (s, 4H), 3.14

(s, 4H), 1.41 (s, 9H); ^{13}C NMR (500 MHz, d_6-DMSO) δ = 159.2, 156.1, 152.4, 122.9, 122.5, 84.4, 61.4, 54.6 (2), 33.4. LRMS (ESI) m/z [M+H]+ calcd for $C_{16}H_{23}N_3O_5$ = 337.2; found = 238.1 (loss of Boc group). Tert-butyl 4-(2-methoxy-4-nitrophenyl)piperazine-1-carboxylate (400 mg, 1.19 mmol, 1.0 eq) was dissolved in MeOH (10 mL, 0.1M), after which Pd(C) (40 mg, 10%wt) was added. The stirring solution was flushed through with hydrogen gas for 10 mins and the reaction was stirred at RT for 16 h. Reaction completion was monitored via TLC (CH_2Cl_2/MeOH/NH_4OH, 92:7:1). Upon completion, the reaction was vacuum filtered through celite and washed with MeOH to separate Pd and crude product. The crude material was adsorbed onto silica gel, then purified by flash column chromatography eluting with hexanes/EtOAc to afford the title compound. (black solid, yield = 74%): ^{1}H NMR (400 MHz, $CDCl_3$) δ = 6.75 (d, J = 7.6 Hz, 1H), 6.28-6.25 (m, 2H), 3.83 (s, 3H), 3.60-3.50 (m, 6H), 2.90 (s, 4H), 1.49 (s, 9H); ^{13}C NMR (400 MHz, $CDCl_3$) δ = 150.1, 148.6, 138.2, 128.5, 114.7, 102.0, 95.2, 74.8, 50.6, 46.6 (2), 23.7; LRMS (ESI) m/z [M+H]+ calcd for $C_{16}H_{25}N_3O_3$ = 307.2; found = 208.0 (loss of Boc group).

tert-butyl 4-(4-((3-carbamoyl-6-chloro-5-ethylpyrazin-2-yl)amino)-2-methoxyphenyl)piperazine-1-carboxylate (**20**). To a stirring solution of 3,5-Dichloro-6-ethylpyrazine-2-carboxamide (200 mg, 0.909 mmol, 1.0 eq) in Dioxane (5 mL, 0.2M), **19** (279 mg, 0.909 mmol, 1.0 eq) and DIPEA (318 mL, 1.82 mmol, 2.0 eq) were added. The reaction was stirred at 110°C for 16 h. Reaction completion was monitored via TLC (CH_2Cl_2/MeOH/NH_4OH, 58:7:1). Upon completion, the reaction mixture was dissolved in EtOAc and partitioned with saturated $NaHCO_3$ and the product was extracted with EtOAc (3x). The organic layers were combined and washed with saturated $NaHCO_3$,

water (3x), and saturated NaCl, then dried over Na_2SO_4 and concentrated to dryness. The crude material was adsorbed onto silica gel, then purified by flash column chromatography eluting with CH_2Cl_2/MeOH/NH_4OH, 192:7:1 to yield the title compound. (dark yellow solid, yield = 80%): ^{1}H NMR (400 MHz, d_6-DMSO) δ = 11.02 (s, 1H), 8.20 (s, 1H), 7.98 (s, 1H), 7.27 (s, 1H), 7.09 (d, J = 8.4 Hz, 1H), 6.86 (d, J = 8.4 Hz, 1H), 3.78 (s, 3H), 3.42 (s, 4H), 2.85 (s, 4H), 2.78 (q, J = 7.5 Hz, 2H), 1.40 (s, 9H), 1.23 (t, J = 7.4 Hz, 3H); ^{13}C NMR (400 MHz, d_6-DMSO) δ = 168.5, 154.3, 152.6, 149.6, 147.1, 141.7, 137.0, 134.6, 125.2, 119.0, 112.3, 105.1, 79.3, 55.8, 50.8, 28.5, 27.2, 26.6, 12.4.

tert-butyl 4-(4-((3-carbamoyl-5-ethyl-6-((tetrahydro-2H-pyran-4-yl)amino)pyrazin-2-yl)amino)-2-methoxyphenyl)piperazine-1-carboxylate (**21**). To a stirring solution of **20** (250 mg, 0.509 mmol, 1.0 eq) in NMP (5 mL, 0.1M), was added 4-aminotetrahydropyran (210 mL, 2.04 mmol, 4.0 eq) and DIPEA (355 mL, 2.04 mmol. 4.0 eq). The reaction was stirred at 150°C for 16 h. Reaction completion was monitored via TLC (CH_2Cl_2/MeOH/NH_4OH, 92:7:1). Upon completion, the reaction mixture was dissolved in EtOAc and partitioned with saturated $NaHCO_3$ and the product was extracted with EtOAc (3x). The organic layers were combined and washed with saturated $NaHCO_3$, water (3x), and saturated NaCl, then dried over Na_2SO_4 and concentrated to dryness. The crude material was adsorbed onto silica gel, then purified by flash column chromatography eluting with CH_2Cl_2/MeOH/NH_4OH, 92:7:1 to yield the title compound. (dark yellow solid, yield = 60%): ^{1}H NMR (400 MHz, d_6-DMSO) δ = 11.03 (s, 1H), 7.52 (s, 1H), 7.29 (d, J = 8 Hz, 1H), 7.21 (s, 1H), 7.00 (s, 1H), 6.82 (d, J = 8.4 Hz, 1H), 6.77 (d, J = 6.8 Hz, 1H), 4.10 (s, 1H), 3.90 (d, J = 9.2 Hz, 2H), 3.80 (s, 3H), 3.43-3.35 (m,

6H), 2.84 (s, 4H), 2.56 (d, J = 7.2 Hz, 2H), 1.83 (d, J = 10.8 Hz, 2H), 1.62 (d, J = 10 Hz, 2H), 1.40 (s, 9H), 1.17 (t, J = 7.2 Hz, 3H); ^{13}C NMR (400 MHz, d_6-DMSO) δ = 170.1, 154.3, 152.8, 152.2, 150.6, 136.3, 136.1, 132.0, 119.0, 112.1, 111.9, 105.1, 72.3, 66.9, 56.1 (2), 51.0, 48.0, 32.6, 28.5, 24.6, 11.4.

6-ethyl-3-((3-methoxy-4-(piperazin-1-yl)phenyl)amino)-5-((tetrahydro-2H-pyran-4-yl)amino)pyrazine-2-carboxamide (**22**). **21** (170 mg, 0.305 mmol, 1.0 eq) was dissolved in CH_2Cl_2 (0.1M). Trifluoroacetic acid (0.1M) was added to the reaction and left stirring at RT for 2 h. Reaction completion was monitored via TLC (CH_2Cl_2/MeOH/NH_4OH, 92:7:1). Upon completion, the solvent was removed under vacuum and the crude material was adsorbed onto silica gel, then purified by flash column chromatography eluting with CH_2Cl_2/MeOH/NH_4OH, 58:7:1 to afford the title compound. (yellow foam, yield = 90%): ^{1}H NMR (400 MHz, d_6-DMSO) δ = 11.00 (s, 1H), 7.51 (s, 1H), 7.25 (d, J = 8.8 Hz, 1H), 7.20 (s, 1H), 7.01 (s, 1H), 6.80-6.75 (m, 2H), 4.10 (s, 1H), 3.90 (d, J = 9.2 Hz, 2H), 3.80 (s, 3H), 3.34 (t, J = 11.4 Hz, 2H), 2.82 (s, 8H), 2.56 (q, J = 7.3 Hz, 2H), 1.83 (d, J = 11.4 Hz, 2H), 1.62 (q, J = 9.5 Hz, 2H), 1.17 (t, J = 7.2 Hz, 3H); ^{13}C NMR (400 MHz, d_6-DMSO) δ = 170.1, 152.7, 152.2, 150.6, 137.1, 135.8, 131.9, 118.5, 112.2, 112.1, 105.4, 66.9, 56.1, 52.1, 48.0, 46.2, 32.6, 24.6, 11.4.

3-((4-(4-((4-(N-(2-((1H-pyrrolo[2,3-b]pyridin-5-yl)oxy)-4-(4-((4'-chloro-5,5-dimethyl-3,4,5,6-tetrahydro-[1,1'-biphenyl]-2-yl)methyl)piperazin-1-yl)benzoyl)sulfamoyl)-2-nitrophenyl)glycyl)piperazin-1-yl)-3-methoxyphenyl)amino)-6-ethyl-5-((tetrahydro-2H-pyran-4-yl)amino)pyrazine-2-carboxamide (**6**, CG-3-246). **13a** and **22** were reacted on a 0.107 mmol scale according to General Procedure C to deliver the title compound. (off white solid, yield = 68%): ^{1}H NMR (400 MHz, DMSO) δ = 11.71 (s, 1H), 11.37 (s, 1H),

11.09 (s, 1H), 9.15 (s, 1H), 8.63 (s, 1H), 8.06 (s, 1H), 7.90 (d, J = 8.4 Hz, 1H), 7.56 (s, 2H), 7.53-7.51 (m, 2H), 7.36 (d, J = 8 Hz, 3H), 7.26 (s, 1H), 7.11-7.04 (m, 4H), 6.88 (d, J = 8.4 Hz, 1H), 6.82 (d, J = 8 Hz, 1H), 6.69 (d, J = 8.4 Hz, 1H), 6.41 (s, 1H), 6.22 (s, 1H), 4.36 (s, 2H), 4.15 (s, 1H), 3.95 (d, J = 9.6 Hz, 2H), 3.87 (s, 3H), 3.72-3.67 (m, 4H), 3.40 (s, 2H), 3.10 (s, 4H), 3.03 (s, 2H), 2.97 (s, 2H), 2.78 (s, 2H), 2.61 (q, J = 7.1 Hz, 2H), 2.23 (s, 4H), 2.16 (s, 2H), 1.97 (s, 2H), 1.88 (d, J = 12.8 Hz, 2H), 1.66 (q, J = 11.6 Hz, 2H), 1.40 (t, J = 5.8 Hz, 2H), 1.22 (t, J = 7.4 Hz, 3H), 0.94 (s, 6H); ^{13}C NMR (400 MHz, d_6-DMSO) δ = 170.1, 166.0, 164.3, 162.8, 158.3, 155.0, 152.8, 152.2, 150.6, 147.0, 146.6, 145.8, 142.4, 136.4, 135.8, 135.7, 134.5, 132.6, 132.1, 131.3, 130.4, 130.2, 128.5, 128.1, 127.9, 120.2, 119.0, 118.3, 116.5, 112.2, 112.0, 109.2, 105.1, 102.9, 100.4, 66.9, 60.1, 56.2, 52.4, 51.0, 48.1, 46.9, 46.8, 45.0, 44.7, 42.5, 36.2, 35.2, 32.6, 31.2, 29.3, 28.4, 25.6, 24.7, 11.4.; HRMS (ESI) m/z [M+H]+ calcd for $C_{64}H_{73}ClN_{14}O_{10}S$ = 1265.5116; found = 1265.5113.

3-((4-(4-(7-((4-(N-(2-((1H-pyrrolo[2,3-b]pyridin-5-yl)oxy)-4-(4-((4'-chloro-5,5-dimethyl-3,4,5,6-tetrahydro-[1,1'-biphenyl]-2-yl)methyl)piperazin-1-yl)benzoyl)sulfamoyl)-2-nitrophenyl)amino)heptanoyl)piperazin-1-yl)-3-methoxyphenyl)amino)-6-ethyl-5-((tetrahydro-2H-pyran-4-yl)amino)pyrazine-2-carboxamide (**7**, CG-3-242). **13b** and **22** were reacted on a 0.111 mmol scale according to General Procedure C to deliver the title compound. (yellow solid, yield = 70%): ^{1}H NMR (400 MHz, d_6-DMSO) δ = 11.71 (s, 1H), 11.37 (s, 1H), 11.08 (s, 1H), 8.58 (s, 2H), 8.06 (s, 1H), 7.83 (d, J = 9.6 Hz, 1H), 7.56-7.50 (m, 4H), 7.36-7.32 (m, 3H), 7.25 (s, 1H), 7.08-7.04 (m, 4H), 6.85-6.80 (m, 2H), 6.69 (d, J = 8.4 Hz, 1H), 6.41 (s, 1H), 6.21 (s, 1H), 4.24 (s, 1H), 3.94 (d, J = 9.2 Hz, 2H), 3.84 (s, 3H), 3.59 (s, 4H), 3.36 (s, 4H), 3.08 (s, 4H), 2.91 (s, 2H), 2.87 (s, 2H), 2.75

(s, 2H), 2.61 (q, J = 7.3 Hz, 2H), 2.36 (t, J = 7 Hz, 2H), 2.21-2.15 (m, 6H), 1.96 (s, 2H), 1.87 (d, J = 12.4 Hz, 2H), 1.66-1.54 (m, 6H), 1.39 (s, 6H), 1.21 (t, J = 7.4 Hz, 3H), 0.93 (s, 6H); ^{13}C NMR (400 MHz, d_6-DMSO) δ = 171.0, 170.1, 158.2, 152.8, 152.2, 150.6, 147.6, 145.9, 142.4, 136.3, 136.0, 135.7, 134.6, 134.4, 132.5, 132.0, 131.2, 130.4 (2), 129.9, 128.5 (2), 128.1 (2), 120.2, 118.9, 118.2, 115.2, 112.2, 112.0, 109.2, 105.1, 103.2, 100.4, 66.9, 60.1, 56.2, 52.4, 51.5, 51.0, 48.0, 46.9 (2), 46.7, 45.7, 42.9, 41.7, 35.2, 32.6 (2), 31.9, 29.3, 28.9, 28.3 (2), 26.6, 25.5, 25.2, 24.7, 11.4; HRMS (ESI) m/z [M+H]+ calcd for $C_{69}H_{83}ClN_{14}O_{10}S$ = 1335.5899; found = 1335.5907.

3-((4-(4-(1-(4-(N-(2-((1H-pyrrolo[2,3-b]pyridin-5-yl)oxy)-4-(4-((4'-chloro-5,5-dimethyl-3,4,5,6-tetrahydro-[1,1'-biphenyl]-2-yl)methyl)piperazin-1-yl)benzoyl)sulfamoyl)-2-nitrophenyl)piperidine-4-carbonyl)piperazin-1-yl)-3-methoxyphenyl)amino)-6-ethyl-5-((tetrahydro-2H-pyran-4-yl)amino)pyrazine-2-carboxamide (**8**, CG-3-245): **13c** and **22** were reacted on a 0.123 mmol scale according to General Procedure C to deliver the title compound. (yellow solid, yield = 68%): ^{1}H NMR (400 MHz, d_6-DMSO) δ = 11.69 (s, 1H), 11.29 (s, 1H), 11.04 (s, 1H), 8.25 (s, 1H), 8.03 (s, 1H), 7.80 (d, J = 9.6 Hz, 1H), 7.53-7.49 (m, 4H), 7.31 (d, J = 7.6 Hz, 3H), 7.23-7.21 (m, 2H), 7.01 (d, J = 8.8 Hz, 3H), 6.82 (d, J = 8.8 Hz, 1H), 6.77 (d, J = 8 Hz, 1H), 6.65 (d, J = 8.8 Hz, 1H), 6.39 (s, 1H), 6.17 (s, 1H), 4.11 (s, 1H), 3.90 (d, J = 9.2 Hz, 2H), 3.81 (s, 3H), 3.66 (s, 2H), 6.59 (s, 2H), 3.38-3.32 (m, 2H), 3.05 (s, 6H), 2.92 (s, 4H), 2.85 (s, 2H), 2.75 (s, 2H), 2.57 (q, J = 7.3 Hz, 2H), 2.48 (s, 1H), 2.20 (s, 4H), 2.12 (s, 2H), 1.92 (s, 2H), 1.84 (d, J = 12.4 Hz, 2H), 1.71-1.58 (m, 6H), 1.35 (t, J = 6 Hz, 2H), 1.17 (t, J = 7.6 Hz, 3H), 0.89 (s, 6H); ^{13}C NMR (400 MHz, d_6-DMSO) δ = 172.6, 170.1, 158.3, 154.9, 152.8, 152.2, 150.6, 148.5, 147.1, 145.9, 142.4, 137.8, 136.4, 135.9, 135.8, 132.8, 132.6, 132.1, 131.3, 130.4, 128.6,

128.2, 127.6, 120.6, 120.3, 119.0, 118.3, 112.2, 112.0, 109.2, 105.1, 102.9, 100.5, 66.9, 60.0, 56.2, 52.4 (2), 51.7, 51.1, 50.2 (2), 48.1, 46.9, 46.8, 45.7, 41.9, 36.5, 35.2, 32.6, 29.3, 28.4 (2), 25.6, 24.7, 11.4; HRMS (ESI) m/z [M+H]+ calcd for $C_{68}H_{79}ClN_{14}O_{10}S$ = 1319.5586; found = 1319.5583.

5.2 Synthesis of FLT3 Covalent Inhibitors to Counter Gatekeeper Mutation

5.2.1 Introduction

Proximal to the binding site of FLT3 exists a solvent exposed cysteine residues (Cys695).[57]As discussed previously, this cysteine is utilized in the design of the covalent FLT3 inhibitor FF-10101 (**Figure 5.2.1.2**) to overcome the gatekeeper mutation that bestows gilteritinib resistance to AML cancer cells.[70] While FF-10101 is performing well in a phase 1 clinical trial, no patients who harbored the F691L gatekeeper mutation were included in the study.[71] To expand the possible solutions to combat the gatekeeper mutation, we sought to create a FLT3 covalent inhibitor by leveraging the structure of gilteritinib. Since gilteritinib is an FDA-approved inhibitor, it has already demonstrated to be a well-tolerated therapeutic and makes for an ideal candidate for modification to recover its anti-leukemic efficacy in resistant AML.[68] By utilizing gilteritinib (**Figure 5.2.1.1**), the high potency of the compound can be leveraged to help guide the addition of an electrophilic warhead to react with Cys695 and ultimately restore an anti-leukemic effect.

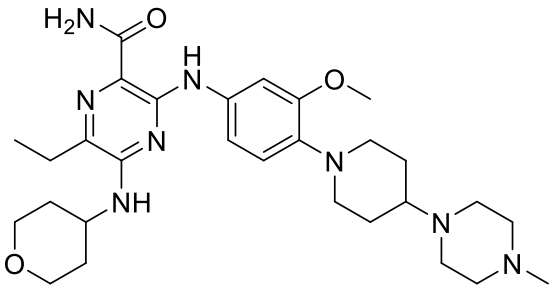

Figure 5.2.1.1: *Structure of gilteritinib*

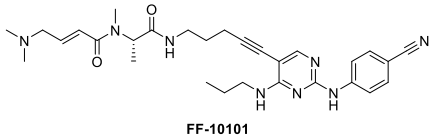

Figure 5.2.1.2: *Structure of FF-10101*

5.2.2 Design Rationale

Looking at the crystal structure of gilteritinib bound to FLT3, there are multiple portions of the molecule that rest outside of the binding site and are solvent exposed.[196] These exit vectors are ideal grafting points for linker groups due to them not interacting with the protein in the bound state.[91] From this structure, we identified two sites where we could modify and add different linking groups and by extension our acrylamide electrophilic warhead for reacting with Cys695 (**Figure 5.2.2.1**). We will modify the piperidine and phenoxy motifs on gilteritinib and graft electrophilic warheads off these modified positions. After identifying these grafting sites, SILCS modeling was conducted by Dr. Erik Nordquist and was utilized to guide our linker design with the goal of creating an inhibitor that can interact with the binding site while reacting with Cys695.[197] From these simulations, FragMaps are overlaid onto the protein that correspond to chemical motifs

that are predicted to favorably bind to that portion of the protein (**Figure 5.2.2.2**).[197] Using these FragMaps, inhibitors were assigned multiple predictive binding values as represented as LGFE Gibbs free energy with the units kcal/mol. We can calculate the predicted dissociation constant using the equation $\Delta G = RT\ln Kd$.[197] LGFE_eq is the predictive binding from the most favorable pose when only factoring in noncovalent interactions between the compound and FLT3. LGFE_rx is the predictive binding from the most favorable pose with the highest overlap with a target cysteine FragMap. Finally, LGFE_rxeq is the predictive binding from the most favorable pose that has a non-zero chance of contacting a target cysteine. These three values are used to guide our inhibitor design because they can be used to predict how certain modifications will impact binding affinity.

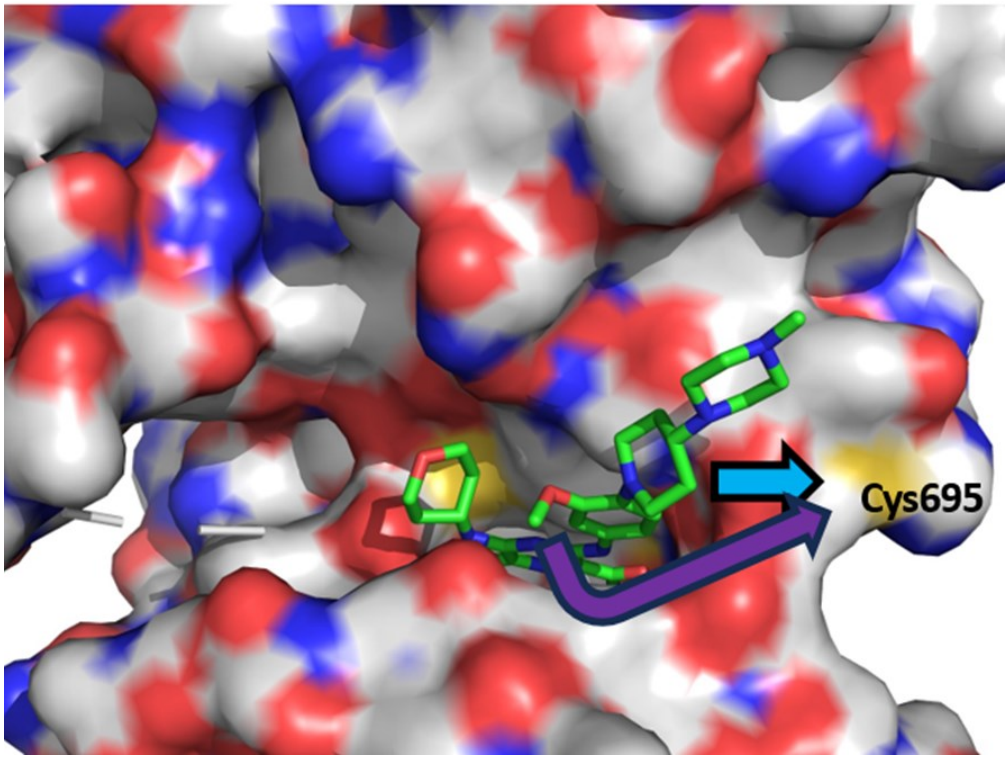

Figure 5.2.2.1: *Crystal structure of gilteritinib bound to FLT3 (PDB ID: 6JQR) with Cys695 residue highlighted. Arrows starting from gilteritinib represent modifiable electorphilic warhead grafting points*

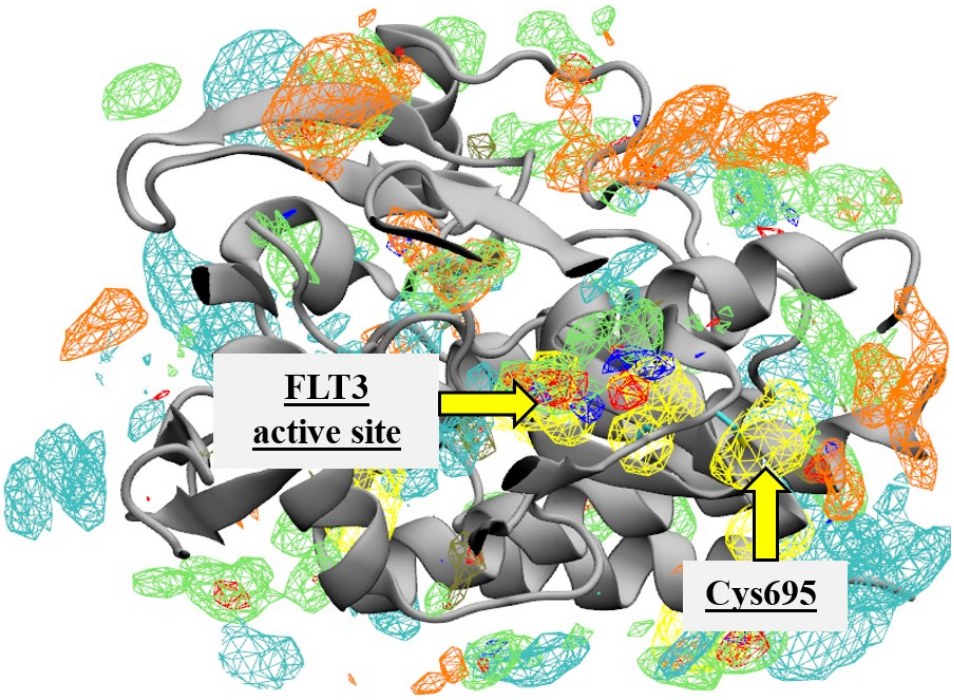

Figure 5.2.2.2: *Crystal structure of gilteritinib bound to FLT3 (PDB ID: 6JQR) with SILCS FragMaps. The FLT3 active site and Cys695 FragMaps are highlighted.*

5.2.3 First Generation FLT3 Covalent Inhibitors

The first grafting spot we explored was by modifying the piperidine-piperazine motif on the original gilteritinib structure. For this class of inhibitors, Dr. Erik Nordquist first tested four compounds using SILCS simulations on the crystal structure of gilteritinib bound to FLT3 (**Table 5.2.3.1**). From these simulations we obtain LGFE values that can be converted into predictive dissociation constants using the equation $\Delta G = RT\ln Kd$.[197] While these individual predictive values are important, by examining the difference between the two LGFE values we can see the predicted loss of binding as our compounds act out their function of binding Cys695. From our list of four compounds, CG-4-163 is

predicted to have the most favorable binding due to the smallest difference between the two LGFE values.

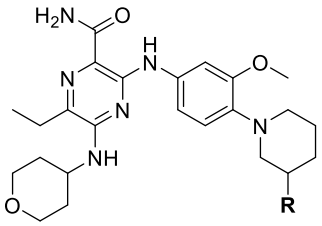

Compound Code	R	LGFE_eq (kcal/mol)	LGFE_rxeq (kcal/mol)
CG-4-156	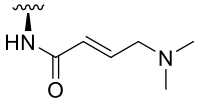	-17.0	-9.6
CG-4-157	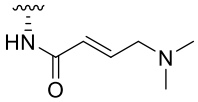	-17.5	-12.5
CG-4-162	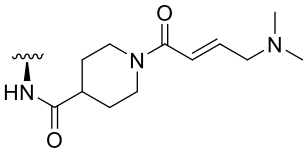	-17.2	-15.9
CG-4-163	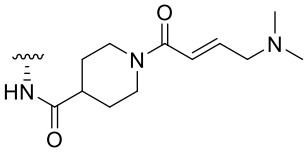	-18.1	-17.2

Table 5.2.3.1: *LGFE values for first generation FLT3 covalent inhibitors*

5.2.3.1 Synthesis of first generation FLT3 Covalent Inhibitors

Figure 5.2.3.1.1 outlines the synthesis of first generation FLT3 inhibitors in which we started with purchased both chiral isomers of 3-(Boc-amino)piperidines and performed S_NAr on 1-fluoro-2-methoxy-4-nitrobenzene and reduced to produce **2**. An S_NAr between 3,5-dichloro-6-ethylpyrazine-2-carboxamide and **2** was guided by anchimeric assistance

from the carboxamide group directing substitution to the ortho carbon affording **3**. Another S_NAr followed using 4-amino tetrahydropyran at 150°C to yield **4**. Standard chemistry followed and two final compounds were synthesized represented by compound **6**. Additional inhibitors were synthesized utilizing **5** and performing a HATU coupling with 1-(tert-butoxycarbonyl)piperidine-4-carboxylic acid along with standard transformations to furnish both chiral isomers of **9**.

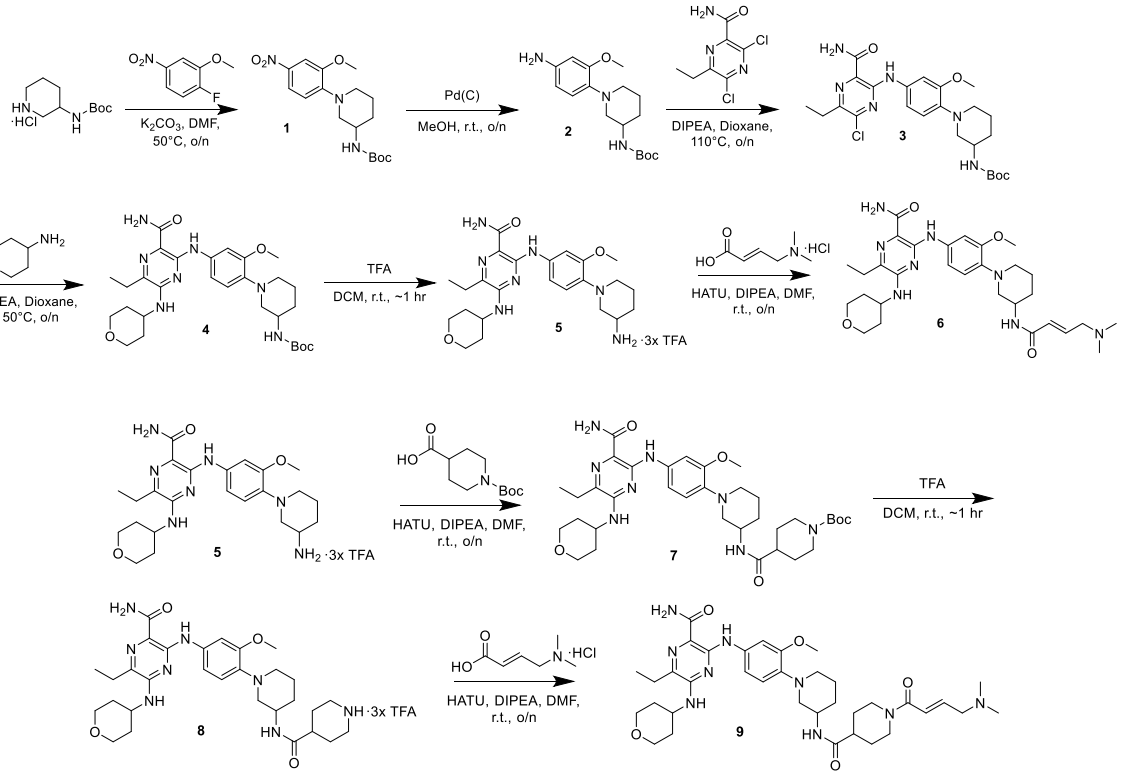

Figure 5.2.3.1.1: *Synthesis of first generation FLT3 covalent inhibitors*

5.2.3.2 Biological Evaluation of first generation FLT3 Covalent Inhibitors

We first tested our 1st generation inhibitors by commissioning Element / Nanosyn to conduct a cell-free TR-FRET assay to measure the IC_{50} of our compounds against WT FLT3 (**Table 5.2.3.2.1**). We had these compounds tested twice in this TR-FRET assay,

once with no additional incubation between our compounds and the FLT3 protein and another experiment where our compounds were incubated with FLT3 for an additional 3 hours. While gilteritinib itself was not tested, the literature IC_{50} value of gilteritinib against FLT3 is ~1nM. The cell-free data suggests that the modifications we performed did not cause a drastic change in gilteritinib inherent binding to FLT3 as all our compounds have a measured IC_{50} value approximately between 2nM-1nM. After the cell-free testing, we conducted AlamarBlue cell proliferation assays to measure the anti-leukemic effects of our inhibitors in various AML cell lines. Starting with MV4;11 and BCL2 OE MV4;11 cells (**Table 5.2.3.2.2**), our compounds demonstrated low nM potency with CG-4-163 demonstrating a similar effect to gilteritinib in the BCL2 overexpressing cell models. After this promising data, we shifted our focus to MOLM14 and MOLM14 F691L FLT3 overexpressing AML cells and tested our compounds potency. Again using an AlamarBlue assay, our compounds demonstrated worse potency when compared to gilteritinib with our best compound CG-4-157 being ~2-fold worse than the control compound (**Table 5.2.3.2.3**).

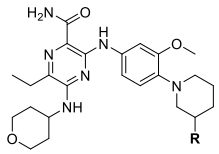

Compound Code	R	FLT3 IC_{50} (nM)	3 hrs. inc. FLT3 IC_{50} (nM)
Staurosporine (Control)		0.063 ± 0.00499	0.0285 ± 0.00242
CG-4-156	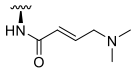	1.14 ± 0.207	1.93 ± 0.194
CG-4-157	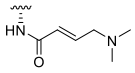	1.37 ± 0.148	1.75 ± 0.244
CG-4-162	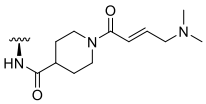	1.19 ± 0.129	1.63 ± 0.285
CG-4-163	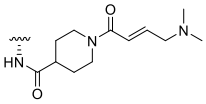	1.24 ± 0.256	1.23 ± 0.245

Table 5.2.3.2.1: *Cell-free inhibition of FLT3 with first generation FLT3 covalent inhibitors*

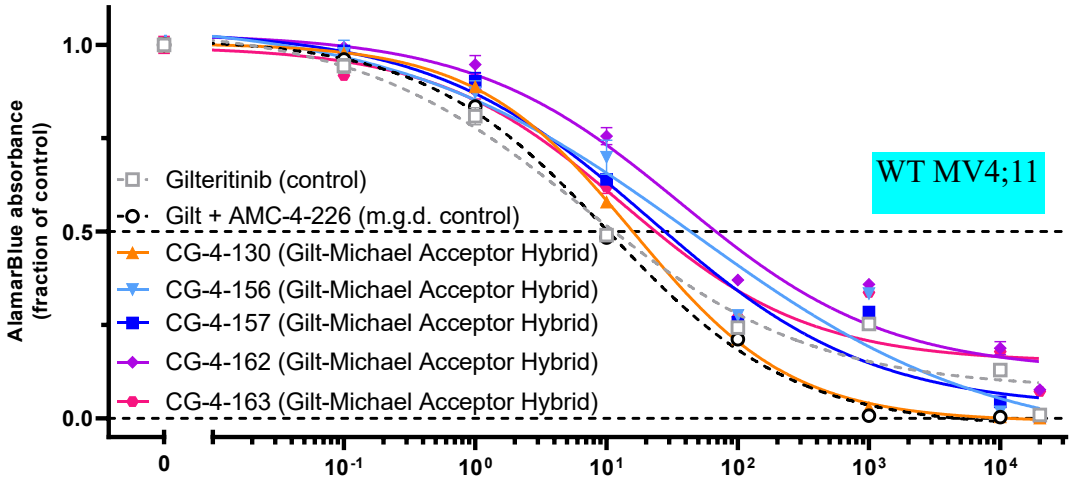

Figure 5.2.3.2.1: *Anti-proliferation effects of first generation FLT3 covalent inhibitors in WT MV4;11 cells*

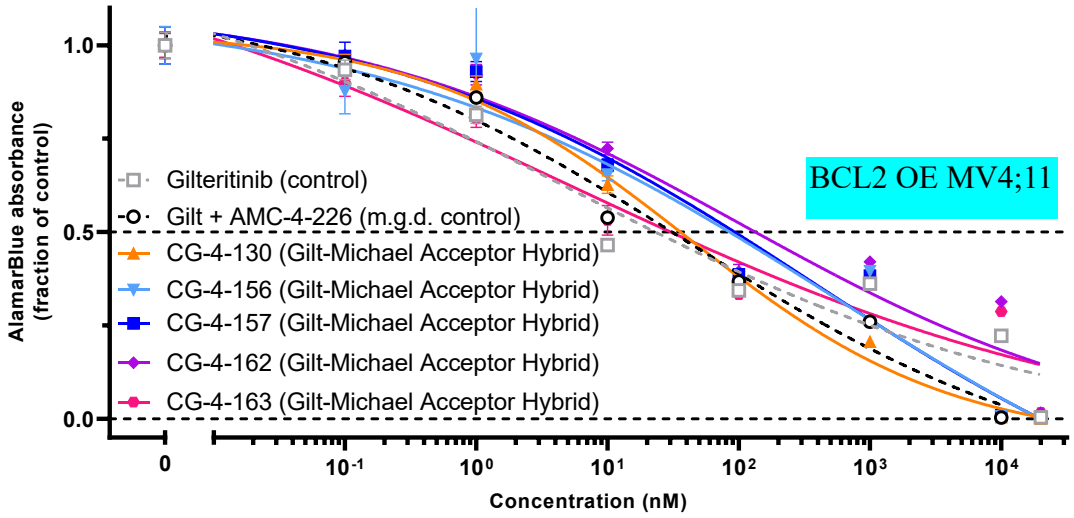

Figure 5.2.3.2.2: *Anti-proliferation effects of first generation FLT3 covalent inhibitors in BCL2 OE MV4;11 cells*

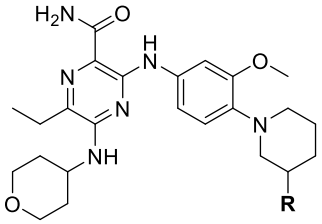

Compound Code	R	WT MV4;11 IC_{50} (nM)	BCL2 OE MV4;11 IC_{50} (nM)
Gilteritinib (Control)		6.8	5.2
CG-4-156	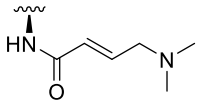	45.2	510.7
CG-4-157	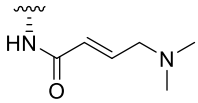	21.6	375.3
CG-4-162	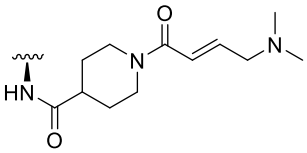	36.4	104.1
CG-4-163	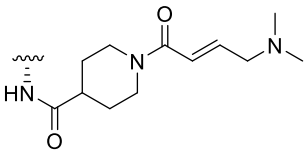	13.3	5.2

Table 5.2.3.2.2: *IC_{50} values for anti-proliferation effects of first generation FLT3 covalent inhibitors in MV4;11 cells*

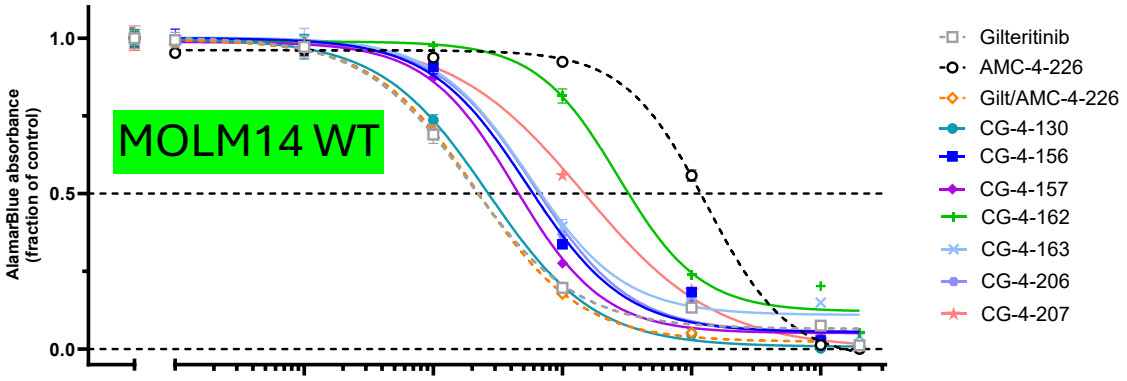

Figure 5.2.3.2.3: *Anti-proliferation effects of first generation FLT3 covalent inhibitors in WT MOLM14 cells*

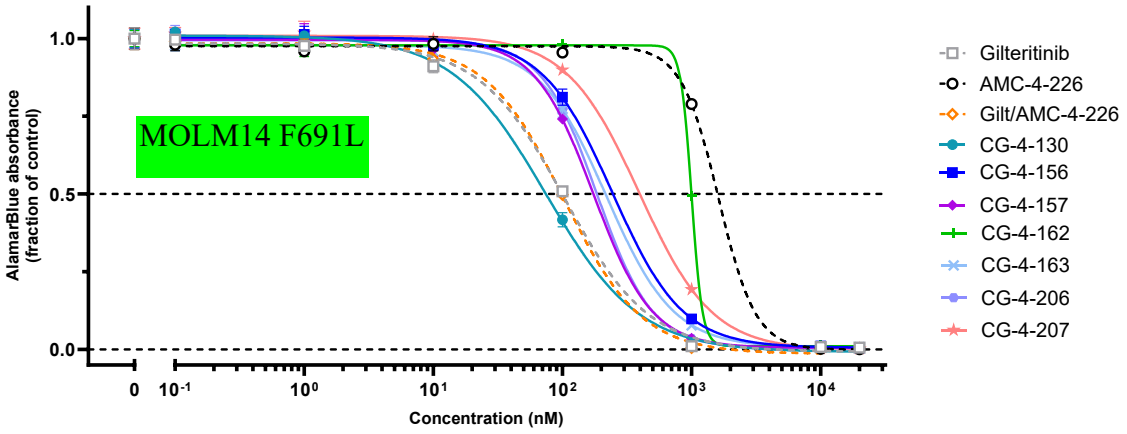

Figure 5.2.3.2.4: *Anti-proliferation effects of first generation FLT3 covalent inhibitors in FLT3 F691L MOLM14 cells*

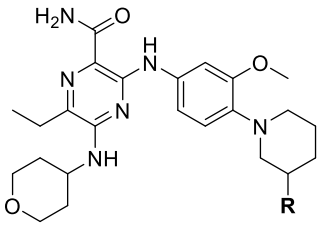

Compound Code	R	WT MOLM14 IC_{50} (nM)	MOLM14 F691L IC_{50} (nM)
Gilteritinib (Control)		19.25	103.1
CG-4-156	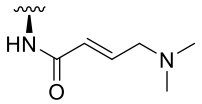	53.61	243.5
CG-4-157	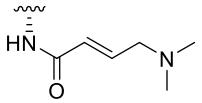	42.93	173.6
CG-4-162	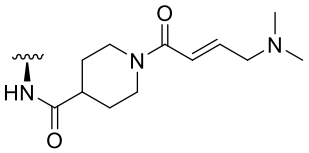	270.1	1000
CG-4-163	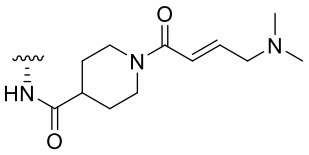	55.23	219.3

Table 5.2.3.2.3: *IC_{50} values for anti-proliferation effects of first generation FLT3 covalent inhibitors in MOLM14 cells*

5.2.4 Second Generation FLT3 Covalent Inhibitors

For our next class of FLT3 covalent inhibitors, we focused on modifying the methoxy group of gilteritinib to graft on various linkers. In a similar manner to before, SILCS simulations were done by Dr. Erik Nordquist on multiple compounds to predict the optimal linker length and rigidity (**Table 5.2.4.1**).

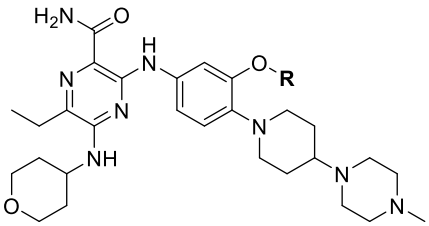

Compound Code	R	LGFE_eq (kcal/mol)	LGFE_rxeq (kcal/mol)
CG-4-206	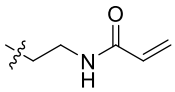	-16.6	-8.9
CG-4-207	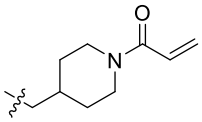	-17.7	-10.4
CG-5-002	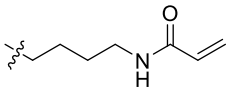	-17.7	-8.9
CG-5-008	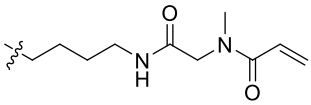	-19.6	-16.4

Table 5.2.4.1: *LGFE values for second generation FLT3 covalent inhibitors*

5.2.4.1 Synthesis of first generation FLT3 covalent Inhibitors

Following **Figure 5.2.4.1.1**, we synthesized the solubilizing group on gilteritinib by performing a reductive amination between N-methyl piperazine and N-boc-4-piperidone after which a boc deprotection was done using TFA to create **11**. We started by alkylating 2-fluoro-5-nitrophenol with tert-butyl (2-bromoethyl)carbamate to afford **12**. Similar chemistry found in the previous section was done on **12** to form the penultimate intermediate **17** which was acylated with acryloyl chloride resulted in **18**. Similar steps

were taken to form our next two final compound from **Figure 5.2.4.1.2** and **Figure 5.2.4.1.3**. Alkylating 2-fluoro-5-nitrophenol with tert-butyl 4-(bromomethyl)piperidine-1-carboxylate yields **19** which underwent the same chemistry as **12** to afford final compound **25**. 2-fluoro-5-nitrophenol was used again in which a Mitsunobu reaction with tert-butyl (4-hydroxybutyl)carbamate formed **26** and similar chemistry used to form our last two final compounds was conducted to yield final compound **32**. The last two compounds were created by following **Figure 5.2.4.1.4** in which HATU coupling **31** and Boc-sarcosine together makes **33**. Compound **33** then had the Boc group removed and the resulting intermediate **34** was acylated with either acryloyl chloride or propionyl chloride yielding **35** and **36**.

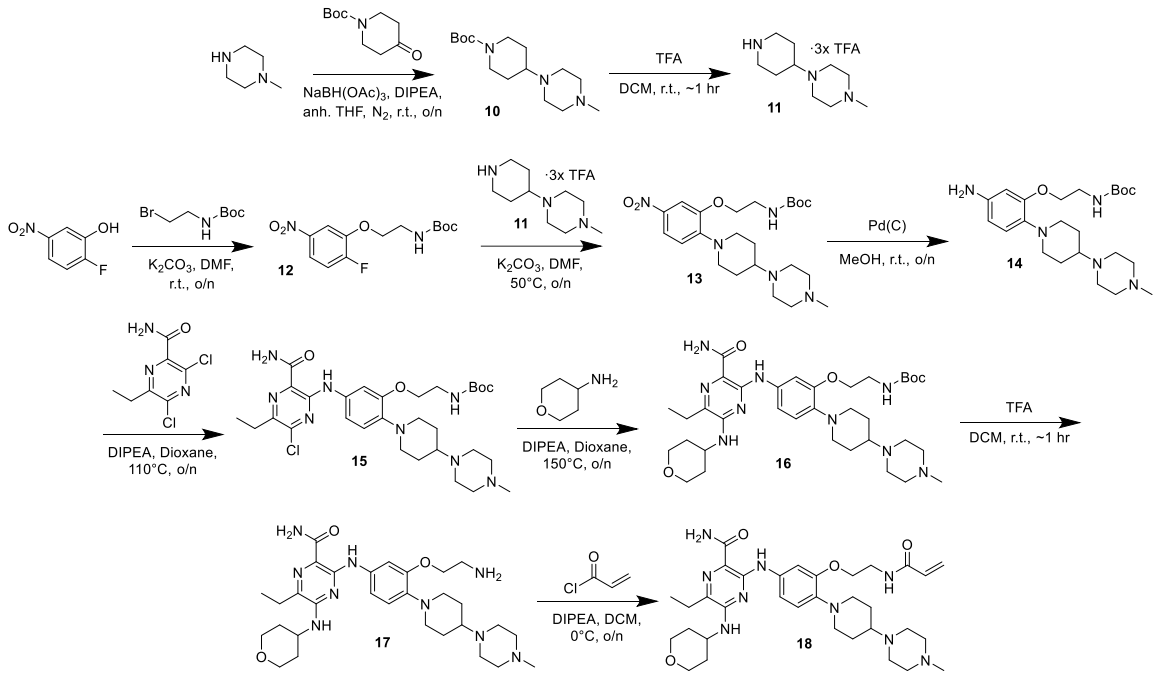

Figure 5.2.4.1.1: *Synthesis of second generation FLT3 covalent inhibitor CG-4-206*

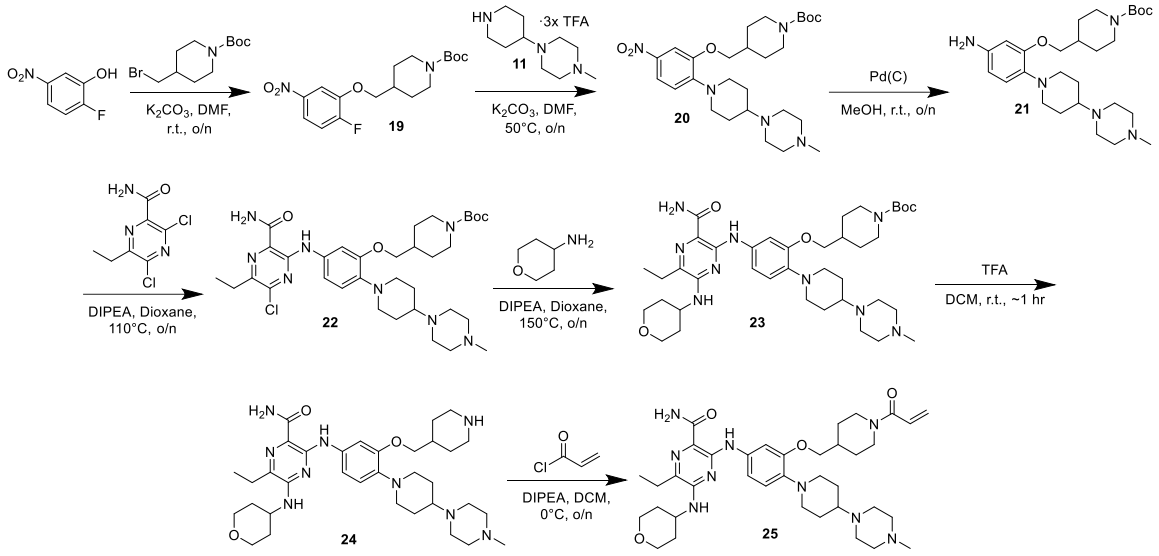

Figure 5.2.4.1.2: *Synthesis of second generation FLT3 covalent inhibitor CG-4-207*

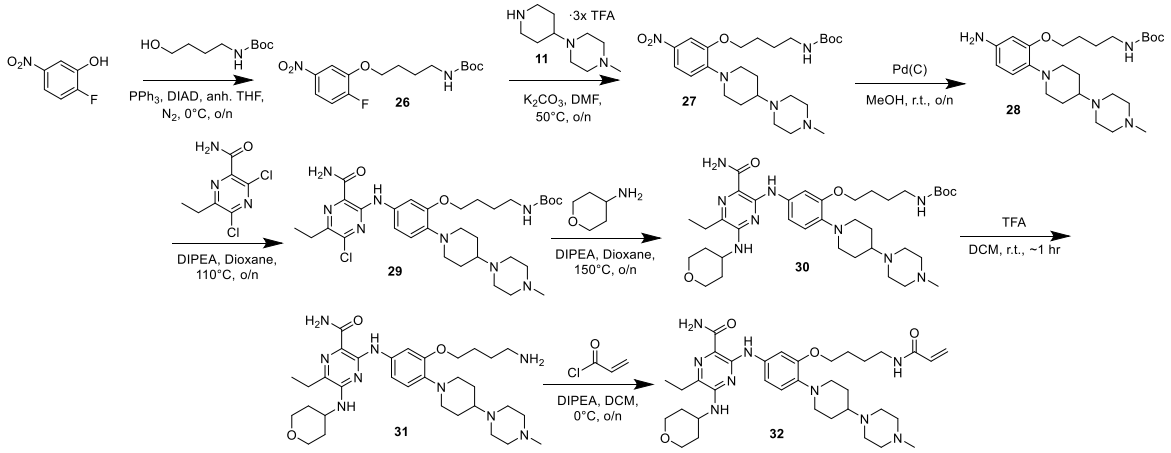

Figure 5.2.4.1.3: *Synthesis of second generation FLT3 covalent inhibitor CG-4-208*

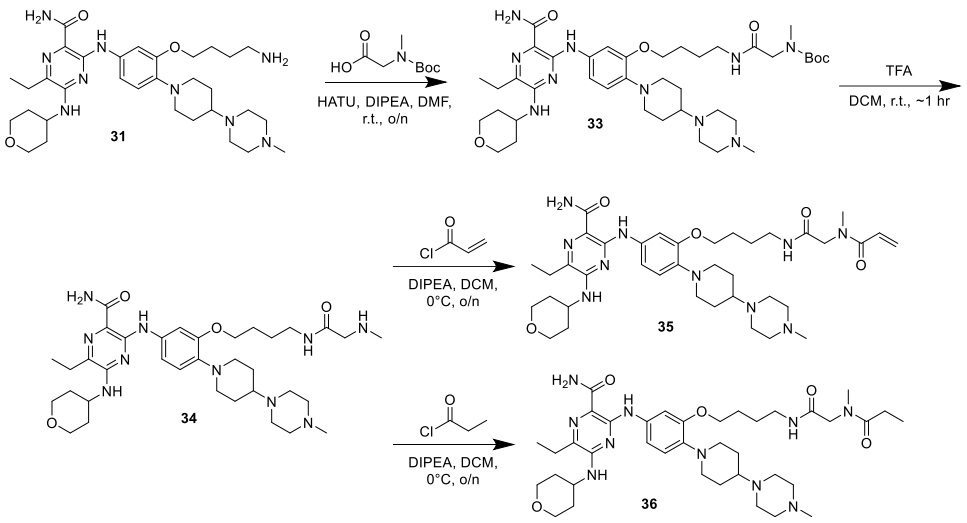

Figure 5.2.4.1.4: *Synthesis of second generation FLT3 covalent inhibitor CG-5-008 & CG-5-024*

5.2.4.2 Biological Evaluation of second generation FLT3 Covalent Inhibitors

In a similar manner to before, we had our compounds tested in a cell-free assay. We commissioned DiscoverX to conduct a KINOMEscan assay to evaluate the K_d of our inhibitors against FLT3 (**Table 5.2.4.2.1***)*. Excitingly, CG-5-008 recorded a K_d value in the picoM range against FLT3. Again, we conducted an AlamarBlues cell proliferation assay with our 2nd generation inhibitors using MOLM14 and MOLM14 F691L FLT3 overexpressing AML cell lines (**Table 5.2.4.2.2**). Excitingly, CG-5-008 performs the best out of all our compounds with a similar potency as gilteritinib in WT MOLM14 cells and less than a 2-fold decrease in potency when tested in MOLM14 F691L FLT3 cells. Additionally, our deactivated compound CG-5-024 loses all potency when the acrylamide is swapped for the inactive propionyl motif. This drastic shift in measured IC50 values between CG-5-008 and CG-5-024 supports the importance of the electrophilic warhead with respect to binding FLT3.

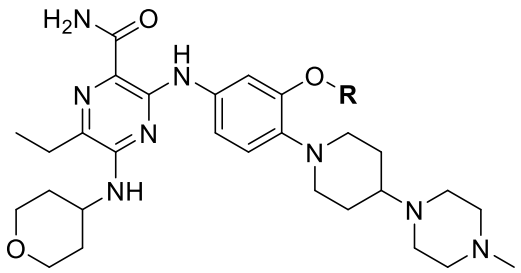

Compound Code	R	FLT3 K_d (nM)
Gilteritinib (Control)		1.5 ± 0.554
CG-4-206	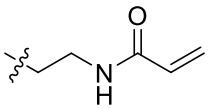	Not Tested
CG-4-207	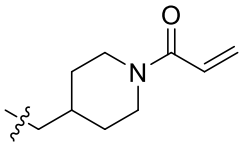	Not Tested
CG-5-002	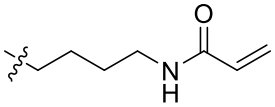	1.5 ± 0.139
CG-5-008	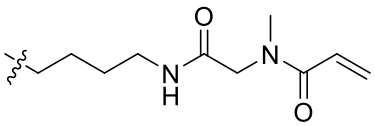	0.87 ± 0.284
CG-5-024	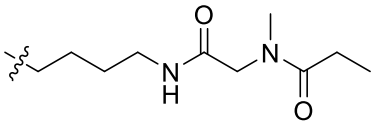	Not Tested

Table 5.2.4.2.1: *Cell-free inhibition of FLT3 with second generation FLT3 covalent inhibitors*

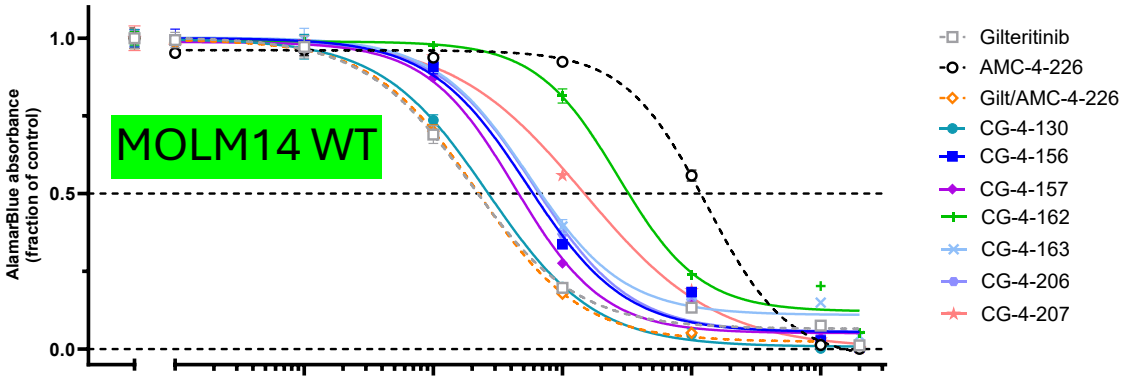

Figure 5.2.3.4.1: *Anti-proliferation effects of second generation FLT3 covalent inhibitors in WT MOLM14 cells*

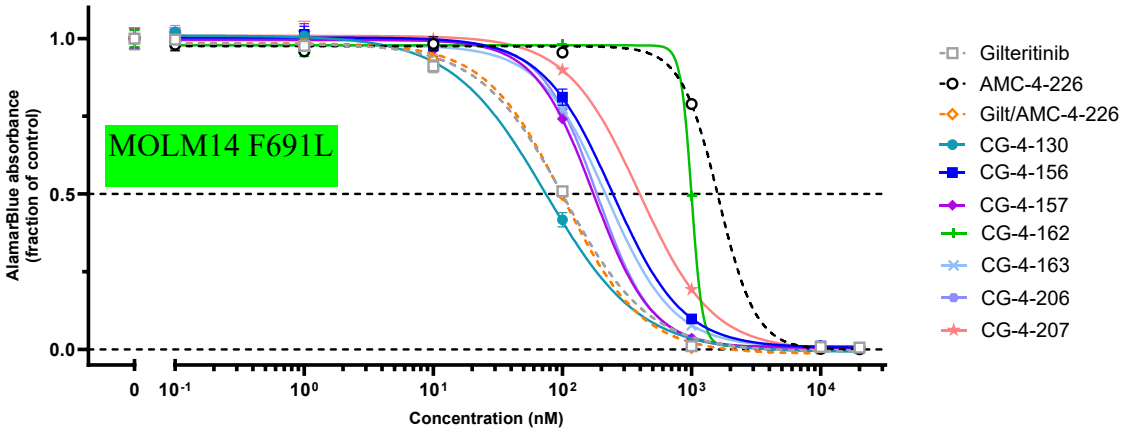

Figure 5.2.3.4.2: *Anti-proliferation effects of second generation FLT3 covalent inhibitors in FLT3 F691L MOLM14 cells*

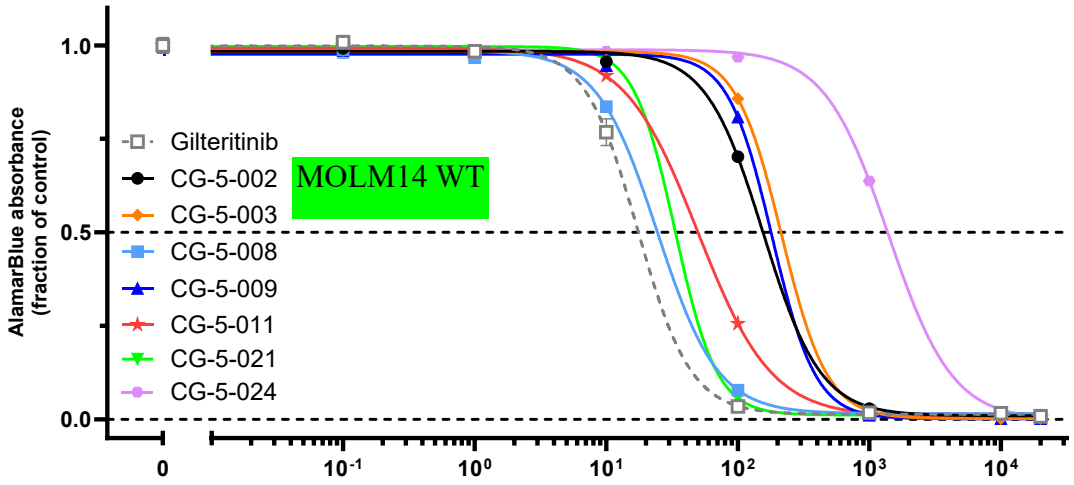

Figure 5.2.3.4.3: *Anti-proliferation effects of second generation FLT3 covalent inhibitors in WT MOLM14 cells*

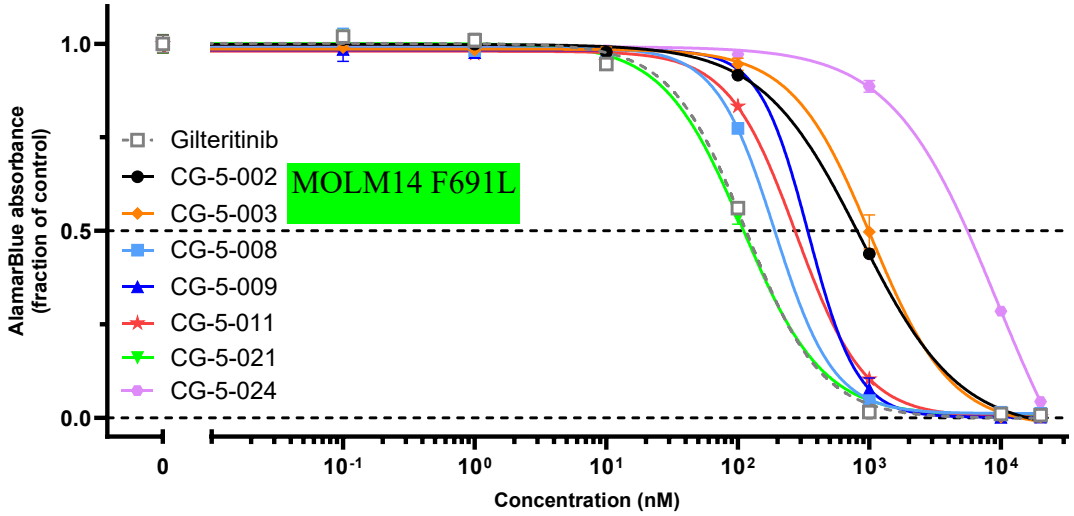

Figure 5.2.3.4.4: *Anti-proliferation effects of second generation FLT3 covalent inhibitors in FLT3 F691L MOLM14 cells*

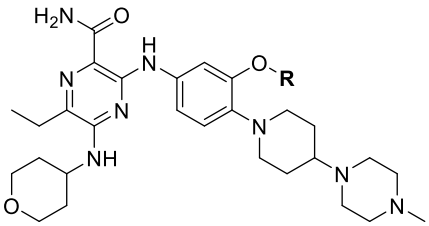

Compound Code	R	WT MOLM14 IC_{50} (nM)	MOLM14 F691L IC_{50} (nM)
Gilteritinib (Control)		18.3	109.4
CG-4-206	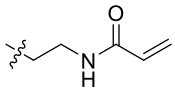	60.4	185.2
CG-4-207	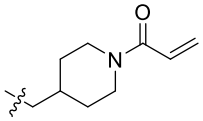	147.4	393.9
CG-5-002	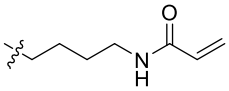	156.3	855.3
CG-5-008	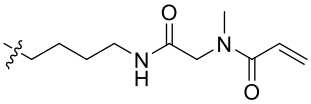	24.5	190.8
CG-5-024	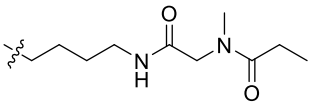	1399	9373

Table 5.2.4.2.2: *IC_{50} values for anti-proliferation effects of second generation FLT3 covalent inhibitors in MOLM14 cells*

5.2.5 Third Generation FLT3 Covalent Inhibitor

For our last class of compounds we created a "merged" covalent inhibitor by utilizing the structure of gilteritinib and FF-10101.[65,70] Analyzing the crystal structures of gilteritinib

and FF-10101 bound to gilteritinib, we noticed that the phenyl carbon para to the aniline was spatially near the start of the linker on FF-10101 (**Figure 5.2.5.1**).[196,198] Towards increasing our inhibitor diversity, we devised a compound that utilizes the noncovalent portion of gilteritinib and grafted on the linker and electrophilic warhead of FF-10101 to target Cys695 which is outlined in **Figure 5.2.5.2**.

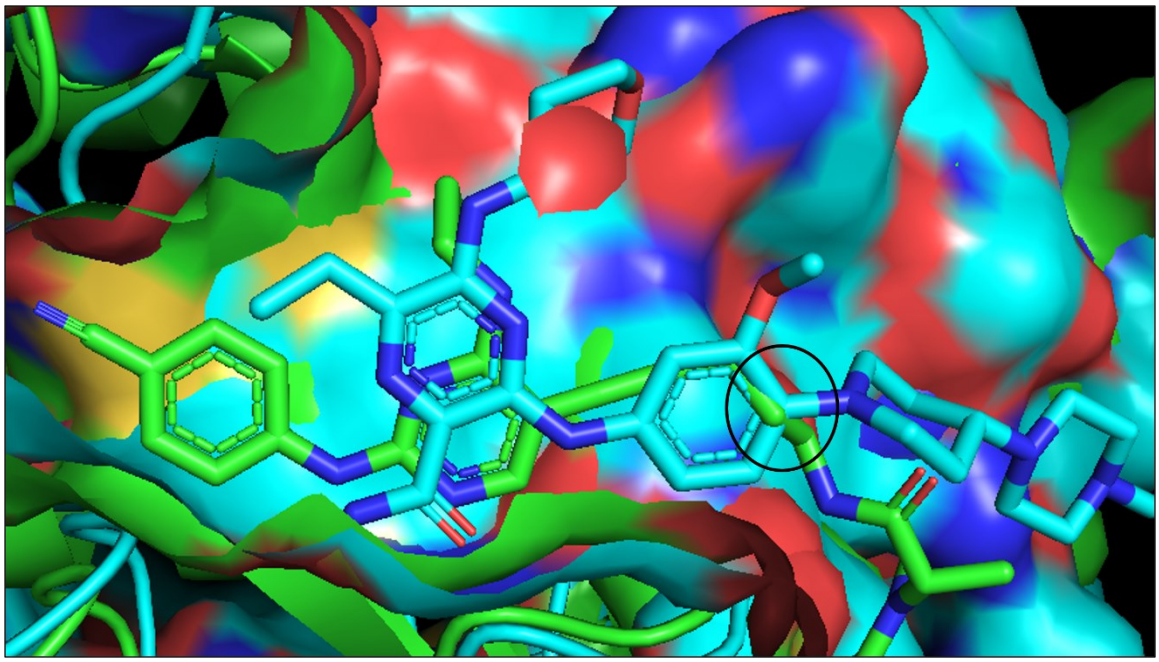

Figure 5.2.5.1: *Crystal structure of gilteritinib (PDB ID: 6JQR) overlayed crystal structure of FF-10101 bound to FLT3 (PDB ID: 5X02). Black circle highlights spatial overlap between the para carbon on the benzyl group of gilteritinib and the start of the electrophilic warhead tail of FF-10101.*

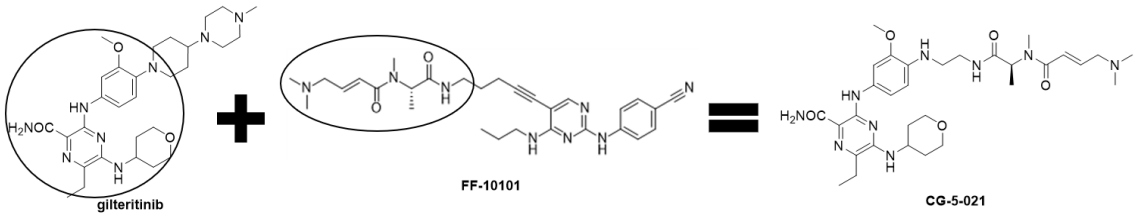

Figure 5.2.5.2: *Schematic showing the design rational of our third generation FLT3 covalent inhibitor*

5.2.5.1 Synthesis of Third Generation FLT3 Covalent Inhibitor

To synthesize this inhibitor, we utilized **Figure 5.2.5.1.1** to conduct an S_NAr between 1-fluoro-2-methoxy-4-nitrobenzene and tert-butyl (2-aminoethyl)carbamate was done to afford **37**. From this intermediate **37**, standard chemistry, as well as chemistry already outlines by the previous sections, was used to create final compound **44**.

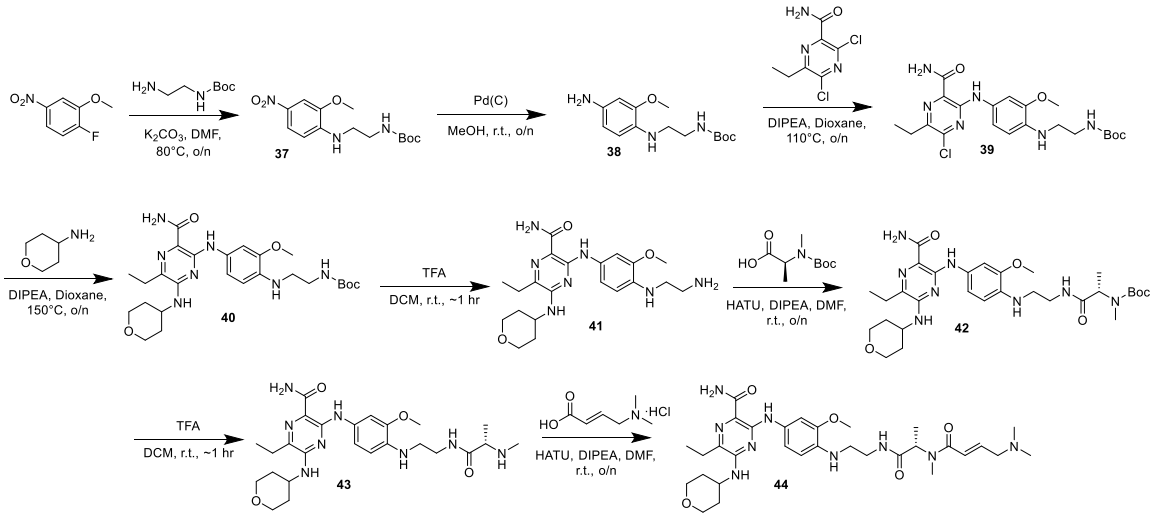

Figure 5.2.5.1.1: *Synthesis of third generation FLT3 covalent inhibitor CG-5-024*

5.2.5.2 Biological Evaluation of 3rd generation FLT3 Covalent Inhibitors

Below is the structure of the only compound synthesized for this generation. Again, an AlamarBlue assay was conducted on our compound against MOLM14 and MOLM14

F691L FLT3 cells (**Table 5.2.5.2.1**). From this, the IC_{50} value of our 3rd generation inhibitor is comparable to the control compound gilteritinib in MOLM14 F691L FLT3 cells. This is the first inhibitor we created that has a similar IC_{50} value in gilteritinib resistant cells.

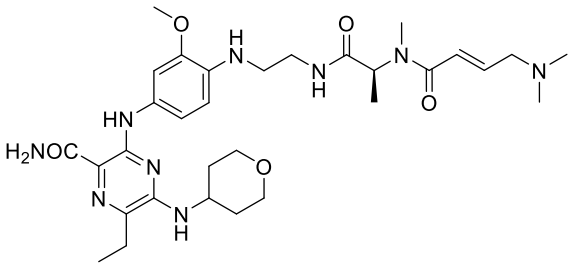

Compound Code	R	WT MOLM14 IC_{50} (nM)	MOLM14 F691L IC_{50} (nM)
Gilteritinib (Control)		17.4	115.6
CG-5-021		33.4	109.6

Table 5.2.5.2.1: *Cell-free inhibition of FLT3 with third generation FLT3 covalent inhibitor*

5.2.6 Conclusions and Future Directions

Based off our three generations of inhibitor design, we currently have two leading compounds that are demonstrating a slight increase in biological evaluations compared to gilteritinib. Using this biological data, we plan to conduct further SILCS experiments to optimize both CG-5-008 and CG-5-021 and create a superior FLT3 covalent inhibitor that demonstrates a heightened potency in F691L FLT3 expressing AML cell lines.

5.2.7 Methods

Chemistry

All reactions were performed in oven-dried glassware under non-inert atmosphere, unless otherwise stated. All chemicals and solvents were used as supplied without additional purification. ^{1}H and ^{13}C NMR spectra were obtained on a Varian 400 or 500 MHz NMR spectrometer at 298.1K. Chemical shifts are reported in parts per million (ppm) and are referenced to residual non-deuterated solvent peak ($CHCl_3$: δ_H 7.26; DMSO: δ_H 2.50, δ_C 39.5). All final compounds were lyophilized before biological evaluation.

Inhibition of FLT3

Inhibition of FLT3 was determined by NanoSyn (Element) measuring the phosphorylation of a substrate by the tyrosine kinase FLT3 (Millipore lot 2001422E) . Enzyme, substrate (FAM-KKKKEEIYFFF-CONH2), and cofactors (ATP and Mg2+) are combined in a well of a microtiter plate and incubate at 3 hours at 25ºC. At the end of the incubation, the reaction is quenched by the addition of an EDTA-containing buffer. Formation of phospho-tyrosine from kinase reaction is detected with biotinylated-anti-phospho-tyrosine antibodies (Sigma Cat#B1531) and cryptatelabeled streptavidin (CisBio Cat# 610SATLB). TR-FRET signal is measured on Biotek Synergy Neo2 instrument.

DiscoveRx's proprietary KINOMEscan™ is based on a competition binding assay that quantitatively measures the ability of a compound to compete with an immobilized, active-site directed ligand. The assay is performed by combining three components: DNA-tagged kinase; immobilized ligand; and a test compound. The ability of the test compound to compete with the immobilized ligand is measured via quantitative PCR of the DNA tag. For most assays, kinase-tagged T7 phage strains were prepared in an E. coli

host derived from the BL21 strain. E. coli were grown to log-phase and infected with T7 phage and incubated with shaking at 32°C until lysis. The lysates were centrifuged and filtered to remove cell debris. The remaining kinases were produced in HEK-293 cells and subsequently tagged with DNA for qPCR detection. Streptavidin-coated magnetic beads were treated with biotinylated small molecule ligands for 30 minutes at room temperature to generate affinity resins for kinase assays. The liganded beads were blocked with excess biotin and washed with blocking buffer (SeaBlock (Pierce), 1% BSA, 0.05% Tween 20, 1 mM DTT) to remove unbound ligand and to reduce non-specific binding. Binding reactions were assembled by combining kinases, liganded affinity beads, and test compounds in 1x binding buffer (20% SeaBlock, 0.17x PBS, 0.05% Tween 20, 6 mM DTT). Test compounds were prepared as 111X stocks in 100% DMSO. Kds were determined using an 11-point 3-fold compound dilution series with three DMSO control points. All compounds for Kd measurements are distributed by acoustic transfer (non-contact dispensing) in 100% DMSO. The compounds were then diluted directly into the assays such that the final concentration of DMSO was 0.9%. All reactions performed in polypropylene 384-well plate. Each was a final volume of 0.02 ml. The assay plates were incubated at room temperature with shaking for 1 hour and the affinity beads were washed with wash buffer (1x PBS, 0.05% Tween 20). The beads were then re-suspended in elution buffer (1x PBS, 0.05% Tween 20, 0.5 μM nonbiotinylated affinity ligand) and incubated at room temperature with shaking for 30 minutes. The kinase concentration in the eluates was measured by qPCR.

Cell Cultures

Pediatric acute myeloid leukemia cell lines harboring mixed-lineage-leukemia rearrangements were obtained from either ATCC (Manassas, VA) or DSMZ (Branschweig, DEU) (MOLM14, #ACC-777 DSMZ; MV4;11, #CRL-9591, ATCC).

MOLM14 FLT3 F691L cells were a gift from Dr. Shah (UCSF). MV4;11 BCL-2 OE cells were generated via lentiviral transduction using a Transdux MAX kit (SBI, Cat# LV860A-1) following manufacturer's guidelines. The human BCL-2a open reading frame (ORF; 720bp) was amplified with gene-specific primers (BCL2aOE-2243-F: 5'-CTGAGAATTCATGGCGCACGCTGGGAGAACAG-3' and BCL2aOE-2243-R: 5'-CTGAGGTACCTCACTTGTGGCCCAGATAGGCAC-3') from NB4 human leukemia cell cDNA by PCR, and then cloned into pMJK2243 (our control empty lentivector) using EcoRI and KpnI restriction enzyme sites. pMJK2243 is a bidirectional dual promoter lentivector including the EF1a and hUbC promoters. In the BCL-2a expression lentivector, the EF1a promoter drives expression of the BCL-2a ORF, whereas the hUbC promoter drives expression of the green fluorescence protein (GFP) and puromycin resistance ($Puro^R$) genes. Lentiviruses (LVs) were generated in HEK293T cells as described previously.[195] The BCL-2 OE LV was validated in MOLM14 cells (>95% GFP^+ by the puromycin selection) with a 5-fold increase in BCL-2 protein levels compared to WT MOLM14 cells. Before proceeding with cell metabolic/viability and apoptosis/death assays, MV4;11 BCL-2 OE cells were cultured in puromycin-containing media until >95% GFP^+.

Cell lines were cultured in RPMI1640 media (Cellgro, # MDT-10-040-CV) containing 10% fetal bovine serum (Gemini BioProducts #100-106) and passaged twice per week to maintain cultures in log-phase-growth. Upon receipt, cell lines were expanded and

multiple aliquots cryopreserved in DMSO-containing medium in the vapor phase of liquid nitrogen. Cryopreserved cells were genetically authenticated and confirmed to be mycoplasma-negative prior to cryopreservation. Cells from a given cryopreserved aliquot were cultured for no more than 3-4 months.

Cell metabolic/viability assays

Cell metabolism/viability was assessed by alamarBlue assays (Thermo Fisher, cat# DAL1100) according to manufacturer's guidelines. Cells and concentrations of each compound were combined in culture for 48h. Cells were then incubated with alamarBlue reagent for a minimum of 5hr before absorbance was read using a Perkin Elmer Victor X3. Reads were normalized to the corresponding equimolar DMSO (vehicle) controls. IC50s were generated in Prism's GraphPad by modeling a non-linear fit (4-parameter, variable Hill-slope) against log(inhibitor) vs relative absorbance values. Top and bottom constraints were set to 1 and 0, respectively.

5.2.8 Experimental Procedures

General Procedure 1: Nucleophilic aromatic substitution of aromatic nitro compounds:

Either 1-fluoro-2-methoxy-4-nitrobenzene or prepared phenol ether (1 eq.) was placed in a reaction flask and solubilized in DMF (0.1 M). Selected amines (1.1 eq.) and K_2CO_3 (2.0 eq.) were added to the reaction mixture. The reaction was stirred at 50°C for 16 h. Reaction completion was monitored via TLC. Upon completion, the reaction was partitioned between EtOAc and brine. The organic layer was washed five times with brine to remove the DMF and excess amine. The organic layer was then collected, dried

with Na_2SO_4, filtered and concentrated. The crude material was adsorbed onto silica gel, then purified by flash column chromatography.

General Procedure 2: Palladium catalyzed reduction of aromatic nitro compounds:

To a stirring solution of the starting nitro compound (1.0 eq) in methanol (0.1 M, 150 mL maximum), catalytic palladium on carbon (10% wt) was added. H_2(g) was bubbled through solution for 15 minutes and the reaction was stirred at room temperature for 16 hours under H_2(g). Reaction completion was monitored via TLC. Upon completion, the reaction mixture was filtered through celite, rinsing with methanol and concentrated to dryness. The crude material was adsorbed onto silica gel, then purified by flash column chromatography.

General Procedure 3: Nucleophilic aromatic substitution of 3,5-dichloro-6-ethylpyrazine-2-carboxamide:

Various amines (1 eq.) were placed in a reaction flask and solubilized in Dioxane (0.1 M). 3,5-dichloro-6-ethylpyrazine-2-carboxamide (1.0 eq) and DIPEA (2.0 eq) were added to the reaction mixture. The reaction was stirred at 110°C for 16 h. Reaction completion was monitored via TLC. Upon completion, the reaction was partitioned between EtOAc and H_2O. The aqueous was basified with saturated sodium bicarbonate and the product was extracted into ethyl acetate x3. The organic layers were combined and washed with water: saturated sodium bicarbonate x3 and saturated sodium chloride, then dried over sodium sulfate and concentrated to dryness. The crude material was adsorbed onto silica gel, then purified by flash column chromatography.

General Procedure 4: Nucleophilic aromatic substitution of mono substituted 5-chloro-6-ethylpyrazine-2-carboxamide:

Different pyrazines (1.0 eq) were placed in a reaction flask and solubilized in NMP (0.1 M). 4-Aminotetrahydropyran (4.0 eq) and DIPEA (4.0 eq) were added to the reaction mixture. The reaction was stirred at 150°C for 16 h. Reaction completion was monitored via TLC. Upon completion, the reaction was partitioned between EtOAc and H_2O. The aqueous was basified with saturated sodium bicarbonate and the product was extracted into ethyl acetate x3. The organic layers were combined and washed with water: saturated sodium bicarbonate x3 and saturated sodium chloride, then dried over sodium sulfate and concentrated to dryness. The crude material was adsorbed onto silica gel, then purified by flash column chromatography.

General Procedure 5: Boc-deprotection of amines:

To a stirring solution of the boc-protected amine (1.0 eq) in DCM (0.1 M), TFA was added. The reaction mixture was stirred at room temperature for 3 hours. Upon completion, the reaction mixture was concentrated to dryness and azeoptroped with DCM and methanol x3.

General Procedure 6: HATU-mediated condensation reactions:

To a stirring solution of the carboxylic acid (1.0 eq) in DMF (0.1M, 30mL max), DIPEA (1.1 eq) and HATU (1.2 eq) were added followed by the amine (1.0 eq) and additional 1.0 eq DIPEA per HCl salt. The reaction was stirred at room temperature for 16 hours. Reaction completion was monitored via TLC. Upon completion, the reaction was partitioned between EtOAc and H_2O. The aqueous was basified with saturated sodium

bicarbonate and the product was extracted into ethyl acetate x3. The organic layers were combined and washed with water: saturated sodium bicarbonate x3 and saturated sodium chloride, then dried over sodium sulfate and concentrated to dryness. The crude material was adsorbed onto silica gel, then purified by flash column chromatography.

General Procedure 7: Acylation utilizing acid chloride:

Various amines (1.0 eq) were placed in a reaction flask and solubilized in DCM (0.1 M). DIPEA (2.0 eq) was added to the reaction mixture which was then placed in an ice bath at 0°C. Acid chloride (1.2 eq) was added to the reaction mixture which was left stirring for 16 hours. Reaction completion was monitored via TLC. Upon completion, the reaction was partitioned between DCM and H_2O. The aqueous was basified with saturated sodium bicarbonate and the product was extracted into DCM x3. The organic layers were combined and washed with water: saturated sodium bicarbonate x3 and saturated sodium chloride, then dried over sodium sulfate and concentrated to dryness. The crude material was adsorbed onto silica gel, then purified by flash column chromatography.

tert-butyl (R)-(1-(2-methoxy-4-nitrophenyl)piperidin-3-yl)carbamate (CG-4-145): (R)-3-(Boc-amino)piperidine hydrochloride and 1-fluoro-2-methoxy-4-nitrobenzene were reacted on a 4.22 mmol scale according to General Procedure 1, using hexanes:EtOAc to monitor and purify the title compound. (yellow solid, yield = 73%): ^{1}H NMR (400 MHz, DMSO) δ = 7.80 (d, J = 8.8 Hz, 1H), 7.65 (s, 1H), 6.99 (d, J = 9.2 Hz, 1H), 6.86 (d, J = 6.8 Hz, 1H), 3.88 (s, 3H), 3.54-3.46 (m, 3H), 2.69 (t, J = 10.4 Hz, 1H), 2.61 (t, J = 10.2 Hz, 1H), 1.83-1.72 (m, 2H), 1.55 (m, 1H), 1.37 (m, 10H); ^{13}C NMR (400 MHz, DMSO) δ = 155.4, 150.9, 147.9, 140.9, 118.2, 117.5, 107.0, 78.2, 56.4, 55.2, 50.1, 47.3, 30.2, 28.7, 24.1.

tert-butyl (S)-(1-(2-methoxy-4-nitrophenyl)piperidin-3-yl)carbamate (CG-4-146): (S)-3-(Boc-amino)piperidine hydrochloride and 1-fluoro-2-methoxy-4-nitrobenzene were reacted on a 4.22 mmol scale according to General Procedure 1, using hexanes:EtOAc to monitor the reaction and purify the title compound. (yellow solid, yield = 73%): ^{1}H NMR (400 MHz, DMSO) δ = 7.80 (d, J = 8.8 Hz, 1H), 7.65 (s, 1H), 6.99 (d, J = 8.4 Hz, 1H), 6.86 (d, J = 6.8 Hz, 1H), 3.88 (s, 3H), 3.54-3.46 (m, 3H), 2.69 (t, J = 10.4 Hz, 1H), 2.61 (t, J = 10.2 Hz, 1H), 1.83-1.72 (m, 2H), 1.55 (m, 1H), 1.37 (m, 10H); ^{13}C NMR (400 MHz, DMSO) δ = 155.4, 150.9, 147.9, 140.9, 118.2, 117.5, 107.0, 78.2, 56.4, 55.2, 50.1, 47.3, 30.2, 28.7, 24.1.

tert-butyl (R)-(1-(4-amino-2-methoxyphenyl)piperidin-3-yl)carbamate (CG-4-147): CG-4-145 was reacted on a 3.09 mmol scale according to General Procedure 2, using CH_2Cl_2/MeOH/NH_4OH, 192:7:1 to monitor the reaction and purify the title compound. (brown oil, yield = 87%): ^{1}H NMR (400 MHz, DMSO) δ = 6.67 (d, J = 7.6 Hz, 1H), 6.60 (d, J = 8.8 Hz, 1H), 6.21 (s, 1H), 6.07 (d, J = 7.6 Hz, 1H), 5.02 (s, 2H), 3.67 (s, 3H), 3.45 (s, 1H), 2.95 (t, J = 10.6 Hz, 2H), 2.43-2.33 (m, 2H), 1.72-1.52 (m, 3H), 1.37 (s, 9H), 1.23 (m, 1H); ^{13}C NMR (400 MHz, DMSO) δ = 155.3, 153.7, 145.3, 131.7, 120.5, 106.1, 99.8, 78.0, 57.7, 55.5, 52.0, 47.7, 30.3, 28.7, 24.4.

tert-butyl (S)-(1-(4-amino-2-methoxyphenyl)piperidin-3-yl)carbamate (CG-4-148): CG-4-146 was reacted on a 3.09 mmol scale according to General Procedure 2, using CH_2Cl_2/MeOH/NH_4OH, 192:7:1 to monitor the reaction and purify the title compound. (brown oil, yield = 73%): ^{1}H NMR (400 MHz, DMSO) δ = 6.67 (d, J = 6.8 Hz, 1H), 6.59 (d, J = 8.4 Hz, 1H), 6.20 (s, 1H), 6.05 (d, J = 8.8 Hz, 1H), 4.88 (s, 2H), 3.66 (s, 3H), 3.44 (s, 1H), 2.94 (t, J = 11.0 Hz, 2H), 2.41-2.29 (m, 2H), 1.72-1.51 (m, 3H), 1.37 (s, 9H),

1.22 (m, 1H); ^{13}C NMR (400 MHz, DMSO) δ = 155.3, 153.7, 145.4, 131.7, 120.4, 106.0, 99.8, 78.0, 57.7, 55.5, 52.0, 47.8, 30.3, 28.7, 24.4.

tert-butyl (R)-(1-(4-((3-carbamoyl-6-chloro-5-ethylpyrazin-2-yl)amino)-2-methoxyphenyl)piperidin-3-yl)carbamate (CG-4-149): CG-4-147 was reacted on a 1.12 mmol scale according to General Procedure 3, using CH_2Cl_2/MeOH/NH_4OH, 92:7:1 to monitor the reaction and hexanes:EtOAc to purify the title compound. (orange-red solid, yield = 74%): ^{1}H NMR (400 MHz, DMSO) δ = 11.02 (s, 1H), 8.23 (s, 1H), 8.00 (s, 1H), 7.26 (s, 1H), 7.07 (d, J = 8.8 Hz, 1H), 6.84 (d, J = 8.8 Hz, 1H), 6.73 (d, J = 8.0 Hz, 1H), 3.78 (s, 3H), 3.49 (s, 1H), 3.15 (m, 2H), 2.78 (q, J = 7.2 Hz, 2H), 2.49-2.34 (m, 2H), 1.77-1.55 (m, 3H), 1.38 (s, 9H), 1.29-1.22 (m, 4H); ^{13}C NMR (400 MHz, DMSO) δ = 168.5, 155.3, 152.6, 149.6, 147.2, 141.6, 137.6, 134.2, 125.1, 119.2, 112.4, 105.1, 78.0, 56.8, 55.8, 51.3, 47.6, 30.4, 28.7, 26.6, 24.4, 12.5.

tert-butyl (S)-(1-(4-((3-carbamoyl-6-chloro-5-ethylpyrazin-2-yl)amino)-2-methoxyphenyl)piperidin-3-yl)carbamate (CG-4-150): CG-4-148 was reacted on a 0.975 mmol scale according to General Procedure 3, using CH_2Cl_2/MeOH/NH_4OH, 92:7:1 to monitor the reaction and hexanes:EtOAc to purify the title compound. (orange-red solid, yield = 78%): ^{1}H NMR (400 MHz, DMSO) δ = 11.02 (s, 1H), 8.23 (s, 1H), 8.00 (s, 1H), 7.26 (s, 1H), 7.07 (d, J = 8.8 Hz, 1H), 6.84 (d, J = 8.8 Hz, 1H), 6.73 (d, J = 8.0 Hz, 1H), 3.78 (s, 3H), 3.49 (s, 1H), 3.15 (m, 2H), 2.78 (q, J = 7.2 Hz, 2H), 2.49-2.36 (m, 2H), 1.77-1.55 (m, 3H), 1.38 (s, 9H), 1.29-1.22 (m, 4H); ^{13}C NMR (400 MHz, DMSO) δ = 168.5, 155.3, 152.6, 149.6, 147.2, 141.6, 137.6, 134.2, 125.1, 119.2, 112.4, 105.1, 78.0, 56.8, 55.8, 51.3, 47.6, 30.4, 28.7, 26.6, 24.4, 12.5.

tert-butyl (R)-(1-(4-((3-carbamoyl-5-ethyl-6-((tetrahydro-2H-pyran-4-yl)amino)pyrazin-2-yl)amino)-2-methoxyphenyl)piperidin-3-yl)carbamate (CG-4-151): CG-4-149 was reacted on a 0.461 mmol scale according to General Procedure 4, using hexanes:EtOAc to monitor the reaction and purify the title compound. (yellow solid, yield = 90%): ^{1}H NMR (400 MHz, DMSO) δ = 11.01 (s, 1H), 7.51 (s, 1H), 7.26 (d, J = 8.4 Hz, 1H), 7.20 (s, 1H), 7.01 (s, 1H), 6.80 (d, J = 8.4 Hz, 1H), 6.76 (d, J = 6.8 Hz, 1H), 6.69 (d, J = 8.0 Hz, 1H), 4.10 (s, 1H), 3.90 (d, J = 9.2 Hz, 2H), 3.80 (s, 3H), 3.49 (s, 1H), 3.38-3.31 (m, 2H), 3.12 (s, 2H), 2.59-2.54 (m, 2H), 2.49-2.40 (m, 2H), 1.85-1.58 (m, 7H), 1.38 (s, 9H), 1.29-1.26 (m, 1H), 1.20-1.14 (m, 3H); ^{13}C NMR (400 MHz, DMSO) δ = 170.1, 155.3, 152.8, 152.2, 150.6, 136.7, 136.0, 132.0, 119.2, 112.1, 105.3, 78.0, 66.9, 60.2, 56.9, 56.2, 51.5, 48.0, 47.7, 32.6, 28.7, 28.5, 24.6, 24.4, 11.4.

tert-butyl (S)-(1-(4-((3-carbamoyl-5-ethyl-6-((tetrahydro-2H-pyran-4-yl)amino)pyrazin-2-yl)amino)-2-methoxyphenyl)piperidin-3-yl)carbamate (CG-4-152): CG-4-150 was reacted on a 0.461 mmol scale according to General Procedure 4, using hexanes:EtOAc to monitor the reaction and purify the title compound. (yellow solid, yield = 84%): ^{1}H NMR (400 MHz, DMSO) δ = 11.00 (s, 1H), 7.51 (s, 1H), 7.26 (d, J = 8.4 Hz, 1H), 7.20 (s, 1H), 7.01 (s, 1H), 6.80 (d, J = 8.4 Hz, 1H), 6.76 (d, J = 6.8 Hz, 1H), 6.69 (d, J = 7.2 Hz, 1H), 4.10 (s, 1H), 3.90 (d, J = 9.2 Hz, 2H), 3.80 (s, 3H), 3.49 (s, 1H), 3.38-3.32 (m, 2H), 3.12 (s, 2H), 2.59-2.54 (m, 2H), 2.49-2.37 (m, 2H), 1.85-1.58 (m, 7H), 1.38 (s, 9H), 1.29-1.26 (m, 1H), 1.19-1.14 (m, 3H); ^{13}C NMR (400 MHz, DMSO) δ = 170.1, 155.3, 152.8, 152.2, 150.6, 136.7, 136.0, 132.0, 119.2, 112.1, 105.3, 78.1, 66.9, 56.9, 56.2, 55.4, 51.4, 48.0, 47.7, 32.6, 28.7, 28.5, 24.6, 24.4, 11.4.

(R)-3-((4-(3-aminopiperidin-1-yl)-3-methoxyphenyl)amino)-6-ethyl-5-((tetrahydro-2H-pyran-4-yl)amino)pyrazine-2-carboxamide (CG-4-153): CG-4-151 was reacted on a 0.415 mmol scale according to General Procedure 5, using hexanes:EtOAc to monitor the formation of the title compound with no further purification. (off brown solid, yield = 59%): ^{1}H NMR (400 MHz, DMSO) δ = 11.07 (s, 1H), 7.98 (s, 3H), 7.55 (s, 1H), 7.32 (d, J = 7.6 Hz, 1H), 7.26 (s, 1H), 7.01 (s, 1H), 6.83 (d, J = 7.2 Hz, 2H), 4.11 (s, 1H), 3.92 (d, J = 9.2 Hz, 2H), 3.82 (s, 3H), 3.36 (m, 3H), 3.12 (s, 1H), 3.00 (s, 1H), 2.81 (s, 1H), 2.73 (s, 1H), 2.57 (m, 2H), 1.83 (m, 4H), 1.62 (m, 4H), 1.18 (m, 3H); ^{13}C NMR (400 MHz, DMSO) δ = 170.1, 152.8, 152.2, 150.5, 136.5, 135.8, 132.1, 119.5, 112.1, 111.8, 104.7, 66.9, 56.1, 54.5, 50.9, 48.0, 47.4, 32.6, 27.8, 24.7, 22.6, 11.4.

(S)-3-((4-(3-aminopiperidin-1-yl)-3-methoxyphenyl)amino)-6-ethyl-5-((tetrahydro-2H-pyran-4-yl)amino)pyrazine-2-carboxamide (CG-4-154): CG-4-151 was reacted on a 0.388 mmol scale according to General Procedure 5, using hexanes:EtOAc to monitor the formation of the title compound with no further purification. (off brown solid, yield = 57%): ^{1}H NMR (400 MHz, DMSO) δ = 11.06 (s, 1H), 7.96 (s, 3H), 7.54 (s, 1H), 7.32 (d, J = 7.6 Hz, 1H), 7.25 (s, 1H), 7.01 (s, 1H), 6.83 (d, J = 8.8 Hz, 2H), 4.11 (s, 1H), 3.92 (d, J = 10.0 Hz, 2H), 3.82 (s, 3H), 3.36 (m, 3H), 3.12 (d, J = 10.0 Hz, 1H), 3.00 (s, 1H), 2.81 (s, 1H), 2.73 (s, 1H), 2.57 (q, J = 7.3 Hz, 2H), 1.83 (m, 4H), 1.64-1.53 (m, 4H), 1.18 (t, J = 7.2 Hz, 3H); ^{13}C NMR (400 MHz, DMSO) δ = 170.1, 152.8, 152.2, 150.5, 136.5, 135.8, 132.1, 119.5, 112.1, 111.8, 104.7, 66.9, 56.1, 54.5, 50.9, 48.0, 47.4, 32.6, 27.8, 24.7, 22.5, 11.4.

(R,E)-3-((4-(3-(4-(dimethylamino)but-2-enamido)piperidin-1-yl)-3-methoxyphenyl)amino)-6-ethyl-5-((tetrahydro-2H-pyran-4-yl)amino)pyrazine-2-

carboxamide (CG-4-156): CG-4-153 and trans-4-Dimethylaminocrotonic acid hydrochloride were reacted on a 0.0823 mmol scale according to General Procedure 6, using CH_2Cl_2/MeOH/NH_4OH, 92:7:1 to monitor the reaction and purify the title compound. (off yellow solid, yield = 77%): ^{1}H NMR (400 MHz, DMSO) δ = 11.04 (s, 1H), 7.91 (d, J = 6.8 Hz, 1H), 7.53 (s, 1H), 7.28-7.24 (m, 2H), 7.01 (s, 1H), 6.80 (t, J = 7.4 Hz, 2H), 6.58-6.51 (m, 1H), 6.07 (d, J = 15.6 Hz, 1H), 4.10 (s, 1H), 3.91 (d, J = 12.0 Hz, 3H), 3.78 (s, 3H), 3.35 (m, 2H), 3.14 (t, J = 12.6 Hz, 2H), 2.98 (d, J = 6.4 Hz, 2H), 2.57 (q, J = 7.3 Hz, 3H), 2.47 (m, 1H), 2.13 (s, 6H), 1.85-1.74 (m, 4H), 1.60 (m, 3H), 1.31 (m, 1H), 1.21-1.15 (m, 4H); ^{13}C NMR (400 MHz, DMSO) δ = 170.1, 164.3, 152.8, 152.2, 150.6, 139.7, 136.6, 136.0, 132.0, 126.7, 119.1, 111.9, 105.1, 66.9 (2), 60.2, 56.5, 56.2, 51.5, 48.0, 46.3, 45.5, 32.6, 30.2, 24.7, 24.3, 11.4. HRMS-ESI: m/z found 579.3407 [M+H]+, $C_{30}H_{44}N_8O_4$ requires 579.3413.

(S,E)-3-((4-(3-(4-(dimethylamino)but-2-enamido)piperidin-1-yl)-3-methoxyphenyl)amino)-6-ethyl-5-((tetrahydro-2H-pyran-4-yl)amino)pyrazine-2-carboxamide (CG-4-157): CG-4-154 and trans-4-Dimethylaminocrotonic acid hydrochloride were reacted on a 0.0823 mmol scale according to General Procedure 6, using CH_2Cl_2/MeOH/NH_4OH, 92:7:1 to monitor the reaction and purify the title compound. (off yellow solid, yield = 97%): ^{1}H NMR (400 MHz, DMSO) δ = 11.04 (s, 1H), 7.92 (d, J = 7.6 Hz, 1H), 7.53 (s, 1H), 7.28-7.24 (m, 2H), 7.01 (s, 1H), 6.80 (t, J = 6.6 Hz, 2H), 6.56-6.53 (m, 1H), 6.07 (d, J = 15.6 Hz, 1H), 4.10 (s, 1H), 3.90 (d, J = 9.2 Hz, 3H), 3.78 (s, 3H), 3.35 (m, 2H), 3.14 (t, J = 12.6 Hz, 2H), 2.98 (d, J = 5.6 Hz, 2H), 2.57 (q, J = 7.3 Hz, 3H), 2.47 (m, 1H), 2.13 (s, 6H), 1.85-1.74 (m, 4H), 1.60 (m, 3H), 1.31 (m, 1H), 1.21-1.15 (m, 4H); ^{13}C NMR (400 MHz, DMSO) δ = 170.1, 164.3, 152.8,

152.2, 150.6, 139.7, 136.6, 136.0, 132.0, 126.7, 119.1, 112.1, 111.9, 105.1, 66.9, 60.2, 56.5, 56.2, 51.5, 48.0, 46.3, 45.5, 32.6, 30.2, 24.7, 24.3, 11.4. HRMS-ESI: m/z found 579.3407 [M+H]+, $C_{30}H_{44}N_8O_4$ requires 579.3413.

tert-butyl (R)-4-((1-(4-((3-carbamoyl-5-ethyl-6-((tetrahydro-2H-pyran-4-yl)amino)pyrazin-2-yl)amino)-2-methoxyphenyl)piperidin-3-yl)carbamoyl)piperidine-1-carboxylate (CG-4-158): CG-4-153 and N-Boc-piperidine-4-carboxylic acid were reacted on a 0.0941 mmol scale according to General Procedure 6, using hexanes:EtOAc to monitor the reaction and purify the title compound. (yellow solid, yield = 77%): ^{1}H NMR (400 MHz, DMSO) δ = 11.05 (s, 1H), 7.67 (d, J = 8.0 Hz, 1H), 7.55 (s, 1H), 7.29 (d, J = 8.4 Hz, 1H), 7.24 (s, 1H), 7.06 (s, 1H), 6.84 (d, J = 8.4 Hz, 1H), 6.80 (d, J = 8.0 Hz, 1H), 4.13 (s, 1H), 3.95-3.93 (m, 4H), 3.83 (s, 3H), 3.41-3.35 (m, 2H), 3.11 (s, 2H), 2.75-2.71 (m, 3H), 2.63-2.58 (m, 3H), 2.50-2.47 (m, 2H), 2.32 (t, J = 11.4 Hz, 1H), 1.87 (d, J = 12.4 Hz, 2H), 1.78-1.76 (m, 2H), 1.69-1.61 (m, 5H), 1.46-1.34 (m, 11H), 1.25-1.18 (m, 3H); ^{13}C NMR (400 MHz, DMSO) δ = 173.8, 170.1, 154.3, 152.8, 152.2, 150.6, 136.7, 136.0, 132.0, 119.2, 112.1 (2), 105.3, 79.0, 66.9, 60.2, 56.6, 56.2, 51.5, 48.0, 46.0, 42.1, 39.3, 32.6, 28.8, 28.5, 24.6, 24.2, 11.4.

tert-butyl (S)-4-((1-(4-((3-carbamoyl-5-ethyl-6-((tetrahydro-2H-pyran-4-yl)amino)pyrazin-2-yl)amino)-2-methoxyphenyl)piperidin-3-yl)carbamoyl)piperidine-1-carboxylate (CG-4-159): CG-4-154 and N-Boc-piperidine-4-carboxylic acid were reacted on a 0.0941 mmol scale according to General Procedure 6, using hexanes:EtOAc to monitor the reaction and purify the title compound. (yellow solid, yield = 95%): ^{1}H NMR (400 MHz, DMSO) δ = 11.05 (s, 1H), 7.67 (d, J = 8.0 Hz, 1H), 7.55 (s, 1H), 7.29 (d, J = 8.4 Hz, 1H), 7.24 (s, 1H), 7.06 (s, 1H), 6.84 (d, J = 8.4 Hz, 1H), 6.80 (d, J = 8.0 Hz, 1H),

4.13 (s, 1H), 3.95-3.93 (m, 4H), 3.41-3.35 (m, 2H), 3.13 (s, 2H), 2.60 (q, J = 7.3 Hz, 2H), 2.52-2.50 (m, 5H), 2.32 (t, J = 11.4 Hz, 1H), 1.87 (d, J = 11.6 Hz, 2H), 1.78-1.76 (m, 2H), 1.69-1.61 (m, 5H), 1.46-1.34 (m, 11H), 1.21 (t, J = 7.0 Hz, 3H); ^{13}C NMR (400 MHz, DMSO) δ = 173.8, 170.1, 154.3, 152.8, 152.2, 150.6, 136.7, 136.0, 132.0, 119.2, 112.1 (2), 105.3, 79.0, 66.9, 56.6, 56.2, 55.4, 51.5, 48.0, 46.1, 42.1, 32.6, 30.1, 28.8, 28.5, 24.6, 24.2, 11.4.

(R)-6-ethyl-3-((3-methoxy-4-(3-(piperidine-4-carboxamido)piperidin-1-yl)phenyl)amino)-5-((tetrahydro-2H-pyran-4-yl)amino)pyrazine-2-carboxamide (CG-4-160): CG-4-158 was reacted on a 0.0667 mmol scale according to General Procedure 5, using hexanes:EtOAc to monitor the formation of the title compound with no further purification. (white solid, yield = 89%): ^{1}H NMR (400 MHz, DMSO) δ = 11.47 (s, 1H), 8.72 (d, J = 9.2 Hz, 1H), 8.40 (d, J = 9.2 Hz, 1H), 8.16 (d, J = 6.8 Hz, 1H), 7.64 (d, J = 8.8 Hz, 1H), 7.48 (d, J = 8.4 Hz, 1H), 7.24 (s, 1H), 6.95 (d, J = 7.2 Hz, 1H), 4.17 (s, 2H), 3.99-3.95 (m, 5H), 3.51-3.39 (m, 5H), 3.32 (d, J = 12.0 Hz, 2H), 2.91 (s, 2H), 2.71 (s, 2H), 2.64 (q, J = 7.3 Hz, 2H), 2.46 (t, J = 11.0 Hz, 1H), 1.99-1.87 (m, 7H), 1.78-1.65 (m, 4H), 1.55 (s, 1H), 1.22 (t, J = 7.4 Hz, 3H); ^{13}C NMR (400 MHz, DMSO) δ = 173.4, 169.9, 159.0, 158.7, 152.3, 152.1, 150.0, 133.4, 117.4, 114.5, 112.7, 111.3, 104.3, 66.9, 56.9 (2), 55.3, 48.2, 44.4, 42.9, 38.7, 32.5, 25.6, 25.5, 24.8, 11.3.

(S)-6-ethyl-3-((3-methoxy-4-(3-(piperidine-4-carboxamido)piperidin-1-yl)phenyl)amino)-5-((tetrahydro-2H-pyran-4-yl)amino)pyrazine-2-carboxamide (CG-4-161): CG-4-159 was reacted on a 0.122 mmol scale according to General Procedure 5, using hexanes:EtOAc to monitor the formation of the title compound with no further purification. (white solid, yield = 93%): ^{1}H NMR (400 MHz, DMSO) δ = 11.47 (s, 1H),

8.73 (d, J = 10.0 Hz, 1H), 8.41 (d, J = 9.6 Hz, 1H), 8.17 (d, J = 6.8 Hz, 1H), 7.64 (d, J = 8.8 Hz, 1H), 7.48 (d, J = 7.6 Hz, 1H), 7.24 (s, 1H), 6.96 (d, J = 7.2 Hz, 1H), 4.17 (s, 2H), 3.99-3.95 (m, 5H), 3.51-3.39 (m, 5H), 3.30-3.25 (m, 4H), 2.93 (t, J = 11.4 Hz, 2H), 2.65 (q, J = 7.3 Hz, 2H), 2.46 (t, J = 10.6 Hz, 1H), 2.00-1.87 (m, 7H), 1.78-1.65 (m, 4H), 1.55 (s, 1H), 1.22 (t, J = 7.4 Hz, 3H); ^{13}C NMR (400 MHz, DMSO) δ = 173.4, 169.9, 159.0, 158.7, 152.3, 152.1, 150.0, 133.4, 117.4, 114.5, 112.7, 111.3, 104.3, 66.9, 56.9, 55.3, 53.7, 48.2, 44.4, 42.9, 32.5, 25.6, 25.5, 25.1, 24.8, 11.2.

(R,E)-3-((4-(3-(1-(4-(dimethylamino)but-2-enoyl)piperidine-4-carboxamido)piperidin-1-yl)-3-methoxyphenyl)amino)-6-ethyl-5-((tetrahydro-2H-pyran-4-yl)amino)pyrazine-2-carboxamide (CG-4-162): CG-4-160 and trans-4-Dimethylaminocrotonic acid hydrochloride were reacted on a 0.0593 mmol scale according to General Procedure 6, using CH_2Cl_2/MeOH/NH_4OH, 92:7:1 to monitor the reaction and CH_2Cl_2/MeOH/NH_4OH, 58:7:1 to purify the title compound. (dark yellow solid, yield = 80%): ^{1}H NMR (400 MHz, DMSO) δ = 11.02 (s, 1H), 7.69 (d, J = 7.6 Hz, 1H), 7.53 (s, 1H), 7.27-7.24 (m, 2H), 7.01 (s, 1H), 6.81-6.79 (m, 2H), 6.57-6.55 (m, 2H), 4.38 (d, J = 10.8 Hz, 1H), 4.11-4.01 (m, 2H), 3.90 (d, J = 9.2 Hz, 2H), 3.79 (s, 4H), 3.34 (s, 2H), 3.08-3.02 (m, 5H), 2.62-2.36 (m, 5H), 2.14 (s, 6H), 1.83 (d, J = 11.6 Hz, 2H), 1.66-1.57 (m, 7H), 1.41-1.30 (m, 3H), 1.21-1.15 (m, 4H); ^{13}C NMR (400 MHz, DMSO) δ = 173.6, 170.1, 164.5, 152.2, 150.6, 141.8, 139.2, 136.6, 136.0, 132.0, 123.2, 119.2, 112.0, 105.2, 66.9, 60.3, 56.6, 56.2, 51.5, 48.0, 46.1, 45.4 (2), 42.2, 41.5, 32.6, 30.1, 29.7, 28.7, 24.7, 24.2. HRMS-ESI: m/z found 690.4094 [M+H]+, $C_{36}H_{53}N_9O_5$ requires 690.4097.

(S,E)-3-((4-(3-(1-(4-(dimethylamino)but-2-enoyl)piperidine-4-carboxamido)piperidin-1-yl)-3-methoxyphenyl)amino)-6-ethyl-5-((tetrahydro-2H-pyran-4-yl)amino)pyrazine-2-

carboxamide (CG-4-163): CG-4-161 and trans-4-Dimethylaminocrotonic acid hydrochloride were reacted on a 0.113 mmol scale according to General Procedure 6, using CH_2Cl_2/MeOH/NH_4OH, 92:7:1 to monitor the reaction and CH_2Cl_2/MeOH/NH_4OH, 58:7:1 to purify the title compound. (dark yellow solid, yield = 59%): ^{1}H NMR (400 MHz, DMSO) δ = 11.02 (s, 1H), 7.69 (d, J = 7.6 Hz, 1H), 7.53 (s, 1H), 7.27-7.24 (m, 2H), 7.01 (s, 1H), 6.81-6.79 (m, 2H), 6.57-6.55 (m, 2H), 4.38 (d, J = 11.6 Hz, 1H), 4.11-4.01 (m, 2H), 3.90 (d, J = 9.2 Hz, 2H), 3.79 (s, 4H), 3.35 (s, 2H), 3.09 (s, 2H), 3.02 (d, J = 4 Hz, 2H), 2.62-2.36 (m, 6H), 2.14 (s, 6H), 1.83 (d, J = 12.4 Hz, 2H), 1.72-1.57 (m, 7H), 1.41-1.30 (m, 3H), 1.21-1.15 (m, 4H); ^{13}C NMR (400 MHz, DMSO) δ = 173.6, 170.1, 164.5, 152.8, 152.2, 150.6, 141.8, 136.6, 136.0, 132.0, 123.2, 119.2, 112.0, 105.2, 66.9, 60.3, 56.6, 56.2, 51.5, 48.0, 46.0, 45.4 (2), 42.2, 32.6, 30.1, 29.7, 28.7, 24.7, 24.2, 11.4. HRMS-ESI: m/z found 690.4092 [M+H]+, $C_{36}H_{53}N_9O_5$ requires 690.4097.

tert-butyl 4-(4-methylpiperazin-1-yl)piperidine-1-carboxylate (CG-4-176): 1-methylpiperazine (20 mmol, 1.0 eq) was dissolved in anh. THF (0.1M) with DIPEA (1.0). Tert-butyl 4-oxopiperidine-1-carboxylate (2.0 eq) was added to the reaction mixture followed by sodium triacetoxyborohydride (3.0 eq). The reaction mixture was stirred at room temperature for 16 hours under N_2(g). Reaction completion was monitored via TLC (CH_2Cl_2/MeOH/NH_4OH, 92:7:1). Upon completion, the reaction was diluted with ethyl acetate and partitioned with water and the aqueous was basified with saturated sodium bicarbonate. The product was extracted from the aqueous layer x3. The organic layers were combined and washed with saturated sodium bicarbonate, water x3, and saturated sodium chloride then dried over sodium sulfate and concentrated to dryness. The crude

material was adsorbed onto silica gel, then purified by flash column chromatography eluting with CH_2Cl_2/MeOH/NH_4OH, 192:7:1 to yield the title compound. (yellow oil, yield = 61%): ^{1}H NMR (400 MHz, DMSO) δ = 3.90 (d, J = 10.8 Hz, 2H), 3.37 (s, 4H), 2.71 (s, 2H), 2.43 (s, 4H), 2.28 (s, 4H), 1.69 (d, J = 12.0 Hz, 2H), 1.67 (s, 9H), 1.20 (q, J = 12.1 Hz, 2H); ^{13}C NMR (400 MHz, DMSO) δ = 79.0, 61.2, 55.6 (2), 48.9 (2), 46.2, 28.5, 28.3.

1-methyl-4-(piperidin-4-yl)piperazine (CG-4-179): CG-4-176 was reacted on a 12.0 mmol scale according to General Procedure 5, using CH_2Cl_2/MeOH/NH_4OH, 92:7:1 to monitor the formation of the title compound with no further purification. (white solid, yield = 87%): ^{1}H NMR (400 MHz, DMSO) δ = 5.71 (s, 1H), 3.49-3.12 (m, 6H), 2.91-2.8 (m, 8H), 2.49 (s, 2H), 2.01 (d, J = 12.4 Hz), 1.63 (q, J = 10.9 Hz, 2H); ^{13}C NMR (400 MHz, DMSO) δ = 58.6, 52.0, 46.0, 42.6, 42.4, 24.7.

tert-butyl (2-(2-fluoro-5-nitrophenoxy)ethyl)carbamate (CG-4-174): 2-fluoro-5-nitrophenol (3.18 mmol, 1.0 eq) was dissolved in DMF (0.1M) with K_2CO_3 (3.0 eq). Tert-butyl (2-bromoethyl)carbamate (1.5 eq) was added to the reaction mixture and the reaction mixture was stirred at room temperature for 16 hours. Reaction completion was monitored via TLC (hexanes:EtOAc). Upon completion, the reaction was partitioned between EtOAc and brine. The organic layer was washed five times with brine to remove the DMF. The organic layer was then collected, dried with Na_2SO_4, filtered and concentrated. The crude material was adsorbed onto silica gel, then purified by flash column chromatography eluting with hexanes:EtOAc to yield the title compound. (off white solid, yield = 90%): ^{1}H NMR (400 MHz, DMSO) δ = 9.97 (d, J = 6.8 Hz, 1H), 7.88 (m, 1H), 7.51 (t, J = 9.8 Hz, 1H), 7.05 (s, 1H), 4.19 (t, J = 5.4 Hz, 2H), 3.31 (s, 2H), 1.35

(s, 9H); ^{13}C NMR (400 MHz, DMSO) δ = 156.1, 154.9, 117.7, 117.6, 117.3, 117.1, 110.6, 78.3, 68.6, 28.6 (2).

tert-butyl (2-(2-(4-(4-methylpiperazin-1-yl)piperidin-1-yl)-5-nitrophenoxy)ethyl)carbamate (CG-4-180): CG-4-174 and CG-4-179 were reacted on a 1.67 mmol scale according to General Procedure 1, using CH_2Cl_2/MeOH/NH_4OH, 92:7:1 to monitor and purify the title compound. (dark yellow solid, yield = 68%): ^{1}H NMR (400 MHz, DMSO) δ = 7.80 (d, J = 9.6 Hz, 1H), 7.63 (s, 1H), 6.99-6.96 (m, 2H), 4.07 (t, J = 4.8 Hz, 2H), 3.71 (d, J = 12.4 Hz, 2H), 2.69 (t, J = 11.2 Hz, 2H), 2.49 (s, 4H), 2.30 (m, 5H), 2.11 (m, 2H), 1.80 (d, J = 11.6 Hz, 2H), 1.52 (q, J = 10 Hz, 2H), 1.37 (s, 12H); ^{13}C NMR (400 MHz, DMSO) δ = 156.0, 150.0, 148.4, 140.6, 118.4, 117.4, 108.1, 78.2, 67.6, 61.1, 55.6, 49.6, 49.0, 48.9, 46.2, 28.7, 28.5.

tert-butyl (2-(5-amino-2-(4-(4-methylpiperazin-1-yl)piperidin-1-yl)phenoxy)ethyl)carbamate (CG-4-187): CG-4-180 was reacted on a 1.08 mmol scale according to General Procedure 2, using CH_2Cl_2/MeOH/NH_4OH, 92:7:1 to monitor the reaction and purify the title compound. (black oil, yield = 72%): ^{1}H NMR (400 MHz, DMSO) δ = 6.94 (d, J = 5.0 Hz, 1H), 6.59 (d, J = 8.4 Hz, 1H), 6.18 (s, 1H), 6.07 (d, J = 7.6 Hz, 1H), 4.67 (s, 2H), 3.84 (m, 2H), 3.26 (m, 2H), 3.15 (m, 2H), 2.40 (m, 6H), 2.19 (s, 5H), 1.76 (d, J = 11.6 Hz, 2H), 1.53 (q, J = 9.6 Hz, 2H), 1.36 (s, 12H); ^{13}C NMR (400 MHz, DMSO) δ = 156.0, 152.7, 145.2, 132.7, 119.8, 106.8, 102.0, 78.2, 67.6, 61.5, 5.2, 51.4, 48.7, 45.8, 42.5, 28.9, 28.7.

tert-butyl (2-(5-((3-carbamoyl-6-chloro-5-ethylpyrazin-2-yl)amino)-2-(4-(4-methylpiperazin-1-yl)piperidin-1-yl)phenoxy)ethyl)carbamate (CG-4-190): CG-4-187 was reacted on a 0.775 mmol scale according to General Procedure 3, using

CH_2Cl_2/MeOH/NH_4OH, 92:7:1 to monitor the reaction and purify the title compound. (yellow solid, yield = 57%): ^{1}H NMR (400 MHz, DMSO) δ = 10.96 (s, 1H), 8.20 (s, 1H), 7.98 (s, 1H), 7.23 (s, 1H), 7.08 (d, J = 7.6 Hz, 1H), 6.92 (s, 1H), 6.85 (d, J = 7.6 Hz, 1H), 3.97 (t, J = 5.2 Hz, 2H), 3.38-3.31 (m, 4H), 2.78 (q, J = 7.5 Hz, 2H), 2.49-2.44 (m, 4H), 2.30-2.18 (m, 6H), 2.13 (s, 3H), 1.79 (d, J = 10.8 Hz, 2H), 1.55 (q, J = 10.4 Hz, 2H), 1.36 (s, 9H), 1.25-1.17 (m, 4H); ^{13}C NMR (400 MHz, DMSO) δ = 168.5 (2), 156.4, 151.6, 149.7, 147.2, 141.6, 138.5, 133.9, 126.4, 118.8, 113.1, 107.3, 78.2, 67.6, 61.5, 55.7, 50.8, 49.0, 46.2, 28.9, 28.7, 26.6, 12.5.

tert-butyl (2-(5-((3-carbamoyl-5-ethyl-6-((tetrahydro-2H-pyran-4-yl)amino)pyrazin-2-yl)amino)-2-(4-(4-methylpiperazin-1-yl)piperidin-1-yl)phenoxy)ethyl)carbamate (CG-4-200): CG-4-190 was reacted on a 0.442 mmol scale according to General Procedure 4, using CH_2Cl_2/MeOH/NH_4OH, 92:7:1 to monitor the reaction and purify the title compound. (yellow foam solid, yield = 83%): ^{1}H NMR (400 MHz, DMSO) δ = 11.0 (s, 1H), 7.52 (s, 1H), 7.23 (s, 2H), 7.07 (s, 1H), 6.94 (t, J = 5.0 Hz, 1H), 6.79 (t, J = 7.8 Hz, 2H), 4.06 (s, 1H), 3.98 (t, J = 5.6 Hz, 2H), 3.90 (s, J = 9.2 Hz, 2H), 3.39-3.27 (m, 6H), 2.56 (q, J = 7.3 Hz, 2H), 2.46 (m, 4H), 2.28-2.17 (m, 5H), 2.12 (s, 3H), 1.81 (t, J = 15.2 Hz, 4H), 1.57 (m, 4H), 1.36 (s, 10H), 1.23-1.15 (m, 4H); ^{13}C NMR (400 MHz, DMSO) δ = 170.1, 156.0, 152.2, 151.8, 150.5, 137.6, 135.7, 132.0, 118.8, 112.9, 112.1, 107.7, 78.2, 68.2, 66.9 (2), 61.5, 55.7, 51.0, 49.1, 48.1, 46.2, 32.6, 28.9, 28.7, 24.7, 11.4.

3-((3-(2-aminoethoxy)-4-(4-(4-methylpiperazin-1-yl)piperidin-1-yl)phenyl)amino)-6-ethyl-5-((tetrahydro-2H-pyran-4-yl)amino)pyrazine-2-carboxamide (CG-4-203): CG-4-200 was reacted on a 0.293 mmol scale according to General Procedure 5, using CH_2Cl_2/MeOH/NH_4OH, 58:7:1 to monitor the reaction and purify the title compound.

(yellow solid, yield = 82%): ^{1}H NMR (400 MHz, DMSO) δ = 11.0 (s, 1H), 7.52 (s, 1H), 7.23 (s, 2H), 7.07 (s, 1H), 6.80 (s, 2H), 4.07 (s, 1H), 3.96 (t, J = 5.4 Hz, 2H), 3.91 (d, J = 10.0 Hz, 2H), 3.32 (s, 6H), 2.88 (t, J = 5.2 Hz, 2H), 2.56 (q, J = 7.3 Hz, 2H), 2.49 (s, 4H), 2.29-2.17 (m, 5H), 2.12 (s, 3H), 1.82 (t, J = 11.8 Hz, 4H), 1.65-1.49 (m, 4H), 1.17 (t, J = 7.6 Hz, 3H); ^{13}C NMR (400 MHz, DMSO) δ = 170.1, 152.2, 151.9, 150.5, 137.5, 135.8, 132.0, 118.8, 112.6, 112.1, 107.3, 71.3, 66.9, 61.4, 55.7, 51.0, 49.1, 48.1, 46.3, 41.5, 32.6, 29.0, 24.7, 11.4.

3-((3-(2-acrylamidoethoxy)-4-(4-(4-methylpiperazin-1-yl)piperidin-1-yl)phenyl)amino)-6-ethyl-5-((tetrahydro-2H-pyran-4-yl)amino)pyrazine-2-carboxamide (CG-4-206): CG-4-203 and acryloyl chloride were reacted on a 0.120 mmol scale according to General Procedure 7, using CH_2Cl_2/MeOH/NH_4OH, 58:7:1 to monitor the reaction and purify the title compound. (yellow solid, yield = 54%): ^{1}H NMR (400 MHz, DMSO) δ = 11.0 (s, 1H), 8.27 (s, 1H), 7.52 (s, 1H), 7.27-7.24 (m, 2H), 7.03 (s, 1H), 6.79 (d, J = 8.8 Hz, 2H), 6.23 (q, J = 10 Hz, 1H), 6.08 (d, J = 14.8 Hz, 1H), 5.58 (d, J = 10 Hz, 1H), 4.05 (m, 3H), 3.90 (d, J = 10.4 Hz, 2H), 3.52 (d, J = 4.8 Hz, 2H), 3.36 (6H), 2.56 (q, J = 7.3 Hz, 2H), 2.49-2.41 (m, 4H), 2.30-2.20 (m, 5H), 2.13 (s, 3H), 1.83 (d, J = 12.4 Hz, 2H), 1.73 (d, J = 11.6 Hz, 2H), 1.62-1.48 (m, 4H), 1.17 (t, J = 7.6 Hz, 3H); ^{13}C NMR (400 MHz, DMSO) δ = 170.1, 165.2, 152.2, 151.7, 150.5, 137.4, 135.6, 132.1, 131.9, 125.6, 118.8, 112.7, 112.1, 107.0, 67.2, 66.9, 61.5, 55.6 (2), 50.9, 49.0, 48.1, 46.2, 32.6, 28.8, 24.7, 11.4. HRMS-ESI: m/z found 634.3829 [M+H]+, $C_{33}H_{49}N_9O_4$ requires 634.3835.

tert-butyl 4-((2-fluoro-5-nitrophenoxy)methyl)piperidine-1-carboxylate (CG-4-175): 2-fluoro-5-nitrophenol (3.18 mmol, 1.0 eq) was dissolved in DMF (0.1M) with K_2CO_3 (3.0 eq). tert-butyl 4-(bromomethyl)piperidine-1-carboxylate (1.5 eq) was added to the

reaction mixture and the reaction mixture was stirred at room temperature for 16 hours. Reaction completion was monitored via TLC (hexanes:EtOAc). Upon completion, the reaction was partitioned between EtOAc and brine. The organic layer was washed five times with brine to remove the DMF. The organic layer was then collected, dried with Na_2SO_4, filtered and concentrated. The crude material was adsorbed onto silica gel, then purified by flash column chromatography eluting with hexanes:EtOAc to yield the title compound. (off white solid, yield = 49%): ^{1}H NMR (400 MHz, DMSO) δ = 7.95 (d, J = 7.2 Hz, 1H), 7.90-7.86 (m, 1H), 7.51 (t, J = 9.8 Hz, 1H), 4.06 (d, J = 6.4 Hz, 2H), 3.96 (d, J = 10 Hz, 2H), 2.74 (s, 2H), 1.97 (s, 1H), 1.73 (d, J = 12 Hz, 2H), 1.38 (s, 9H), 1.17 (q, J = 12.3 Hz, 2H); ^{13}C NMR (400 MHz, DMSO) δ = 157.3, 154.8, 154.3, 144.6, 117.6, 117.5, 117.2, 117.0, 110.4, 79.0, 73.7, 35.5, 28.5.

tert-butyl 4-((2-(4-(4-methylpiperazin-1-yl)piperidin-1-yl)-5-nitrophenoxy)methyl)piperidine-1-carboxylate (CG-4-181): CG-4-175 and CG-4-179 were reacted on a 1.41 mmol scale according to General Procedure 1, using CH_2Cl_2/MeOH/NH_4OH, 92:7:1 to monitor and purify the title compound. (yellow solid, yield = 72%): ^{1}H NMR (400 MHz, $CDCl_3$) δ = 7.86 (d, J = 8.4 Hz, 1H), 7.68 (s, 1H), 6.87 (d, J = 9.2 Hz, 1H), 4.19 (s, 2H), 3.92 (d, J = 6.4 Hz, 2H), 3.76 (d, J = 11.6 Hz, 2H), 2.81-2.66 (m, 6H), 2.51 (s, 4H), 2.42-2.36 (m, 2H), 2.30 (s, 3H), 2.01-1.84 (m, 4H), 1.69 (q, J = 11.5 Hz, 2H), 1.49-1.46 (m, 11H), 1.34 (q, J = 12.5 Hz, 2H); ^{13}C NMR (400 MHz, $CDCl_3$) δ = 150.0, 145.6, 143.1, 136.8, 113.1, 112.0, 102.6, 74.8, 68.4, 56.8, 50.6, 45.1, 44.5, 44.2, 41.3, 31.6, 24.3, 23.9, 23.7.

tert-butyl 4-((5-amino-2-(4-(4-methylpiperazin-1-yl)piperidin-1-yl)phenoxy)methyl)piperidine-1-carboxylate (CG-4-188): CG-4-181 was reacted on a

0.964 mmol scale according to General Procedure 2, using CH_2Cl_2/MeOH/NH_4OH, 92:7:1 to monitor the reaction and purify the title compound. (brown solid, yield = 95%): ^{1}H NMR (400 MHz, DMSO) δ = 6.60 (d, J = 8.4 Hz, 1H), 6.21 (s, 1H), 6.06 (d, J = 8.0 Hz, 1H), 4.65 (s, 2H), 4.58 (d, J = 3.2 Hz, 1H), 4.02 (d, J = 11.6 Hz, 2H), 3.73 (d, J = 5.6 Hz, 2H), 3.52 (s, 1H), 3.35 (s, 3H), 3.04 (d, J = 6.4 Hz, 2H), 2.75 (m, 3H), 2.55-2.52 (m, 4H), 1.93 (s, 1H), 1.78 (d, J = 9.2 Hz, 4H), 1.53-1.42 (m, 13H), 1.23 (q, J = 12.0 Hz, 2H); ^{13}C NMR (400 MHz, $CDCl_3$) δ = 162.8, 154.3, 152.9, 145.0, 132.5, 119.7, 106.0, 100.8, 78.9, 72.1, 66.9, 55.4, 49.8 (2), 36.3, 35.5 (2), 29.0, 28.6.

tert-butyl 4-((5-((3-carbamoyl-6-chloro-5-ethylpyrazin-2-yl)amino)-2-(4-(4-methylpiperazin-1-yl)piperidin-1-yl)phenoxy)methyl)piperidine-1-carboxylate (CG-4-191): CG-4-181 was reacted on a 0.636 mmol scale according to General Procedure 3, using CH_2Cl_2/MeOH/NH_4OH, 92:7:1 to monitor the reaction and purify the title compound. (yellow solid, yield = 80%): ^{1}H NMR (400 MHz, DMSO) δ = 11.0 (s, 1H), 8.20 (s, 1H), 7.97 (s, 1H), 7.22 (s, 1H), 7.06 (d, J = 7.2 Hz, 1H), 6.82 (d, J = 8 Hz, 1H), 3.99 (d, J = 10.8 Hz, 2H), 3.84 (d, J = 5.6 Hz, 2H), 3.33 (s, 2H), 2.78 (q, J = 7.2 Hz, 5H), 2.49 (s, 2H), 2.31 (s, 4H), 2.20 (m, 1H), 2.14 (s, 3H), 1.94 (s, 1H), 1.82-1.73 (m, 4H), 1.48 (q, J = 9.2 Hz, 2H), 1.37 (s, 11H), 1.28-1.19 (m, 6H). ^{13}C NMR (400 MHz, DMSO) δ = 168.5, 154.2, 151.8, 149.7, 147.2, 141.5, 138.0, 133.9, 125.1, 118.7, 112.4, 106.0, 78.9, 72.4, 61.5, 55.6, 50.7 (2), 49.0, 48.8, 46.1, 36.2, 29.0, 28.6, 26.6, 12.4.

tert-butyl 4-((5-((3-carbamoyl-5-ethyl-6-((tetrahydro-2H-pyran-4-yl)amino)pyrazin-2-yl)amino)-2-(4-(4-methylpiperazin-1-yl)piperidin-1-yl)phenoxy)methyl)piperidine-1-carboxylate (CG-4-201): CG-4-191 was reacted on a 0.446 mmol scale according to General Procedure 4, using CH_2Cl_2/MeOH/NH_4OH, 92:7:1 to monitor the reaction and

purify the title compound. (yellow foam solid, yield = 73%): ^{1}H NMR (400 MHz, DMSO) δ = 11.0 (s, 1H), 7.50 (s, 1H), 7.26 (d, J = 8.4 Hz, 1H), 7.19 (s, 1H), 6.92 (s, 1H), 6.77 (t, J = 8.2 Hz, 2H), 4.07-3.98 (m, 3H), 3.90 (d, J = 10.8 Hz, 2H), 3.86 (d, J = 4.8 Hz, 2H), 3.34 (m, 2H), 3.32 (s, 2H), 2.56 (q, J = 7.3 Hz, 2H), 2.49 (s, 2H), 2.28-2.16 (m, 5H), 2.12 (s, 3H), 1.91-1.72 (m, 8H), 1.66-1.44 (m, 4H), 1.38 (s, 11H), 1.29-1.15 (m, 6H); ^{13}C NMR (400 MHz, DMSO) δ = 170.1, 154.2, 152.2, 152.0, 150.6, 137.1, 135.6, 131.9, 121.9, 118.6, 112.2, 112.1, 106.2, 78.9, 72.7, 66.9, 61.5, 55.7, 50.9 (2), 49.1, 48.1, 46.3, 36.4, 32.6, 29.0, 28.6, 24.6, 11.4.

6-ethyl-3-((4-(4-(4-methylpiperazin-1-yl)piperidin-1-yl)-3-(piperidin-4-ylmethoxy)phenyl)amino)-5-((tetrahydro-2H-pyran-4-yl)amino)pyrazine-2-carboxamide (CG-4-204): CG-4-201 was reacted on a 0.271 mmol scale according to General Procedure 5, using CH_2Cl_2/MeOH/NH_4OH, 58:7:1 to monitor the reaction and purify the title compound. (yellow solid, yield = 80%): ^{1}H NMR (400 MHz, DMSO) δ = 11.0 (s, 1H), 7.50 (s, 1H), 7.27 (d, J = 8.4 Hz, 1H), 7.20 (s, 1H), 6.93 (d, J = 8.8 Hz, 1H), 6.79-6.75 (m, 2H), 4.06 (s, 1H), 3.90 (d, J = 9.2 Hz, 2H), 3.80 (d, J = 5.6 Hz, 2H), 3.38-3.32 (m, 4H), 3.09 (d, J = 11.6 Hz, 2H), 3.01 (d, J = 9.6 Hz, 1H), 2.67-2.54 (m, 4H), 2.49 (s, 3H), 2.28-2.16 (m, 5H), 2.12 (s, 2H), 2.04 (s, 1H), 1.89-1.70 (m, 9H), 1.66-1.42 (m, 5H), 1.30 (q, J = 12 Hz, 2H), 1.17 (t, J = 7.6 Hz, 3H); ^{13}C NMR (400 MHz, DMSO) δ = 170.1, 152.2 (2), 150.6, 137.2, 135.6, 131.9, 118.6, 112.1, 106.5, 73.1, 66.9, 61.5, 55.7, 51.9, 50.9, 49.1, 48.1, 46.3, 45.2, 36.0, 32.6, 29.0, 28.7, 24.6, 11.4.

3-((3-((1-acryloylpiperidin-4-yl)methoxy)-4-(4-(4-methylpiperazin-1-yl)piperidin-1-yl)phenyl)amino)-6-ethyl-5-((tetrahydro-2H-pyran-4-yl)amino)pyrazine-2-carboxamide (CG-4-207): CG-4-204 and acryloyl chloride were reacted on a 0.110 mmol scale

according to General Procedure 7, using CH_2Cl_2/MeOH/NH_4OH, 58:7:1 to monitor the reaction and purify the title compound. (yellow solid, yield = 49%): ^{1}H NMR (400 MHz, DMSO) δ = 11.0 (s, 1H), 7.52 (s, 1H), 7.27 (d, J = 8.4 Hz, 1H), 7.22 (s, 1H), 6.89 (s, 1H), 6.85-6.75 (m, 3H), 6.09 (d, J = 16.4 Hz, 1H), 5.64 (d, J = 10.4 Hz, 1H), 4.48 (d, J = 11.6 Hz, 1H), 4.13-4.05 (m, 2H), 3.91-3.84 (m, 4H), 3.34 (m, 6H), 3.09 (t, J = 12.6 Hz, 1H), 2.66 (t, J = 12.2 Hz, 1H), 2.56 (q, J = 7.3 Hz, 2H), 2.49-2.45 (m, 4H), 2.29 (s, 3H), 2.21-2.13 (m, 5H), 2.03 (s, 1H), 1.84-1.75 (m, 6H), 1.60 (q, J = 10.4 Hz, 2H), 1.45 (q, J = 10.7 Hz, 2H), 1.25 (m, 2H), 1.17 (t, J = 7.6 Hz, 3H); ^{13}C NMR (400 MHz, DMSO) δ = 170.0, 164.4, 152.2, 152.0, 150.6, 137.0, 135.5, 131.9, 128.9, 127.4, 118.5, 112.1, 105.7, 72.2, 66.9, 61.5, 55.6, 50.9, 49.0, 48.1, 46.2, 45.5, 42.0, 36.4, 32.6, 30.0, 29.0, 24.6, 11.4. HRMS-ESI: m/z found 688.4300 [M+H]+, $C_{37}H_{55}N_9O_4$ requires 688.4304.

tert-butyl (4-(2-fluoro-5-nitrophenoxy)butyl)carbamate (CG-4-213): 2-fluoro-5-nitrophenol (12.7 mmol, 1.0 eq) was dissolved in anh. THF (0.1M) and the reaction mixture was then placed in an ice bath at 0°C under N_2(g). tert-butyl (4-hydroxybutyl)carbamate (1.1 mmol), triphenylphosphine (1.1 mmol) and diisopropyl azodicarboxylate (1.1 mmol) were added to the reaction mixture which was left stirring for 16 hours. Reaction completion was monitored via TLC (hexanes:EtOAc). Upon completion, the reaction was partitioned between EtOAc and H_2O. The aqueous was basified with saturated sodium bicarbonate and the product was extracted into ethyl acetate x3. The organic layers were combined and washed with water: saturated sodium bicarbonate x3 and saturated sodium chloride, then dried over sodium sulfate and concentrated to dryness. The crude material was adsorbed onto silica gel, then purified by flash column chromatography eluting with hexanes:EtOAc to yield the title compound.

(off white solid, yield = 72%): ^{1}H NMR (400 MHz, DMSO) δ = 7.94 (d, J = 7.2 Hz, 1H), 7.87 (d, J = 9.2 Hz, 1H), 7.50 (t, J = 9.8 Hz, 1H), 6.84 (s, 1H), 4.18 (t, J = 6.2 Hz, 2H), 2.97 (t, J = 6 Hz, 2H), 1.73 (t, J = 7 Hz, 2H), 1.52 (t, J = 7 Hz, 2H), 1.35 (s, 9H), 1.17 (d, J = 5.6 Hz, 2H); ^{13}C NMR (400 MHz, DMSO) δ = 117.5, 117.4, 117.2, 117.0, 110.4 (2), 77.8, 69.6, 68.3, 28.7, 26.4, 26.3, 22.4.

tert-butyl (4-(2-(4-(4-methylpiperazin-1-yl)piperidin-1-yl)-5-nitrophenoxy)butyl)carbamate (CG-4-223): CG-4-213 and CG-4-179 were reacted on a 4.57 mmol scale according to General Procedure 1, using CH_2Cl_2/MeOH/NH_4OH, 92:7:1 to monitor and purify the title compound. (yellow solid, yield = 43%): ^{1}H NMR (400 MHz, DMSO) δ = 7.78 (d, J = 8.4 Hz, 1H), 7.63 (s, 1H), 6.96 (d, J = 8.8 Hz, 1H), 6.85 (s, 1H), 4.06 (t, J = 5.8 Hz, 2H), 3.69 (d, J = 11.6 Hz, 2H), 2.98 (q, J = 6.5 Hz, 2H), 2.70 (d, J = 11.8 Hz, 2H), 2.49 (s, 4H), 2.32 (s, 4H), 2.14 (s, 3H), 1.83 (d, J = 11.6 Hz, 2H), 1.74 (t, J = 6.6 Hz, 2H), 1.56-1.46 (m, 4H), 1.36 (s, 10H); ^{13}C NMR (400 MHz, DMSO) δ = 156.1, 150.3, 148.2, 140.8, 118.1, 117.3, 107.5, 77.8, 68.5, 61.1, 55.6, 49.5, 49.0, 46.1, 28.7 (2), 28.5, 26.7, 26.6.

tert-butyl (4-(5-amino-2-(4-(4-methylpiperazin-1-yl)piperidin-1-yl)phenoxy)butyl)carbamate (CG-4-242): CG-4-223 was reacted on a 1.95 mmol scale according to General Procedure 2, using CH_2Cl_2/MeOH/NH_4OH, 92:7:1 to monitor the reaction and purify the title compound. (black solid, yield = 44%): ^{1}H NMR (400 MHz, DMSO) δ = 6.83 (s, 1H), 6.57 (d, J = 8.8 Hz, 1H), 6.17 (s, 1H), 6.03 (d, J = 8.4 Hz, 1H), 4.65 (s, 2H), 3.81 (t, J = 5.8 Hz, 2H), 3.15 (d, J = 11.2 Hz, 2H), 2.97 (q, J = 6.3 Hz, 2H), 2.49-2.37 (m, 6H), 2.30 (s, 4H), 2.13 (s, 4H), 1.76-1.65 (m, 4H), 1.57-1.46 (m, 4H), 1.36

(s, 9H); ^{13}C NMR (400 MHz, DMSO) δ = 156.0, 152.9, 145.1, 132.3 (2), 119.7 (2), 106.0, 100.9, 77.8, 67.4, 61.7, 55.6, 51.5, 49.0, 46.2, 29.0, 28.7, 26.9.

tert-butyl (4-(5-((3-carbamoyl-6-chloro-5-ethylpyrazin-2-yl)amino)-2-(4-(4-methylpiperazin-1-yl)piperidin-1-yl)phenoxy)butyl)carbamate (CG-4-247): CG-4-242 was reacted on a 1.43 mmol scale according to General Procedure 3, using CH_2Cl_2/MeOH/NH_4OH, 92:7:1 to monitor the reaction and purify the title compound. (orange solid, yield = 53%): ^{1}H NMR (400 MHz, DMSO) δ = 11.0 (s, 1H), 8.12 (s, 1H), 7.97 (s, 1H), 7.22 (s, 1H), 7.04 (d, J = 7.6 Hz, 1H), 6.84-6.82 (m, 2H), 3.95 (t, J = 5.8 Hz, 2H), 3.37 (m, 2H), 2.98 (q, J = 6.3 Hz, 2H), 2.78 (q, J = 7.2 Hz, 2H), 2.49-2.44 (m, 5H), 2.29-2.21 (m, 5H), 2.13 (s, 3H), 1.81-1.71 (m, 4H), 1.58-1.52 (m, 4H), 1.35 (s, 10H), 1.23 (t, J = 7.4 Hz, 3H); ^{13}C NMR (400 MHz, DMSO) δ = 168.5, 156.0, 151.8, 149.7, 147.2, 141.5, 138.0, 133.8, 125.1, 118.7, 112.4 (2), 106.1, 77.8, 67.8 (2), 61.5, 55.7, 50.7, 49.0, 46.2, 28.9, 28.7, 26.8, 26.6, 12.5.

tert-butyl (4-(5-((3-carbamoyl-5-ethyl-6-((tetrahydro-2H-pyran-4-yl)amino)pyrazin-2-yl)amino)-2-(4-(4-methylpiperazin-1-yl)piperidin-1-yl)phenoxy)butyl)carbamate (CG-4-252): CG-4-247 was reacted on a 0.697 mmol scale according to General Procedure 4, using CH_2Cl_2/MeOH/NH_4OH, 92:7:1 to monitor the reaction and purify the title compound. (yellow solid, yield = 67%): ^{1}H NMR (400 MHz, DMSO) δ = 11.0 (s, 1H), 7.50 (s, 1H), 7.21-7.19 (m, 2H), 7.00 (1H), 6.83-6.74 (m, 3H), 4.08 (s, 1H), 3.96-3.89 (m, 4H), 3.34 (m, 4H), 2.98 (q, J = 6.27 Hz, 2H), 2.59-2.44 (m, 6H), 2.29-2.12 (m, 5H), 2.12 (s, 3H), 1.81 (t, J = 13.6 Hz, 4H), 1.70-1.50 (m, 9H), 1.35 (s, 10H), 1.17 (t, J = 7.6 Hz, 3H); ^{13}C NMR (400 MHz, DMSO) δ = 170.1, 156.2 (2), 152.2, 152.0, 150.6, 137.2,

135.6, 131.9, 118.6, 112.2 (2), 106.3, 77.8, 68.2, 66.9, 61.6, 55.7, 50.9, 49.0, 48.0, 46.3, 32.6, 28.9, 28.7, 27.0, 26.9, 24.6, 11.4.

3-((3-(4-aminobutoxy)-4-(4-(4-methylpiperazin-1-yl)piperidin-1-yl)phenyl)amino)-6-ethyl-5-((tetrahydro-2H-pyran-4-yl)amino)pyrazine-2-carboxamide (CG-5-001): CG-4-252 was reacted on a 0.464 mmol scale according to General Procedure 5, using CH_2Cl_2/MeOH/NH_4OH, 58:7:1 to monitor the reaction and purify the title compound. (yellow solid, yield = 69%): ^{1}H NMR (400 MHz, DMSO) δ = 11.0 (s, 1H), 7.51 (s, 1H), 7.22-7.20 (m, 2H), 7.00 (s, 1H), 6.80-6.75 (m, 2H), 4.08 (s, 1H), 3.97-3.89 (m, 4H), 3.35 (m, 4H), 2.64 (t, J = 7.2 Hz, 2H), 2.56 (q, J = 7.3 Hz, 2H), 2.49 (m, 7H), 2.29-2.18 (m, 4H), 2.12 (s, 3H), 1.85-1.72 (m, 6H), 1.65-1.50 (m, 6H), 1.17 (t, J = 7.6 Hz, 3H); ^{13}C NMR (400 MHz, DMSO) δ = 170.1, 152.0 (2), 150.6, 137.2, 135.6, 131.9, 118.6, 112.2, 106.4, 103.0, 68.4, 66.9, 61.5, 55.7, 50.9, 49.1, 48.1, 46.3, 41.4, 32.6, 29.4, 29.0, 27.0, 24.6, 11.4.

3-((3-(4-acrylamidobutoxy)-4-(4-(4-methylpiperazin-1-yl)piperidin-1-yl)phenyl)amino)-6-ethyl-5-((tetrahydro-2H-pyran-4-yl)amino)pyrazine-2-carboxamide (CG-5-002): CG-5-001 and acryloyl chloride were reacted on a 0.0264 mmol scale according to General Procedure 7, using CH_2Cl_2/MeOH/NH_4OH, 92:7:1 to monitor the reaction and purify the title compound. (off yellow solid, yield = 86%): ^{1}H NMR (400 MHz, DMSO) δ = 11.0 (s, 1H), 8.14 (s, 1H), 7.52 (s, 1H), 7.23 (s, 2H), 7.00 (s, 1H), 6.78 (d, J = 8 Hz, 2H), 6.23-6.16 (m, 1H), 6.05 (d, J = 16 Hz, 1H), 5.55 (d, J = 10.4 Hz, 1H), 4.09 (s, 1H), 3.97 (t, J = 5.8 Hz, 2H), 3.90 (d, J = 9.2 Hz, 2H), 3.34 (s, 4H), 3.20 (q, J = 6.1 Hz, 2H), 2.59-2.44 (m, 6H), 2.31-2.22 (m, 5H), 2.14 (s, 3H), 1.84-1.74 (m, 6H), 1.64-1.46 (m, 6H), 1.21-1.15 (m, 5H); ^{13}C NMR (400 MHz, DMSO) δ = 170.1, 164.9, 152.2 (2), 150.6, 137.1, 135.6,

132.3, 131.9, 125.3 (2), 118.6, 112.1, 106.2, 67.4, 66.9, 61.5, 55.6, 50.9, 48.9, 47.2, 46.2, 38.7, 32.6, 28.8, 27.1, 26.5, 24.6, 11.4. HRMS-ESI: m/z found 662.4142 [M+H]+, $C_{35}H_{53}N_9O_4$ requires 662.4148.

tert-butyl (2-((4-(5-((3-carbamoyl-5-ethyl-6-((tetrahydro-2H-pyran-4-yl)amino)pyrazin-2-yl)amino)-2-(4-(4-methylpiperazin-1-yl)piperidin-1-yl)phenoxy)butyl)amino)-2-oxoethyl)(methyl)carbamate (CG-5-006): CG-5-001 and N-(tert-butoxycarbonyl)-N-methylglycine were reacted on a 0.483 mmol scale according to General Procedure 6, using CH_2Cl_2/MeOH/NH_4OH, 92:7:1 to monitor the reaction and purify the title compound. (yellow solid, yield = 64%): ^{1}H NMR (400 MHz, DMSO) δ = 11.0 (s, 1H), 7.85 (t, J = 5.6 Hz, 1H), 7.50 (s, 1H), 7.23-7.19 (m, 2H), 6.99 (s, 1H), 6.8.-6.75 (m, 2H), 4.08 (s, 1H), 3.97-3.89 (m, 4H), 3.70 (d, J = 15.2 Hz, 2H), 3.37-3.31 (m, 4H), 3.14 (d, J = 5.6 Hz, 2H), 2.77 (s, 3H), 2.59-2.45 (m, 7H), 2.30-2.18 (m, 5H), 2.13 (s, 3H), 1.85-1.66 (m, 6H), 1.66-1.49 (m, 6H), 1.38-1.32 (m, 10H), 1.17 (t, J = 7.2 Hz, 3H); ^{13}C NMR (400 MHz, DMSO) δ = 170.1, 152.2 (2), 152.0, 150.6, 137.2, 135.6 (2), 131.9, 118.6, 112.3 (2), 112.1, 106.4 (2), 68.1, 66.9, 61.5, 55.7, 50.9, 49.1, 48.1, 46.2, 38.7, 32.6, 29.0, 28.5 (2), 27.0, 26.5, 24.6, 11.4.

6-ethyl-3-((3-(4-(2-(methylamino)acetamido)butoxy)-4-(4-(4-methylpiperazin-1-yl)piperidin-1-yl)phenyl)amino)-5-((tetrahydro-2H-pyran-4-yl)amino)pyrazine-2-carboxamide (CG-5-007): CG-5-006 was reacted on a 0.298 mmol scale according to General Procedure 5, using CH_2Cl_2/MeOH/NH_4OH, 58:7:1 to monitor the reaction and purify the title compound. (yellow solid, yield = 92%): ^{1}H NMR (400 MHz, DMSO) δ = 11.0 (s, 1H), 7.90 (t, J = 5.4 Hz, 1H), 7.51 (s, 1H), 7.23 (m, 2H), 7.00 (s, 1H), 6.79-6.75 (m, 2H), 4.09 (s, 1H), 3.98-3.89 (m, 4H), 3.38-3.31 (m, 6H), 3.17 (q, J = 6.27 Hz, 2H),

3.09 (s, 2H), 2.59-2.31 (m, 6H), 2.26-2.13 (m, 9H), 2.11 (s, 3H), 1.85-1.71 (m, 6H), 1.65-1.46 (m, 6H), 1.17 (t, J = 7.2 Hz, 3H); ^{13}C NMR (400 MHz, DMSO) δ = 170.4, 170.1, 152.2, 152.0, 150.6, 137.2, 135.6, 118.6 (2), 112.2 (2), 106.4, 68.1, 66.9, 61.5, 55.6, 54.0, 50.9, 49.0, 48.0, 46.2, 38.4, 26.0, 32.6, 28.9, 27.0, 26.6, 24.6, 11.4.

6-ethyl-3-((3-(4-(2-(N-methylacrylamido)acetamido)butoxy)-4-(4-(4-methylpiperazin-1-yl)piperidin-1-yl)phenyl)amino)-5-((tetrahydro-2H-pyran-4-yl)amino)pyrazine-2-carboxamide (CG-5-008): CG-5-007 and acryloyl chloride were reacted on a 0.0733 mmol scale according to General Procedure 7, using CH_2Cl_2/MeOH/NH_4OH, 92:7:1 to monitor the reaction and purify the title compound. (off yellow solid, yield = 76%): ^{1}H NMR (400 MHz, DMSO) δ = 11.0 (s, 1H), 8.14 (s, 0.5H), 7.95 (s, 0.5H), 7.52 (s, 1H), 7.22 (s, 2H), 6.99 (s, 1H), 6.79-6.74 (m, 2.5H), 6.55 (q, J = 8.8 Hz, 0.5H), 6.08 (t, J = 16.6 Hz, 1H), 5.68 (d, J = 10.4 Hz, 0.5H), 5.60 (d, J = 10.4 Hz, 0.5H), 4.09 (s, 1H), 4.01-3.89 (m, 6H), 3.35 (m, 3H), 3.14 (t, J = 7.4 Hz, 2H), 3.04 (s, 2H), 2.83 (s, 2H), 2.59-2.44 (m, 7H), 2.28-2.17 (m, 5H), 2.12 (s, 3H), 1.84-1.72 (m, 6H), 1.65-1.48 (m, 6H), 1.17 (t, J = 7.2 Hz, 4H); ^{13}C NMR (400 MHz, DMSO) δ = 170.1, 168.3 (2), 152.2, 152.0, 150.6, 137.1, 135.6, 131.9, 128.8, 127.8, 127.4, 118.6, 112.1, 106.2, 68.1, 66.9, 61.5, 55.7, 52.5, 50.9 (2), 49.1, 48.1, 46.3, 38.7, 32.6, 28.9, 27.0, 26.5, 24.6, 11.4. HRMS-ESI: m/z found 733.4514 [M+H]+, $C_{38}H_{58}N_{10}O_5$ requires 733.4519.

6-ethyl-3-((4-(4-(4-methylpiperazin-1-yl)piperidin-1-yl)-3-(4-(2-(N-methylpropionamido)acetamido)butoxy)phenyl)amino)-5-((tetrahydro-2H-pyran-4-yl)amino)pyrazine-2-carboxamide (CG-5-024): CG-5-007 and propionyl chloride were reacted on a 0.147 mmol scale according to General Procedure 7, using CH_2Cl_2/MeOH/NH_4OH, 92:7:1 to monitor the reaction and purify the title compound.

(off yellow solid, yield = 51%): ^{1}H NMR (400 MHz, DMSO) δ = 11.0 (s, 1H), 8.06 (s, 0.5H), 7.82 (t, J = 5 Hz, 0.5H), 7.50 (s, 1H), 7.23-7.20 (m, 2H), 6.99 (s, 1H), 6.81-6.75 (m, 2H), 4.07 (s, 1H), 3.96-3.86 (m, 6H), 3.37-3.21 (m, 3H), 3.14 (q, J = 6.53 Hz, 2H), 2.93 (s, 2H), 2.76 (s, 2H), 2.59-2.44 (m, 6H), 2.35-2.29 (m, 5H), 2.24-2.14 (m, 6H), 1.85-1.72 (m, 6H), 1.65-1.49 (m, 6H), 1.26-1.15 (m, 4H), 0.98-0.91 (m, 3H); ^{13}C NMR (400 MHz, DMSO) δ = 173.6, 170.1, 168.6, 152.2, 152.0, 150.6, 137.2, 135.6, 131.9, 118.6, 112.2, 106.3, 68.1, 66.9, 61.5, 55.6, 52.5, 50.9, 50.7, 49.0, 48.0, 46.2, 40.6, 38.9, 38.7, 26.4, 34.7, 32.6, 28.9, 24.6, 11.4, 9.5. HRMS-ESI: m/z found 735.4670 [M+H]+, $C_{38}H_{60}N_{10}O_5$ requires 735.4675.

tert-butyl (2-((2-methoxy-4-nitrophenyl)amino)ethyl)carbamate (SP-2-128): 1-fluoro-2-methoxy-4-nitrobenzene and tert-butyl (2-aminoethyl)carbamate were reacted on a 11.69 mmol scale according to General Procedure 1, using hexanes:EtOAc to monitor and purify the title compound. (yellow solid, yield = 96%): ^{1}H NMR (400 MHz, DMSO) δ = 7.80 (d, J = 9.6 Hz, 1H), 7.55 (s, 1H), 7.00 (t, J = 5 Hz, 1H), 6.64 (d, J = 9.6 Hz, 1H), 6.60 (t, J = 5.6 Hz, 1H), 3.88 (s, 3H), 3.25 (q, J = 5.7 Hz, 2H), 3.11 (q, J = 5.6 Hz, 2H), 1.36 (s, 9H); ^{13}C NMR (400 MHz, DMSO) δ = 156.4, 145.3, 135.7, 120.4, 106.8, 104.9, 78.3, 56.3, 42.8, 39.3, 28.6, 28.4.

tert-butyl (2-((4-amino-2-methoxyphenyl)amino)ethyl)carbamate (CG-5-015): SP-2-128 was reacted on a 6.42 mmol scale according to General Procedure 2, using CH_2Cl_2/MeOH/NH_4OH, 192:7:1 to monitor the reaction and purify the title compound. (black solid, yield = 97%): ^{1}H NMR (400 MHz, DMSO) δ = 6.88 (s, 1H), 6.28-6.21 (m, 2H), 6.06 (s, 1H), 4.32 (s, 3H), 3.67 (s, 3H), 3.07 (s, 2H), 2.95 (s, 2H), 1.37 (s, 9H); ^{13}C

NMR (400 MHz, DMSO) δ = 156.3, 147.9, 139.6, 129.6, 112.3 (2), 99.8, 78.1, 55.5, 44.5 (2), 28.7.

tert-butyl (2-((4-((3-carbamoyl-6-chloro-5-ethylpyrazin-2-yl)amino)-2-methoxyphenyl)amino)ethyl)carbamate (CG-5-016): CG-5-015 was reacted on a 1.77 mmol scale according to General Procedure 3, using CH_2Cl_2/MeOH/NH_4OH, 192:7:1 to monitor the reaction and purify the title compound. (orange solid, yield = 66%): ^{1}H NMR (400 MHz, DMSO) δ = 11.0 (s, 1H), 8.18 (s, 1H), 7.95 (s, 1H), 7.08 (s, 1H), 7.00-6.98 (m, 2H), 6.52 (d, J = 8.8 Hz, 1H), 4.89 (s, 1H), 3.77 (s, 3H), 3.09 (s, 4H), 2.76 (q, J = 7.3 Hz, 2H), 1.38 (s, 9H), 1.23 (t, J = 7.4 Hz, 3H); ^{13}C NMR (400 MHz, DMSO) δ = 168.6, 156.4, 150.1, 147.4, 146.6, 140.7, 134.9, 127.9, 124.8, 113.7, 109.1, 104.7, 78.2, 55.7, 43.5, 39.3, 28.7, 26.6, 12.5.

tert-butyl (2-((4-((3-carbamoyl-5-ethyl-6-((tetrahydro-2H-pyran-4-yl)amino)pyrazin-2-yl)amino)-2-methoxyphenyl)amino)ethyl)carbamate (CG-5-017): CG-5-016 was reacted on a 1.07 mmol scale according to General Procedure 4, using CH_2Cl_2/MeOH/NH_4OH, 192:7:1 to monitor the reaction and purify the title compound. (yellow solid, yield = 88%): ^{1}H NMR (400 MHz, DMSO) δ = 10.8 (s, 1H), 7.46 (s, 1H), 7.17-7.13 (m, 2H), 6.94-6.90 (m, 2H), 6.68 (d, J = 7.2 Hz, 1H), 6.51 (d, J = 8.8 Hz, 1H), 4.07 (s, 1H), 3.89 (d, J = 9.6 Hz, 2H), 3.78 (s, 3H), 3.13-3.06 (m, 4H), 2.56 (q, J = 8.3 Hz, 2H), 2.16 (t, J = 8.2 Hz, 2H), 1.89 (q, J = 7.6 Hz, 2H), 1.60 (q, J = 11.7 Hz, 2H), 1.38 (s, 9H), 1.17 (t, J = 7.2 Hz, 3H); ^{13}C NMR (400 MHz, DMSO) δ = 170.2, 152.3, 1509, 146.8, 129.8, 113.2, 109.3, 104.5, 66.9, 66.4, 56.0, 48.9, 47.9, 43.8, 33.6, 32.7, 30.6, 29.4, 28.7, 24.6, 17.7, 11.5.

3-((4-((2-aminoethyl)amino)-3-methoxyphenyl)amino)-6-ethyl-5-((tetrahydro-2H-pyran-4-yl)amino)pyrazine-2-carboxamide (CG-5-018): CG-5-017 was reacted on a 0.886 mmol scale according to General Procedure 5, using CH_2Cl_2/MeOH/NH_4OH, 192:7:1 to monitor the reaction and purify the title compound. (yellow solid, yield = 73%): ^{1}H NMR (400 MHz, DMSO) δ = 10.8 (s, 1H), 7.46 (s, 1H), 7.14-7.13 (m, 2H), 6.92 (s, 1H), 6.69 (d, J = 8 Hz, 1H), 6.47 (d, J = 8 Hz, 1H), 4.69 (s, 1H), 4.07 (s, 1H), 3.90 (d, J = 9.6 Hz, 2H), 3.79 (s, 3H), 3.35-3.13 (m, 2H), 3.00 (s, 1.5H), 2.75 (t, J = 5.8 Hz, 1.5H), 2.55 (q, J = 7.2 Hz, 2H), 1.83 (d, J = 12.4 Hz, 2H), 1.61 (q, J = 11.7 Hz, 2H), 1.17 (t, J = 7.2 Hz, 3H); ^{13}C NMR (400 MHz, DMSO) δ = 170.2, 152.3, 150.9, 147.0, 134.3, 131.2, 129.8, 113.2, 111.8, 109.7, 104.5, 66.9, 56.0, 47.9, 46.5, 41.1, 32.7, 24.6, 11.5.

tert-butyl (S)-(1-((2-((4-((3-carbamoyl-5-ethyl-6-((tetrahydro-2H-pyran-4-yl)amino)pyrazin-2-yl)amino)-2-methoxyphenyl)amino)ethyl)amino)-1-oxopropan-2-yl)(methyl)carbamate (CG-5-019): CG-5-018 and N-(tert-butoxycarbonyl)-N-methyl-L-alanine were reacted on a 0.604 mmol scale according to General Procedure 6, using CH_2Cl_2/MeOH/NH_4OH, 92:7:1 to monitor the reaction and purify the title compound. (dark yellow solid, yield = 85%): ^{1}H NMR (400 MHz, DMSO) δ = 10.8 (s, 1H), 7.91 (t, J = 5 Hz, 1H), 7.46 (s, 1H), 7.15-7.13 (m, 2H), 6.92 (s, 1H), 6.68 (d, J = 7.2 Hz, 1H), 6.53 (d, J = 8.4 Hz, 1H), 4.71 (s, 1H), 4.60-4.2 (m, 1H), 4.07 (s, 1H), 3.89 (d, J = 9.6 Hz, 2H), 3.77 (s, 3H), 3.35-3.23 (m, 2H), 3.10 (d, J = 5.6 Hz, 2H), 2.72-2.67 (m, 4H), 2.55 (q, J = 7.5 Hz, 2H), 1.82 (d, J = 12 Hz, 2H), 1.60 (q, J = 11.6 Hz, 2H), 1.40 (s, 9H), 1.21-1.15 (m, 6H); ^{13}C NMR (400 MHz, DMSO) δ = 170.2, 152.3, 150.9, 146.9, 133.9, 131.2, 129.9, 113.2, 111.8, 109.4 (2), 104.6 (2), 79.3, 66.9 (2), 56.1, 47.9, 43.4, 38.6, 32.7 (2), 28.5 (2), 24.6, 11.5.

(S)-6-ethyl-3-((3-methoxy-4-((2-(2-(methylamino)propanamido)ethyl)amino)phenyl)amino)-5-((tetrahydro-2H-pyran-4-yl)amino)pyrazine-2-carboxamide (CG-5-020): CG-5-019 was reacted on a 0.487 mmol scale according to General Procedure 5, using CH_2Cl_2/MeOH/NH_4OH, 92:7:1 to monitor the reaction and purify the title compound. (yellow solid, yield = 75%): ^{1}H NMR (400 MHz, DMSO) δ = 10.8 (s, 1H), 7.98 (d, J = 5.6 Hz, 1H), 7.46 (s, 1H), 7.13-7.11 (m, 2H), 6.92 (s, 1H), 6.68 (d, J = 7.2 Hz, 1H), 6.53 (d, J = 8.4 Hz, 1H), 4.70 (t, J = 5.4 Hz, 1H), 4.07 (s, 1H), 3.89 (d, J = 9.6 Hz, 2H), 3.77 (s, 3H), 3.346-3.29 (m, 3H), 3.11 (d, J = 5.6 Hz, 2H), 2.92 (q, J = 6.8 Hz, 1H), 2.55 (q, J = 7.47 Hz, 2H), 2.18 (s, 3H), 1.82 (d, J = 12.8 Hz, 2H), 1.60 (q, J = 11.7 Hz, 2H), 1.17 (t, J = 7.4 Hz, 3H), 1.09 (d, J = 7.2 Hz, 3H); ^{13}C NMR (400 MHz, DMSO) δ = 175.3, 170.2, 152.3, 150.9, 146.9, 134.0, 131.2, 129.9, 113.2, 111.8, 109.6, 104.6, 66.9, 59.8, 56.1, 47.9, 43.6, 38.2, 34.6, 32.7, 24.6, 19.5, 11.5.

(S,E)-3-((4-((2-(2-(4-(dimethylamino)-N-methylbut-2-enamido)propanamido)ethyl)amino)-3-methoxyphenyl)amino)-6-ethyl-5-((tetrahydro-2H-pyran-4-yl)amino)pyrazine-2-carboxamide (CG-5-021): CG-5-020 and trans-4-Dimethylaminocrotonic acid hydrochloride were reacted on a 0.0969 mmol scale according to General Procedure 6, using CH_2Cl_2/MeOH/NH_4OH, 58:7:1 to monitor the reaction and purify the title compound. (off yellow solid, yield = 74%): ^{1}H NMR (400 MHz, DMSO) δ = 10.8 (s, 1H), 8.14 (s, 0.25H), 8.02 (s, 0.25 H), 7.93 (s, 0.5H), 7.46 (1H), 7.13 (s, 2H), 6.92 (s, 1H), 6.70-6.48 (m, 4H), 4.71 (s, 1H), 4.08 (s, 1H), 3.89 (d, J = 10.4 Hz, 2H), 3.78 (s, 3H), 3.32 (m, 6H), 3.11 (s, 2H), 3.02-2.96 (m, 2H), 2.88 (s, 2H), 2.73 (s, 1H), 2.55 (q, J = 7.2 Hz, 2H), 2.11 (d, J = 15.6 Hz, 4H), 1.82 (d, J = 12.8 Hz, 2H), 1.60 (q, J = 11.7 Hz, 2H), 1.28-1.10 (m, 6H); ^{13}C NMR (400 MHz, DMSO) δ =

170.2, 152.3, 150.9, 146.8, 142.6, 133.9, 131.2, 129.9, 123.3, 113.2, 111.8, 109.5 (2), 104.6, 66.9, 60.4, 56.1, 52.1, 47.9, 45.6, 43.3, 38.6, 32.7, 31.2, 29.8, 24.6, 14.8, 11.5. HRMS-ESI: m/z found 624.3621 [M+H]+, $C_{31}H_{47}N_9O_5$ requires 624.3627.

Chapter 6: Transformation of the pan-CDK Inhibitor AT7519 into AMC-3-221, a CDK9-Selective Degrader

6.1 Introduction

CDKs are responsible for the phosphorylation of other proteins, thereby activating them and initiating cell proliferation, differentiation, apoptosis, and DNA repair.[73] In particular, CDK9 influences gene transcription through the phosphorylation of RNA polymerase II; this activation results in the downstream synthesis of key drivers of cancers, namely MYC and MCL-1, which are long-sought targets for cancer therapeutics.[73] MYC is the most amplified oncogene in human cancers, though its intrinsically disordered nature renders the rational design of inhibitors challenging.[75] MCL-1 is one of the anti-apoptotic proteins of the BCL-2 family which is often dysregulated in cancer and a major factor resistance to cancer treatments, including venetoclax.[30-32] Direct inhibition of MCL-1 requires inhibition of its protein-protein interactions with characteristic large, shallow hydrophobic areas which demand picomolar affinities for substantial inhibition.[30-32] Furthermore, direct inhibition of MCL-1 has been associated with severe adverse effects including cardiotoxicities which have brought two clinical trials to a halt.[146,147] Dysregulation of CDK9 is evident in a variety of cancer types and has been shown to impact malignant cell development and disease progression.[73] This overexpression may also lead to the downstream upregulation of MYC and MCL-1. Therefore, we have created a library of CDK9 PROTACs with the intention of downregulating MCL-1 on the transcriptional level, which is hypothesized to mitigate the toxicities seen by direct MCL-1 inhibition. Additionally, these compounds are designed for efficacy in BCL-2 resistant cell lines due to their upregulation of MCL-1.[81-85]

6.2 Design Rationale

AT7519 is a CDK inhibitor which shows the most potency towards CDK9, developed using a fragment-based x-ray crystallography method.[85] While this inhibitor shows exquisite potency for CDK9 (IC_{50} < 10nM) it also shows double digit nanomolar potency against CDK2 and CDK5 (IC_{50} = 47nM and 13nM, respectively).[85] Its potent inhibition has resulted in therapeutic efficacy in a variety of human cancer cell lines as well as xenograft models.[85,87] Furthermore, AT7519 has been used in clinical trials both as a single agent and in combination with other treatments for a variety of cancer types including both hematological and solid tumors.[86,88] Additionally, the use of AT7519 has been shown to downregulate MCL-1 through deactivation of RNA polymerase II.[85] Although little is known about resistance to CDK9 inhibitors, intrinsic and acquired resistance to kinase inhibitors is well documented.[199] We aimed to develop a CDK9 PROTAC as these degraders are less prone to resistance than traditional inhibitors.[200] This approach has been utilized with the CDKi SNS-032 by Gray, et al. What Grey and co. showcased was that by linking SNS-032 to thalidomide, an E3 ligase ligand for cereblon (CRBN), they created a selective CDK9 protein degrader in a cereblon dependent manner. Importantly, this study only showcased their protein degrader function within cells and a follow up paper was never published, leaving CDK9 protein degraders unexplored completely.[83] AT7519 was selected as the protein of interest ligand in the PROTAC design for its synthetic accessibility as well as possession of a readily-accessible piperidine, which is directed away from the protein surface, that is used as the exit vector to graft the linking group as well as E3 ligase ligands for our PROTACs.[85]

In addition to the use of AT7519 as the ligand for our protein of interest, CDK9, we have also used a modified version of thalidomide, which includes a synthetic handle for attachment of linking groups. As stated before, thalidomide is a commonly used ligand for the E3 ligase protein CRBN. CRBN is often recruited for the use of targeted protein degraders as it has been shown to result in rapid degradation of proteins and is a naturally highly active E3 ligase.[121] Additionally, ligands for this protein such as thalidomide are very well studied and have possess low molecular weights and increased drug-like properties when compared to other E3 ligase ligands.[121]

6.3 First Generation AT7519 PROTACs

An initial library of eight PROTACs were synthesized using AT7519 and the modified thalidomide. These compounds were synthesized using several alkyl and PEG linkers as well as some piperidine derivatives to explore the importance of linker length on CDK9 degradation. Currently, optimal linking groups for heterobifunctional compounds are discovered using an empirical approach, in which optimal linker length and rigidity is discovered through creating and testing multiple analogues. Linking groups are a crucial element to PROTAC design as they are highly dependent on the protein being targeted as well as the E3 ligase to be recruited.[97,121] This may be due in part to the cooperative or uncooperative effects between the two proteins which can either contribute to ternary complex formation or result in the repulsion of the two proteins, therefore having a negative impact.[97,113,121]

6.3.1: Synthesis of AT7519

The synthesis of AT7519 is shown in **Figure 6.3.1.1.** 4-nitro-1h-pyrazole-5-carboxylic acid (**1**) was condensed with 1-Boc-4-aminopiperidine (**2**) using HATU then reduced to

give the pyrazole amine (**3**). The acid chloride of 2,6-dichlorobenzoic acid (**4**) was made using oxalyl chloride and coupled to compound **3**. Finally, the boc group was removed with 4M HCl in dioxane to yield AT7519 as the HCl salt (**5**).

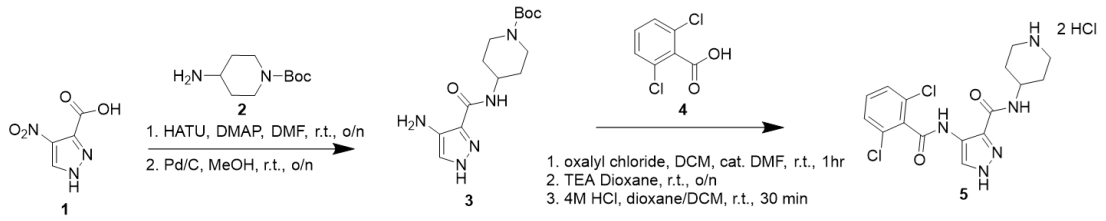

Figure 6.3.1.1: *Synthesis of AT7519*

6.3.2: Synthesis of Modified AT7519

The synthesis of the modified version of AT7519 is shown in **Figure 6.3.2.1**. 4-nitro-1h-pyrazole-5-carboxylic acid (**1**) was esterified with thionyl chloride in methanol, resulting in the methyl ester. The nitro group was then reduced to the amine with catalytic palladium on carbon (**6**). Separately, 2,6-dichlorobenzoic acid (**4**) was converted to the acid chloride using oxalyl chloride and catalytic DMF. The resulting acid chloride was then coupled with pyrazole (**6**) then was saponified to the carboxylic acid (**7**). In parallel, 4-benzyloxycarbonylamino-piperidine (**8**) was alkylated with tert-butyl bromoacetate (**9**), resulting in compound then debenzylated with catalytic palladium on carbon to give free amine **10**. A HATU-mediated coupling was performed between carboxylic acid **7** and amine **10**. The tert-butyl ester was removed with 4M HCl in dioxane to yield AT7519 with the synthetic handle (**11**) ready for attachment of the linking groups.

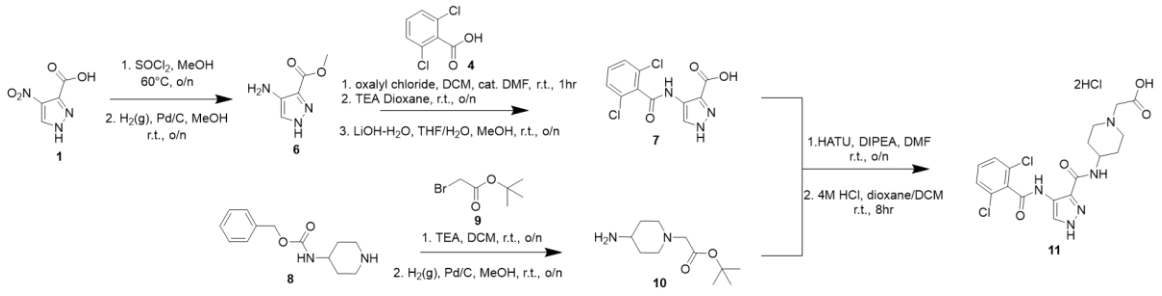

Figure 6.3.2.1: *Synthesis of modified AT7519*

6.3.3: Synthesis of Modified Thalidomide

The synthesis for the modified version of thalidomide is shown in **Figure 6.3.3.1**. 3-hydroxyphthalic anhydride (**12**) was condensed with 3-aminopiperidine-2,6-dione hydrochloride (**13**) in pyridine, resulting in compound **14**. The tert-butyl bromoacetate (**9**) was reacted at the hydroxyl position of (**14**). The tert-butyl ester was removed with trifluoroacetic acid to give the modified thalidomide with readily-accessible carboxylic acid for PROTAC synthesis (**15**).

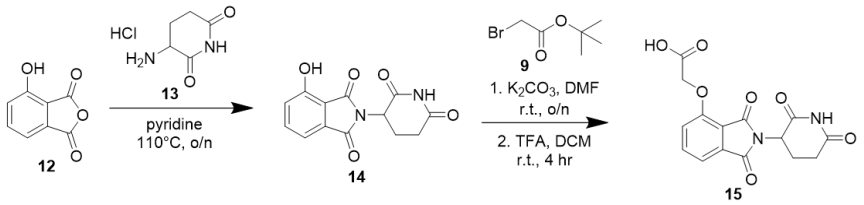

Figure 6.3.3.1: *Synthesis of modified thalidomide*

6.3.4 Synthesis of First Generation CDK9 PROTACs

The first generation of CDK9 PROTACs were synthesized starting with AT7519 or a modified version of AT7519 to include a synthetic handle used for attachment of

additional linking groups (**Figure 6.3.4.1**). Dr. Alexandria Carlson aided in creating three final compounds for this class of CDK9 PROTACs. Protein of interest ligand was HATU-coupled to the linking group followed by boc-deprotection of the linker. The final synthetic step is a condensation reaction with the modified thalidomide to yield the final CDK9 PROTACs.

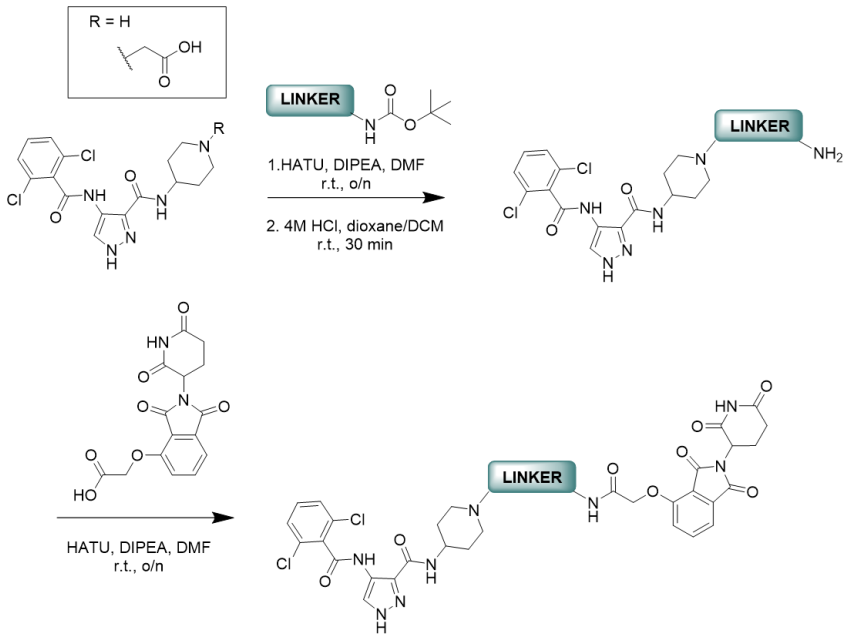

***Figure 6.3.4.1**: General synthesis of first generation CDK9 PROTACs*

6.3.5 Biological Evaluation for First Generation CDK9 PROTACs

As PROTAC design consists of an inhibitor as the ligand for CDK9, maintenance of protein binding was determined through the ability of the heterobifunctional compounds to retain CDK9 inhibition. This was determined by the company NanoSyn, which uses an electrophoretic mobility shift assay (EMSA) which is performed on a microfluidic chip. When compared to the parent compound, AT7519 (IC_{50} = 2.06 nM), the PROTACs

maintained their inhibitory activity against CDK9 with IC_{50} values in the single digit nanomolar range (IC_{50} = 1.66-4.49 nM) as seen in **Table 6.3.5.1**.

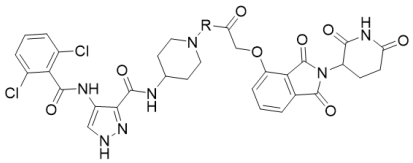

Compound Code	R	CDK9 IC_{50} (nM)	Compound Code	R	CDK9 IC_{50} (nM)
AT7519 (control)	—	2.06	AMC-3-104	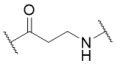	2.82
AMC-3-097	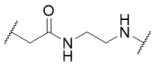	3.96	CG-3-071	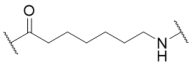	2.85
AMC-3-106	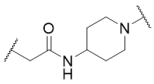	3.04	SF-8-140	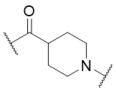	1.66
CG-3-066	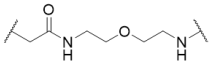	3.32	SF-8-141	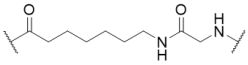	4.49
CG-3-067	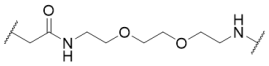	3.89			

Table 6.3.5.1: *Cell-free inhibition of CDK9 with first generation PROTACs*

The library of CDK9 PROTACs was then tested for their anti-leukemic effects in MOLM14 cells, an adult AML cell line, using an alamarBlue proliferation assay. Unfortunately, all eight of the PROTACs did not perform as well as the AT7519 control when observing their anti-proliferation effects (**Figure 6.3.5.1** and **Table 6.3.5.2**) following 48 hours of treatment. However, these compounds did provide insight on linker length for the design of future compounds. Due to the differences in performance of our library of compounds in the cell-free and cell proliferation assays, we hypothesized the

compounds were limited in their ability to permeate the cell membrane, preventing anti-proliferation activity.

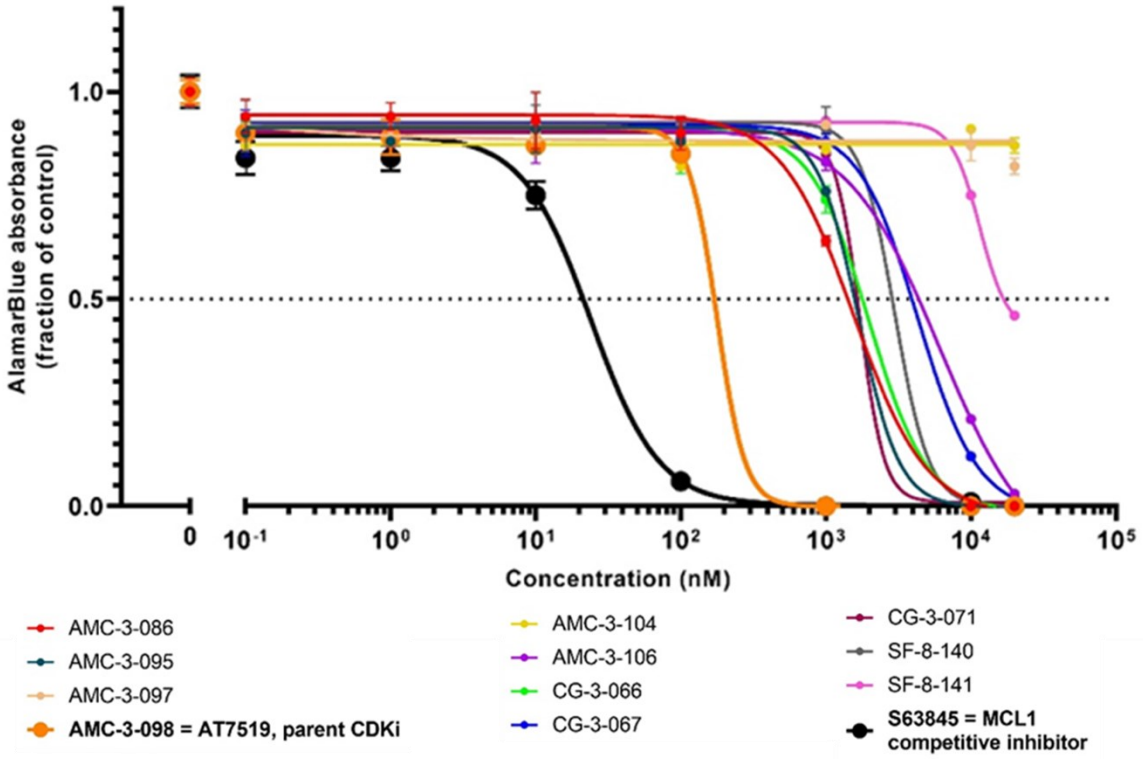

Figure 6.3.5.1: *Anti-proliferation effects of first generation PROTACs in MOLM14 cells*

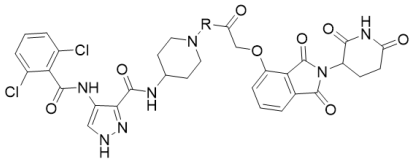

Compound Code	R	MOLM14 IC_{50} (μM)	Compound Code	R	MOLM14 IC_{50} (μM)
AT7519 (control)	—	0.1175	AMC-3-104	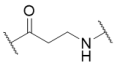	>20
AMC-3-097	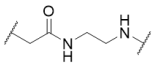	>20	CG-3-071	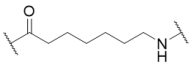	1.713
AMC-3-106	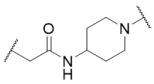	6.067	SF-8-140	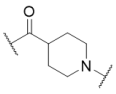	2.998
CG-3-066	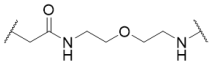	1.973	SF-8-141	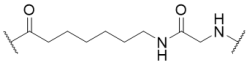	11.50
CG-3-067	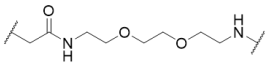	4.317			

Table 6.3.5.2: *IC_{50} values for anti-proliferation effects of first generation PROTACs*

6.4 Second Generation AT7519 PROTACs

Given the results from our first generation of compounds, several modifications were made to the second library of five CDK9 PROTACs. These include changes to the linking group as well as the E3 ligase ligand. The linking groups for the new compounds were designed with increased rigidity as many of the previous compounds were highly flexible. Recent literature has shown that an increase in linker rigidity can promote ternary complex formation.[97,113,121] These compounds were also designed to decrease the number of amide bonds while introducing tertiary amines to aide in compound solubility.[96] One compound was synthesized retaining the flexible linker as a control compound, given the other alterations that were made to degrader design. Additionally, a

fluorinated derivative of thalidomide was used to increase compound lipophilicity as well as cell permeability.[98]

6.4.1 Synthesis of Second Generation CDK9 PROTACs

A second generation of five CDK9 PROTACs were synthesized in a similar manner to the first generation in which AT7519 or a modified version with synthetic handle were used (**Figure 6.4.1.1**). Dr. Alexandria Carlson was instrumental with this class of CDK9 PROTACs as she synthesized all final compounds. Compounds synthesized using the modified AT7519 were condensed with the corresponding linker using HATU. The linker was then boc-deprotected using 4M HCl in dioxane to yield the HCl salt of the free amine. In the case of AMC-3-227, an additional synthetic step was performed to extend the linker via reductive amination with *N*-Boc-4-piperidine carboxaldehyde, which was then boc-deprotected with 4M HCl to yield the free piperidine amine as an HCl salt. The deprotected linkers then undergo an S_NAr with 2-(2,6-dioxopiperidin-3-yl)-5,6-difluoroisoindoline-1,3-dione to give the final second generation PROTACs with the fluorinated thalidomide modification.

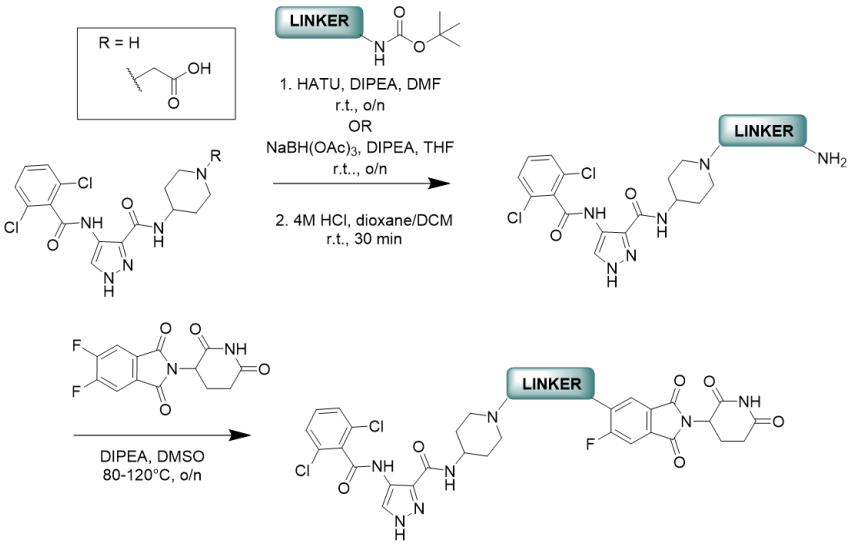

Figure 6.4.1.1: *General Synthesis of second generation CDK9 PROTACs*

6.4.2 Biological Evaluation of Second Generation CDK9 PROTACs

Compounds were once again tested for their inhibitory activity against CDK9 by NanoSyn to determine if the compounds have maintained binding affinity to the protein (**Table 6.4.2.1**). As was expected due to similar modifications which were made to AT7519 as our previous compounds, the second generation of compounds maintained inhibitory activity against CDK9. Surprisingly, compounds within this library showed increased activity when compared to the control inhibitor. In fact, AMC-3-227 achieved sub-nanomolar inhibition of CDK9 (IC_{50} = 0.887 nM). We propose the slightly increased inhibition is due to additional interactions between the linking group and the protein surface, outside of the catalytic pocket, as these types of interactions have been targeted with the use of more rigid linkers and are amongst the advantages of these groups.

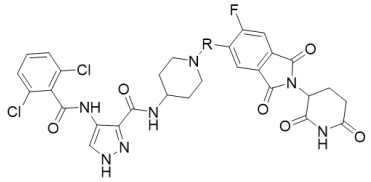

Compound Code	R	CDK9 IC_{50} (nM)	Compound Code	R	CDK9 IC_{50} (nM)
AT7519 (control)	—	2.06	AMC-3-221	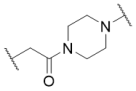	1.73
AMC-3-201	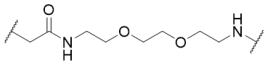	2.25	AMC-3-225		4.95
AMC-3-207	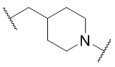	1.57	AMC-3-227	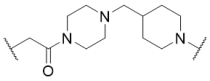	0.887

Table 6.4.2.1: *Cell-free inhibition of CDK9 with second generation PROTACs*

Second generation PROTACs were also tested for their anti-leukemic activity using the aforementioned anti-proliferation assay in MOLM14 cells after 48 hours of treatment (**Figure 6.4.2.1** and **Table 6.4.2.2**). In this cell line, there were three PROTACs which outperformed the parent inhibitor while one had very similar anti-leukemic effects and the final PROTAC was slightly less effective than AT7519. The control compound bearing the flexible PEG linker (AMC-3-201) had lesser anti-proliferation effects than the parent inhibitor, though was more potent than the corresponding first-generation compound with the same linking group (CG-3-067). This provides evidence towards the increased cell permeability due to fluorination of the thalidomide E3 ligase ligand. The best PROTAC (AMC-3-227) had an IC_{50} value of 12.07 nM, which is nearly 15 times more potent than AT7519 (IC_{50} = 177.5 nM). The high potency seen by these PROTACs exemplifies the benefits of an event-driven pharmacologic approach over the traditional occupancy driven compounds.

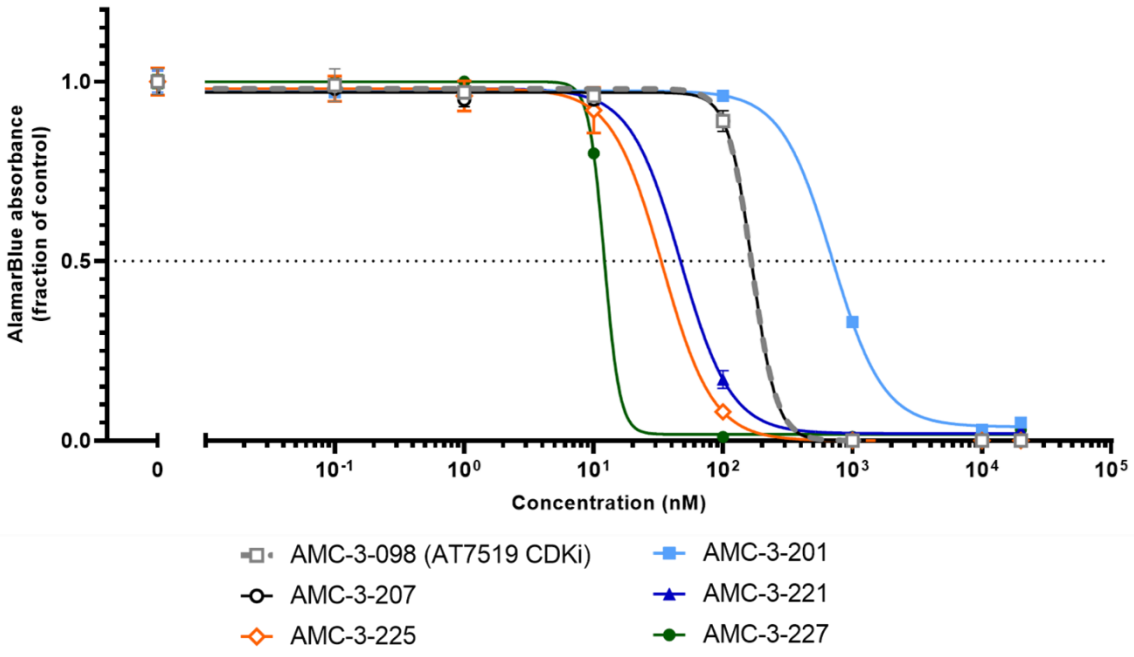

Figure 6.4.2.1: *Anti-proliferation effects of second generation PROTACs in MOLM14 cells*

To further investigate the effects of these degraders, the second generation of compounds was also tested in MV411 cells, which are a pediatric AML cell line (**Figure 6.4.2.2** and **Table 6.4.2.2**). Though they are both classified as the same disease, recent studies show that adult and pediatric populations can have significant variations in terms of their genomic landscape and thereby the cause of the disease and the subsequent gene and protein expression levels that contribute to progression.[201] Therefore, treatments which are effective in adults do not always translate to pediatric patients. For this reason, we have tested the efficacy of our compounds in a pediatric cell line. Anti-proliferation assays in MV411 cells show that all five of the second generation CDK9 PROTACs have improved anti-leukemic effects over the parent inhibitor (IC_{50} = 250.3 nM). The three best PROTACs in MOLM14 cells remain the most potent in MV411 cells with AMC-3-

227 showing the highest anticancer activity (IC_{50} = 18.21 nM). Results from these studies support the differences in adult and pediatric populations while also emphasizing the advantages of protein degradation. The three PROTACs which showed the highest anti-leukemic effects were subjected to additional evaluation.

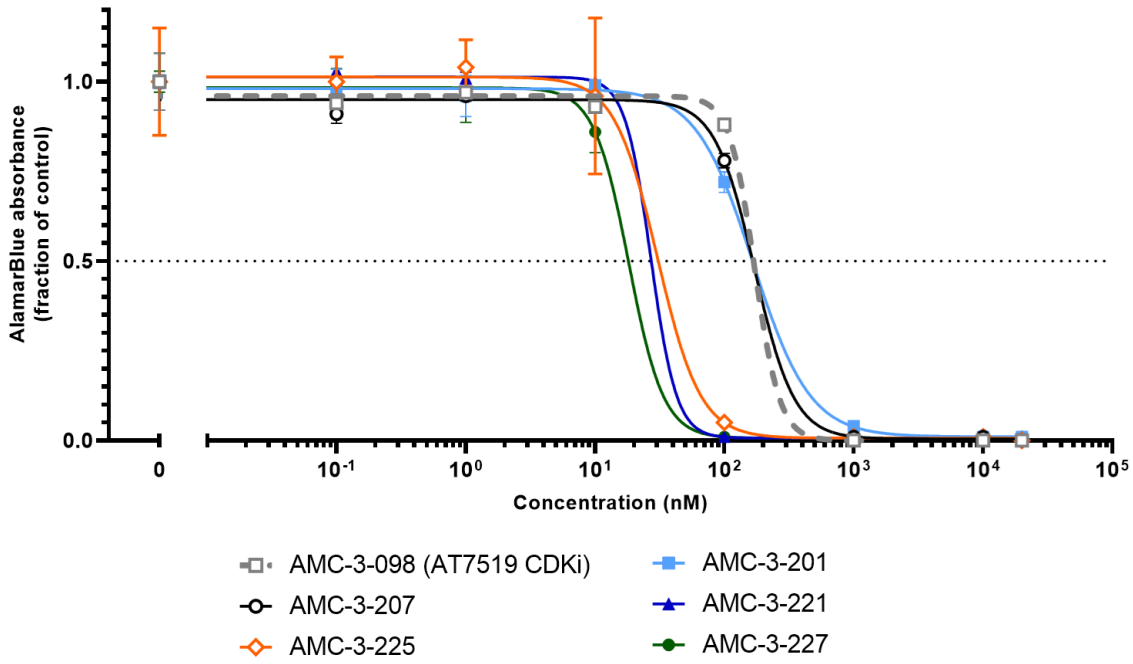

Figure 6.4.2.2: *Anti-proliferation effects of second generation PROTACs in MV411 cells*

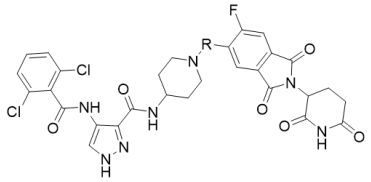

Compound Code	R	MOLM14 IC_{50} (nM)	MV411 IC_{50} (nM)
AT7519	---	177.5	250.3
AMC-3-201	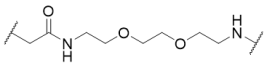	696.4	166.4
AMC-3-207	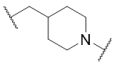	167.6	171.2
AMC-3-221	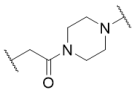	46.89	26.93
AMC-3-225		33.86	30.33
AMC-3-227	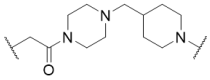	12.07	18.21

Table 6.4.2.2: *IC_{50} values for anti-proliferation effects of second generation PROTACs*

6.5 Flow Cytometry

Flow cytometry using Annexin V and 7-aminoactinomycin D (7-AAD) apoptotic stains were performed to better understand the rate at which the PROTACs were exhibiting anticancer effects as well as confirm malignant cell death along with the anti-proliferation activity (**Figure 6.5.1**). This was monitored at several timepoints from 1hr to 24 hrs with the PROTACs dosed at 200 nM and AT7519 at 1000 nM in MOLM14 cells. Presence of Annexin V begins between 2-3 hrs of treatment indicating cells are entering an early stage of apoptosis. The PROTACs were inducing early apoptosis at a faster rate than the AT7519 control, which was dosed at 5x the concentration. 7-AAD appears around 8hr

after treatment, indicating the cells are entering late apoptosis, and presence of this stain continues to increase after this time. These studies confirm the anticancer effect of our compounds is due to apoptosis of malignant cells while also revealing the quick onset of early apoptosis induced by our PROTACs.

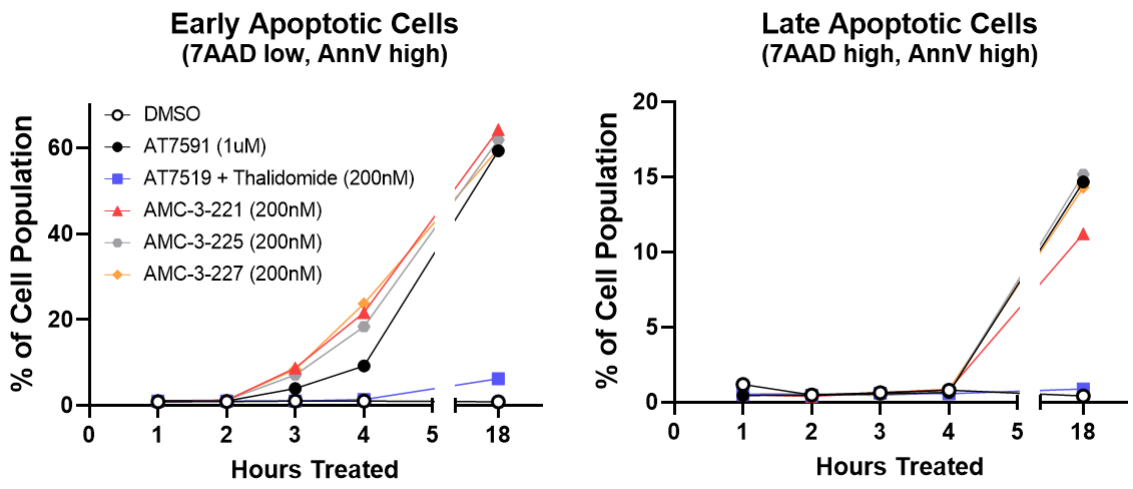

Figure 6.5.1: *Quantification of flow cytometry data staining for apoptosis represented by percent cell population in early (left) or late (right) apoptosis vs. time*

6.6 Degradation of CDK9 and Downregulation of MCL-1

Western blot analysis was used to confirm the degradation of CDK9 as well as the downregulation of MCL-1 (**Figure 6.6.1**). This was once again performed in MOLM14 cells with PROTACs dosed at 200 nM and AT7519 control at both 200 nM and 1000 nM. The assay was performed after 4 hrs of treatment as cellular apoptosis occurring at later timepoints impacts the presence of tubulin controls. Treatment with all three PROTACs results in the degradation of CDK9 after 4 hrs of treatment as well as the subsequent downregulation of MCL-1. These effects were not seen by treatment of AT7519 control or the fluorinated E3 ligase ligand as single agents at identical concentrations, nor the

combination treatment of these two drugs. Downregulation of MCL-1 was seen by the high dose of AT7519, which was similar to that of the PROTACs, though at 5x the concentration. These results confirm the PROTAC-mediated degradation of our target protein as well as the downregulation of anti-apoptotic protein MCL-1.

An additional western blot analysis was done on our three PROTACs to measure selectivity for CDK9 over other CDKs (**Figure 6.6.2**). In a similar manner to the previous analysis, MOLM14 cells were treated with the same controls at the same concentrations along with our three PROTACs. Two of our PROTACs, AMC-3-221 and AMC-3-227 show selectivity for CDK9 over the other CDKs. AMC-3-221 demonstrated the highest level of selectivity for CDK9 as the relative protein level of all other CDK proteins did not go below 50%. Both of these experiments showcase AMC-3-221 to be a selective CDK9 protein degrader that also leads to a lower level in MCL-1 protein.

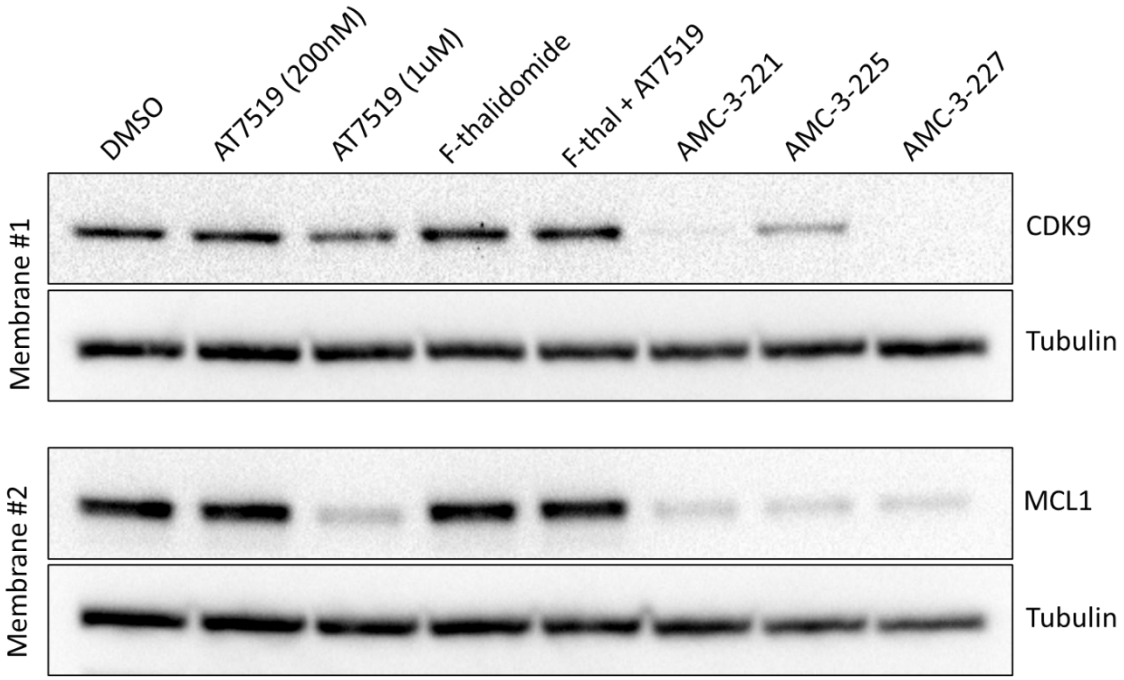

Figure 6.6.1: *Western blot analysis for degradation of CDK9 and downregulation of MCL-1 in MOLM14 cells after 4 hour treatment*

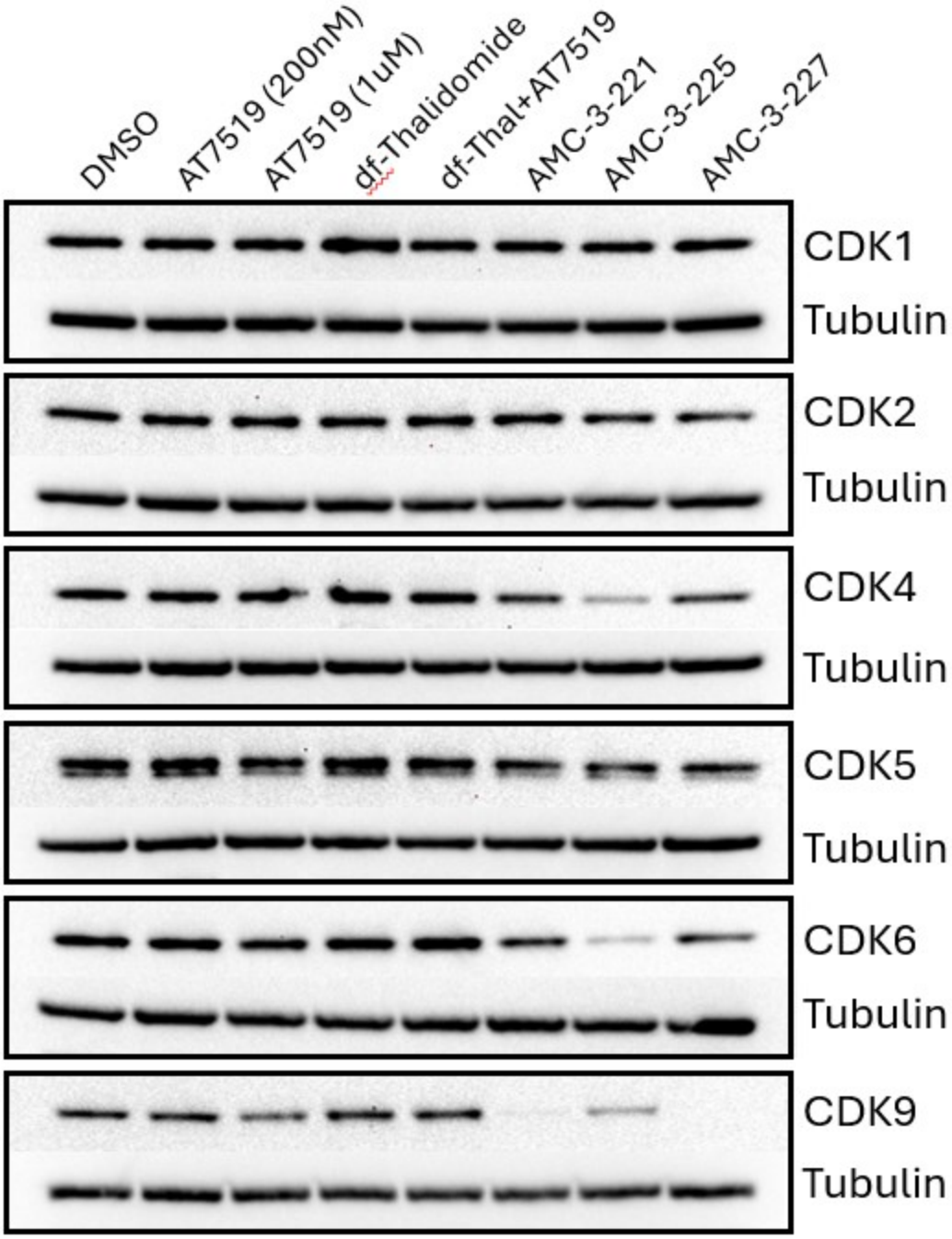
DMSO
AT7519 (200nM)
AT7519 (1uM)
df-Thalidomide
df-Thal+AT7519
AMC-3-221
AMC-3-225
AMC-3-227
CDK1
Tubulin
CDK2
Tubulin
CDK4
Tubulin
CDK5
Tubulin
CDK6
Tubulin
CDK9
Tubulin

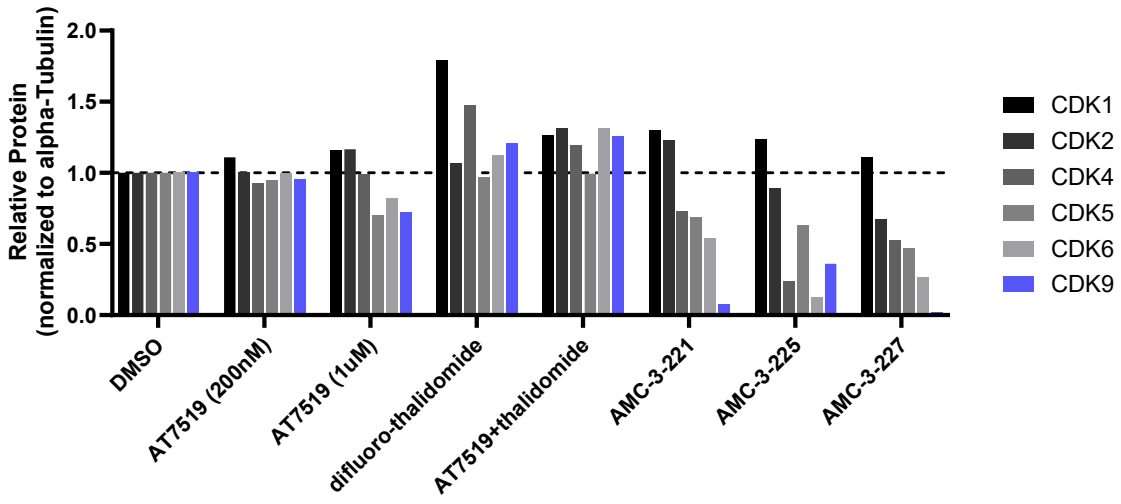

Figure 6.6.2: *Western blot analysis for degradation of CDKs in MOLM14 cells after 4-hour treatment [200nM]*

6.7 CDK9 PROTACs in Additional Cancer Models

The three best PROTACs as well as AT7519 control were tested in additional cancer cell lines using a WST-1 proliferation assay to determine their anticancer effects after 72 hrs of treatment (**Table 6.7.1**). The cell lines include leukemia cell lines (MOLM13, MV4-11, THP1, K562) as well as ovarian cancer (A2780), non-small cell lung cancer (A549), colon cancer (HCT116), and breast cancer (MCF7). AMC-3-227 and AMC-3-225 consistently outperformed AT7519 across the cancer cell lines tested. Results from previous AML cell lines were also corroborated using the WST-1 assay. Variations in the IC50 values allude to the selectivity of these compounds over general toxicity, though our next study focused on determining cytotoxic effects of our compounds.

Cell Line	AT7519 IC_{50} (nM)	AMC-3-221 IC_{50} (nM)	AMC-3-225 IC_{50} (nM)	AMC-3-227 IC_{50} (nM)
THP1	484	405	180	65
K562	607	417	97	31
A2780	321	55	52	8
A549	1022	475	129	21
HCT116	139	198	60	16
MCF7	308	279	92	20

Table 6.7.1: *IC_{50} values for several cancer cell lines for the best three PROTACs*

6.8 CDK9 PROTACs in Fibroblast Cells

Our three best PROTACs were then tested for their cytotoxic effects in the healthy fibroblast cell line MRC-5. Again, we used a WST-1 proliferation assay to determine their cytotoxic effects after 72 hrs of treatment (**Table 6.8.1**). The IC_{50} value of AT7519 roughly followed the reported literature value of 980 nM in this same cell line.[85] AMC-3-221 demonstrated the least cytotoxic effects of our three compounds.

Cell Line	AT7519 IC_{50} (nM)	AMC-3-221 IC_{50} (nM)	AMC-3-225 IC_{50} (nM)	AMC-3-227 IC_{50} (nM)
MRC-5	1223 ± 606	396 ± 141	170 ± 70	16.2 ± 6

Table 6.8.1: *IC_{50} values for cytotoxic effects for the best three PROTACs*

6.9 In Vivo Evaluation of AMC-3-221

Maximum tolerated dose studies were conducted with AMC-3-221 due to the compound being more potent than AT7519 in AML cells, being the most selective degrader for CDK9 over the sister kinase proteins and because it is associated with the lowest rate of cytotoxicity in healthy cells. To measure acute toxicity, Mice were injected via IP with various concentrations of AMC-3-221 once and their body weight was monitored for 12 days. From this, the mice who were administered via IP up to 25 mg/kg of the drug did not have a steep decline in body weight while the mouse administered 50 mg/kg of AMC-3-221 lost around 5% of total body weight (**Figure 6.9.1**). Next, we measured the maximum tolerated dose of AMC-3-221 where mice were tested in cohorts of three in which the test group were administered 15 mg/kg of AMC-3-221 via IP for five days in a row and their body weight was recorded each day. The lowest loss was detected on the eighth day when the cohort had on average lost 8% of body weight, however, after the eighth day the cohort regained weight rapidly and matched the control group on day 12 (**Figure 6.9.2**). MTD of AMC-3-221 was determined, in NRG mice, to be 25 mg/kg IP for a single dose, or 15 mg/kg/d PI x5d every 14 days.

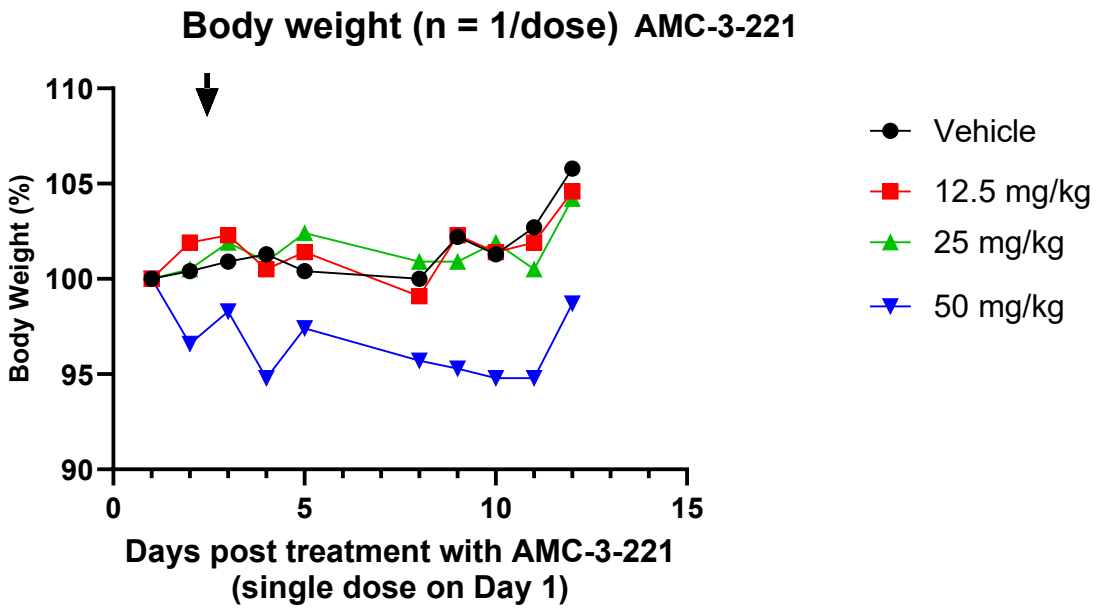

Figure 6.9.1: *Acute toxicity determination of single dose AMC-3-221 in NRG mice*

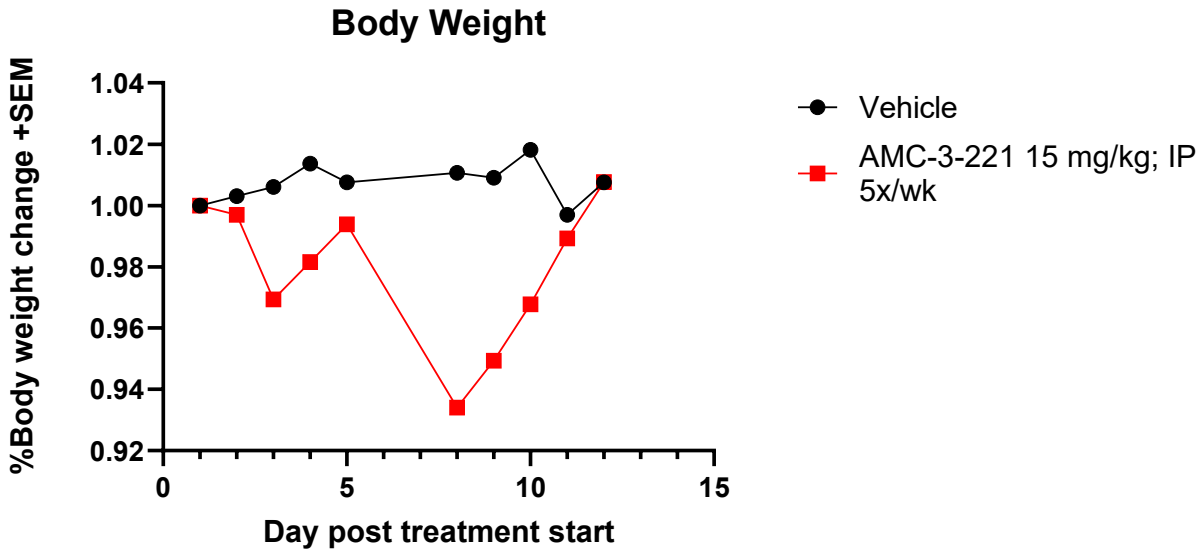

Figure 6.9.2: *Tolerability of 15 mg/kg AMC-3-221 5x/wk IP in NRG mice*

6.10 Conclusions and Future Directions

We have generated a library of CDK9 PROTACs from which AMC-3-221 has emerged as the lead compound due to its *in vitro* anti-leukemic capabilities and low measured toxicity in cells and in NRG mice. Through evaluation of this library, our results have coincided with previous reports both on the importance of linker length and rigidity for PROTAC design as well as the increased biologic effect resulting from fluorination of the E3 ligase ligand, likely due to increased cell permeability. We have developed CDK9 PROTACs which consistently outperform the AT7519 control inhibitor during *in vitro* anticancer evaluation. These compounds also provide evidence for the therapeutic advantage of PROTAC degraders over traditional small molecule inhibitors.[97,121] Currently, vivo studies are underway to determine the anti-leukemic effects of AMC-3-221 in NRG mice.

6.11 Methods

Chemistry

All reactions were performed in oven-dried glassware under non-inert atmosphere, unless otherwise stated. All chemicals and solvents were used as supplied without additional purification. ^{1}H and ^{13}C NMR spectra were obtained on a Varian 400 or 500 MHz NMR spectrometer at 298.1K. Chemical shifts are reported in parts per million (ppm) and are referenced to residual non-deuterated solvent peak ($CHCl_3$: δ_H 7.26; DMSO: δ_H 2.50, δ_C 39.5). All final compounds were lyophilized before biological evaluation.

Inhibition of CDK9

Inhibition of CDK9 was determined by NanoSyn (Element) measuring the phosphorylation of a substrate by the CDK9/CyclinT1 protein (Carna Bio, Cat#04-110) . Enzyme, substrate (H-ACSYSPTSPSYSPTSPSYSPTSPSKK-NH2), and cofactors (ATP and Mg2+) are combined in a well of a microtiter plate and incubate at 22ºC for 17 hours. At the end of the incubation, the reaction is quenched and conversion is detected by luminescence using the Promega ADP-GloTM Kinase Assay kit (catalog # V9102). The assay is read and analyzed on the BioTek Synergy microplate reader using BioTek Gen5 software.

Cell culture:

Pediatric acute myeloid leukemia cell lines harboring mixed-lineage-leukemia rearrangements were obtained from either ATCC (Manassas, VA) or DSMZ (Branschweig, DEU) (MOLM14, #ACC-777 DSMZ; MV4;11, #CRL-9591, ATCC; THP1, #TIB-202, ATCC). Cell lines were cultured in RPMI media containing 10% fetal bovine serum and passaged twice per week to maintain cultures in log-phase-growth.

Cell-metabolic assays:

Cell metabolism was assessed by alamarBlue assays (Life Technologies, Grand Island, NY) following the manufacturer's guidelines. Cells and compounds were combined in culture for 48hrs. Cells would then undergo incubation with alamarBlue reagent for a minimum of 5 hours before absorbance was read using a Perkin Elmer Victor X3.

Apoptosis staining:

Cell death was verified by Annexin V/7-aminoactinomycin D (AnnV/7AAD) staining (BioLegend, San Diego, CA # BLD-640930) per the manufacturer's guidelines. Cell

numbers were determined by acridine orange/propidium iodide staining and quantified using a Nexcelcom K2 cell counter (#CS2-0106). Per sample, a total of 2.5x10^5 cells were stained with AnnV/7AAD and fluorescence was assessed by flow cytometry using a Becton Dickinson Accuri C6.

Western blotting

Cellular protein was extracted, quantitated, electrophoresed, and western blotted with monoclonal antibodies. Antibody-specific band intensities were quantitated by densitometry (ChemiDOC XRS+ and Image Laboratory system; Bio-Rad, Hercules, CA) and normalized to alpha-tubulin.

Antibody	Manufacturer	Catalogue #
MCL1	Cell Signaling Technology	94296
BCL2	Cell Signaling Technology	4223
CDK1	Cell Signaling Technology	28439
CDK2	Cell Signaling Technology	2546T
CDK4	Cell Signaling Technology	12790
CDK5	Cell Signaling Technology	2506
CDK6	Cell Signaling Technology	13331T
CDK9	Cell Signaling Technology	2316S
phospho-CDK9 (Thr186)	Cell Signaling Technology	2549S
alpha-Tubulin	Cell Signaling Technology	3873S

Acute Toxicity Studies

Acute Toxicity experiments were approved by the UMB IACUC, AUP-1021001-Amd-65. Female Immunodeficient NRG Mice for these studies came from Requisition #V012237 (Jax, delivered 7/17 @ 8 weeks of age), and #V014094 (UMB Veterinary Resources, bred from Jax stocks, delivered 9/3/24 @ 5-6 weeks of age and aged on our rack) Mice were 2-3 months old for the studies. This is a 15-day experiment in which mice will be sorted into groups of 1. On day one, mice will be injected once IP with varying doses of AMC-3-221 (see table below). Following injections, mice will be monitored continuously for 30 minutes for signs of toxicity. Mice will be checked at ~1 hr, ~1.5 hr, ~2 hr, ~3 hr, ~4 hr, 6-8 hr, the next morning, and at ~24, ~48, ~72 hrs, then M-F until the end of the study after 2 weeks. Mice will be weighed at least 2x/wk and euthanized if they lose >20% BW or if they reach an alternative endpoint described in the parent protocol.

Group	N	Dose AMC-3-221	Route	Freq
1	1	0 mg/kg (Vehicle)	IP	1x
2	1	12.5 mg/kg	IP	1x
3	1	25 mg/kg	IP	1x
4	1	50 mg/kg	IP	1x

Dissolve AMC-3-221 powder in DMSO then add the HCl already diluted in PBS to make stock of 50 mg/mL = 1.85 mg + 37 ul DMSO. Store powder at 4°C; can make 1 week of dosing (for tolerability study) at a time and store in 4°C; freeze stock solutions at 20°C.

Group	Dose Conc	Stock	DMSO	HCl/PBS	TV
Vehicle	0 mg/mL	0	30 µl	270 □l	300 µl

12.5 mg/kg	1.25 mg/ml	7.5 µl	22.5 µl	270 µl	300 µl
25 mg/kg	2.5 mg/ml	15 µl	15 µl	270 µl	300 µl
50 mg/kg	5 mg/ml	30 µl	0 µl	270 µl	300 µl

Maximum Tolerated Dose

Maximum tolerated dose experiments were approved by the UMB IACUC, AUP-1021001-Amd-65. Female Immunodeficient NRG Mice for these studies came from Requisition #V012237 (Jax, delivered 7/17 @ 8 weeks of age), and #V014094 (UMB Veterinary Resources, bred from Jax stocks, delivered 9/3/24 @ 5-6 weeks of age and aged on our rack) Mice were 2-3 months old for the studies. Mice will be sorted into groups of 3. Mice will be dosed as described in the table below. Mice will be dosed 5 days in a row and monitored at least 5x/week. If the 5-day dose is tolerated, a second 5-day cycle will start either the next week or 1-2 weeks later. Mice will be weighed at least 2x/wk and euthanized if they lose >20% BW or if they reach an alternative endpoint described in the parent protocol.

Group	N	Dose AMC-3-221	Route	Freq
1	3	0 mg/kg (Vehicle)	IP	5x
2	3	15 mg/kg	IP	5x

Dissolve AMC-3-221 powder in DMSO then add the HCl already diluted in PBS to make stock of 50 mg/mL = 1.85 mg + 37 µl DMSO. Store powder at 4°C; can make 1 week of dosing (for tolerability study) at a time and store in 4°C; freeze stock solutions at 20°C.

Group	Dose Conc	Stock	DMSO	HCl/PBS	TV

Vehicle	0 mg/mL	0	100 µl	900 µl	1 ml
15 mg/kg	15 mg/mL	30 µl	70 µl	900 µl	1 ml

6.12 Experimental Procedures

General Procedure A: HATU-mediated condensation reactions

To a stirring solution of the carboxylic acid (1.0 eq) in DMF (0.1M, 30mL max), DIPEA (1.1 eq) and HATU (1.1 eq) were added followed by the amine (1.0 eq) and additional 1.0 eq DIPEA per HCl salt. The reaction was stirred at room temperature for 16 hours.

General Procedure B: Boc-deprotection of amines

To a stirring solution of the boc-protected amine (1.0 eq) in DCM (0.1 M), 4M HCl in dioxane was added. The reaction mixture was stirred at room temperature for 3 hours. Upon completion, the reaction mixture was concentrated to dryness and azeoptroped with DCM and methanol x3.

General Procedure C: Formation of Acid Chloride and Subsequent Condensation

To a stirring solution of the carboxylic acid (1.1 eq) in anhydrous DCM (0.1 M), oxalyl chloride (1.3 eq) was added followed by catalytic DMF. The reaction mixture was stirred for 2 hours under inert atmosphere. Upon completion, the reaction mixture was concentrated to dryness and azeotroped with DCM x3. The reaction was then left at room temperature under reduced pressure for 1 hour. Following this time, the acid chloride was dissolved in dioxane and the amine (1.0 eq) was added with TEA (3.0 eq). The reaction was stirred at room temperature for 16 hours.

General Procedure D: Palladium catalyzed Reduction/Benzyl Deprotection

To a stirring solution of the starting compound (1.0 eq) in methanol (0.1 M, 150 mL maximum), catalytic palladium on carbon (10% wt) was added. H_2(g) was bubbled through solution for 15 minutes and the reaction was stirred at room temperature for 16 hours under H_2(g). Upon completion, the reaction mixture was filtered through celite, rinsing with methanol and concentrated to dryness.

General Procedure E: Reductive Amination

The amine (1.0 eq) was dissolved in THF (0.1M) with DIPEA (1.0 eq per HCl salt). The corresponding carbonyl derivative (1.0 eq) was added to the reaction mixture followed by sodium triacetoxyborohydride (1.5 eq). The reaction mixture was stirred at room temperature for 16 hours. Upon completion, the reaction was diluted with ethyl acetate and partitioned with water and the aqueous was basified with saturated sodium bicarbonate. The product was extracted from the aqueous layer x3. The organic layers were combined and washed with saturated sodium bicarbonate, water x3, and saturated sodium chloride then dried over sodium sulfate and concentrated to dryness.

General Procedure F: S_NAr with Fluorinated Thalidomide

The amine (1.0 eq) was dissolved in DMSO (0.1M) with DIPEA (4.0 eq). 2-(2,6-dioxopiperidin-3-yl)-5,6-difluoroisoindoline-1,3-dione (1.0 eq) was added to the reaction mixture and stirred at 80°C for 16 hours. Upon completion the reaction mixture was dissolved in ethyl acetate and partitioned with water. The aqueous was basified with saturated sodium bicarbonate and product was extracted into ethyl acetate x3. The organic layers were combined and washed with water: saturated sodium bicarbonate x3

and saturated sodium chloride, then dried over sodium sulfate and concentrated to dryness.

Synthesis of *tert*-butyl 4-(4-amino-1*H*-pyrazole-3-carboxamido)piperidine-1-carboxylate (**3**): To a stirring solution of 4-nitro-1h-pyrazole-5-carboxylic acid (9.548 mmol, 1.0 eq) in DMF (30 mL), HATU (11.458 mmol, 1.2 eq) was added, followed by DMAP (0.955 mmol, 0.1 eq), and finally 1-Boc-aminopeiperidine (10.503mmol, 1.1 eq). The reaction was stirred at room temperature for 16 hours. Upon completion, the reaction was dissolved in ethyl acetate and partitioned with water. The product was extracted from the aqueous layer x3. The organic layers were combined and washed with 1M HCl, saturated sodium bicarbonate, water x3, and saturated sodium chloride then dried over sodium sulfate and concentrated to dryness. The product was isolated via gravity column chromatography on silica gel using a solution of 92 DCM: 7 methanol: 1 ammonium hydroxide, resulting in *tert*-butyl 4-(4-nitro-1*H*-pyrazole-3-carboxamido)piperidine-1-carboxylate. (white solid, yield = 94%). ^{1}H NMR: (400 MHz, d_6 DMSO) δ8.69 (1H, s), 8.57 (1H, d, J = 7.2 Hz), 3.94 (1H, t, J =4.0 Hz), 3.85 (2H, d, J =13.2), 2.91 (2H, m), 1.80 (2H, d, J = 11.6), 1.40 (9H, s), 1.33 (2H, m). *Tert*-butyl 4-(4-nitro-1*H*-pyrazole-3-carboxamido)piperidine-1-carboxylate (9.991 mmol) was reacted according to *General Procedure D* with no further purification. (purple solid, yield = 99%).

Synthesis of 4-(2,6-dichlorobenzamido)-*N*-(piperidin-4-yl)-1*H*-pyrazole-3-carboxamide (**5**): 2,6-dichlorobenzoic acid (10.99 mmol) was reacted according to *General Procedure C* with **3** (9.991 mmol). Upon completion, the reaction mixture was diluted with ethyl acetate and partitioned with water. The product was extracted from the aqueous layer x3. The organic layers were combined and washed with saturated sodium bicarbonate, water

x3, and saturated sodium chloride then dried over sodium sulfate and concentrated to dryness. The product was isolated via gravity column chromatography on silica gel using a solution of 1 hexanes: 4 ethyl acetate, resulting in *tert*-butyl 4-(4-(2,6-dichlorobenzamido)-1*H*-pyrazole-3-carboxamido)piperidine-1-carboxylate (white solid, yield = 55%) *Tert*-butyl 4-(4-(2,6-dichlorobenzamido)-1*H*-pyrazole-3-carboxamido)piperidine-1-carboxylate was reacted according to *General Procedure B* resulting in 4-(2,6-dichlorobenzamido)-*N*-(piperidin-4-yl)-1*H*-pyrazole-3-carboxamide without further purification. ^{1}H NMR: (500 MHz, d6 DMSO) δ10.13 (1H, s), 8.81 (1H, s), 8.68 (1H ,d, *J* = 7.5 Hz), 8.48 (1H, s), 8.35 (1H, s), 7.58 (2H, d, *J* =7.0 Hz), 7.52 (1H, q, *J* =6.0 Hz), 3.99 (1H, m), 3.28 (2H, d, *J* = 13.0 Hz), 2.92 (2H, t, *J* = 12.0 Hz), 1.90 (2H, d, *J* =12.0 Hz), 1.79 (2H, t, *J* = 10.0 Hz).

Synthesis of methyl 4-amino-1*H*-pyrazole-3-carboxylate (**6**): To a stirring solution of 4-nitro-1h-pyrazole-5-carboxylic acid (19.10 mmol, 1.0 eq) in methanol, thionyl chloride (40.10 mmol, 2.1 eq) was added, dropwise at 0°C. The reaction mixture was warmed to 60°C and stirred for 16 hours. Upon completion, the reaction mixture was concentrated to dryness and azeotroped with DCM x3. The reaction mixture was dissolved in ethyl acetate and partitioned with saturated sodium bicarbonate. The organic layer was washed with brine and dried over sodium sulfate, then concentrated to dryness yielding methyl 4-nitro-1*H*-pyrazole-3-carboxylate with no further purification. (pale yellow solid, yield = 74%). Methyl 4-nitro-1*H*-pyrazole-3-carboxylate (14.20 mmol) was reacted according to *General Procedure D* with no further purification resulting in methyl 4-amino-1*H*-pyrazole-3-carboxylate (purple solid, yield = 94%). ^{1}H NMR: (500 MHz, d_6 DMSO) δ12.81 (1H, s), 7.08 (1H, s), 4.81 (2H, s), 3.76 (3H, s).

Synthesis of 4-(2,6-dichlorobenzamido)-1*H*-pyrazole-3-carboxylic acid (**7**): 2,6-dichlorobenzoic acid (14.76 mmol) was reacted according to *General Procedure C* with **6** (13.42 mmol). Upon completion, the reaction mixture was diluted with ethyl acetate and partitioned with water. The product was extracted from the aqueous layer x3. The organic layers were combined and washed with saturated sodium bicarbonate, water x3, and saturated sodium chloride then dried over sodium sulfate and concentrated to dryness. The product was isolated via gravity column chromatography on silica gel using a solution of 2 hexanes: 3 ethyl acetate, resulting in methyl 4-(2,6-dichlorobenzamido)-1*H*-pyrazole-3-carboxylate. (white solid, yield = 99%) To a stirring solution of methyl 4-(2,6-dichlorobenzamido)-1*H*-pyrazole-3-carboxylate (14.62 mmol, 1.0 eq) in 3 THF: methanol: water (0.1 M), lithium hydroxide monohydrate (58.47 mmol, 4.0 eq) was added. The reaction was stirred at room temperature for 16 hrs. Upon completion, the reaction mixture was concentrated to remove THF and methanol then dissolved in ethyl acetate and partitioned with water. The aqueous layer was acidified with 1M HCl and the product was extracted from the aqueous x3 with ethyl acetate. The organic layers were combined, washed with saturated sodium chloride, and dried over sodium sulfate. The product was concentrated to dryness, yielding 4-(2,6-dichlorobenzamido)-1*H*-pyrazole-3-carboxylic acid with no further purification. (white solid, yield = 93%) ^{1}H NMR: (400 MHz, d_6 DMSO) δ13.42 (1H, s) 9.83 (1H, s) 8.26 (1H, s), 7.53 (2H, d, J = 7.2 Hz), 7.47 (1H, t, J = 6.0 Hz).

Synthesis of *tert*-butyl 2-(4-aminopiperidin-1-yl)acetate (**10**): 4-benzyloxycarbonylamino-piperidine hydrochloride (11.08 mmol, 1.0 eq) was dissolved in DMF (0.1 M) followed by the addition of tert-butyl bromoacetate (12.19 mmol, 1.1 eq)

and potassium carbonate (33.24 mmol, 3.0 eq). The reaction mixture was stirred at room temperature for 16 hours. Upon completion the reaction mixture was dissolved in ethyl acetate and partitioned with water. The aqueous was basified with saturated sodium bicarbonate and the product was extracted into ethyl acetate x3. The organic layers were combined and washed with water: saturated sodium bicarbonate x3 and saturated sodium chloride, then dried over sodium sulfate and concentrated to dryness yielding *tert*-butyl 2-(4-(2-phenylacetamido)piperidin-1-yl)acetate with no further purification. (orange solid, yield = 99%). *Tert*-butyl 2-(4-(2-phenylacetamido)piperidin-1-yl)acetate (13.75 mmol) was reacted according to *General Procedure D* with no further purification, resulting in *tert*-butyl 2-(4-aminopiperidin-1-yl)acetate. (yield = 96%). ^{1}H NMR: (400 MHz, d_6 DMSO) δ8.26 (2H, s), 3.30 (2H, m), 2.41 (1H, m), 1.87 (2H, d, J = 8.8 Hz), 1.23 (2H, m), 1.43 (2H, m), 1.41 (9H, s).

Synthesis of 2-(4-(4-(2,6-dichlorobenzamido)-1*H*-pyrazole-3-carboxamido)piperidin-1-yl)acetic acid (**11**): **7** (8.67 mmol) and **10** (8.67 mmol) were reacted according to *General Procedure A*. Upon completion, the reaction mixture was dissolved in ethyl acetate and partitioned with water. The aqueous was basified with saturated sodium bicarbonate and product was extracted into ethyl acetate x3. The organic layers were combined and washed with water: saturated sodium bicarbonate x3 and saturated sodium chloride, then dried over sodium sulfate and concentrated to dryness. The product was isolated via gravity column chromatography on silica gel using a solution of 5% methanol in chloroform, yielding *tert*-butyl 2-(4-(4-(2,6-dichlorobenzamido)-1*H*-pyrazole-3-carboxamido)piperidin-1-yl)acetate. (tan solid, yield = 93%). ^{1}H NMR: (500 MHz, d_6 DMSO) δ10.16 (1H, s), 8.33 (3H, t, J = 11.0 Hz), 7.58 (2H, d, J = 7.0 Hz), 7.52 (1H, t, J

=7.0 Hz), 3.68 (1H, q, *J* = 3.0 Hz), 3.07 (2H, s), 2.80 (2H, d, *J* =11.0 Hz), 1.18 (2H, q, *J* =11.0 Hz), 1.64 (2H, m), 1.40 (9H, s); ^{13}C NMR (500 MHz, d_6-DMSO) δ = 174.8, 168.0, 165.6, 139.9, 138.3, 137.2, 136.6, 133.8, 126.9, 126.0, 85.4, 64.8, 56.9, 51.2, 36.5, 33.2. LRMS (ESI) m/z [M+H]+ calcd for $C_{22}H_{28}Cl_2N_5O_4$ = 496.14; found = 440.1 (loss of tert-butyl group). To a stirring solution of *tert*-butyl 2-(4-(4-(2,6-dichlorobenzamido)-1*H*-pyrazole-3-carboxamido)piperidin-1-yl)acetate (4.30 mmol, 1.0 eq) in DCM (20 mL), 4M HCl in dioxane was added. The reaction was stirred at room temperature for 8 hours. Upon completion, the reaction mixture was concentrated to dryness and azeotroped (3x) with DCM, resulting in 2-(4-(4-(2,6-dichlorobenzamido)-1*H*-pyrazole-3-carboxamido)piperidin-1-yl)acetic acid with no further purification. (tan solid, yield = 99%). 1H NMR (500 MHz, d6-DMSO) δ = 13.37 (s, 1H), 10.14 (s, 1H), 8.61-8.33 (m, 2H), 7.58 (d, J = 7.5 Hz, 2H), 7.52 (t, J = 8 Hz, 1H), 4.08 (s, 1H), 3.97 (s, 1 H), 3.17 (s, 4H), 1.98 (s, 4H); 13C NMR (500 MHz, d6-DMSO) δ = 184.6, 173.2, 165.4, 144.7, 140.2, 136.6, 133.8, 128.8, 121.1 (2), 77.5, 75.9, 65.5, 49.0. LRMS (ESI) m/z [M+H]+ calcd for $C_{18}H_{20}Cl_2N_5O_4$ = 440.08; found = 440.1.

Synthesis of 2-(2,6-dioxopiperidin-3-yl)-4-hydroxyisoindoline-1,3-dione (**14**): 3-hydroxyphthalic anhydride was dissolved in pyridine followed by the addition of 3-aminopiperidine-2,6-dione hydrochloride. The reaction mixture was stirred at 110°C for 16 hours. Upon completion, the reaction mixture was concentrated, dissolved in ethyl acetate, and partitioned with 1M HCl. The product was extracted from the aqueous into ethyl acetate (3x). The organic layers were combined and washed with 1M HCl x3 and saturated sodium chloride, then dried over sodium sulfate and concentrated to dryness, resulting in 2-(2,6-dioxopiperidin-3-yl)-4-hydroxyisoindoline-1,3-dione with no further

purification. (green solid, yield = 73%) ^{1}H NMR: (500 MHz, d_6 DMSO) δ11.07 (1H, s), 7.64 (1H, t, J = 8.0 Hz), 7.30 (1H, d, J = 7.2 Hz), 7.24 (1H, d, J = 8.8 Hz), 5.06 (1H, dd, J = 4.8 Hz), 2.87 (1H. m), 2.53 (2H, m), 2.01 (1H, m).

Synthesis of 2-((2-(2,6-dioxopiperidin-3-yl)-1,3-dioxoisoindolin-4-yl)oxy)acetic acid (**15**): To a stirring solution of **14** (10 mmol, 1.0 eq) in DMF (30 mL), tert-butyl bromoacetate (11 mmol, 1.1 eq) was added at 0°C. The reaction was stirred at room temperature for 16 hours. Upon completion, the reaction mixture was diluted with ethyl acetate and partitioned with water. The product was extracted from the aqueous layer x3. The organic layers were combined and washed with water x3, and saturated sodium chloride then dried over sodium sulfate and concentrated to dryness. The product was isolated via flash column chromatography on silica gel using a solution of 1 hexanes: 2 ethyl acetate, resulting in *tert*-butyl 2-((2-(2,6-dioxopiperidin-3-yl)-1,3-dioxoisoindolin-4-yl)oxy)acetate. (white foam, yield = 67%). *Tert*-butyl 2-((2-(2,6-dioxopiperidin-3-yl)-1,3-dioxoisoindolin-4-yl)oxy)acetate (6.18 mmol, 1.0 eq) was dissolved in DCM (31 mL). Trifluoroacetic acid (31 mL) and the rection was stirred at room temperature for 4 hours. Upon completion, the reaction mixture was concentrated to dryness and azeotroped with DCM/methanol x2, followed by DCM, resulting in 2-((2-(2,6-dioxopiperidin-3-yl)-1,3-dioxoisoindolin-4-yl)oxy)acetic acid without further purification. (white solid, yield = 99%). ^{1}H NMR: (500 MHz, d_6 DMSO) δ11.10 (1H, s), 7.79 (1H, t, J = 7.5 Hz), 7.47 (2H, d, J = 7.5 Hz), 7.38, 1H, d, J = 8.5 Hz), 5.09 (1H ,dd, J = 6.0 Hz), 4.98 (2H, s), 2.88, (1H, m), 2.56 (2H, m), 2.04 (1H, m).

Synthesis of 4-(2,6-dichlorobenzamido)-*N*-(1-(2-((2-(2-((2-(2,6-dioxopiperidin-3-yl)-1,3-dioxoisoindolin-4-yl)oxy)acetamido)ethyl)amino)-2-oxoethyl)piperidin-4-yl)-1*H*-

pyrazole-3-carboxamide (**AMC-3-097**): **11** (0.584 mmol) was reacted with 1-Boc-ethylenediamine (0.584 mmol) according to *General Procedure A*. Upon completion, the reaction mixture was dissolved in ethyl acetate and partitioned with water. The aqueous was basified with saturated sodium bicarbonate and product was extracted into ethyl acetate x3. The organic layers were combined and washed with water: saturated sodium bicarbonate x3 and saturated sodium chloride, then dried over sodium sulfate and concentrated to dryness. The product was isolated via gravity column chromatography on silica gel using a solution of 5% methanol in chloroform, yielding *tert*-butyl (2-(2-(4-(4-(2,6-dichlorobenzamido)-1*H*-pyrazole-3-carboxamido)piperidin-1-yl)acetamido)ethyl)carbamate. (white solid, yield = 37%). 1H NMR (500 MHz, d6-DMSO) δ = 13.39 (s, 1H), 10.16 (s, 1H), 8.35 (s, 1H), 8.26 (d, J = 8 Hz, 1H), 7.70 (s, 1H), 7.58 (d, J = 8 Hz, 2H) 7.52 (t, J = 8.25 Hz, 1H), 6.80 (s, 1H), 3.69 (q, J = 7 Hz, 1H), 3.12 (d, J = 5 Hz, 2H), 3.00 (d, J = 6 Hz, 2H), 2.87 (s, 2H), 2.77 (d, J = 10.5 Hz, 2 H), 2.09 (s, 2H), 1.69 (s, 4H), 1.36 (s, 9H); 13C NMR (400 MHz, d6-DMSO) δ = 170.0, 163.1, 160.7, 156.2, 135.8, 133.4, 132.3, 131.7, 128.9, 121.9, 121.2, 78.1, 61.8, 53.0, 46.4, 38.9, 31.5, 28.7. LRMS (ESI) m/z [M+H]+ calcd for $C_{25}H_{34}Cl_2N_7O_5$ = 582.19; found = 582.2. *tert*-butyl (2-(2-(4-(4-(2,6-dichlorobenzamido)-1*H*-pyrazole-3-carboxamido)piperidin-1-yl)acetamido)ethyl)carbamate (0.0738 mmol)was reacted according to *General Procedure B*, yielding *N*-(1-(2-((2-aminoethyl)amino)-2-oxoethyl)piperidin-4-yl)-4-(2,6-dichlorobenzamido)-1*H*-pyrazole-3-carboxamide hydrochloride without further purification. (tan solid, yield = 99%). *N*-(1-(2-((2-aminoethyl)amino)-2-oxoethyl)piperidin-4-yl)-4-(2,6-dichlorobenzamido)-1*H*-pyrazole-3-carboxamide hydrochloride (0.157 mmol) was then reacted with **15** (0.172 mmol, 1.1

eq) according to *General Procedure A*. Upon completion the reaction mixture was diluted with ethyl acetate and partitioned with water. The product was extracted from the aqueous (3x). The organic layers were combined and washed with water (3x) and saturated sodium chloride, then dried over sodium sulfate and concentrated to dryness. The product was isolated via gravity column chromatography in a solution of 10% methanol in chloroform, yielding of 4-(2,6-dichlorobenzamido)-*N*-(1-(2-((2-(2-((2-(2,6-dioxopiperidin-3-yl)-1,3-dioxoisoindolin-4-yl)oxy)acetamido)ethyl)amino)-2-oxoethyl)piperidin-4-yl)-1*H*-pyrazole-3-carboxamide. (white solid, yield = 62%) ^{1}H NMR: (400 MHz, d_6 DMSO) δ10.15 (1H, s), 8.35 (1H, s), 8.24 (1H, d, *J* = 7.0 Hz), 7.79 (1H, t, *J* = 8.0 Hz), 7.75 (1H, s), 7.58 (2H, d, *J* = 7.0 Hz), 7.52 (1H, t, *J* = 7.0 Hz), 7.48 (1H, d, *J* = 7.0 Hz), 7.38 (1H, d, *J* =9.0 Hz), 5.75 (2H, s), 5.10 (1H, dd, 5.0 Hz), 3.66 (1H, q, *J* = 8.0 Hz), 3.20 (4H, m) 2.87 (2H, m), 2.75 (2H, d, *J* = 11.0 Hz), 2.56 (1H, m), 2.04 (2H, m), 1.67 (4H, s).^{13}C NMR: (500 MHz, d_6 DMSO) δ173.35, 170.45, 170.37, 167.78, 167.32, 166.05, 160.94, 155.64, 137.53, 135.97, 133.65, 132.46, 131.87, 129.00, 122.10, 121.05, 117.46, 116.67, 68.27, 61.93, 60.36, 53.14, 49.43, 46.54, 38.93, 38.68, 31.62, 31.55, 22.61, 21.36, 14.68. HRMS (ESI) m/z [M+H]+ calcd for $C_{35}H_{35}Cl_2N_9O_9$ = 796.2008; found = 796.2029.

Synthesis of 4-(2,6-dichlorobenzamido)-*N*-(1-(2-((1-(2-((2-(2,6-dioxopiperidin-3-yl)-1,3-dioxoisoindolin-4-yl)oxy)acetyl)piperidin-4-yl)amino)-2-oxoethyl)piperidin-4-yl)-1*H*-pyrazole-3-carboxamide (**AMC-3-106**): **11** (0.585 mmol) was reacted with 1-Boc-4-aminopiperidine (0.644 mmol, 1.1 eq) according to *General Procedure A*. Upon completion, the reaction mixture was diluted with ethyl acetate and partitioned with water. The product was extracted from the aqueous (3x). The organic layers were

combined and washed with water (3x) and saturated sodium chloride, then dried over sodium sulfate and concentrated to dryness. The product was isolated via gravity column chromatography in a solution of 192 DCM: 7 methanol: 1 ammonium hydroxide, resulting in *tert*-butyl 4-(2-(4-(4-(2,6-dichlorobenzamido)-1*H*-pyrazole-3-carboxamido)piperidin-1-yl)acetamido)piperidine-1-carboxylate. (white solid, yield = 72%). 1H NMR (400 MHz, d6-DMSO) δ = 13.38 (s, 1H), 10.15 (s, 1H), 8.33 (s, 1H), 8.25 (d, J = 7.2 Hz, 1H), 7.58-7.55 (m, 3H), 7.50 (t, J = 7.4 Hz, 1H), 3.82-3.67 (m, 4H), 2.86 (s, 4H), 2.76 (d, J = 10.8 Hz, 2H), 2.08 (s, 2H), 1.67 (s, 6H), 1.37 (s, 9H), 1.27 (q, J = 10.2 Hz, 2H); 13C NMR (400 MHz, d6-DMSO) δ = 169.0, 163.4, 160.7, 154.3, 135.8, 132.3, 131.7, 128.9 (2), 121.9, 121.1, 79.1, 61.6, 52.8, 52.8, 46.3, 45.8, 31.8, 31.5, 28.5. LRMS (ESI) m/z [M+H]+ calcd for $C_{28}H_{38}Cl_2N_7O_5$ = 622.22; found = 622.2. *Tert*-butyl 4-(2-(4-(4-(2,6-dichlorobenzamido)-1*H*-pyrazole-3-carboxamido)piperidin-1-yl)acetamido)piperidine-1-carboxylate (0.196 mmol) was reacted according to *General Procedure B* resulting in 4-(2,6-dichlorobenzamido)-*N*-(1-(2-oxo-2-(piperidin-4-ylamino)ethyl)piperidin-4-yl)-1*H*-pyrazole-3-carboxamide without further purification. (tan solid, yield = 99%). 4-(2,6-dichlorobenzamido)-*N*-(1-(2-oxo-2-(piperidin-4-ylamino)ethyl)piperidin-4-yl)-1*H*-pyrazole-3-carboxamide (0.287 mmol) was reacted with **15** (0.316 mmol, 1.1 eq) according to *General Procedure A*. Upon completion, the reaction mixture was diluted with ethyl acetate and partitioned with water. The product was extracted from the aqueous (3x). The organic layers were combined and washed with water (3x) and saturated sodium chloride, then dried over sodium sulfate and concentrated to dryness. The product was isolated via gravity column chromatography in a solution of 92 DCM: 7 methanol: 1 ammonium hydroxide, resulting in 4-(2,6-

dichlorobenzamido)-*N*-(1-(2-((1-(2-((2-(2,6-dioxopiperidin-3-yl)-1,3-dioxoisoindolin-4-yl)oxy)acetyl)piperidin-4-yl)amino)-2-oxoethyl)piperidin-4-yl)-1*H*-pyrazole-3-carboxamide. (white solid, yield =38%) ^{1}H NMR: (400 MHz, d_6 DMSO) δ10.15 (1H, s), 8.34 (1H, s), 8.27 (1H, d, *J* = 4.6 Hz), 7.74 (1H, t, *J* =6.8 Hz), 7.62 (1H, d, *J* = 7.2 Hz), 7.57 (2H, d, *J* = 7.2 Hz), 7.48 (1H, t, 6.8 Hz) 7.43 (1H, d, 7.2 Hz), 7.30 (1H, d, *J* =8.8 Hz), 5.17 (1H, s), 5.08 (1H, dd, 4.8 Hz), 4.12 (1H, d, *J* = 12.4 Hz), 3.83 (1H, m), 3.71 (1H, q, *J* = 4.8 Hz), 2.88 (2H, s), 2.78 (2H, d, *J* =10.4 Hz), 2.55 (2H, m), 2.03 (3H, m), 1.67 (4H, m). ^{13}C NMR: (500 MHz, d_6 DMSO) δ173.38, 170.53, 169.18, 167.41, 165.85, 165.36, 163.27, 156.28, 137.10, 135.96, 133.70, 133.52, 132.47, 131.57, 129.01, 122.09, 120.73, 116.74, 116.03, 66.68, 61.73, 60.36, 52.96, 49.38, 46.41, 45.91, 43.38, 40.90, 32.33, 31.667, 22.62, 21.35, 14.68. HRMS (ESI) m/z [M+H]+ calcd for $C_{38}H_{39}Cl_2N_9O_9$ = 836.2321; found = 836.2339.

Synthesis of 4-(2,6-dichlorobenzamido)-*N*-(1-(2-((2-(2-(2-((2-(2,6-dioxopiperidin-3-yl)-1,3-dioxoisoindolin-4-yl)oxy)acetamido)ethoxy)ethyl)amino)-2-oxoethyl)piperidin-4-yl)-1*H*-pyrazole-3-carboxamide (**CG-3-066**): **11** (0.809 mmol) was reacted with Boc-2-(2-aminoethoxy) ethylamine (0.889 mmol, 1.1 eq) according to *General Procedure A*. Upon completion, the reaction mixture was diluted with ethyl acetate and partitioned with water. The product was extracted from the aqueous (3x). The organic layers were combined and washed with water (3x) and saturated sodium chloride, then dried over sodium sulfate and concentrated to dryness. The product was isolated via gravity column chromatography in a solution of 92 DCM: 7 methanol: 1 ammonium hydroxide, resulting in *tert*-butyl (2-(2-(2-(4-(4-(2,6-dichlorobenzamido)-1*H*-pyrazole-3-carboxamido)piperidin-1-yl)acetamido)ethoxy)ethyl)carbamate. (pale yellow foam, yield

= 40%). 1H NMR (400 MHz, d6-DMSO) δ = 13.38 (s, 1H), 10.15 (s, 1H), 8.33 (s, 1H), 8.27 (d, J = 7.2 Hz, 1H), 7.63 (t, J = 5 Hz, 1H), 7.56 (d, J = 7.2 Hz, 2H), 7.50 (t, J = 7.8 Hz, 1H), 6.72 (s, 1H), 3.69-3.64 (m, 2H), 3.37 (d, J = 6.4 Hz, 2H), 3.22 (d, J = 5.2 Hz, 2H), 3.04 (d, J = 6 Hz, 2H), 2.87 (s, 2H), 2.77 (d, J = 10.8 Hz, 2H), 2.08 (s, 2H), 1.67 (s, 4H), 1.33 (s, 10H); 13C NMR (400 MHz, d6-DMSO) δ = 169.8, 163.1, 160.9, 156.0, 135.8, 132.3, 131.7, 128.9 (2), 121.9, 121.1, 78.1, 69.4, 69.2, 61.7, 53.0, 46.3, 38.6, 31.5, 28.7. LRMS (ESI) m/z [M+H]+ calcd for $C_{27}H_{38}Cl_2N_7O_6$ = 626.22; found = 626.1. *Tert*-butyl (2-(2-(2-(4-(4-(2,6-dichlorobenzamido)-1*H*-pyrazole-3-carboxamido)piperidin-1-yl)acetamido)ethoxy)ethyl)carbamate (0.240 mmol) was reacted according to *General Procedure B*, resulting in *N*-(1-(2-((2-(2-aminoethoxy)ethyl)amino)-2-oxoethyl)piperidin-4-yl)-4-(2,6-dichlorobenzamido)-1*H*-pyrazole-3-carboxamide hydrochloride without further purification. (tan solid, yield = 99%). *N*-(1-(2-((2-(2-aminoethoxy)ethyl)amino)-2-oxoethyl)piperidin-4-yl)-4-(2,6-dichlorobenzamido)-1*H*-pyrazole-3-carboxamide hydrochloride (0.240 mmol) was reacted with **15** (0.240 mmol) according to *General Procedure A*. Upon completion, the reaction mixture was diluted with ethyl acetate and partitioned with water. The product was extracted from the aqueous (3x). The organic layers were combined and washed with water (3x) and saturated sodium chloride, then dried over sodium sulfate and concentrated to dryness. The product was isolated via gravity column chromatography in a solution of 92 DCM: 7 methanol: 1 ammonium hydroxide, resulting in 4-(2,6-dichlorobenzamido)-*N*-(1-(2-((2-(2-(2-((2-(2,6-dioxopiperidin-3-yl)-1,3-dioxoisoindolin-4-yl)oxy)acetamido)ethoxy)ethyl)amino)-2-oxoethyl)piperidin-4-yl)-1*H*-pyrazole-3-carboxamide. (white solid, yield = 33%). ^{1}H NMR: (500 MHz, d_6 DMSO) δ13.39 (1H, s), 11.10 (1H, s(, 10.15 (1H, s), 8.35 (1H, s),

8.29 (1H, s), 8.00 (1H, t, *J* = 6.0 Hz), 7.80 (1H, t, *J* = 7.5 Hz), 7.66 (1H, s), 7.55 (2H, d, *J* = 7.5 Hz), 7.49 (2H, m), 7.39 (1H, d, *J* = 9.0 Hz), 5.11 (1H, dd, *J* = 5.0 Hz), 4.79 (2H, s), 3.70 (1H, s), 3.44 (4H, p, *J* = 6.0 Hz), 3.31 (5H, m), 3.26 (2H, q, *J* = 6.0 Hz), 2.89 (2H, m), 2.79 (2H, m), 2.55 (3H, m), 2.04 (2H, m), 1.69 (4H, m). ^{13}C NMR: (500 MHz, *d*$_6$ DMSO) δ173.36, 170.47, 167.53, 167.32, 166.09, 163.29, 160.90, 155.55, 137.54, 135.97, 133.63, 133.50, 132.48, 131.86, 129.02, 122.08, 121.32, 120.97, 117.39, 116.67, 69.43, 69.19, 68.14, 53.01, 49.43, 38.98, 38.72, 31.56, 22.61. HRMS (ESI) m/z [M+H]+ calcd for $C_{37}H_{39}Cl_2N_9O_{10}$ = 840.2270; found = 840.2301.

Synthesis of 4-(2,6-dichlorobenzamido)-*N*-(1-(14-((2-(2,6-dioxopiperidin-3-yl)-1,3-dioxoisoindolin-4-yl)oxy)-2,13-dioxo-6,9-dioxa-3,12-diazatetradecyl)piperidin-4-yl)-1*H*-pyrazole-3-carboxamide (**CG-3-067**): To a stirring solution of NH_2-2PEG-NH_2 (67.48 mmol, 10 eq) in DCM (150 mL) at 0°C, a solution of boc-anhydride (6.748 mmol, 1.0 eq) in DCM (40 mL) was added dropwise. The reaction was stirred at room temperature for 16 hours. Upon completion, the reaction mixture was quenched with water and partitioned between water and DCM. The product was extracted into DCM 2x, washed with water and saturated sodium bicarbonate, then dried over sodium sulfate and concentrated to dryness, yielding *tert*-butyl (2-(2-(2-aminoethoxy)ethoxy)ethyl)carbamate without further purification. (pale yellow oil, yield = 99%). *Tert*-butyl (2-(2-(2-aminoethoxy)ethoxy)ethyl)carbamate (0.889 mmol, 1.1 eq) was reacted with **11** (0.809 mmol), according to *General Procedure A.* Upon completion, the reaction mixture was diluted with ethyl acetate and partitioned with water. The product was extracted from the aqueous (3x). The organic layers were combined and washed with water (3x) and saturated sodium chloride, then dried over sodium sulfate

and concentrated to dryness. The product was isolated via gravity column chromatography in a solution of 92 DCM: 7 methanol: 1 ammonium hydroxide, resulting in *tert*-butyl (2-(2-(2-(2-(4-(4-(2,6-dichlorobenzamido)-1*H*-pyrazole-3-carboxamido)piperidin-1-yl)acetamido)ethoxy)ethoxy)ethyl)carbamate. (pale yellow oil, yield = 38%). 1H NMR (400 MHz, d6-DMSO) δ = 13.38 (s, 1H), 10.15 (s, 1H), 8.33 (s, 1H), 8.29 (d, J = 7.6 Hz, 1H), 7.62 (t, J = 5.4 Hz, 1H), 7.56 (d, J = 8 Hz, 2H), 7.50 (t, J = 8.2 Hz, 1H), 6.72 (s, 1H), 3.71-3.65 (m, 1H), 3.48 (s, 4H), 3.40 (t, J = 5.4 Hz, 2H), 3.35 (t, J = 6.2 Hz, 2H), 3.23 (d, J = 5.6 Hz, 2H), 3.03 (d, J = 6 Hz, 2H), 2.87 (s, 2H), 2.77 (d, J = 11.6 Hz, 2H), 2.07 (s, 2H), 1.67 (s, 4H), 1.34 (s, 9H); 13C NMR (400 MHz, d6-DMSO) δ = 169.8, 163.1, 160.7, 156.3, 135.8, 132.3, 131.7, 128.9, 121.9, 121.1, 78.0, 69.9, 69.6, 69.5, 61.7, 53.0, 46.3, 38.6, 31.5, 28.7. LRMS (ESI) m/z [M+H]+ calcd for $C_{29}H_{42}Cl_2N_7O_7$ = 670.24; found = 670.2. *Tert*-butyl (2-(2-(2-(2-(4-(4-(2,6-dichlorobenzamido)-1*H*-pyrazole-3-carboxamido)piperidin-1-yl)acetamido)ethoxy)ethoxy)ethyl)carbamate (0.224 mmol) was reacted according to *General Procedure B*, resulting in *N*-(1-(2-((2-(2-(2-aminoethoxy)ethoxy)ethyl)amino)-2-oxoethyl)piperidin-4-yl)-4-(2,6-dichlorobenzamido)-1*H*-pyrazole-3-carboxamide without further purification. (tan solid, yield = 99%). *N*-(1-(2-((2-(2-(2-aminoethoxy)ethoxy)ethyl)amino)-2-oxoethyl)piperidin-4-yl)-4-(2,6-dichlorobenzamido)-1*H*-pyrazole-3-carboxamide (0.224 mmol) was reacted with **15** (0.224 mmol) according to *General Procedure A.* Upon completion, the reaction mixture was diluted with ethyl acetate and partitioned with water. The product was extracted from the aqueous (3x). The organic layers were combined and washed with water (3x) and saturated sodium chloride, then dried over sodium sulfate and concentrated to dryness.

The product was isolated via gravity column chromatography in a solution of 92 DCM: 7 methanol: 1 ammonium hydroxide, resulting in 4-(2,6-dichlorobenzamido)-*N*-(1-(14-((2-(2,6-dioxopiperidin-3-yl)-1,3-dioxoisoindolin-4-yl)oxy)-2,13-dioxo-6,9-dioxa-3,12-diazatetradecyl)piperidin-4-yl)-1*H*-pyrazole-3-carboxamide. (white solid, yield = 33%) ^{1}H NMR: (500 MHz, d_6 DMSO) δ13.36 (1H, s), 11.98 (1H, s), 10.36 (1H, s), 8.33 (1H, s), 8.28 (1h, d, *J* = 8.0 Hz), 7.99 (1H, t, *J* = 5.5 Hz), 7.79 (1H, t, *J* = 7.5 Hz), 7.62 (1H, t, *J* = 5.5 Hz), 7.57 (2H, d, *J* = 7.5 Hz), 7.50 (2H, m), 7.38 (1H, d, *J* = 8.5 Hz), 5.10 (1H, dd, *J* = 6.0 Hz), 4.78 (2H, s), 3.70 (1H, m), 3.51 (4H, s), 3.45 (2H, t, *J* = 6.0 Hz), 3.41 (2H, t, *J* = 6.0 Hz), 3.23 (2H, q, *J* = 5.5 Hz), 2.87 (3H, m), 2.77 (2H, d, *J* =11.5 Hz), 2.57 (2H, m), 2.08 (4H, m), 1.68 (4H, m). ^{13}C NMR: (500 MHz, d_6 DMSO) δ173.37, 170.46, 170.01, 167.51, 167.33, 166.05, 160.96, 155.55, 137.53, 135.97, 133.64, 132.47, 131.86, 129.02, 122.10, 120.95, 117.38, 116.66, 70.23, 70.09, 69.65, 69.45, 68.14, 63.63, 61.85, 53.10, 49.43, 46.78, 39.02, 38.70, 31.69, 31.56, 22.61. HRMS (ESI) m/z [M+H]+ calcd for $C_{39}H_{43}Cl_2N_9O_{11}$ = 884.2532; found = 884.2571.

Synthesis of 4-(2,6-dichlorobenzamido)-*N*-(1-(3-(2-((2-(2,6-dioxopiperidin-3-yl)-1,3-dioxoisoindolin-4-yl)oxy)acetamido)propanoyl)piperidin-4-yl)-1*H*-pyrazole-3-carboxamide (**AMC-3-104**): **5** (0.659 mmol) was reacted with Boc-beta-Ala-OH (0.725 mmol, 1.1 eq) according to *General Procedure A*. Upon completion, the reaction mixture was diluted with ethyl acetate and partitioned with water. The product was extracted from the aqueous (3x). The organic layers were combined and washed with water (3x) and saturated sodium chloride, then dried over sodium sulfate and concentrated to dryness. The product was isolated via gravity column chromatography in a solution of 5% methanol in chloroform, resulting in *tert*-butyl (3-(4-(4-(2,6-dichlorobenzamido)-1*H*-

pyrazole-3-carboxamido)piperidin-1-yl)-3-oxopropyl)carbamate. (white solid, yield = 69%). 1H NMR (400 MHz, d6-DMSO) δ = 13.39 (s, 1H), 10.14 (s, 1H), 8.37-8.34 (m, 2H), 7.56 (d, J = 8.8 Hz, 2H), 7.50 (t, J = 7.8 Hz, 1H), 6.64 (s, 1H), 4.33 (d, J = 12.4 Hz, 1H), 3.94 (s, 1H), 3.80 (d, J = 13.2 Hz, 1H), 3.10 (d, J = 5.6 Hz, 2H), 3.01 (t, J = 12 Hz, 1H), 2.56 (t, J = 12Hz, 1H), 2.42 (t, J = 7Hz, 2H), 1.73 (t, J = 15.6 Hz, 2H), 1.55-1.41 (m, 2H), 1.35 (s, 9H); 13C NMR (400 MHz, d6-DMSO) δ = 169.3, 163.1, 160.7, 155.9, 135.8, 133.3, 132.3, 131.7, 128.9, 121.9, 121.2, 78.1, 46.4, 44.4, 37.0, 33.3, 32.1, 31.3, 28.7. LRMS (ESI) m/z [M+H+Na]+ calcd for $C_{24}H_{30}Cl_2N_6O_5Na$ = 575.16; found = 575.0. *Tert*-butyl (3-(4-(4-(2,6-dichlorobenzamido)-1*H*-pyrazole-3-carboxamido)piperidin-1-yl)-3-oxopropyl)carbamate (0.365 mmol) was reacted according to *General Procedure B*, yielding *N*-(1-(3-aminopropanoyl)piperidin-4-yl)-4-(2,6-dichlorobenzamido)-1*H*-pyrazole-3-carboxamide hydrochloride without further purification. (tan solid, yield = 99%). *N*-(1-(3-aminopropanoyl)piperidin-4-yl)-4-(2,6-dichlorobenzamido)-1*H*-pyrazole-3-carboxamide hydrochloride (0.553 mmol) was reacted with **15** (0.608 mmol, 1.1 eq) according to *General Procedure A*. Upon completion, the reaction mixture was diluted with ethyl acetate and partitioned with water. The product was extracted from the aqueous (3x). The organic layers were combined and washed with water (3x) and saturated sodium chloride, then dried over sodium sulfate and concentrated to dryness. The product was isolated via gravity column chromatography in a solution of 92: DCM: 7 methanol: 1 ammonium hydroxide, resulting in 4-(2,6-dichlorobenzamido)-*N*-(1-(3-(2-((2-(2,6-dioxopiperidin-3-yl)-1,3-dioxoisoindolin-4-yl)oxy)acetamido)propanoyl)piperidin-4-yl)-1*H*-pyrazole-3-carboxamide. (white solid, yield =27 %) ^{1}H NMR: (400 MHz, d_6 DMSO) δ13.99 (1H, s),

11.09 (1H, s), 10.14 (1H, s), 8.36 (1H, d, *J* = 7.6), 8.34 (1H, s), 7.98 (1H, t, *J* = 6.0 Hz), 7.79 (1H, t, *J* = 7.6 Hz), 7.56 (2H, d, *J* = 7.2 Hz), 7.47 (2H, m), 7.37 (1H, d, *J* = 8.8 Hz), 5.09 (1H, dd, *J* = 5.6 Hz), 4.76 (2H, s), 4.34 (1H, d, 12.8 Hz), 3.93 (1H, m), 3.79 (1H, d, *J* = 13.6 Hz), 3.36 (2H, m), 3.00 (1H, t, *J* = 12.4 Hz), 2.84 (1H, m), 2.56 (3H, m), 2.02 (1H, m), 1.73 (1H, t, *J* =5.2 Hz), 1.73 (2H, t, *J* =14.0 Hz), 1.46 (2H, m). ^{13}C NMR: (500 MHz, *d₆* DMSO) δ173.37, 170.48, 169.28, 167.44, 167.33, 165.99, 163.27, 160.92, 155.62, 137.50, 135.95, 133.67, 133.50, 132.45, 131.87, 129.00, 122.13, 121.35, 121.04, 117.41, 116.68, 68.12, 60.36, 49.43, 46.56, 44.50, 40.81, 35.57, 32.94, 32.21, 31.56, 31.45, 22.62, 21.34, 14.67. HRMS (ESI) m/z [M+H]+ calcd for $C_{34}H_{32}Cl_2N_8O_9$ = 767.1742; found = 767.1751.

Synthesis of 4-(2,6-dichlorobenzamido)-*N*-(1-(7-(2-((2-(2,6-dioxopiperidin-3-yl)-1,3-dioxoisoindolin-4-yl)oxy)acetamido)heptanoyl)piperidin-4-yl)-1*H*-pyrazole-3-carboxamide (**CG-3-071**): **5** (0.659 mmol) was reacted with Boc-7-aminoheptanoic acid (0.725 mmol, 1.1 eq) according to *General Procedure A*. Upon completion, the reaction mixture was diluted with ethyl acetate and partitioned with water. The product was extracted from the aqueous (3x). The organic layers were combined and washed with water (3x) and saturated sodium chloride, then dried over sodium sulfate and concentrated to dryness. The product was isolated via gravity column chromatography in a solution of 92: DCM: 7 methanol: 1 ammonium hydroxide, resulting in *tert*-butyl (7-(4-(4-(2,6-dichlorobenzamido)-1*H*-pyrazole-3-carboxamido)piperidin-1-yl)-7-oxoheptyl)carbamate. (pale yellow solid, yield = 58%). 1H NMR (400 MHz, d6-DMSO) δ = 13.39 (s, 1H), 10.14 (s, 1H), 8.38-8.33 (m, 2H), 7.56 (d, J = 7.2 Hz, 2H), 7.50 (t, J = 7.8 Hz, 1H), 6.73 (s, 1H), 4.35 (d, J = 12.8 Hz, 1H), 3.94 (s, 1H), 3.87 (d, J = 13.6 Hz,

1H), 3.00 (t, J = 12.6 Hz, 1H), 2.87-2.84 (m, 3H), 2.54 (t, J = 12.4 Hz, 2H), 2.25 (t, J = 7 Hz, 2H), 1.72 (t, J = 17.2 Hz, 2H), 1.43 (s, 4H), 1.34 (s, 9H), 1.22 (s, 4H); 13C NMR (400 MHz, d6-DMSO) δ = 170.8, 163.1, 160.5, 156.0, 135.8, 132.3, 131.7, 128.9, 121.9, 121.2, 77.7, 46.5, 44.5, 32.7, 32.2, 31.4, 29.9, 28.9, 28.7, 26.6, 25.3. LRMS (ESI) m/z [M+H+Na]+ calcd for $C_{28}H_{38}Cl_2N_6O_5Na$ = 631.22; found = 631.1. *Tert*-butyl (7-(4-(4-(2,6-dichlorobenzamido)-1*H*-pyrazole-3-carboxamido)piperidin-1-yl)-7-oxoheptyl)carbamate (0.377 mmol) was reacted according to *General Procedure B*, resulting in *N*-(1-(7-aminoheptanoyl)piperidin-4-yl)-4-(2,6-dichlorobenzamido)-1*H*-pyrazole-3-carboxamide without further purification. (tan solid, yield = 99%) *N*-(1-(7-aminoheptanoyl)piperidin-4-yl)-4-(2,6-dichlorobenzamido)-1*H*-pyrazole-3-carboxamide (0.189 mmol) was reacted with **15** (0.189 mmol) according to *General Procedure A*. Upon completion, the reaction mixture was diluted with ethyl acetate and partitioned with water. The product was extracted from the aqueous (3x). The organic layers were combined and washed with water (3x) and saturated sodium chloride, then dried over sodium sulfate and concentrated to dryness. The product was isolated via gravity column chromatography in a solution of 92: DCM: 7 methanol: 1 ammonium hydroxide, resulting in 4-(2,6-dichlorobenzamido)-*N*-(1-(7-(2-((2-(2,6-dioxopiperidin-3-yl)-1,3-dioxoisoindolin-4-yl)oxy)acetamido)heptanoyl)piperidin-4-yl)-1*H*-pyrazole-3-carboxamide. (white solid, yield = 39%). ^{1}H NMR: (400 MHz, d_6 DMSO) δ13.40 (1H, s), 11.09 (1H, s), 10.15 (1H, s), 8.36 (1H, d, *J* = 8.0 Hz), 8.32 (1H, s), 7.90 (1H, t, *J* = 5.6 Hz), 7.79 (1H, t, *J* = 7.6 Hz), 7.56 (2H, d, *J* = 7.2 Hz), 7.50 (2H, m), 3.37 (1H, d, *J* = 8.8 Hz), 5.10 (1H, dd, *J* = 7.6 Hz), 4.75 (2H, s), 4.35 (1H, d, *J* =12.8 Hz), 3.93 (1H, m), 3.82 (1H, m), 3.13 (2H, q, *J* = 6.4 Hz), 3.00 (1H, t, *J* = 12.4 Hz), 2.87 (3H, m), 2.68 (2H, m),

2.56 (5H, m), 2.26 (2H, t, *J* = 7.6 Hz), 2.02 (2H, m), 1.72 (2H, t, *J* =16.4 Hz), 1.51 (6H, m), 1.26 (4H, m). ^{13}C NMR: (500 MHz, d_6 DMSO) δ173.37, 171.02, 170.46, 167.33, 167.23, 166.14, 162.91, 160.96, 155.62, 137.53, 135.97, 133.63, 132.46, 131.87, 129.01, 122.13, 121.02, 117.46, 116.67, 68.31, 49.44, 46.62, 44.48, 40.81, 38.92, 36.38, 32.87, 32.40, 31.56, 31.37, 29.48, 29.06, 26.76, 25.44, 22.61. HRMS (ESI) m/z [M+H]+ calcd for $C_{38}H_{40}Cl_2N_8O_9$ = 823.2368; found = 823.2393.

Synthesis of 4-(2,6-dichlorobenzamido)-*N*-(1-(1-(2-((2-(2,6-dioxopiperidin-3-yl)-1,3-dioxoisoindolin-4-yl)oxy)acetyl)piperidine-4-carbonyl)piperidin-4-yl)-1*H*-pyrazole-3-carboxamide (**SF-8-140**): Iosnipecotic acid (7.75 mmol, 1.1 eq) was dissolved in dioxane:water (20 mL). Sodium carbonate (7.05 mmol, 1.0 eq) was added to the reaction mixture followed by boc-anhydride (7.05 mmol, 1.0 eq). The reaction was stirred at room temperature for 16 hours. Upon completion, the reaction was concentrated to remove the dioxane, diluted with ethyl acetate, and partitioned with 1M HCl. The product was extracted into ethyl acetate. The organic layers were combined, dried over sodium sulfate, and concentrated to dryness, resulting in 1-(*tert*-butoxycarbonyl)piperidine-4-carboxylic acid without further purification. (white solid, yield = 97%). **5** (0.659 mmol) was reacted with 1-(*tert*-butoxycarbonyl)piperidine-4-carboxylic acid (0.725 mmol, 1.1 eq) according to *General Procedure A*. Upon completion, the reaction mixture was diluted with ethyl acetate and partitioned with water. The product was extracted from the aqueous (3x). The organic layers were combined and washed with water (3x) and saturated sodium chloride, then dried over sodium sulfate and concentrated to dryness, resulting in *tert*-butyl 4-(4-(4-(2,6-dichlorobenzamido)-1*H*-pyrazole-3-carboxamido)piperidine-1-carbonyl)piperidine-1-carboxylate without further purification. (white solid, yield =

65%). 1H NMR (400 MHz, d6-DMSO) δ = 13.39 (s, 1H), 10.14 (s, 1H), 8.37 (d, J = 7.6 Hz, 1H), 8.34 (s, 1H), 7.57 (d, J = 7.2 Hz, 2H), 7.50 (t, J = 8.2 Hz, 1H), 4.35 (d, J = 12.8 Hz, 1H), 3.93 (m, 4H), 3.04 (t, J = 12.6 Hz, 1H), 2.84-2.71 (m, 3H), 2.55 (t, J = 12.4 Hz, 2H), 1.78-1.69 (m, 2H), 1.55 (d, J = 12.4 Hz, 3H), 1.37 (s, 11H); 13C NMR (400 MHz, d6-DMSO) δ = 172.6, 163.1, 160.7, 154.3, 135.8, 133.3, 132.3, 131.7, 128.9, 121.9, 121.2, 79.0, 46.4, 44.3, 39.3, 37.3, 32.5, 31.4, 28.5. LRMS (ESI) m/z [M+H+Na]+ calcd for $C_{27}H_{34}Cl_2N_6O_5Na$ = 615.19; found = 615.1. *Tert*-butyl 4-(4-(4-(2,6-dichlorobenzamido)-1*H*-pyrazole-3-carboxamido)piperidine-1-carbonyl)piperidine-1-carboxylate (0.379 mmol) was reacted according to *General Procedure B*, resulting in 4-(2,6-dichlorobenzamido)-*N*-(1-(piperidine-4-carbonyl)piperidin-4-yl)-1*H*-pyrazole-3-carboxamide hydrochloride without further purification. (tan solid, yield = 99%). 4-(2,6-dichlorobenzamido)-*N*-(1-(piperidine-4-carbonyl)piperidin-4-yl)-1*H*-pyrazole-3-carboxamide hydrochloride (0.234 mmol) was reacted with **15** (0.234 mmol) according to *General Procedure A.* Upon completion, the reaction mixture was diluted with ethyl acetate and partitioned with water. The product was extracted from the aqueous (3x). The organic layers were combined and washed with water (3x) and saturated sodium chloride, then dried over sodium sulfate and concentrated to dryness. The product was isolated via gravity column chromatography on silica gel, using a solution of 79 DCM: 9 methanol: 1 water, resulting in of 4-(2,6-dichlorobenzamido)-*N*-(1-(1-(2-((2-(2,6-dioxopiperidin-3-yl)-1,3-dioxoisoindolin-4-yl)oxy)acetyl)piperidine-4-carbonyl)piperidin-4-yl)-1*H*-pyrazole-3-carboxamide. (white solid, yield = 64%). ^{1}H NMR: (500 MHz, d_6 DMSO) δ13.41 (1H, s), 11.10 (1H, s), 10.16 (1H, s), 8.36 (2H, m), 7.75 (1H, t, *J* = 7.5 Hz), 7.56 (2H, d, *J* = 7.5 Hz), 7.50 (1H, m), 7.46 (1H, d, *J* = 7.0 Hz), 7.31 (1H, d, *J* = 8.5 Hz), 5.17

(3H, m), 4.38 (1H, d, *J* = 11.5 Hz), 4.28 (1H, app. t), 4.00 (2H, m), 3.80 (1H, m), 3.68 (1H, dd, *J* =5.0 Hz), 3.49 (1H, dd, *J* = 4.5 Hz), 3.10 (2H, m), 2.89 (3H, m), 2.72 (3H, m), 2.52 (3H, m), 2.03 (1H, m), 1.77 (2H, m), 1.62 (4H, m), 1.44 (3H, m), 1.21 (1H, m). ^{13}C NMR: (500 MHz, *d6* DMSO) δ173.40, 172.61, 170.54, 167.41, 165.86, 160.897, 156.33, 137.10, 135.96, 133.68, 132.47, 131.87, 129.02, 122.13, 120.79, 116.72, 116.01, 66.72, 60.82, 49.38, 46.60, 44.49, 44.01, 41.35, 41.06, 38.83, 37.45, 32.69, 31.58, 28.22, 22.62. HRMS (ESI) m/z [M+H]+ calcd for $C_{37}H_{36}Cl_2N_8O_9$ = 807.2055; found = 807.2065.

Synthesis of 4-(2,6-dichlorobenzamido)-*N*-(1-(7-(2-(2-((2-(2,6-dioxopiperidin-3-yl)-1,3-dioxoisoindolin-4-yl)oxy)acetamido)acetamido)heptanoyl)piperidin-4-yl)-1*H*-pyrazole-3-carboxamide (**SF-8-141**): **15** (0.500 mmol) was reacted with tert-butyl bromoacetate (0.550 mmol, 1.1 eq) according to *General Procedure A*. Upon completion, the reaction mixture was diluted with ethyl acetate and partitioned with water. The product was extracted from the aqueous (3x). The organic layers were combined and washed with water (3x) and saturated sodium chloride, then dried over sodium sulfate and concentrated to dryness, resulting in *tert*-butyl (2-((2-(2,6-dioxopiperidin-3-yl)-1,3-dioxoisoindolin-4-yl)oxy)acetyl)glycinate without further purification. (white solid, yield = 98%). 1H NMR (500 MHz, d6-DMSO) δ = 11.12 (s, 1H), 8.30 (t, J = 5.3 Hz, 1H), 7.81 (t, J = 8.3 Hz, 1H), 7.50 (d, J = 7.5 Hz, 1H), 7.41 (d, J = 6.8 Hz, 1H), 5.11 (dd, J = 4.9, 12.1 Hz, 1H), 4.86 (s, 2H), 3.82 (d, J = 5.8 Hz, 2H), 2.61-2.50 (m, 3H), 2.04 (s, 1H), 1.40 (s, 9H); 13C NMR (500 MHz, d6-DMSO) δ = 178.1, 175.2, 173.9, 172.8, 172.1, 170.7, 160.3, 142.3, 138.4, 125.8, 122.2, 121.5, 86.3, 72.8, 54.2, 46.5, 36.3, 33.1, 27.4. LRMS (ESI) m/z [M+H+Na]+ calcd for $C_{21}H_{23}N_3O_8Na$ = 468.14; found = 468.1. *Tert*-butyl (2-((2-(2,6-dioxopiperidin-3-yl)-1,3-dioxoisoindolin-4-yl)oxy)acetyl)glycinate (0.500

mmol) was dissolved in DCM (5 mL) and trifluoroacetic acid (5 mL) was added. The reaction mixture was stirred at room temperature for 4 hours. Upon completion, the reaction was concentrated to dryness and azeotroped 2x with DCM/methanol then with DCM, resulting in (2-((2-(2,6-dioxopiperidin-3-yl)-1,3-dioxoisoindolin-4-yl)oxy)acetyl)glycine without further purification. (white solid, yield = 99%). (2-((2-(2,6-dioxopiperidin-3-yl)-1,3-dioxoisoindolin-4-yl)oxy)acetyl)glycine (0.189 mmol) was reacted with *N*-(1-(2-((2-(2-(2-aminoethoxy)ethoxy)ethyl)amino)-2-oxoethyl)piperidin-4-yl)-4-(2,6-dichlorobenzamido)-1*H*-pyrazole-3-carboxamide (0.189 mmol) according to *General Procedure A.* Upon completion, the reaction mixture was diluted with ethyl acetate and partitioned with water. The product was extracted from the aqueous (3x). The organic layers were combined and washed with water (3x) and saturated sodium chloride, then dried over sodium sulfate and concentrated to dryness. The product was isolated via gravity column chromatography on silica gel, using a solution of 79 DCM: 9 methanol: 1 water, resulting in 4-(2,6-dichlorobenzamido)-*N*-(1-(7-(2-(2-((2-(2,6-dioxopiperidin-3-yl)-1,3-dioxoisoindolin-4-yl)oxy)acetamido)acetamido)heptanoyl)piperidin-4-yl)-1*H*-pyrazole-3-carboxamide. ^{1}H NMR: (500 MHz, d_6 DMSO) δ13.38 (1H, s), 11.11 (1H, s), 10.16 (1H, s), 8.37 (1H, d, *J* = 8.0 Hz), 8.34 (1H, s), 8.20 (1H, t, 5.0 Hz), 7.88 (1H, t, *J* = 4.5 Hz), 7.79 (1H, t, 7.5 Hz), 7.56 (2H, d, *J* = 7.5 Hz), 7.49 (2H, m), 7.41 (1H, d, *J* = 8.5 Hz), 5.11 (1H, dd, *J* =4.5 Hz), 4.82 (2H, s), 4.36 (1H, d, *J* = 12.0 Hz), 3.95 (1H, m), 3.84 (1H, d, *J* =13.0 Hz), 3.76 (2H, d, *J* = 5.5 Hz), 3.03 (3H, m), 2.86 (1H, m), 2.54 (3H, m), 2.26 (2H, t, *J* =7.0 Hz), 2.03 (1H, m), 1.73 (2H, m), 1.44 (7H, m), 1.24 (4H, m). ^{13}C NMR: (500 MHz, d_6 DMSO) δ173.37, 171.02, 170.47, 168.61, 167.81, 167.35, 165.97, 160.96, 155.65, 137.49, 135.96, 133.66, 132.47, 131.87, 129.02, 122.12, 121.00, 117.32,

116.62, 68.05, 49.43, 46.62, 44.67, 42.37, 40.81, 39.14, 32.87, 32.40, 31.56, 29.60, 29.08, 26.80, 25.44, 22.61. HRMS (ESI) m/z [M+H]+ calcd for $C_{40}H_{43}Cl_2N_9O_{10}$ = 880.2583; found = 880.2583.

Synthesis of 4-(2,6-dichlorobenzamido)-*N*-(1-(2-((2-(2-(2-((2-(2,6-dioxopiperidin-3-yl)-6-fluoro-1,3-dioxoisoindolin-5-yl)amino)ethoxy)ethoxy)ethyl)amino)-2-oxoethyl)piperidin-4-yl)-1*H*-pyrazole-3-carboxamide (**AMC-3-201**): *Tert*-butyl (2-(2-(2-aminoethoxy)ethoxy)ethyl)carbamate (0.206 mmol) reacted according to *General Procedure F* at 120°C for 4 hours. The product was isolated via flash column chromatography on a gradient of 1 hexanes: 4 ethyl acetate to yield *tert*-butyl (2-(2-(2-((2-(2,6-dioxopiperidin-3-yl)-6-fluoro-1,3-dioxoisoindolin-5-yl)amino)ethoxy)ethoxy)ethyl)carbamate (green solid, yield = 31%). 1H NMR (400 MHz, d6-DMSO) δ = 11.05 (s, 1H), 7.55 (d, J = 10 Hz, 1H), 7.18 (d, J = 6.8 Hz, 1H), 6.78 (s, 1H), 6.70 (s, 1H), 5.03 (dd, J = 5, 13 Hz, 1H), 3.58 (t, J = 5.4 Hz, 2H), 3.51 (s, 2H), 3.48-3.43 (m, 4H), 3.34 (t, J = 6 Hz, 2H), 3.02 (d, J = 5.6 Hz, 2H), 2.86 (t, J = 12.4 Hz, 1H), 2.54 (t, J = 13.6 Hz, 2H), 2.00 (s, 1H), 1.34 (s, 10H); 13C NMR (400 MHz, d6-DMSO) δ = 173.2, 170.5, 167.6, 166.9, 156.3, 154.7, 152.2, 143.4, 130.3, 117.2, 110.4, 110.2, 106.0, 78.0, 70.2, 69.9, 69.6, 69.2, 49.3, 42.6, 31.4, 28.7, 22.6. LRMS (ESI) m/z [M+H+Na]+ calcd for $C_{24}H_{31}FN_4O_8Na$ = 545.2; found = 545.2. *Tert*-butyl (2-(2-(2-((2-(2,6-dioxopiperidin-3-yl)-6-fluoro-1,3-dioxoisoindolin-5-yl)amino)ethoxy)ethoxy)ethyl)carbamate (0.151 mmol) was reacted according to *General Procedure B* yielding 5-((2-(2-(2-aminoethoxy)ethoxy)ethyl)amino)-2-(2,6-dioxopiperidin-3-yl)-6-fluoroisoindoline-1,3-dione without further purification (green solid, yield = 99%). 5-((2-(2-(2-aminoethoxy)ethoxy)ethyl)amino)-2-(2,6-dioxopiperidin-

3-yl)-6-fluoroisoindoline-1,3-dione (0.151 mmol, 1.0 eq) was reacted with **11** (0.166 mmol, 1.1 eq) according to *General Procedure A*. Upon completion, the reaction mixture was diluted with ethyl acetate and partitioned with water. The product was extracted from the aqueous (3x). The organic layers were combined and washed with water (3x) and saturated sodium chloride, then dried over sodium sulfate and concentrated to dryness. The product was isolated via gravity column chromatography in a solution of 58 DCM: 7 methanol: 1 ammonium hydroxide, yielding 4-(2,6-dichlorobenzamido)-*N*-(1-(2-((2-(2-(2-((2-(2,6-dioxopiperidin-3-yl)-6-fluoro-1,3-dioxoisoindolin-5-yl)amino)ethoxy)ethoxy)ethyl)amino)-2-oxoethyl)piperidin-4-yl)-1*H*-pyrazole-3-carboxamide. (green solid, yield =43 %) ^{1}H NMR: (400 MHz, d_6 DMSO) δ13.36 (1H, s), 11.05 (1H, s), 10.14 (1H, s), 8.33 (1H, s), 8.28 (1H, app. d), 7.55 (6H, m), 7.18 (1H, d, *J* = 6.8 Hz), 6.78 (1H, app. t), 5.02 (1H, dd, *J* = 4.4 Hz), 3.67 (2H, m), 3.58 (2H, m), 3.55 (2H, m), 3.52 (2H, m), 3.50 (2H, m), 3.43 (2H, m), 3.39 (2H, m), 3.20 (2H, m), 2.85 (2H, m), 2.75 (2H, d, *J* = 10.0 Hz), 2.58 (1H, s), 2.53 (1H, s), 2.06 (3H, m), 1.66 (4H, m), 1.21 (1H, s). ^{13}C NMR: (500 MHz, d_6 DMSO) δ173.37, 170.67, 169.89, 168.54, 167.73, 160.91, 152.64, 145.41, 143.40, 140.33, 135.97, 132.48, 131.85, 30.47, 129.03, 122.09, 117.16, 110.40, 106.13, 104.16, 99.29, 72.03, 70.41, 70.12, 69.68, 69.46, 61.80, 57.10, 53.07, 49.46, 46.47, 42.83, 38.69, 31.67, 31.58, 29.62, 22.79. HRMS (ESI) m/z [M+H]+ calcd for $C_{37}H_{40}Cl_2FN_9O_9$ = 844.2383; found = 844.2403.

Synthesis of 4-(2,6-dichlorobenzamido)-*N*-(1-((1-(2-(2,6-dioxopiperidin-3-yl)-6-fluoro-1,3-dioxoisoindolin-5-yl)piperidin-4-yl)methyl)piperidin-4-yl)-1*H*-pyrazole-3-carboxamide (**AMC-3-207**): **5** (0.659 mmol) was reacted with *N*-boc-piperidinecarboxaldehyde (0.659 mmol) according to *General Procedure E*. The product

was isolated via gravity column chromatography on silica gel using a solution of 92 DCM: 7 methanol: 1 ammonium hydroxide, yielding *tert*-butyl 4-((4-(4-(2,6-dichlorobenzamido)-1*H*-pyrazole-3-carboxamido)piperidin-1-yl)methyl)piperidine-1-carboxylate. (white solid, yield = 67%). 1H NMR (400 MHz, d6-DMSO) δ = 13.39 (s, 1H), 10.15 (s, 1H), 8.31 (s, 1H), 8.26 (d, J = 8.8 Hz, 1H), 7.56 (d, J = 8 Hz, 2H), 7.49 (t, J = 4.6 Hz, 1H), 3.88 (d, J = 12 Hz, 2H), 3.67 (s, 1H), 2.78 (d, J = 11.2 Hz, 2H), 2.06 (d, J = 6 Hz, 2H), 1.86 (t, J = 11.2 Hz, 2H), 1.64-1.60 (m, 8H), 1.36 (s, 10H), 0.91 (d, J = 11.2 Hz, 2H); 13C NMR (400 MHz, d6-DMSO) δ = 160.9, 154.3, 135.8, 132.3, 131.7, 128.9 (2), 121.9 (2), 121.1, 78.8, 64.2, 53.3, 46.8, 33.4, 31.7, 30.8, 28.6, 26.3. LRMS (ESI) m/z [M+H]+ calcd for $C_{27}H_{37}Cl_2N_6O_4$ = 579.22; found = 579.2. *Tert*-butyl 4-((4-(4-(2,6-dichlorobenzamido)-1*H*-pyrazole-3-carboxamido)piperidin-1-yl)methyl)piperidine-1-carboxylate (0.390 mmol) was reacted according to *General Procedure B*, resulting in 4-(2,6-dichlorobenzamido)-*N*-(1-(piperidin-4-ylmethyl)piperidin-4-yl)-1*H*-pyrazole-3-carboxamide hydrochloride without further purification. (tan solid, yield = 99%). 4-(2,6-dichlorobenzamido)-*N*-(1-(piperidin-4-ylmethyl)piperidin-4-yl)-1*H*-pyrazole-3-carboxamide hydrochloride (.390mmol) was reacted according to *General Procedure F.* The product was isolated via gravity column chromatography using a solution of 92 DCM: 7 methanol: 1 ammonium hydroxide, resulting in 4-(2,6-dichlorobenzamido)-*N*-(1-((1-(2-(2,6-dioxopiperidin-3-yl)-6-fluoro-1,3-dioxoisoindolin-5-yl)piperidin-4-yl)methyl)piperidin-4-yl)-1*H*-pyrazole-3-carboxamide. (green solid, yield = 32%) ^{1}H NMR: (400 MHz, d_6 DMSO) δ13.17 (1H, s), 11.08 (1H, s), 10.16 (1H, s), 8.31 (1H, s), 8.27 (1H, m), 7.67 (1H, d, J = 11.6 Hz), 7.56 (2H, d, J = 7.2 Hz), 7.51 (1H, t, J = 9.2 Hz), 7.40 (1H, d, J = 7.6 Hz), 5.07 (1H, dd, J = 5.2 Hz), 3.66 (2H, m), 3.57 (3H, m), 2.86 (5H,

m), 2.54 (3H, m), 2.13 (2H, d, *J* =7.2 Hz), 2.02 (2H, m), 1.88 (3H, m), 1.78 (2H, d, *J* =13.2 Hz), 1.66 (6H, m), 1.21 (2H, m). ^{13}C NMR: (500 MHz, d_6 DMSO) δ173.34, 170.49, 167.30, 166.81, 160.91, 158.82, 156.82, 146.50, 135.97, 132.46, 131.87, 129.39, 129.01, 123.30, 122.12, 114.23, 112.34, 72.79, 64.34, 60.82, 53.46, 50.53, 49.65, 41.02, 33.19, 31.88, 31.56, 30.88, 22.70, 14.68. HRMS (ESI) m/z [M+H]+ calcd for $C_{35}H_{35}Cl_2FN_8O_6$ = 753.2113; found = 753.2127.

Synthesis of 4-(2,6-dichlorobenzamido)-*N*-(1-(2-oxo-2-(piperazin-1-yl)ethyl)piperidin-4-yl)-1*H*-pyrazole-3-carboxamide (**A**), common precursor for synthesis of AMC-3-221 and AMC-3-227): **11** (0.974 mmol) was reacted with tert-butyl piperazine-1-carboxylate (1.072 mmol, 1.1 eq) according to *General Procedure A*. Upon completion, the reaction mixture was diluted with ethyl acetate, then partitioned with water. The aqueous layer was basified with saturated sodium bicarbonate and the product was extracted into ethyl acetate (3x). The organic layers were combined and washed with water: saturated sodium bicarbonate (3x) and brine, then dried over sodium sulfate and concentrated to dryness. The product was isolated via gravity column chromatography using a solution of 92 DCM: 7 methanol: 1 ammonium hydroxide, yielding *tert*-butyl 4-(2-(4-(4-(2,6-dichlorobenzamido)-1*H*-pyrazole-3-carboxamido)piperidin-1-yl)acetyl)piperazine-1-carboxylate. (white solid, yield = 56%). 1H NMR (400 MHz, d6-DMSO) δ = 13.37 (s, 1H), 10.15 (s, 1H), 8.33-8.30 (m, 2H), 7.56 (d, J = 8 Hz, 2H), 7.49 (t, J = 4.6 Hz, 1H), 3.69-3.64 (m, 2H), 3.49-3.44 (m, 3H), 3.39 (s, 2H), 3.25 (s, 2H), 3.10 (s, 2H), 2.78 (d, J = 10.4 Hz, 2H), 2.01 (s, 2H), 1.65 (s, 4H), 1.34 (s, 9H); 13C NMR (400 MHz, d6-DMSO) δ = 168.3, 163.3, 160.6, 154.3, 134.9, 132.3, 131.7, 128.9, 128.6, 120.7, 79.6, 72.6, 71.0, 61.1, 60.6, 52.6, 46.2, 45.5, 44.0, 41.5, 31.7, 28.5. LRMS (ESI) m/z [M+H]+ calcd for

$C_{27}H_{36}Cl_2N_7O_5$ = 608.21; found = 608.2. *Tert*-butyl 4-(2-(4-(4-(2,6-dichlorobenzamido)-1*H*-pyrazole-3-carboxamido)piperidin-1-yl)acetyl)piperazine-1-carboxylate (0.848 mmol) was reacted according to *General Procedure B*, resulting in 4-(2,6-dichlorobenzamido)-*N*-(1-(2-oxo-2-(piperazin-1-yl)ethyl)piperidin-4-yl)-1*H*-pyrazole-3-carboxamide without further purification. (tan solid, yield = 99%). ^{1}H NMR: (500 MHz, *d₆* DMSO) δ13.10 (1H, s), 11.02 (1H, s), 10.16 (1H, s), 8.32 (1H, s), 8.29 (1H, d, *J* = 7.5 Hz), 7.58 (2H, d, *J* = 7.0 Hz), 7.52 (1H, t, *J* = 7.0 Hz), 498 (1H, m), 3.69 (1H, m), 3.45 (2H, app. t), 3.16 (1H, s), 3.09 (2H, s), 2.78 (2H, d, *J* =11.5 Hz), 2.71 (2H, app, t), 2.64 (2H, app, t), 2.02 (2H, t, *J* = 11.0 Hz), 1.64 (4H, m). 13C NMR (400 MHz, d6-DMSO) δ = 167.9, 162.9, 160.8, 135.8, 133.1, 132.3, 131.7, 128.9, 121.9, 121.6, 61.1, 52.6, 46.7, 46.3, 45.8, 42.5, 31.6. LRMS (ESI) m/z [M+H]+ calcd for $C_{22}H_{28}Cl_2N_7O_3$ = 508.16; found = 508.1.

Synthesis of 4-(2,6-dichlorobenzamido)-*N*-(1-(2-(4-(2-(2,6-dioxopiperidin-3-yl)-6-fluoro-1,3-dioxoisoindolin-5-yl)piperazin-1-yl)-2-oxoethyl)piperidin-4-yl)-1*H*-pyrazole-3-carboxamide (**AMC-3-221**): **A** (0.172 mmol) was reacted according to *General Procedure F.* The product was isolated via gravity column chromatography using a solution of 92 DCM: 7 methanol: 1 ammonium hydroxide, yielding 4-(2,6-dichlorobenzamido)-*N*-(1-(2-(4-(2-(2,6-dioxopiperidin-3-yl)-6-fluoro-1,3-dioxoisoindolin-5-yl)piperazin-1-yl)-2-oxoethyl)piperidin-4-yl)-1*H*-pyrazole-3-carboxamide. (green solid, yield = 40%) ^{1}H NMR: (400 MHz, *d₆* DMSO) δ13.17 (1H, s), 11.09 (1H, s), 10.15 (1H, s), 8.31 (1H, s), 8.26 (1H, d, *J* = 8.0 Hz), 7.75 (1H, d, *J* = 11.2 Hz), 7.56 (2H, d, *J* = 7.2 Hz), 7.48 (2H, m), 5.09 (1H, dd, *J* = 4.8 Hz), 3.72 (3H, m), 3.60 (2H, m), 3.20 (6H, m), 2.83 (3H, m), 2.58 (2H, m), 2.04 (3H, m), 1.67 (4H, m). ^{13}C

NMR: (500 MHz, d_6 DMSO) δ176.62, 173.35, 170.48, 168.41, 167.21, 166.75, 163.23, 150.83, 145.72, 135.97, 132.48, 131.85, 129.33, 128.02, 124.89, 124.46, 122.06, 114.61, 112.73, 65.21, 61.24, 52.73, 50.12, 49.71, 46.39, 45.60, 41.56, 41.04, 31.82, 31.56, 22.67. HRMS (ESI) m/z [M+H]+ calcd for $C_{35}H_{34}Cl_2FN_9O_7$ = 782.2015; found = 782.2024.

Synthesis of 4-(2,6-dichlorobenzamido)-*N*-(1'-(2-(2,6-dioxopiperidin-3-yl)-6-fluoro-1,3-dioxoisoindolin-5-yl)-[1,4'-bipiperidin]-4-yl)-1*H*-pyrazole-3-carboxamide (**AMC-3-225**): **5** (0.659 mmol) was reacted with 1-boc-piperidin-4-one (0.659 mmol) according to *General Procedure E*. The product was isolated via gravity column chromatography using a solution of 92 DCM: 7 methanol: 1 ammonium hydroxide, yielding *tert*-butyl 4-(4-(2,6-dichlorobenzamido)-1*H*-pyrazole-3-carboxamido)-[1,4'-bipiperidine]-1'-carboxylate. (white solid, yield = 78%). 1H NMR (400 MHz, d6-DMSO) δ = 13.37 (s, 1H), 10.15 (s, 1H), 8.32 (s, 1H), 8.25 (d, J = 7.6 Hz, 1H), 7.56 (d, J = 7.2 Hz, 2H), 7.49 (t, J = 4.6 Hz, 1H), 3.92 (d, J = 11.6 Hz, 2H), 3.65-3.58 (m, 2H), 2.92 (s, 1H), 2.80 (d, J = 10.8 Hz, 2H), 2.36 (t, J = 11 Hz, 1H), 2.12 (t, J = 11 Hz, 2H), 1.65 (s, 4H) 1.55 (q, J = 10.6, 20.6 Hz, 2H), 1.36 (s, 9H), 1.21 (q, J = 9.2, 22 Hz, 2H);13C NMR (400 MHz, d6-DMSO) δ = 160.7, 154.2, 135.8, 132.3, 131.7, 128.9 (2), 121.9 (2), 78.9, 66.1, 61.4, 48.4, 46.9, 34.5, 32.1, 28.5, 28.2. LRMS (ESI) m/z [M+H]+ calcd for $C_{26}H_{35}Cl_2N_6O_4$ = 564.20; found = 565.1. *Tert*-butyl 4-(4-(2,6-dichlorobenzamido)-1*H*-pyrazole-3-carboxamido)-[1,4'-bipiperidine]-1'-carboxylate (0.186 mmol) was then reacted according to *General Procedure B*, resulting in *N*-([1,4'-bipiperidin]-4-yl)-4-(2,6-dichlorobenzamido)-1*H*-pyrazole-3-carboxamide hydrochloride without further purification. (tan solid, yield = 99%). *N*-([1,4'-bipiperidin]-4-yl)-4-(2,6-dichlorobenzamido)-1*H*-pyrazole-3-carboxamide hydrochloride (0.186 mmol) was

reacted according to *General Procedure F*. The product was isolated via gravity column chromatography using a solution of 92 DCM: 7 methanol: 1 ammonium hydroxide, yielding 4-(2,6-dichlorobenzamido)-*N*-(1'-(2-(2,6-dioxopiperidin-3-yl)-6-fluoro-1,3-dioxoisoindolin-5-yl)-[1,4'-bipiperidin]-4-yl)-1*H*-pyrazole-3-carboxamide. (green solid, yield = 44%) ^{1}H NMR: (400 MHz, d_6 DMSO) δ13.38 (1H, s), 11.08 (1H, s), 10.16 (1H, s), 8.32 (1H, s), 8.26 (1H, d, *J* = 6.4 Hz), 7.68 (1H, d, *J* = 10.8 Hz), 7.54 (2H, d, *J* = 8.0 Hz), 7.51 (1H, t, *J* = 8.4 Hz), (7.41 (1H, d, *J* = 7.2 Hz), 5.07 (1H, dd, 5.2 Hz), 3.63 (3H, m), 2.86 (5H, m), 2.55 (2H, m), 2.44 (1H, m), 2.16 (2H, t, *J* = 10.8 Hz2.01 (1H, m), 1.84 (2H, m), 1.68 (2H, m), 1.57 (3H, m). ^{13}C NMR: (500 MHz, d_6 DMSO) δ173.35, 170.50, 167.28, 166.80, 160.92, 156.82, 135.98, 132.48, 131.87, 129.38, 129.03 (2), 123.59, 122.09, 114.29, 112.59, 112.39, 61.18, 50.16 (2), 49.65, 48.61 (2), 47.12, 32.27, 31.56, 28.35, 22.69. HRMS (ESI) m/z [M+H]+ calcd for $C_{34}H_{33}Cl_2FN_8O_6$ = 739.1957; found = 739.1968.

Synthesis of 4-(2,6-dichlorobenzamido)-*N*-(1-(2-(4-((1-(2-(2,6-dioxopiperidin-3-yl)-6-fluoro-1,3-dioxoisoindolin-5-yl)piperidin-4-yl)methyl)piperazin-1-yl)-2-oxoethyl)piperidin-4-yl)-1*H*-pyrazole-3-carboxamide (**AMC-3-227**): **A** (0.405 mmol) was reacted with *N*-boc-4-piperidinecarboxaldehyde (0.405 mmol) according to *General Procedure E.* The produce was isolated via gravity column chromatography using a solution of 92 DCM: 7 methanol: 1 ammonium hydroxide, yielding *tert*-butyl 4-((4-(2-(4-(4-(2,6-dichlorobenzamido)-1*H*-pyrazole-3-carboxamido)piperidin-1-yl)acetyl)piperazin-1-yl)methyl)piperidine-1-carboxylate. (white solid, yield = 94%). 1H NMR (400 MHz, d6-DMSO) δ = 13.38 (s, 1H), 10.15 (s, 1H), 8.32 (s, 2H), 7.56 (d, J = 7.2 Hz, 2H), 7.49 (t, J = 4.6 Hz, 1H), 3.89 (d, J = 11.2 Hz, 2H), 3.67 (s, 1H), 3.49 (s, 2H), 3.39 (s, 2H), 3.08

(s, 2H), 2.77 (d, J = 10.8 Hz, 2H), 2.32 (s, 2H), 2.23 (s, 2H), 2.09 (d, J = 6.4 Hz, 2H), 2.00 (t, J = 10 Hz, 2H), 1.63 (s, 8H), 1.36 (s, 10H), 0.91 (d, J = 10 Hz, 2H);13C NMR (400 MHz, d6-DMSO) δ = 167.9, 160.4, 154.3, 135.8, 132.3, 131.7, 128.9 (2), 121.9, 121.2, 78.8, 64.2, 61.1, 54.1, 53.5, 52.6, 46.3, 45.6, 41.7, 33.0, 31.7, 30.7, 28.6. LRMS (ESI) m/z [M+H]+ calcd for $C_{33}H_{47}Cl_2N_8O_5$ = 705.30; found = 705.2. *Tert*-butyl 4-((4-(2-(4-(4-(2,6-dichlorobenzamido)-1*H*-pyrazole-3-carboxamido)piperidin-1-yl)acetyl)piperazin-1-yl)methyl)piperidine-1-carboxylate (0.395 mmol) was reacted according to *General Procedure B*, resulting in 4-(2,6-dichlorobenzamido)-*N*-(1-(2-oxo-2-(4-(piperidin-4-ylmethyl)piperazin-1-yl)ethyl)piperidin-4-yl)-1*H*-pyrazole-3-carboxamide hydrochloride without further purification. (tan solid, yield = 99%). 4-(2,6-dichlorobenzamido)-*N*-(1-(2-oxo-2-(4-(piperidin-4-ylmethyl)piperazin-1-yl)ethyl)piperidin-4-yl)-1*H*-pyrazole-3-carboxamide hydrochloride (0.395 mmol) was reacted according to *General Procedure F*. The produce was isolated via gravity column chromatography using a solution of 92 DCM: 7 methanol: 1 ammonium hydroxide, yielding 4-(2,6-dichlorobenzamido)-*N*-(1-(2-(4-((1-(2-(2,6-dioxopiperidin-3-yl)-6-fluoro-1,3-dioxoisoindolin-5-yl)piperidin-4-yl)methyl)piperazin-1-yl)-2-oxoethyl)piperidin-4-yl)-1*H*-pyrazole-3-carboxamide. (green solid, yield = 34%). ^{1}H NMR: (400 MHz, d_6 DMSO) δ13.18 (1H, s), 11.08 (1H, s), 10.15 (1H, s), 8.31 (1H, m), 7.68 (1H, d, *J* = 10.8 Hz), 7.56 (2H, d, *J* = 7.2 Hz), 7.51 (1H, t, *J* = 9.2 Hz), 7.41 (1H, d, *J* = 7.2 Hz), 5.01 (1H, dd, *J* = 4.4 Hz), 3.68 (2H, m), 3.59 (3H, d, *J* = 11.6 Hz), 3.51 (2H, m), 3.42 (3H, m), 3.09 (2H, s), 2.87 (3H, t, *J* = 10.8 Hz), 2.56 (1H, m), 2.31 (4H, m), 2.17 (2H, d, *J* = 6.4 Hz), 2.01 (2H, app. t), 1.66 (8H, m), 1.22 (2H, m). ^{13}C NMR: (500 MHz, d_6 DMSO) δ173.35, 170.50, 168.01, 167.31, 166.81, 163.23, 160.88, 158.85, 156.84, 146.49, 135.97,

133.52, 132.46, 131.87, 129.40, 129.01, 123.34, 122.10, 121.25, 114.23, 112.56, 112.36, 64.30, 61.19, 54.30, 53.71, 52.72, 5.53, 49.66, 46.46, 45.82, 41.88, 32.80, 31.81, 31.57, 30.80, 22.71. HRMS (ESI) m/z [M+H]+ calcd for $C_{41}H_{45}Cl_2FN_{10}O_7$ = 877.2761; found = 877.2748.

Chapter 7: Appendix

7.1 BCL-2 G101V Confers Venetoclax resistance

As discussed previously, BCL-2 upregulation contributes to tumorigenesis and the progression of hematological malignancies.[1-3] Previous studies have yielded promising results for targeting Bcl-2, such as the small molecule venetoclax.[27] However, chemoresistance still remains an issue as patients suffering from chronic lymphocytic leukemia (CLL) who are prescribed venetoclax only receive ~17 months of effective treatment.[32] One resistance mechanism is the upregulation of sister anti-apoptotic proteins, but another explanation is the BCL-2 G101V point mutation that has been found in patients previously treated with venetoclax.[32] In addition to the G101V point mutation, predictive resistance studies in mice demonstrated other Bcl-2 mutations, namely F104C, that causes a ~1500-fold decrease in binding.[202]

7.1.1 BCL-2 Protein Degraders

To combat this point mutation resistance mechanism, we converted venetoclax into a BCL-2 PROTAC. Previous work focused on the conversion of BCL-2 family inhibitors into PROTACs have produced exciting results. By leveraging navitoclax (a dual BCL-xL/2 inhibitor), The Zhou lab have synthesized selective degraders of BCL-xL by utilizing a Von Hippel-Lindau (VHL) E3 ligase ligand, which avoids adverse side effects due to VHL not being expressed in platelet cells.[203] Additionally, this lab demonstrated that navitoclax can be converted into a dual degrader by grafting the linker and E3 ligase ligand off different solvent-exposed regions of the molecule to create a more favorable ternary complex with the POI and E3 ligase.[204] Like navitoclax, venetoclax presents a

solvent exposed tetrahydropyran which does not influence binding to BCL-2.[27] Therefore, by utilizing the venetoclax acid, we grafted on various linkers and E3 ligase ligands as well as creating unprecedented Bcl-2 PROTACs. Additionally, we also added various bulky hydrophobic groups to these linkers to create novel BCL-2 hydrophobic degraders.

7.1.2 Synthesis of BCL-2 Hydrophobic Degraders

Following **Figure 7.1.2.1**, Tert-butyl (2-aminoethyl)carbamate was coupled to various acids by EDCI coupling to produce **2**. Next, the boc group was removed using acidic conditions to create **3**. An S_NAr with the sulfonamide was conducted affording **5**. Finally, this was coupled with the VEN acid using stochiometric amounts of EDCI and DMAP to yield the final representative inhibitor **6**. Another set of hydrophobic degraders were created in the same manner described before using tert-butyl (2-(2-(2-aminoethoxy)ethoxy)ethyl)carbamate to ultimately give representative compound **10**.

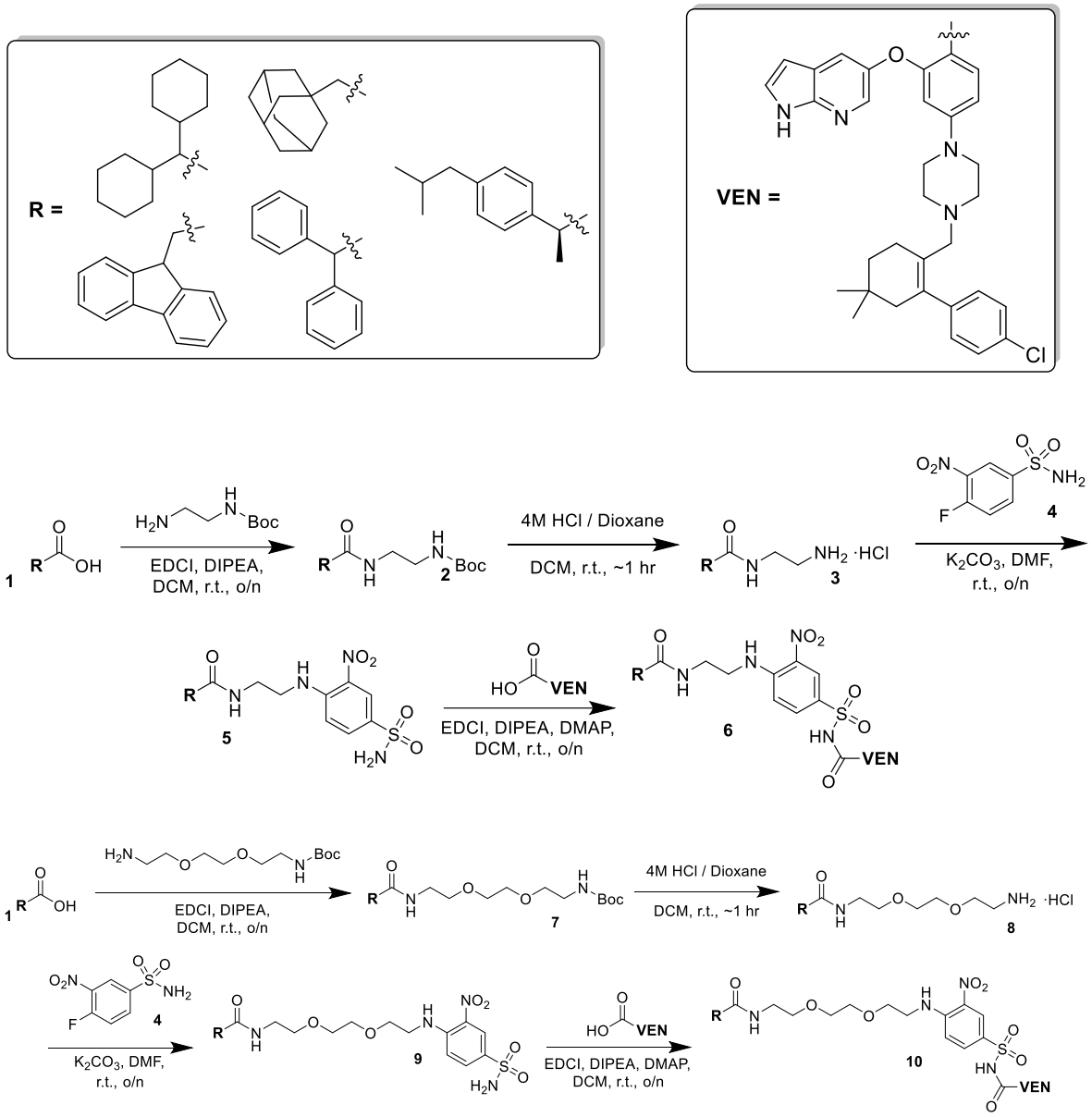

***Figure 7.1.2.1**: Synthesis of BCL-2 Hydrophobic Degraders*

7.1.3 Synthesis of First Generation BCL-2 PROTACs

From **Figure 7.1.3.1**, modified version of Thalidomide was prepared from **11** in which the alcohol was alkylated and the resulting tert-butyl ester was cleaved under acidic conditions to give **13**. Following this, **4** was reacted with numerous amines via S_NAr after

which ven acid was coupled to create **15**. The boc group was removed and the free amine was reacted with **13** via HATU coupling affording four final BCL-2 PROTACs represented by compound **17**. In a similar manner described above, free amines were reacted with idasanutlin via HATU coupling conditions to yield two additional BCL-2 PROTACs represented by compound **18** (**Figure 7.1.3.2**). Three more BCL-2 PROTACs were synthesized utilizing a modified VHL-1 ligand acid, which was formed by reacting the ligand with dihydrofuran-2,5-dione to yield **20**. After a series of SNAr, HATU couplings, and Boc deprotections the prepared amines were coupled to the VHL-1 ligand acid to form our final three BCL-2 PROTACs for this series in compounds **24**, **27** and **30** (**Figure 7.1.3.3**).

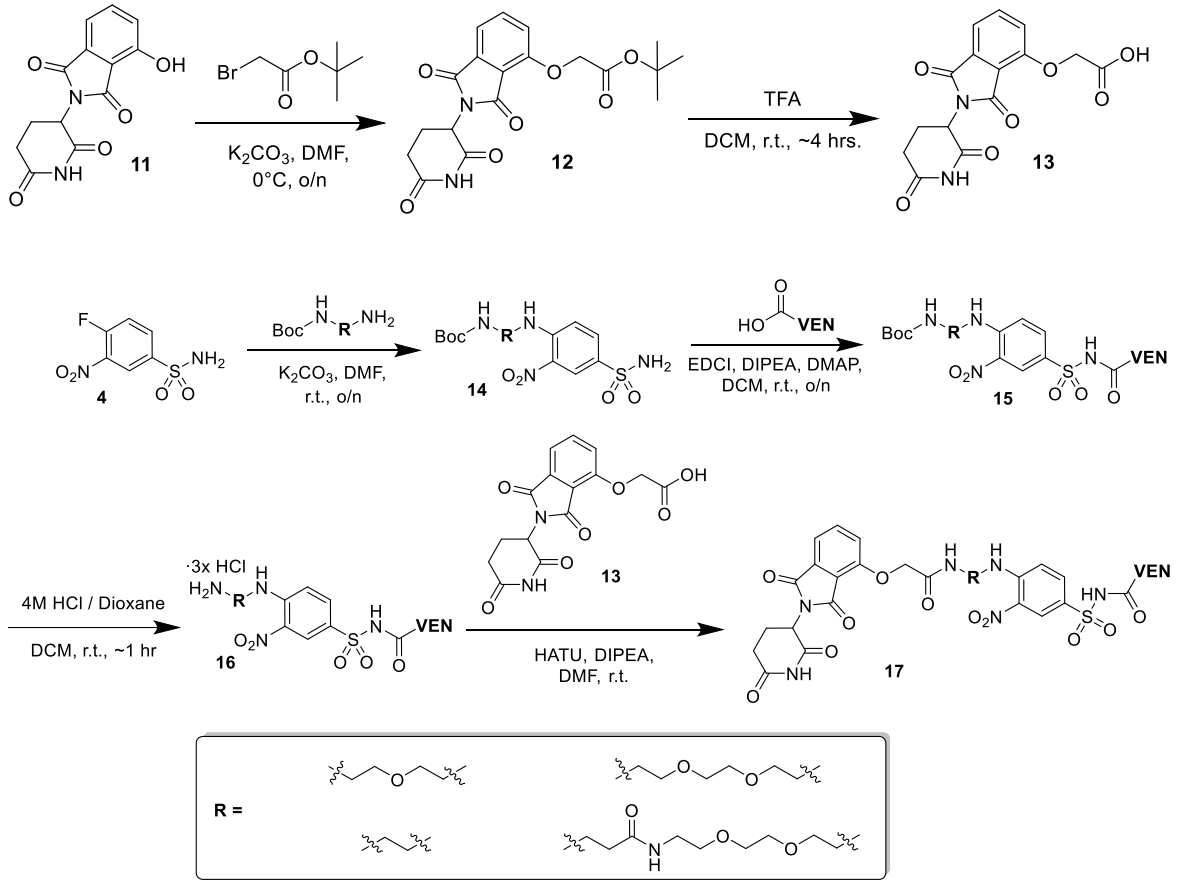

***Figure 7.1.3.1**: Synthesis of BCL-2 Thalidomide PROTACs*

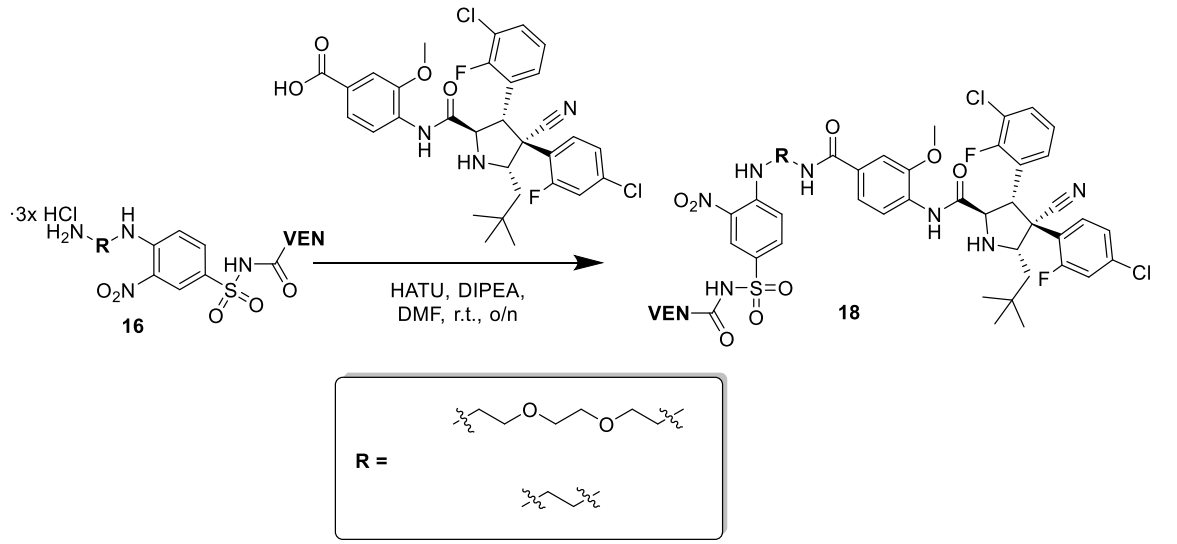

Figure 7.1.3.2: *Synthesis of BCL-2 Idasanutlin PROTACs*

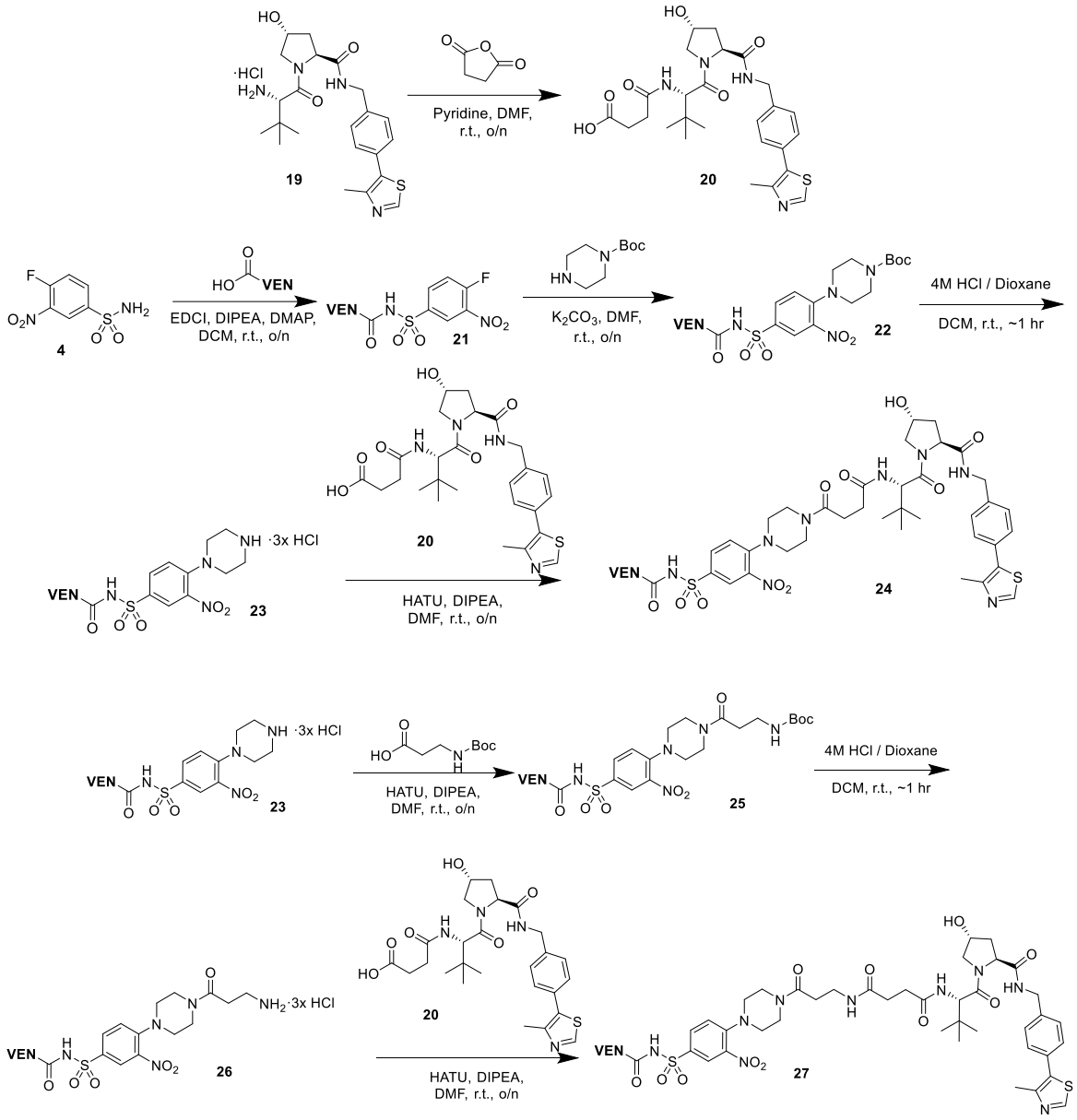

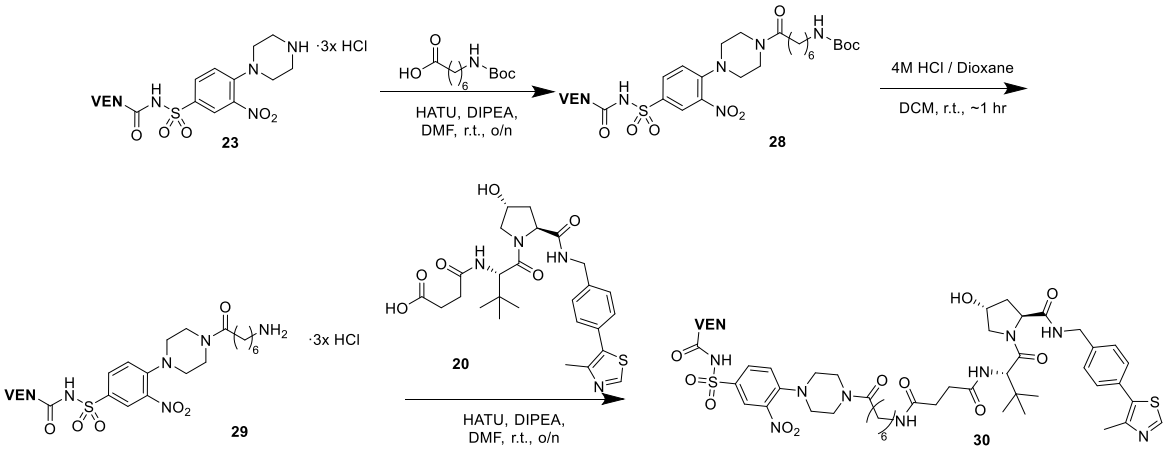

Figure 7.1.3.3: *Synthesis of BCL-2 VHL-1 Ligand PROTACs*

7.1.4 Final Compound Structures of Hydrophobic Degraders and first Generation BCL-2 PROTACs

Below are the 19 final compounds which have been synthesized and were tested in cell-free and cell assays (**Figure 7.1.4.1**).

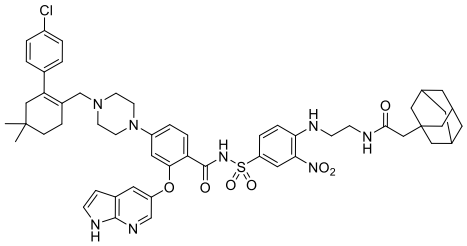

SF-7-330

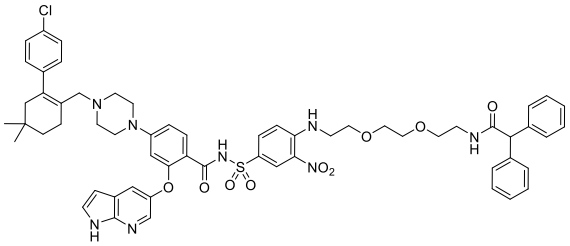

CG-2-132

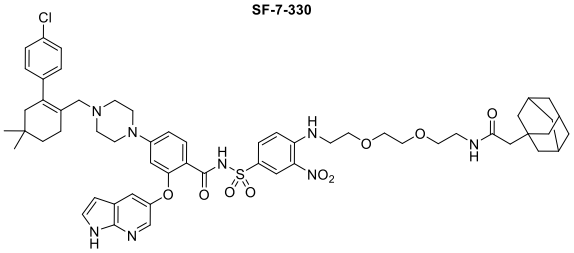

CG-3-003

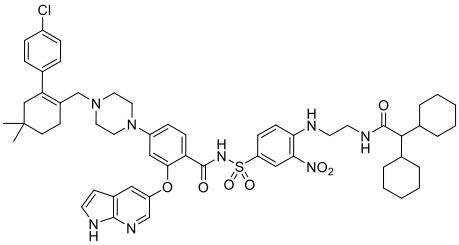

SF-8-108

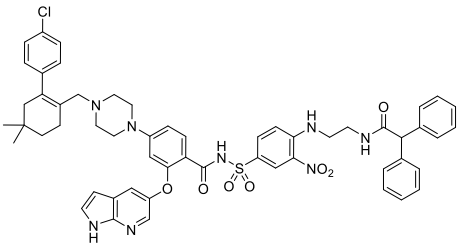

CG-3-004

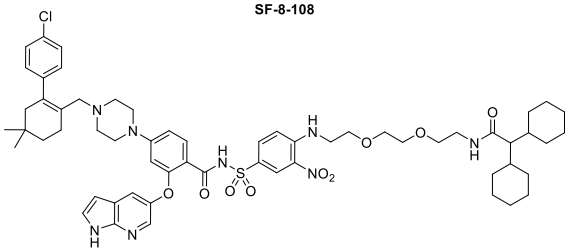

CG-3-051

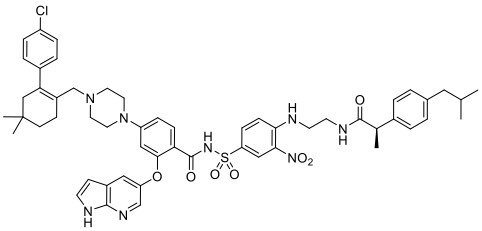

CG-3-006

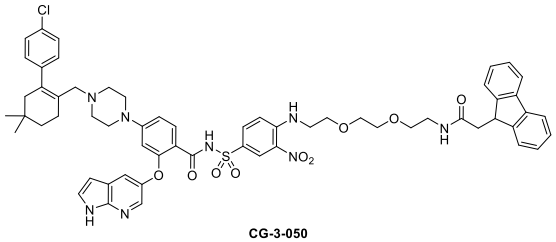

CG-3-050

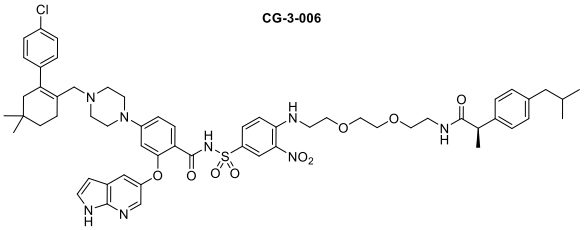

CG-3-005

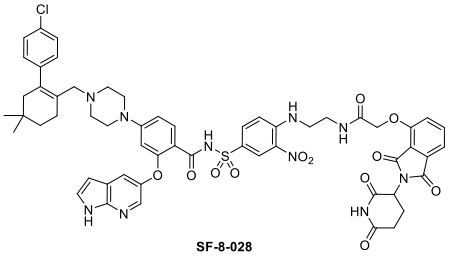

SF-8-028

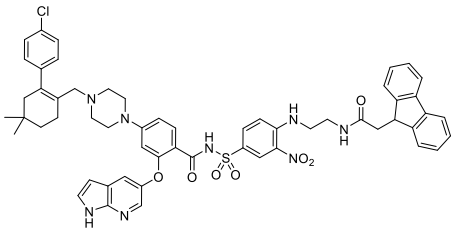

CG-3-058

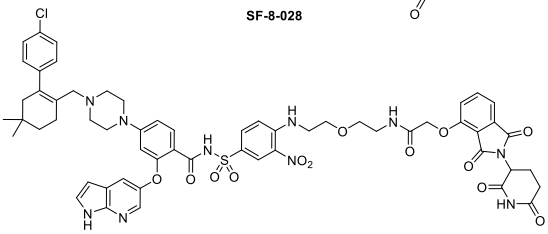

SF-8-033

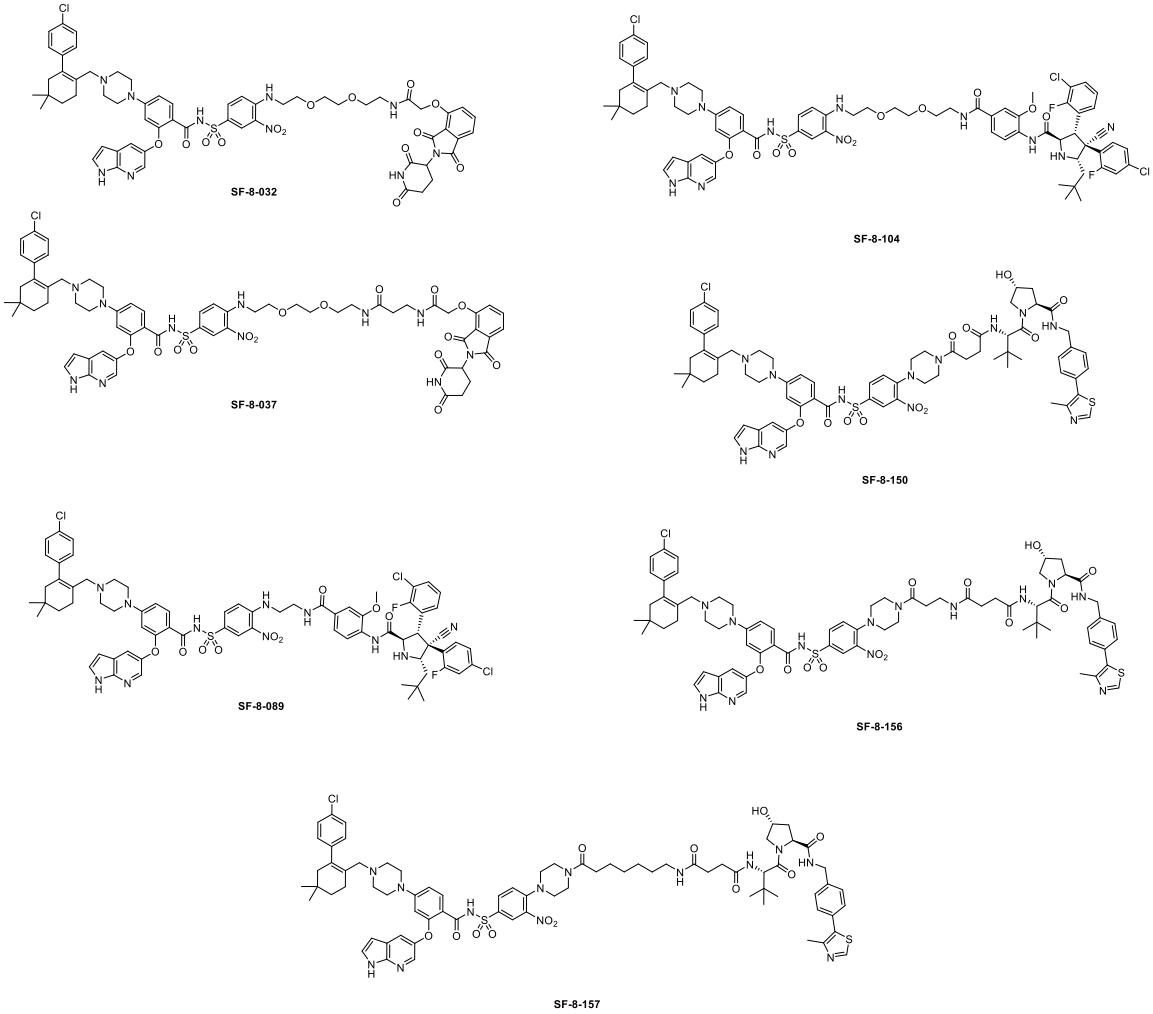

Figure 7.1.4.1: *Final structures of BCL-2 hydrophobic degraders and first generation BCL-2 PROTACs*

7.1.5 Nanosyn Testing of Hydrophobic Degraders and 1st Generation BCL-2 PROTACs

We had 5 compounds, which were either BCL-2 hydrophobic degraders or 1st generation BCL-2 PROTACs, tested by Nanosyn in a TR-FRET cell-free assay to see if there was a loss in potency of venetoclax against BCL-2 due to the conversion of the compound into a hydrophobic degrader or a PROTAC (**Figure 7.1.5.1**). All of our compounds tested demonstrated low nM IC_{50} against BCL-2 and testing continued in cells.

Compound Name	Linker	Head Group	IC_{50} (nM)
CG-3-003	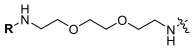		0.426 ± 0.126
CG-3-006		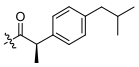	1.44 ± 0.218
SF-8-028		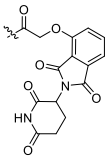	0.439 ± 0.138
SF-8-104	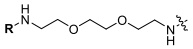	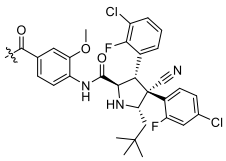	11.5 ± 1.78
SF-8-157	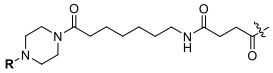	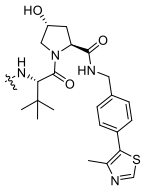	0.5 ± 0.0922
Venetoclax			0.391 ± 0.0566

R =

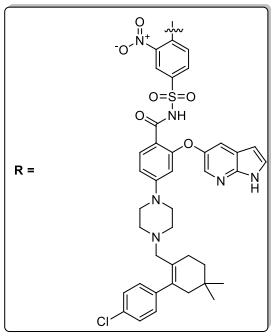

Figure 7.1.5.1: *IC50 values of BCL-2 hydrophobic degraders and first generation PROTACs*

7.1.6 AlamarBlue testing of Hydrophobic Degraders and first Generation BCL-2 PROTACs

Next, we tested our compounds in multiple AlamarBlue cell viability assays to examine our compounds potency in cells (**Figure 7.1.6.1-7.1.6.5**). Cell lines used included AML cell lines MOLM14, MOLM14 empty vector, MOLM14 WT BCL-2 overexpressing cells, MOLM14 G101V BCL-2, and MOLM14 F104C BCL-2. None of the tested compounds outperformed the venetoclax control.

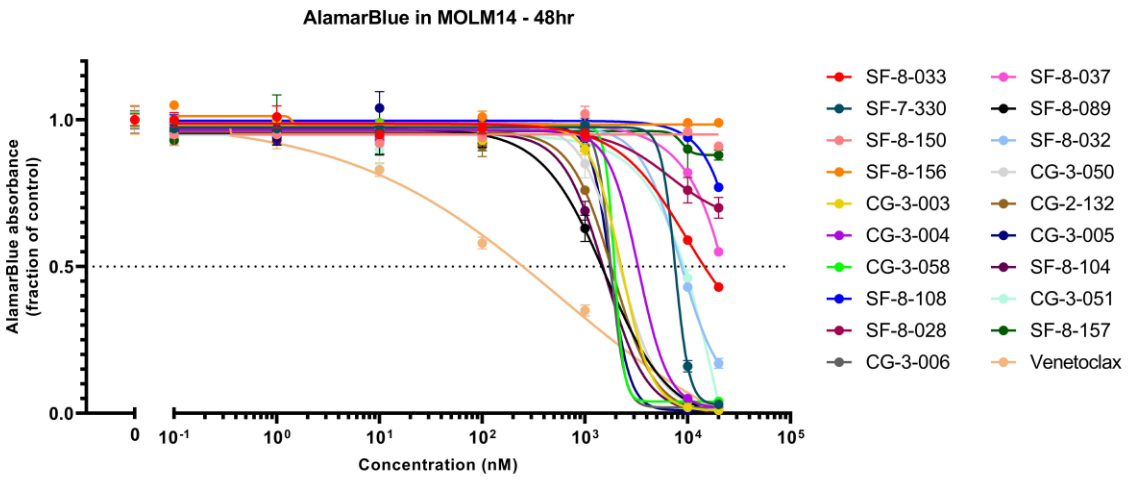

Figure 7.1.6.1: *Anti-proliferation effects of BCL-2 hydrophobic degraders and first generation PROTACs in MOLM14 cells*

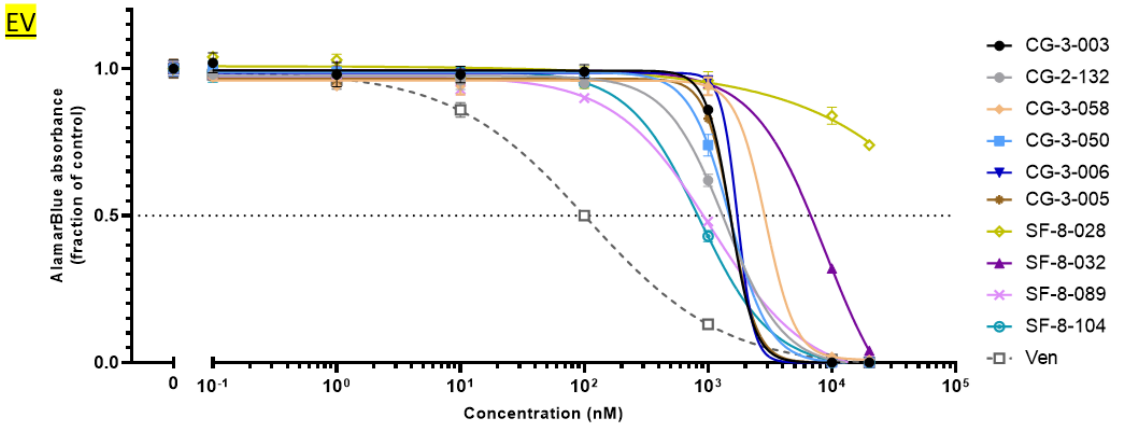

Figure 7.1.6.2: *Anti-proliferation effects of BCL-2 hydrophobic degraders and first generation PROTACs in EV MOLM14 cells*

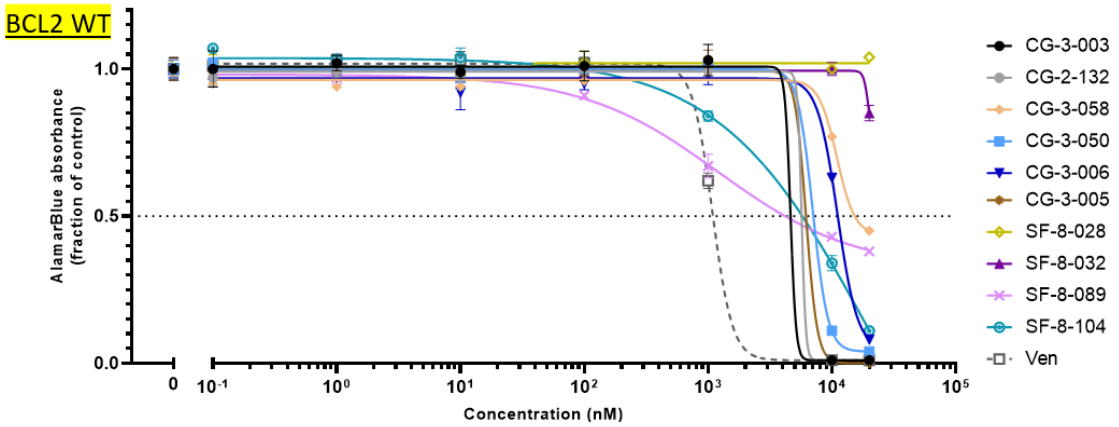

Figure 7.1.6.3: *Anti-proliferation effects of BCL-2 hydrophobic degraders and first generation PROTACs in BCL-2 overexpressing MOLM14 cells*

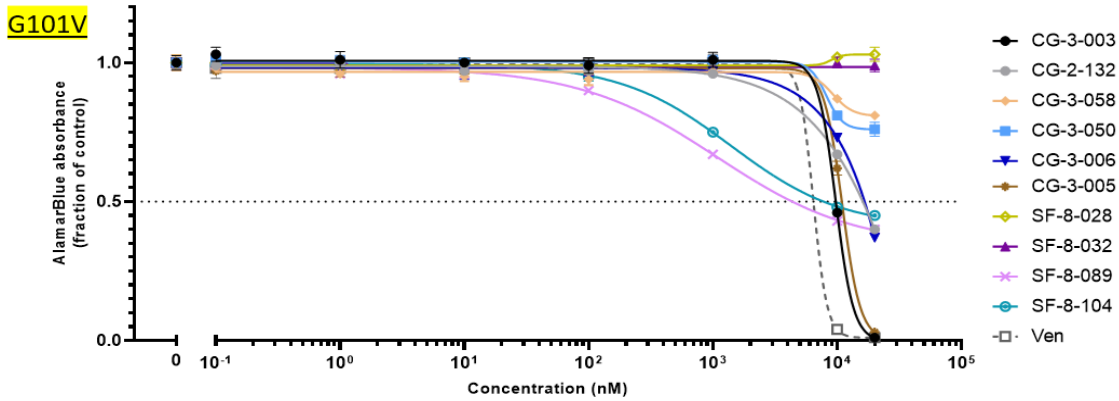

Figure 7.1.6.4: *Anti-proliferation effects of BCL-2 hydrophobic degraders and first generation PROTACs in G101V BCL-2 overexpressing MOLM14 cells*

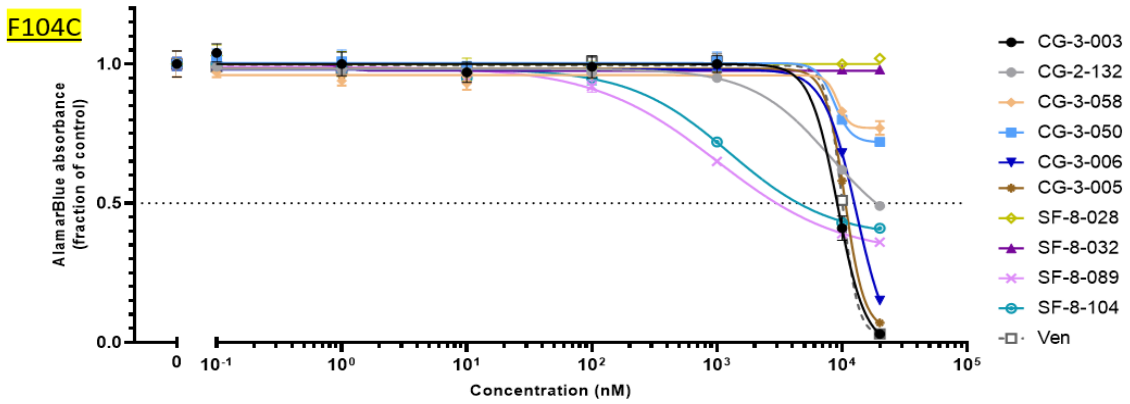

Figure 7.1.6.5: *Anti-proliferation effects of BCL-2 hydrophobic degraders and first generation PROTACs in F104C BCL-2 overexpressing MOLM14 cells*

7.1.7 Synthesis of second generation BCL-2 PROTACs

After the poor cell potency demonstrated by the hydrophobic degraders and 1st generation BCL-2 PROTACs, efforts started to develop another generation of BCL-2 PROTACs (**Figure 7.1.7.1-7.1.7.6**). Starting with the linker synthesis, amines were either purchased or underwent standard transformations to produce compounds **33**, **41**, **47**, **56** and **64**. Once prepared, these linkers were then coupled to idasanutlin or 2-(2,6-dioxopiperidin-3-yl)-5,6-difluoroisoindoline-1,3-dione to create eight 2nd generation BCL-2 PROTACs in compounds **34**, **42**, **48**, **49**, **50**, **51**, **57** and **65**.

Our final BCL-2 PROTAC utilized bestatin as the E3 ligase ligand (**Figure 7.1.7.7**). First we Boc protected bestatin then performed a HATU coupling followed by a boc deprotection to afford **67**. To create a control compound, we took our boc bestatin and coupled to piperidine which then had the boc group removed to give **70**.

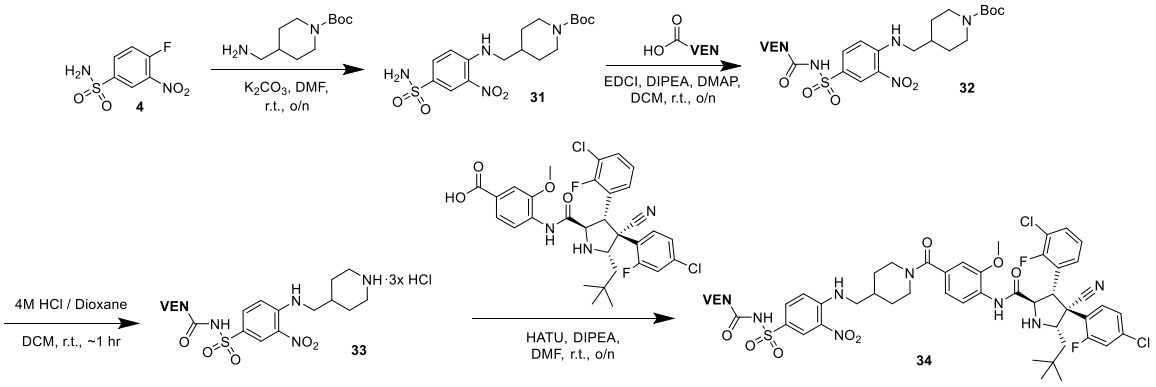

Figure 7.1.7.1: *Synthesis of CG-3-228*

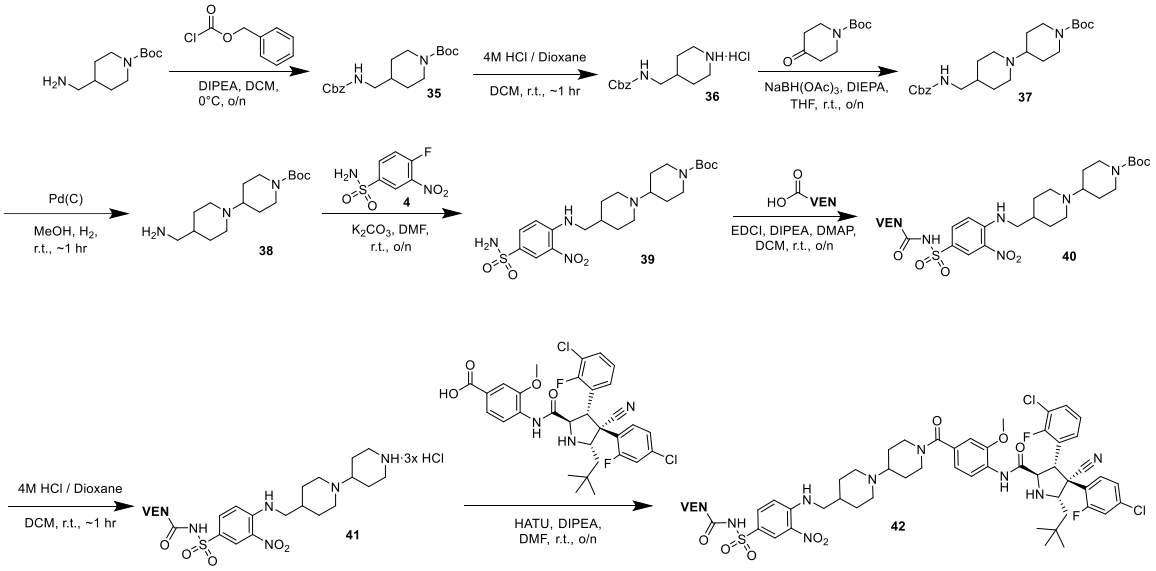

Figure 7.1.7.2: *Synthesis of CG-3-227*

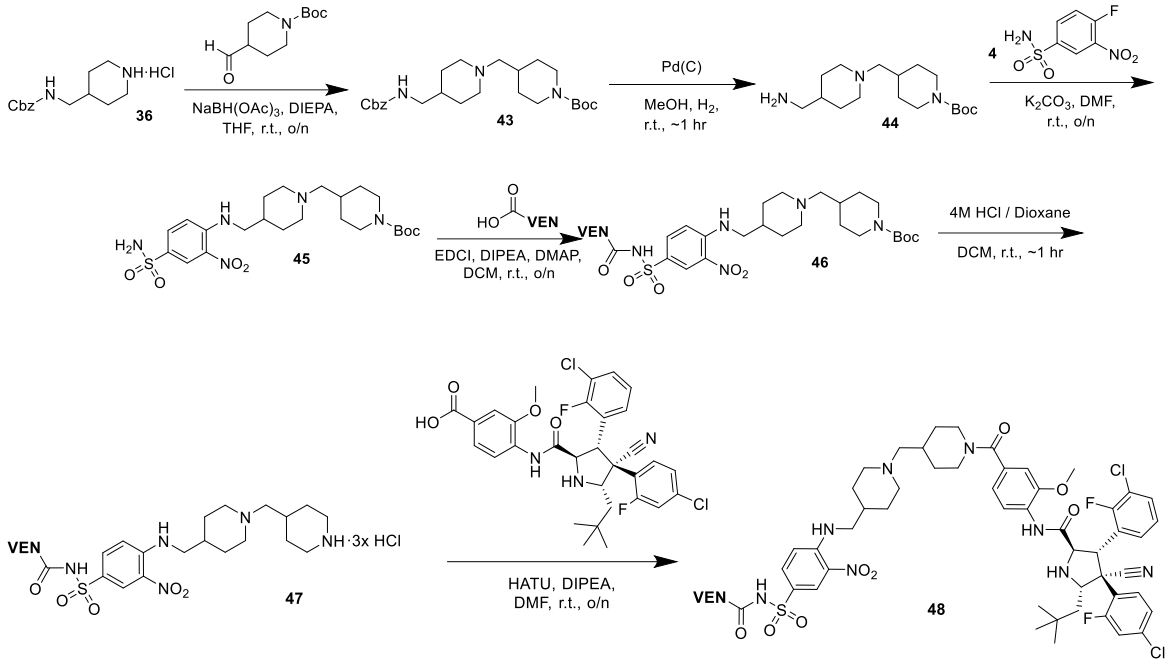

Figure 7.1.7.3: *Synthesis of CG-3-229*

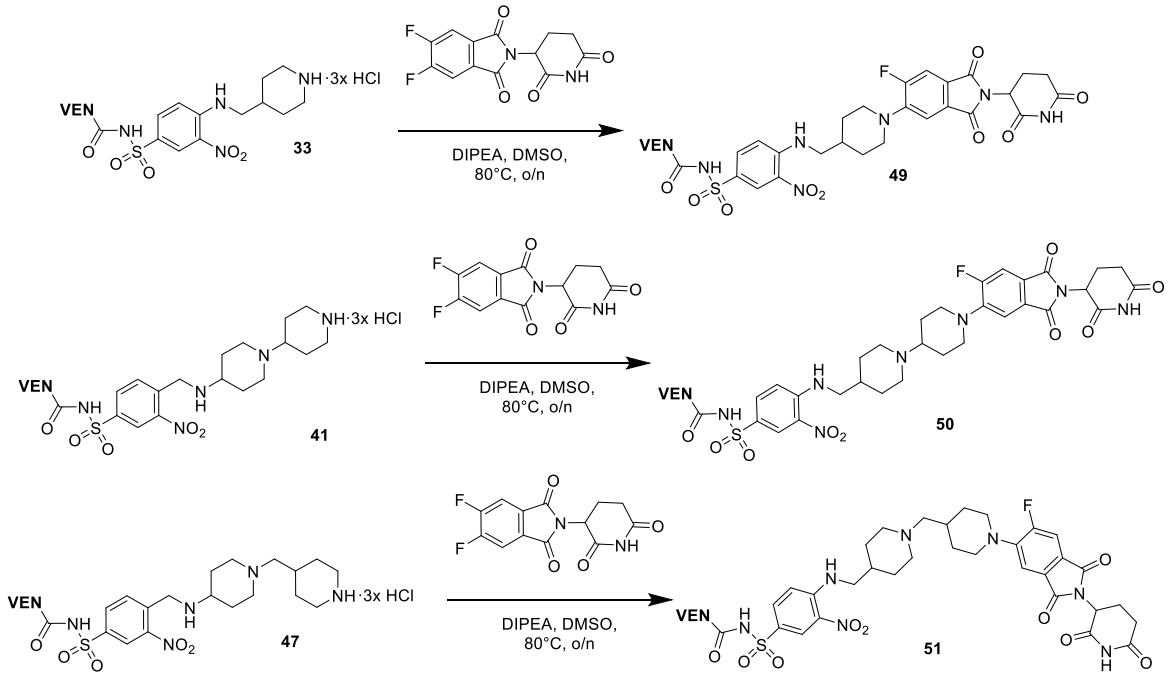

Figure 7.1.7.4: *Synthesis of CG-3-247, CG-3-248, & CG-3-249*

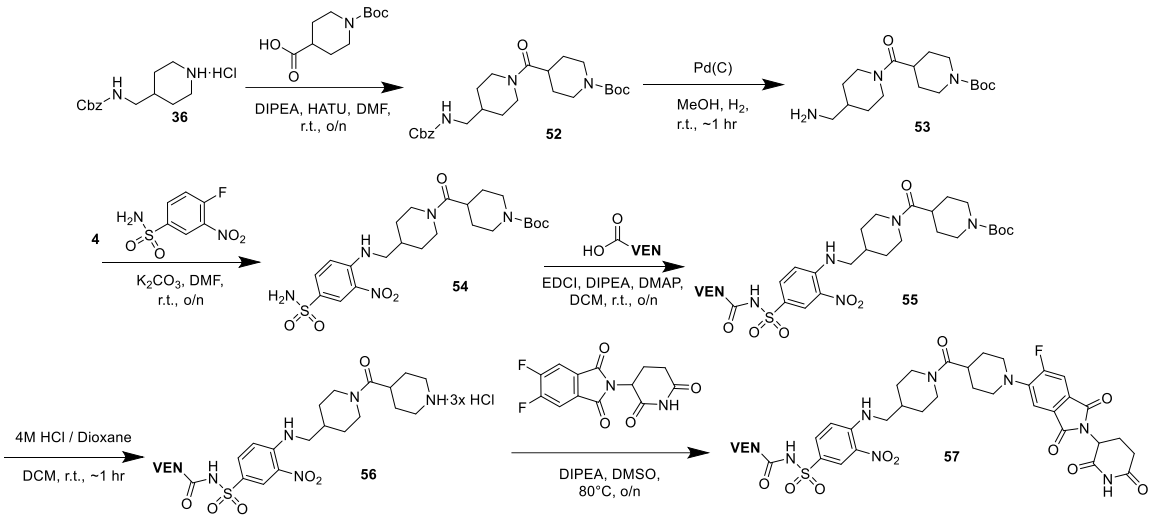

Figure 7.1.7.5: *Synthesis of CG-4-028*

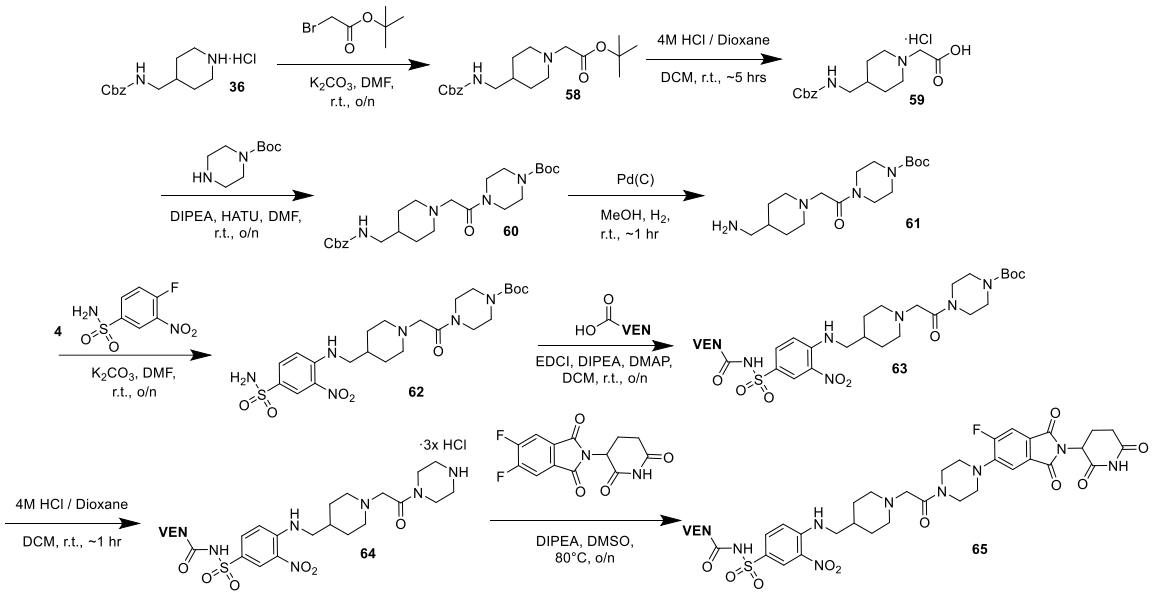

Figure 7.1.7.6: *Synthesis of CG-4-046*

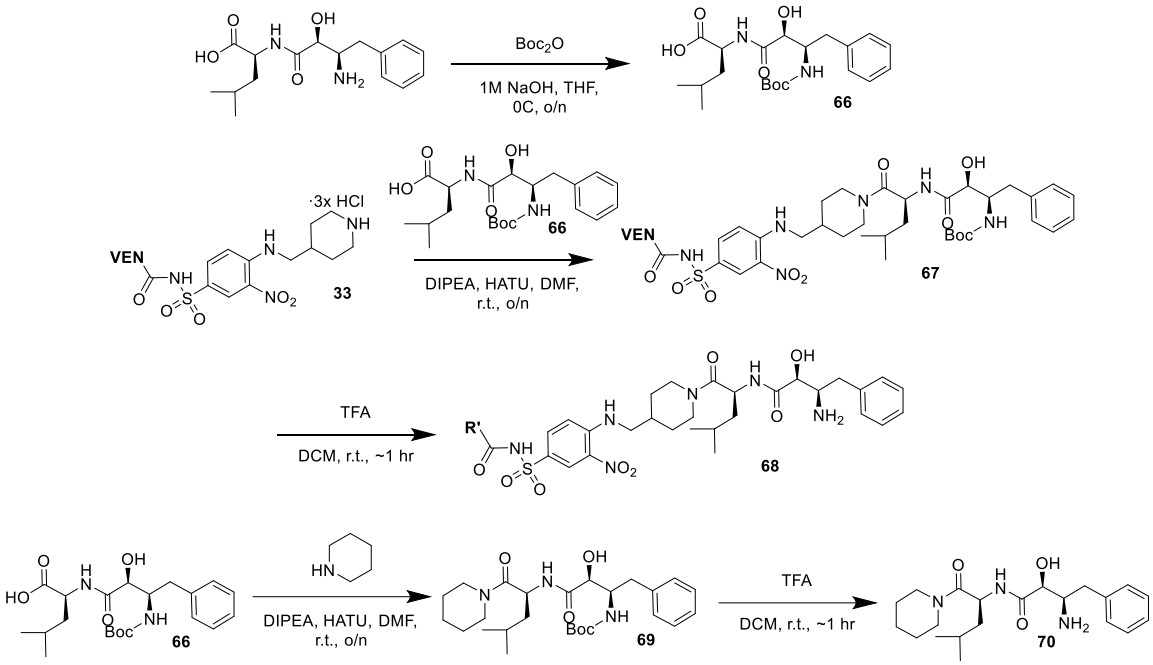

Figure 7.1.7.7: *Synthesis of CG-4-245 & CG-4-246 (control)*

7.1.8 Final Compound Structures of second generation BCL-2 PROTACs

Below are the nine final compounds of the 2nd generation BCL-2 PROTACs. All compounds were fully synthesized and tested in cell assays (**Figure 7.1.8.1**).

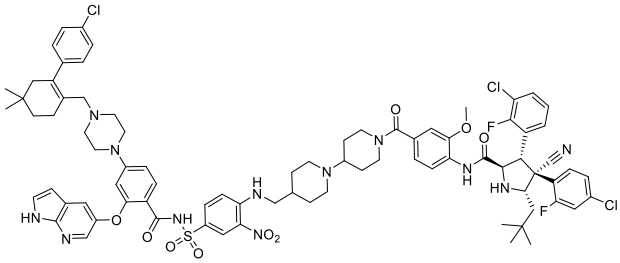

CG-3-227

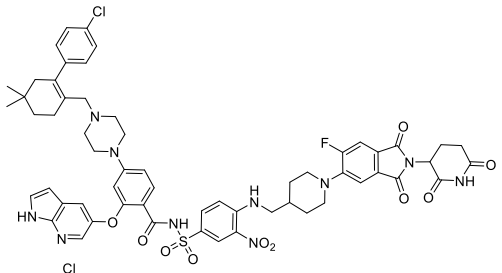

CG-3-247

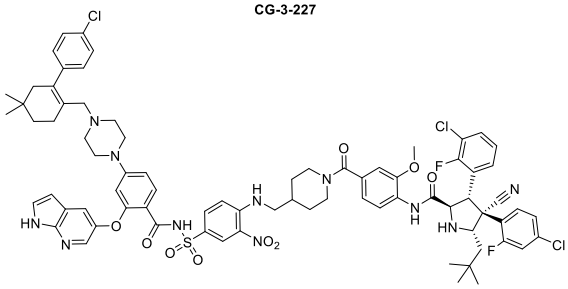

CG-3-228

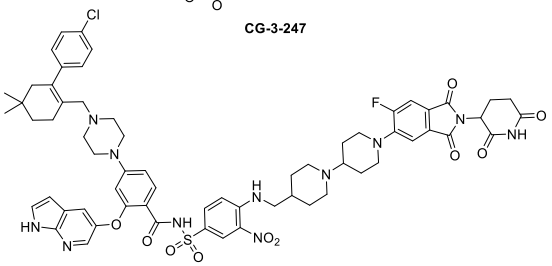

CG-3-248

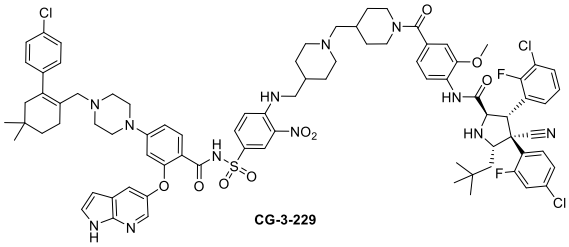

CG-3-229

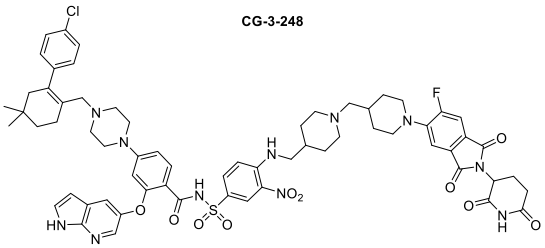

CG-3-249

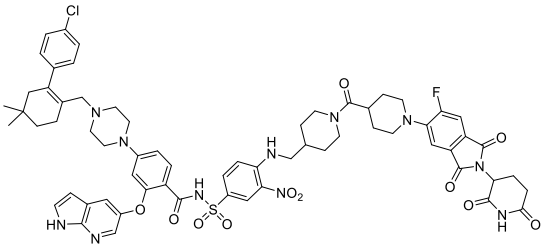

CG-4-028

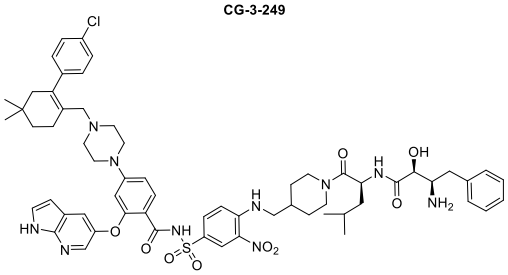

CG-4-245

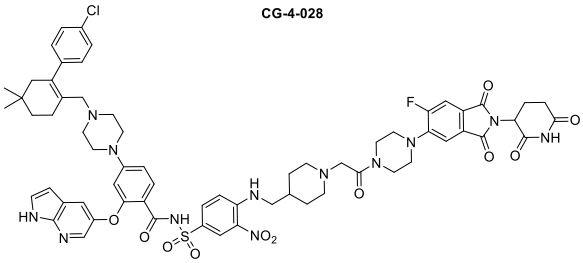

CG-4-046

Figure 7.1.8.1: *Final structures of BCL-2 second generation BCL-2 PROTACs*

7.1.9 AlamarBlue testing of second generation BCL-2 PROTACs

We then conducted AlamarBlue cell viability assays, using MOLM14 AML cells, MV4;11 AML cells and MV4;11 AML cells overexpressing BCL-2, on these 2nd generation BCL-2 PROTACs (**Figure 7.1.9.1-7.1.9.5**).

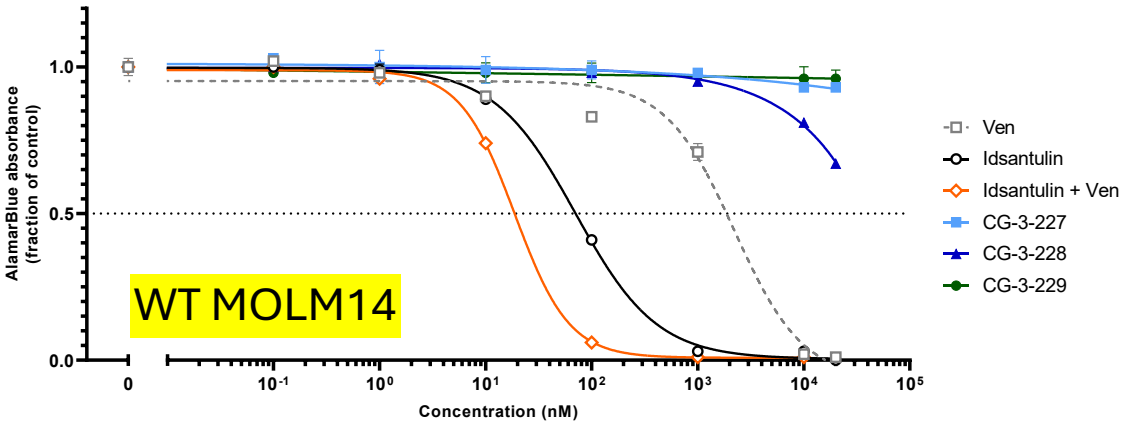

Figure 7.1.9.1: *Anti-proliferation effects of BCL-2 second generation PROTACs in MOLM14 cells*

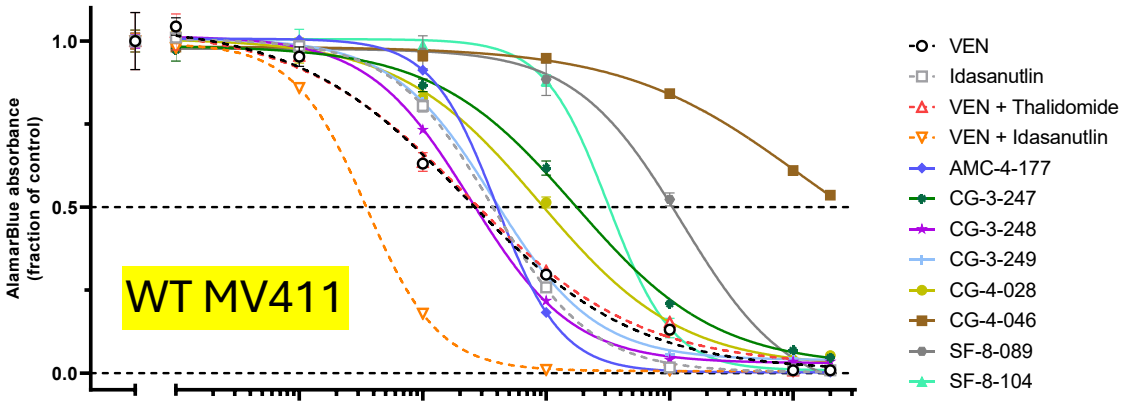

Figure 7.1.9.2: *Anti-proliferation effects of BCL-2 second generation PROTACs in MV;411 cells*

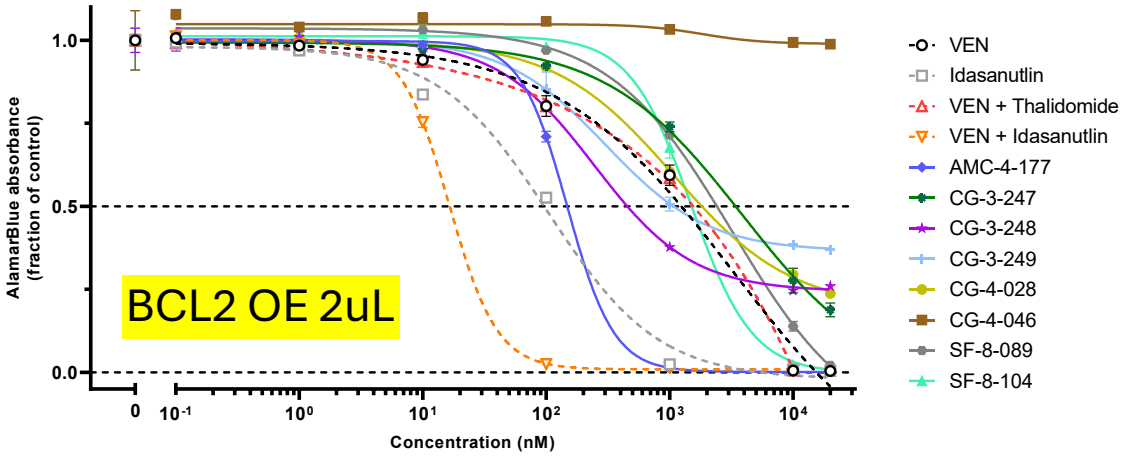

Figure 7.1.9.3: *Anti-proliferation effects of BCL-2 second generation PROTACs in BCL-2 OE MV4;11 cells*

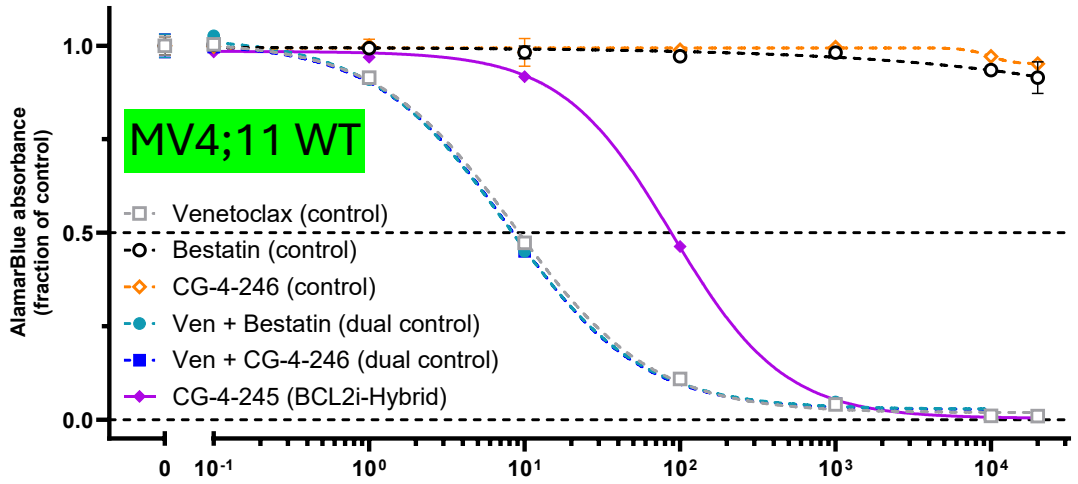

Figure 7.1.9.4: *Anti-proliferation effects of BCL-2 second generation PROTACs in MV4;11 cells*

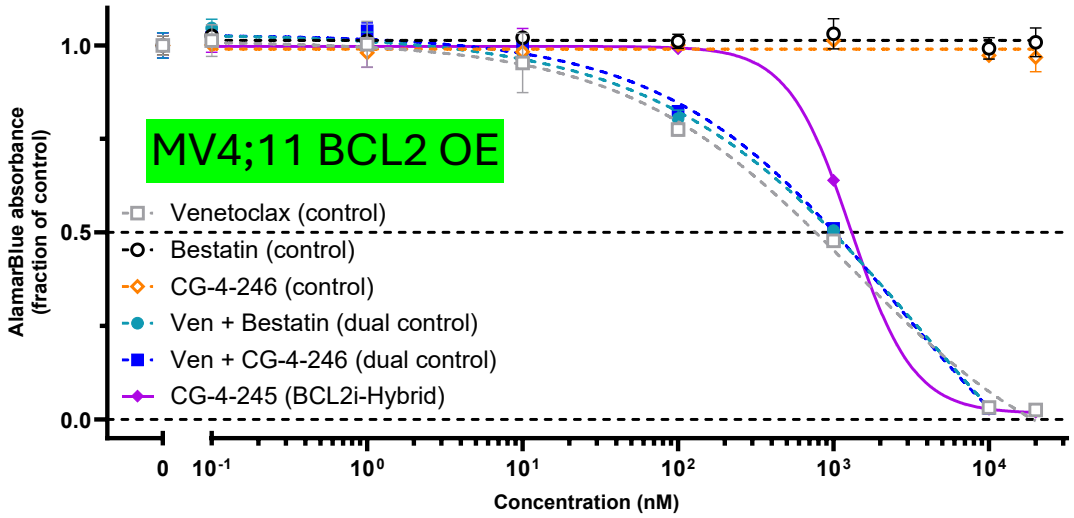

Figure 7.1.9.5: *Anti-proliferation effects of BCL-2 second generation PROTACs in BCL-2 OE MV4;11 cells*

7.2.10 Conclusions and Future Directions

All compounds synthesized have been tested *in vitro* with none of our proposed compounds outperforming control compounds. Future efforts will focus on grafting the linker and E3 ligase ligand off a different position on venetoclax.

7.2 BFL-1 Upregulation Causes Tumorigenesis and Venetoclax Resistance

Multiple cancers can highjack the intrinsic apoptotic pathway and promote tumorigenesis via the upregulation of anti-apoptotic proteins.[1-3] Attempts at directly targeting anti-apoptotic proteins have resulted in venetoclax, an FDA-approved drug, which is a small molecule selective inhibitor for BCL-2.[27] Unfortunately, patients develop resistance within two years of taking venetoclax due to cancer cells upregulating different anti-apoptotic proteins.[27] BFL-1 is a sister anti-apoptotic protein that has been linked to venetoclax resistance due to upregulation of the protein.[205] Compared to the other anti-apoptotic proteins, BFL-1 has received less attention despite being overexpressed in leukemias, lymphomas, and melanomas.[44]

7.2.1 BFL-1 Covalent Inhibitors

The challenge of developing selective inhibitors for anti-apoptotic proteins stems from the fact that each sister protein has a similar BH3 binding groove.[1-3] Fortunately, we can leverage the differences in BFL-1's binding groove to aid in our design of a selective inhibitor.[44] Within the binding groove of BFL-1, there is a unique solvent exposed cysteine residue (Cys55).[44] Other groups targeting BFL-1 have utilized mildly reactive electrophilic warheads for their inhibitor design.[45,46,48] These covalent inhibitors work by first interacting with the protein via noncovalent interactions, and then once bound these warheads react with cysteine residues to create an irreversible covalent bond between the inhibitor and protein.[45,46,48] This design of using mildly reactive electrophilic warheads that only initiate bond formation once in the correct orientation has been associated with less off-target effects.[102]

7.2.2 Inhibitor Design

Because of the lack of any FDA-approved BFL-1 inhibitors, we collaborated with the MacKerell lab and Dr. Mingtian Zhao conducted SILCS simulations on the BFL-1 protein.[197] From this, we conducted a virtual high-throughput screen against the BFL-1 FragMaps to obtain distinct chemical motifs that were predicted to have favorable binding.[197] Additionally, we also utilized previously explored scaffolds that had a high affinity for multiple anti-apoptotic proteins and explored converting those compounds into selective BFL-1 inhibitors by grafting on an electrophilic warhead.[197]

7.2.3 Synthesis of first generation BFL-1 inhibitors

Starting with synthesizing our library of 1st generation BFL-1 inhibitors (**Figure 7.2.3.1**), 5-(dimethylamino)naphthalene-1-sulfonyl chloride and 1,2,3,4-tetrahydroquinoline-8-carboxylic acid were coupled to 2-morpholinoethan-1-amine to create **1** and **2**. Next, 2-(adamantan-1-yl)acetic acid underwent a HBTU mediated coupling with methyl piperidine-4-carboxylate hydrochloride and saponified to yield **4**. 2,4-dichlorothiazole-5-carbaldehyde was oxidized with oxone and was coupled to two amines to afford **7**. Standard transformations on ethyl 2-amino-4-methylthiazole-5-carboxylate created compounds **9** and **11**. Next, 3-methyl-4-nitro-1H-pyrazole-5-carboxylic acid was converted into a methyl ester and an alkylation with 1-iodo-2-methylpropane yielded two distinct products via TLC. These two products correspond to the N-1 and N-2 mono alkylated isomers which were reacted separately to create two product isomers represented by compound **16**. Another set of standard transformations were conducted with methyl 1-methyl-4-nitro-1H-pyrazole-5-carboxylate to create **19**.

Our first BFL-1 inhibitor with an electrophilic warhead was created by using 1H-indazole-3-carboxylic acid and through an EDCI coupling, boc deprotection, and acylation afforded **22**. Another covalent inhibitor was formed by reacting 1-hydroxy-2-naphthoic acid with chlorosulfonic acid to create a key intermediate **23** that will be used to make multiple inhibitors. **23** was then transformed to form **25** which was acylated with two different acid chlorides to make **26** and **27**.

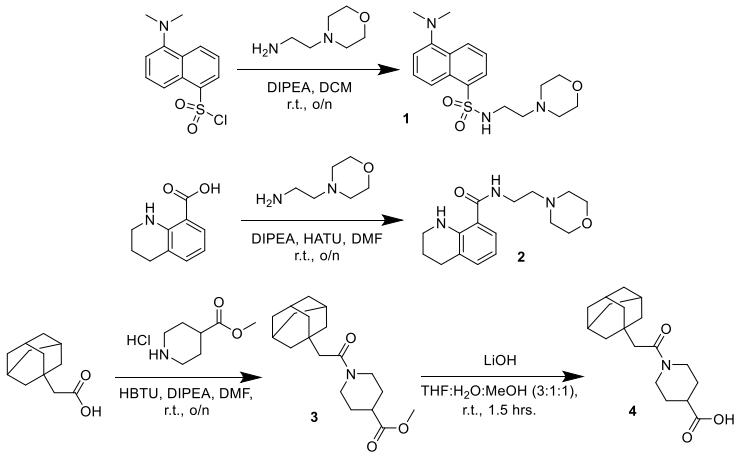

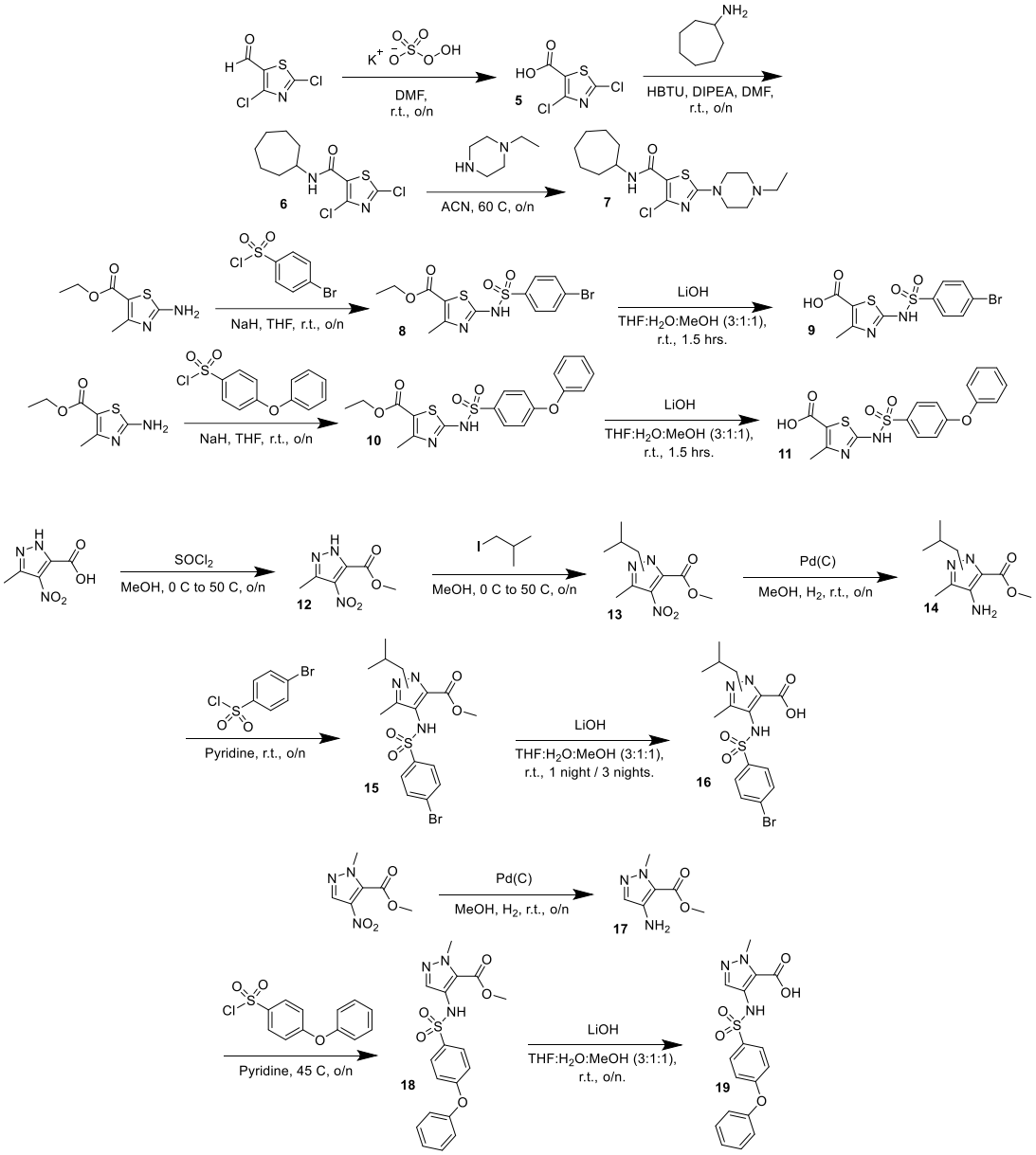
DMF, r.t., o/n
5
HBTU, DIPEA, DMF, r.t., o/n
6
ACN, 60 C, o/n
7
NaH, THF, r.t., o/n
8
LiOH
THF:H2O:MeOH (3:1:1), r.t., 1.5 hrs.
9
NaH, THF, r.t., o/n
10
LiOH
THF:H2O:MeOH (3:1:1), r.t., 1.5 hrs.
11
SOCl2
MeOH, 0 C to 50 C, o/n
12
MeOH, 0 C to 50 C, o/n
13
Pd(C)
MeOH, H2, r.t., o/n
14
Pyridine, r.t., o/n
15
LiOH
THF:H2O:MeOH (3:1:1), r.t., 1 night / 3 nights.
16
Pd(C)
MeOH, H2, r.t., o/n
17
Pyridine, 45 C, o/n
18
LiOH
THF:H2O:MeOH (3:1:1), r.t., o/n.
19

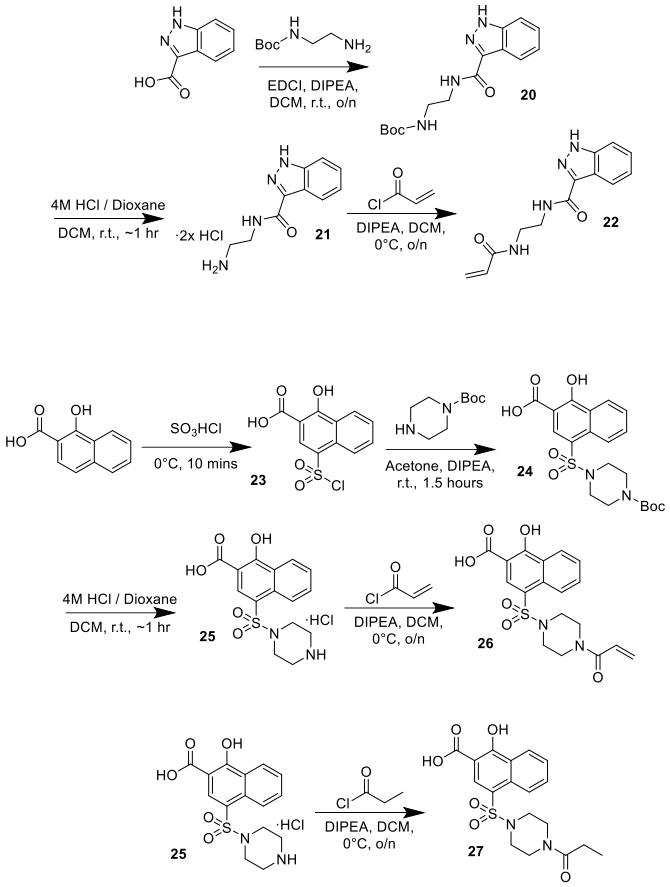

Figure 7.2.3.1: *Synthesis of first generation BFL-1 inhibitors*

7.2.4 Final Compound Structures of 1st generation BFL-1 inhibitors

Below are the 15 final compounds (**Figure 7.2.4.1**). The library was fully synthesized and tested in a cell-free assay. SF-5-290, JY-5-371 and LC-4-118 are pan BCL-2 inhibitors that were included in this series of testing.

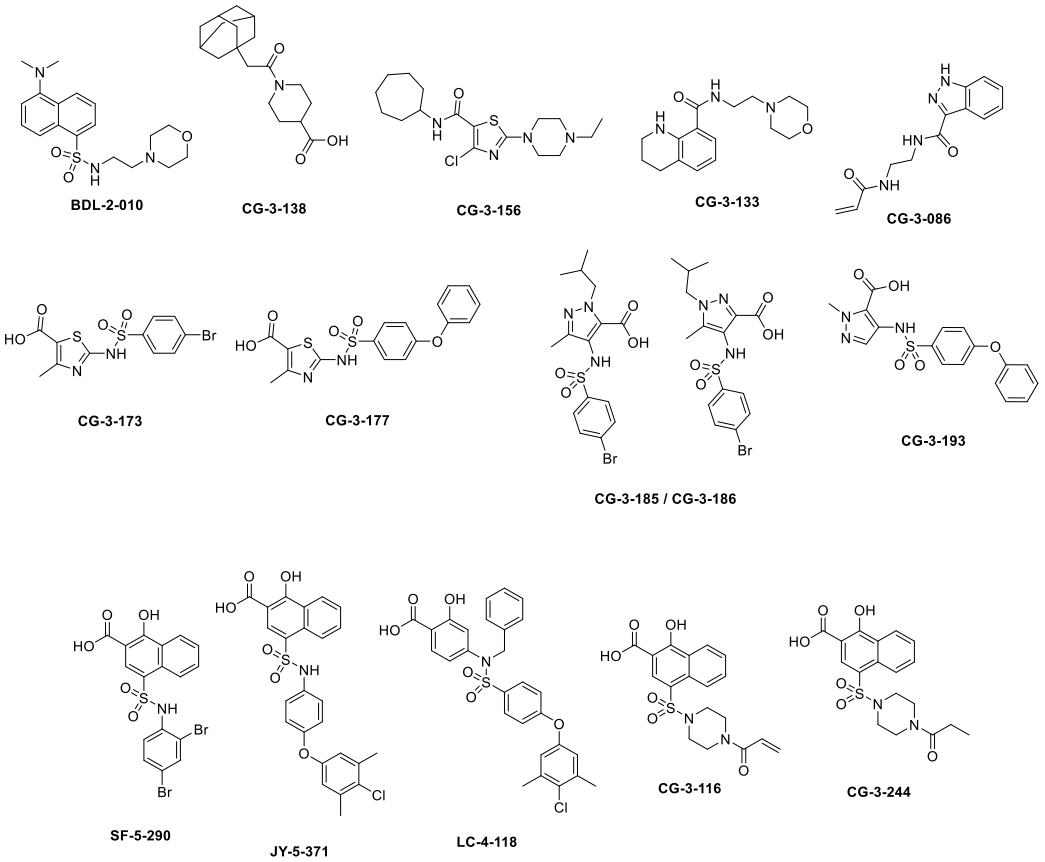

Figure 7.2.4.1: *Final structures of first generation BFL-1 inhibitors*

7.2.5 Cell Free Testing of 1st generation BFL-1 inhibitors

Compounds were tested by Nanosyn in a TR-FRET cell-free assay to measure their IC_{50} against BFL-1 (**Table 7.2.5.1**). From this, we identified CG-3-116 as a lead compound to further optimize through a structure activity relationship (SAR) approach.

Compound Name	BFL1 IC_{50} (mM)	30-min BFL1 IC_{50} (mM)	2-hour BFL1 IC_{50} (mM)
Sabutoclax	0.588		
BDL-2-010	>100	>300	>300

CG-3-086	>100	>300	>300
CG-3-116	0.258	0.301	0.248
CG-3-133	>100	>300	>300
CG-3-138	>100	>300	>300
CG-3-156	>100	>300	>300
CG-3-173	>100	>300	>300
CG-3-177	>100	806	1010
CG-3-185	>100	921	551
CG-3-186	>300		
CG-3-193	>100	907	804
CG-3-244	410		
SF-5-290	>300		
LC-4-118	116		
JY-5-371	20.9		

Table 7.2.5.1: *IC50 values of first generation BFL-1 inhibitors*

7.2.6 Synthesis of CG-3-116 SAR Compounds

Towards optimizing CG-3-116, we conducted an SAR approach to determine what areas of the compound were crucial for the compound to bind to BFL-1. Following **Figure 7.2.6.1**, we started with 1-hydroxy-2-naphthoic acid and the acid was methylated and the same transformations to create **26** were carried to ultimately resulting in **32**. **23** was utilized and alkylated with multiple amines to synthesize representative compound **33**, a boc deprotection and acylated proceeded and eight final compounds were synthesized

represented by **35**. After this, two diamines were mono-acylated with the acrylamide warhead and reacted with **23** to form **37** and **39**. N-boc piperazine was HATU coupled to two elongated acrylamides containing a tertiary amine and ultimately coupled to **23** affording **42** and **45**. Next a benzoic acid and salicylic acid underwent standard transformations to create **48** which represents two final compounds. **24** was taken and doubly alkylated to create intermediate **49** which was then converted into **51**. Finally, **24** was transformed into a tert-butyl ester and the hydroxy group was methylated forming intermediate **53**. From **53**, the tert-butyl group was removed and the resulting product was acylated with the acrylamide to create **55**.

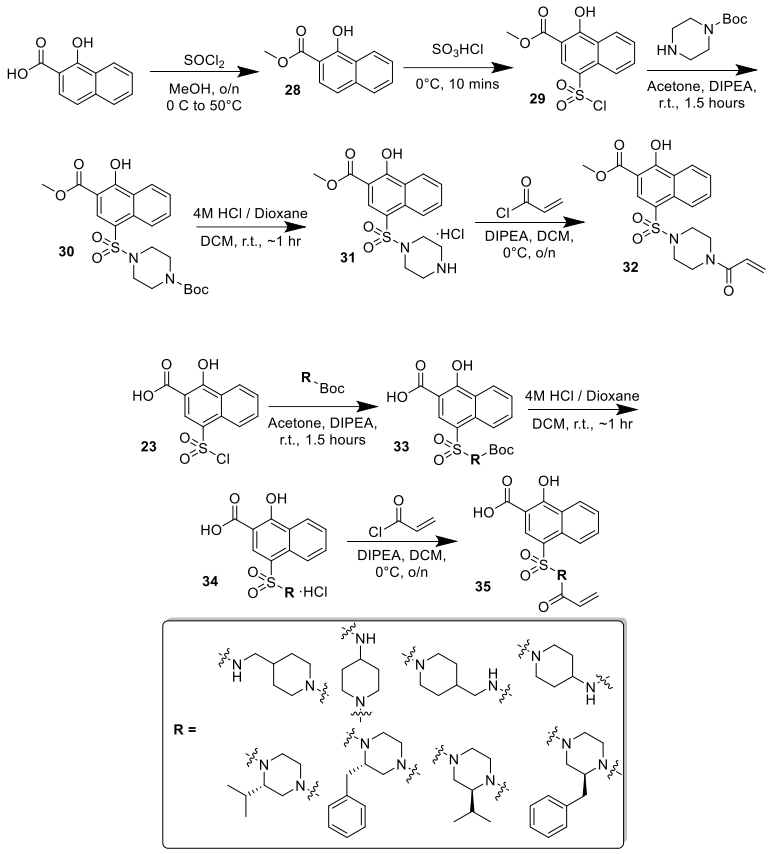

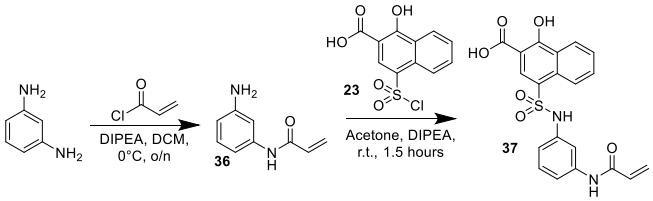
DIPEA, DCM,
0°C, o/n
36
23
Acetone, DIPEA,
r.t., 1.5 hours
37

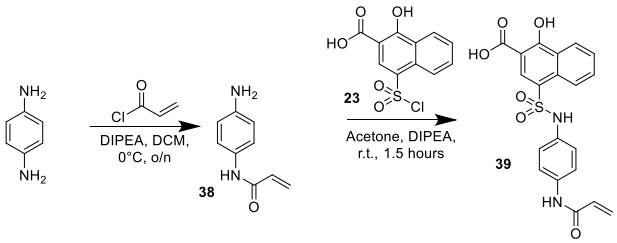
DIPEA, DCM,
0°C, o/n
38
23
Acetone, DIPEA,
r.t., 1.5 hours
39

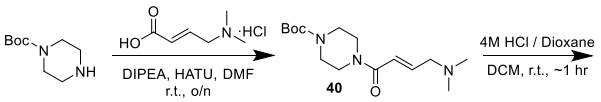
DIPEA, HATU, DMF
r.t., o/n
40
4M HCl / Dioxane
DCM, r.t., ~1 hr

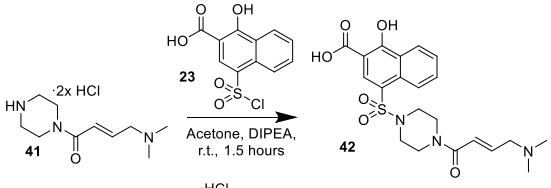
·2x HCl
41
23
Acetone, DIPEA,
r.t., 1.5 hours
42

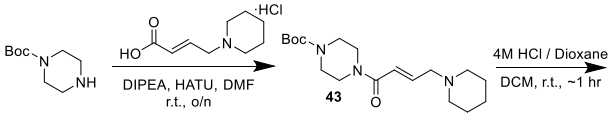
DIPEA, HATU, DMF
r.t., o/n
43
4M HCl / Dioxane
DCM, r.t., ~1 hr

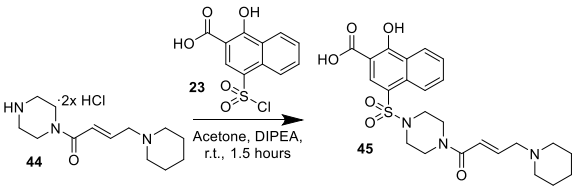
·2x HCl
44
23
Acetone, DIPEA,
r.t., 1.5 hours
45

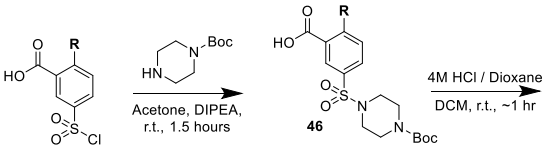
Acetone, DIPEA,
r.t., 1.5 hours
46
4M HCl / Dioxane
DCM, r.t., ~1 hr

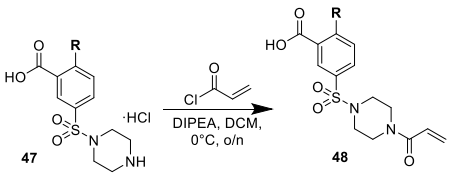
·HCl
47
DIPEA, DCM,
0°C, o/n
48

R = H, OH

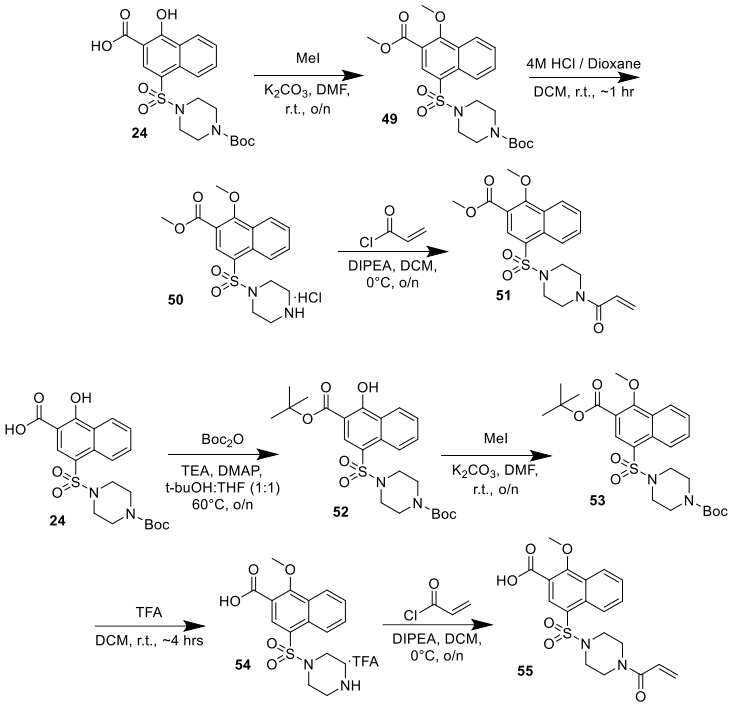

Figure 7.2.6.1: *Synthesis of CG-3-116 SAR compounds*

7.2.7 Final Compound Structures of CG-3-116 SAR Compounds

Below are the 17 final CG-3-116 SAR compounds that have been fully synthesized and tested in a cell-free TR-FRET assay by Nanosyn (**Figure 7.2.7.1**).

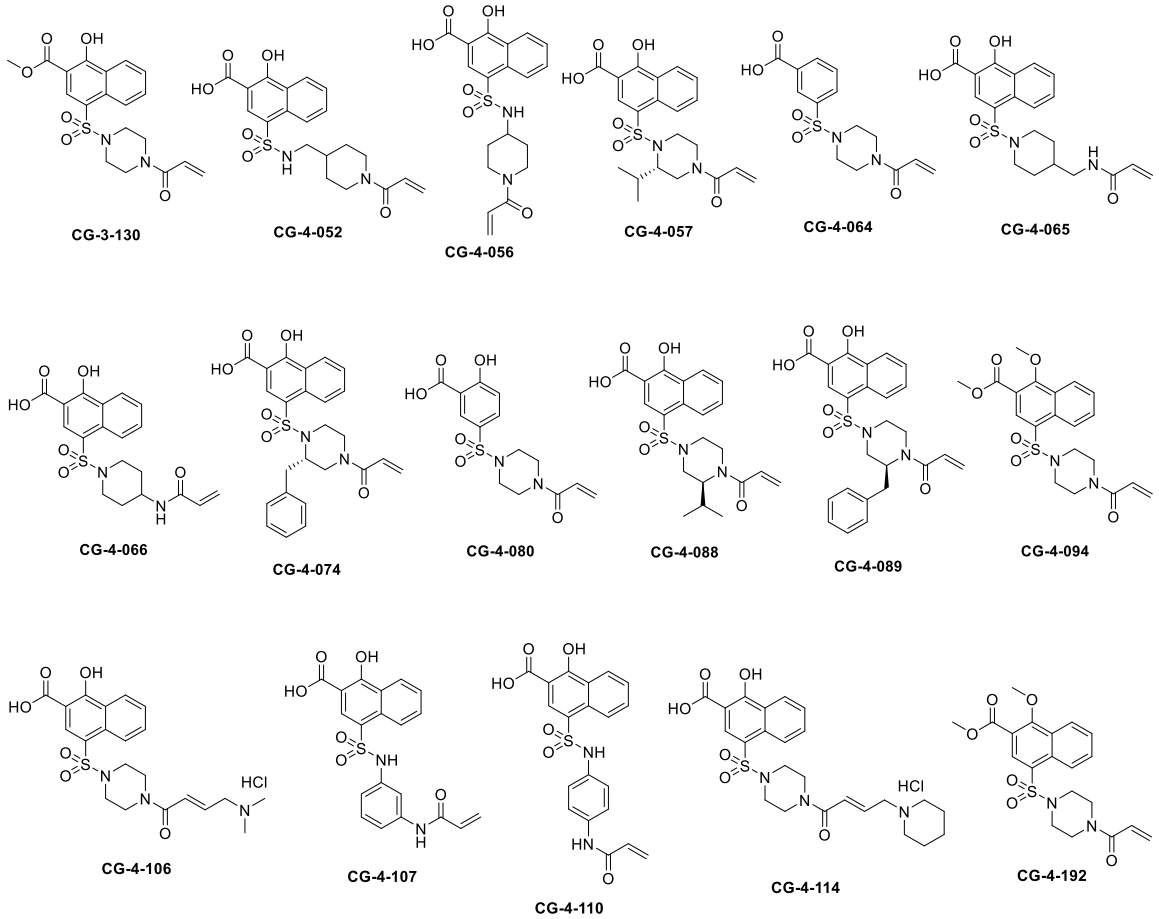

Figure 7.2.7.1: *Final structures of CG-3-116 SAR compounds*

7.2.8 Cell Free Testing of CG-3-116 SAR Compounds

Nanosyn conducted a TR-FRET assay to evaluate IC_{50} values for our compounds (**Table 7.2.8.1**).

Compound Name	BFL1 IC_{50} (mM)
Sabutoclax	0.574
CG-3-130	>30
CG-4-052	3.25

CG-4-056	213
CG-4-057	9.67
CG-4-064	6.56
CG-4-065	15.6
CG-4-066	>300
CG-4-074	11.2
CG-4-080	4.2
CG-4-088	52
CG-4-089	46.9
CG-4-094	>300
CG-4-106	>30
CG-4-107	3.96
CG-4-110	8.41
CG-4-114	>30
CG-4-192	2.23

Table 7.2.8.1: *IC_{50} values of CG-3-116 SAR compounds*

Orthogonal to this data, we had CG-3-116 and CG-3-244 tested via a KINOMEscan by DiscoverX. In this assay, our compounds were identified to have no potency against BFL-1 (**Table 7.2.8.2**).

Compound Name	BFL1 IC_{50} (mM)
CG-3-116	>100
CG-3-244	>100

Table 7.2.8.2: *IC_{50} values of CG-3-116 and control CG-3-244*

7.2.9 Synthesis of Non-Covalent BFL-1 Inhibitors

Due to the false positive observed with CG-3-116, we also explored creating a class of heterocyclic non-covalent BFL-1 inhibitors (**Figure 7.2.9.1**). A Gewald cyclization with cyclohexanone and ethyl 2-cyanoacetate formed **56** which had standard transformations conducted to create **58**. Next, 2-aminobenzonitrile was alkylated and the resulting intermediate was cyclized by a Thorpe–Ziegler reaction followed by standard chemistry to yield **62**. pyrazolo[1,5-a]pyridine-2-carboxylic acid was nitrated and methylated to synthesize **64**. Intermediate **64** was then reduced via two different conditions to afford **65** and **66** which were both transformed into final compounds **69** and **70**.

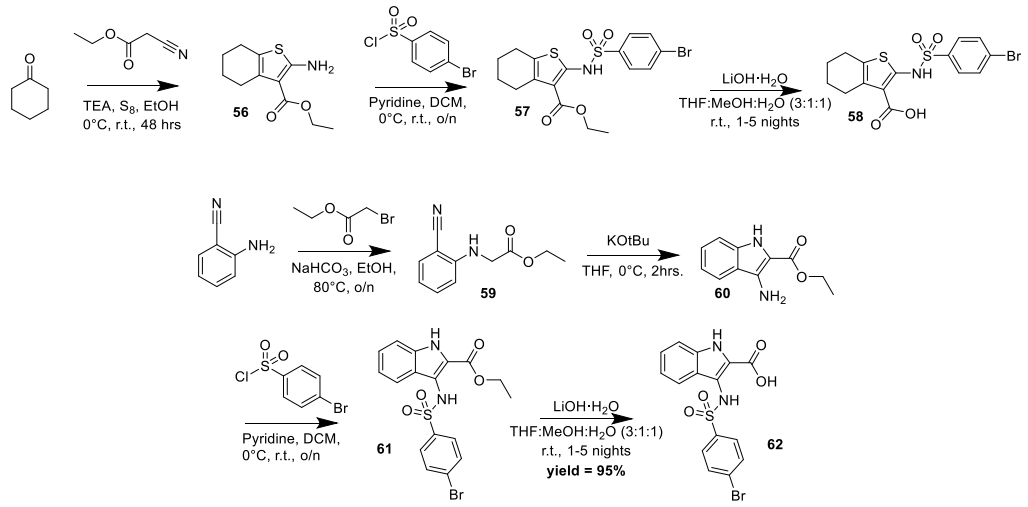

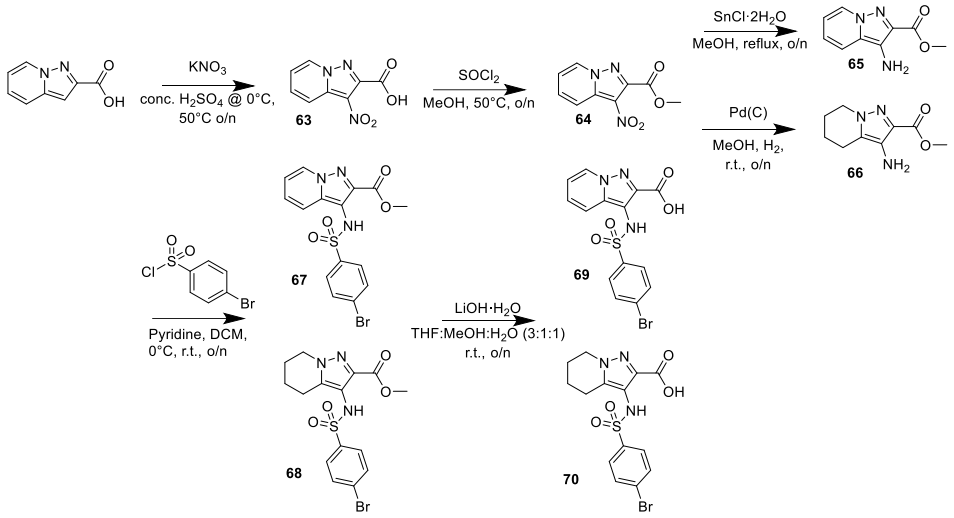

Figure 7.2.9.1*: Synthesis of non-covalent BFL-1 inhibitors*

7.2.10 Final Compound Structures of Non-Covalent BFL-1 Inhibitors

Below are four final non-covalent BFL-1 inhibitors that have been synthesized and three have been tested by Nanosyn in a TR-FRET cell-free assay (**Figure 7.2.10.1**).

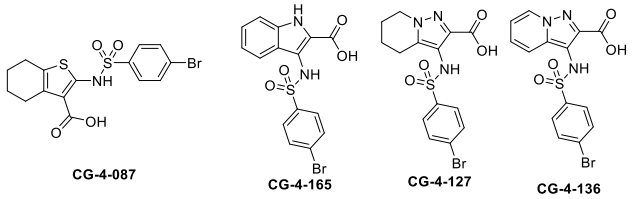

Figure 7.2.10.1: *Final structures of non-covalent BFL-1 inhibitors*

7.2.11 Cell Free Testing of Non-Covalent BFL-1 Inhibitors

Nanosyn conducted a TR-FRET cell-free assay with three non-covalent BFL-1 inhibitors. None of the compounds tested were potent at inhibiting BFL-1 (**Table 7.2.11.1**).

Compound Name	BFL1 IC_{50} (mM)
Sabutoclax	0.574
CG-4-087	94.1
CG-4-127	>30
CG-4-136	>30

Table 7.2.11.1: *IC_{50} values of non-covalent BFL-1 inhibitors*

7.2.12 Synthesis of Indole-Based Covalent BFL-1 Inhibitors

Following **Figure 7.2.12.1**, 1-acetylindolin-3-one underwent a titanium isopropoxide-mediated reductive amination to create **71** which was transformed using standard chemistry into **76**. **71** was used again and the acyl group was saponified before standard transformations resulted in **78** being synthesized. Additionally, **79** was formed using a different acid chloride for the acylation step.

Next, 4-bromo-2-((carboxymethyl)amino)benzoic acid was cyclized using a Dieckmann condensation to create **80** which was then reduced using sodium sulfite and cross coupled with (3-fluorophenyl)boronic acid to afford **82**. The same reductive amination using titanium isopropoxide was used to form **83** and standard chemistry followed resulting in **86**. A deactivated version of **86** was formed by using a different acid chloride during the acylation step and a saponification finished the formation of **88**. Using **83** again, we conducted standard chemistry conditions to synthesize **92**. Finally, **89** underwent a methylation, boc deprotection, and acylation to create **95**.

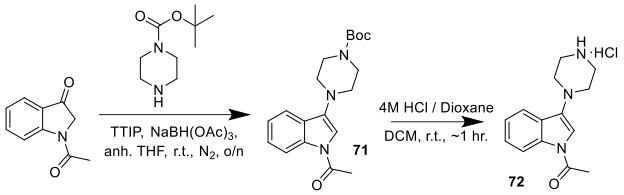
TTIP, NaBH(OAc)3,
anh. THF, r.t., N2, o/n
71
4M HCl / Dioxane
DCM, r.t., ~1 hr.
72

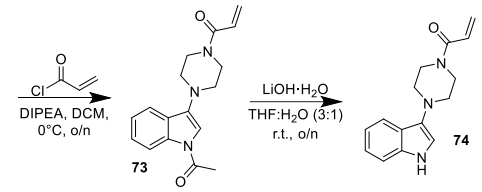
DIPEA, DCM,
0°C, o/n
73
LiOH·H2O
THF:H2O (3:1)
r.t., o/n
74

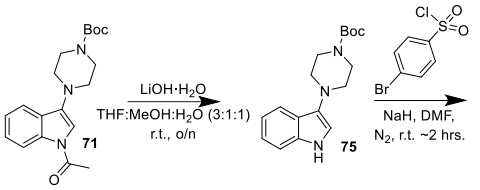
71
LiOH·H2O
THF:MeOH:H2O (3:1:1)
r.t., o/n
75
NaH, DMF,
N2, r.t. ~2 hrs.

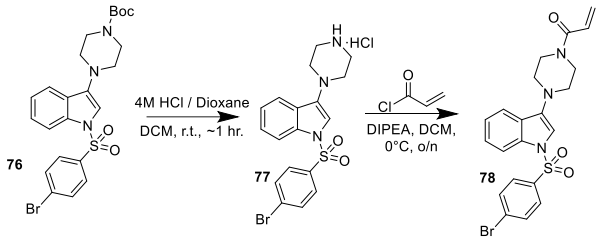
76
4M HCl / Dioxane
DCM, r.t., ~1 hr.
77
DIPEA, DCM,
0°C, o/n
78

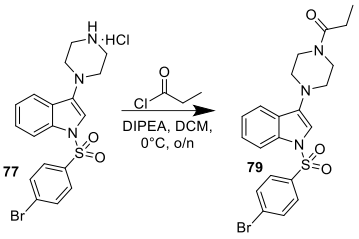
77
DIPEA, DCM,
0°C, o/n
79

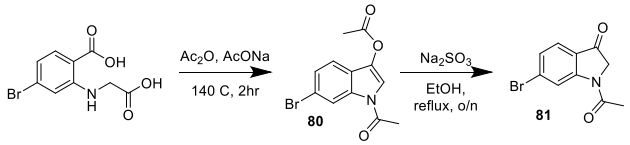
Ac2O, AcONa
140 C, 2hr
80
Na2SO3
EtOH,
reflux, o/n
81

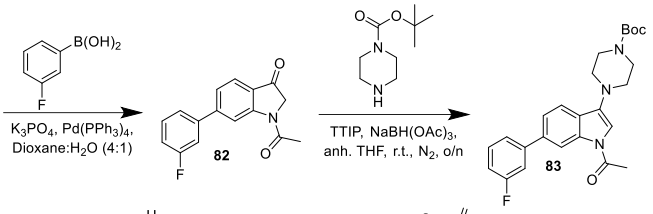
K3PO4, Pd(PPh3)4,
Dioxane:H2O (4:1)
82
TTIP, NaBH(OAc)3,
anh. THF, r.t., N2, o/n
83

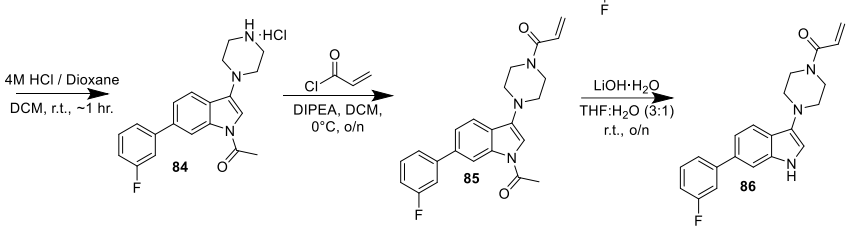
4M HCl / Dioxane
DCM, r.t., ~1 hr.
84
DIPEA, DCM,
0°C, o/n
85
LiOH·H2O
THF:H2O (3:1)
r.t., o/n
86

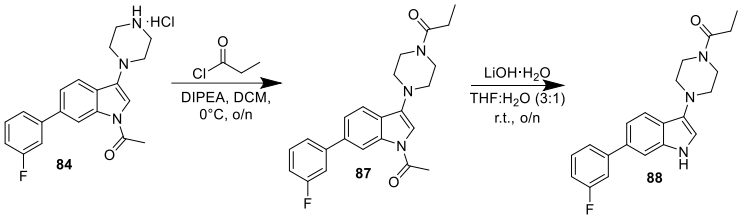
84
DIPEA, DCM,
0°C, o/n
87
LiOH·H2O
THF:H2O (3:1)
r.t., o/n
88

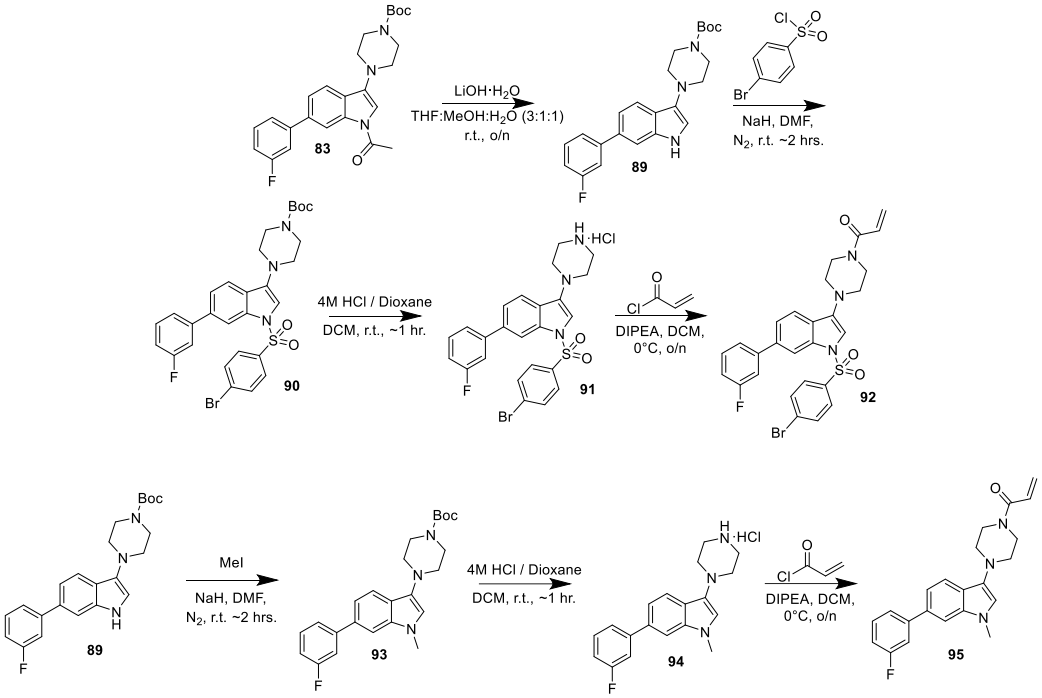

Figure 7.2.12.1: *Synthesis of indole-based BFL-1 covalent inhibitors*

7.2.13 Final Compound Structures of Indole-Based BFL-1 Covalent Inhibitors.

Below are seven final indole-based BFL-1 covalent inhibitors (**Figure 7.2.13.1**). The three compounds with code numbers have been synthesized and tested in a KINOMEscan cell-free assay. The remaining compounds will be fully synthesized and tested in a similar manner.

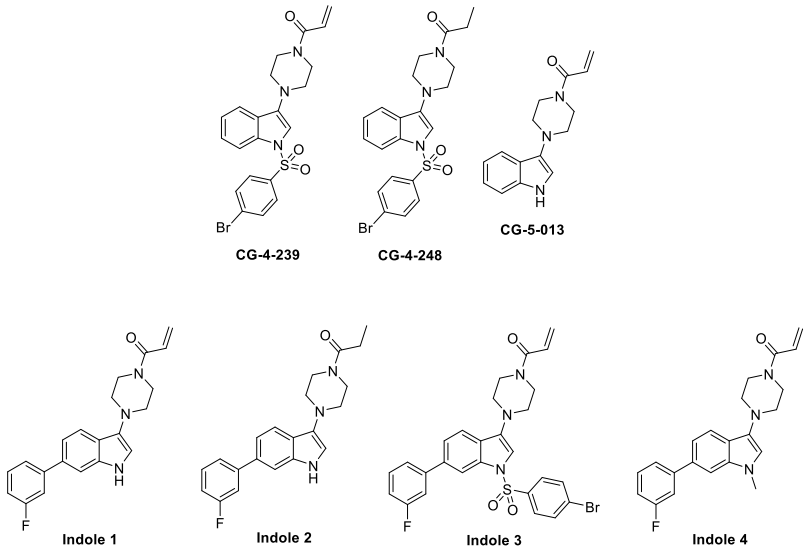

Figure 7.2.13.1: *Final structures of indole-based BFL-1 covalent inhibitors*

7.2.14 Cell Free Testing of Indole-Based BFL-1 Covalent Inhibitors.

DiscoverX conducted a KINOMEscan cell-free assay to measure our compounds and their potency for BFL-1 (**Table 7.2.14.1**). None of our compounds tested had any activity against BFL-1.

Compound Name	BFL1 K_d (mM)
CG-4-239	>100
CG-4-248	>100
CG-5-013	>100

Table 7.2.14.1: *IC_{50} values of indole-based BFL-1 covalent inhibitors*

7.2.15 Conclusions and Future Directions

Current efforts are focused on completing the indole-based library of covalent compounds. Once all compounds have been synthesized, cell-free testing will be done by DiscoverX to assess the BFL-1 K_d value.

Chapter 8: Concluding Remarks

8.1 Future Directions

In summary, we have leveraged several well-characterized inhibitors and employed various molecular strategies as potential adjuvant therapies or single agent therapies in their own right to augment their anti-cancer activities, and potentially overcome the acquired resistance to venetoclax. Both applications of polypharmacology: merged BCL-2/MCL-1 inhibitors and linked BCL-2/FLT3 dual inhibitors, were mildly potent in our cell-free and cell experiments. Additionally, our results demonstrate the effectiveness of a polypharmacy strategy to target multiple proteins of interest. Through transformation of the FDA-approved inhibitor gilteritinib into a putative covalent binder of FLT3, we have shown early success towards recovering the inhibitor's activity against the F691L gatekeeper mutation of the protein. Additionally, our deactivated control of our lead compound loses all activity against FLT3 despite the small structural change. Absolute validation of covalent adduct formation between our covalent inhibitors and FLT3 will be confirmed by intact mass spec analysis. Finally, deploying PROTAC technology, the CDK9 inhibitor AT7519 has been transformed into AMC-3-221, a reasonably selective CDK9 protein degrader that is well tolerated in mice. Next steps include conducting repeat assay experiments to obtain standard deviations of our compounds. Concurrently, western blotting analysis will be conducted to measure the protein abundance of MYC protein, another oncoprotein that is upregulated by CDK9. To conclude the analysis of our CDK9 protein degraders, efficacy studies will be performed in xenograft mouse models harboring MOLM14 AML cells.

Our ultimate goal that ties our various projects together is to combat resistance mechanisms of the anti-leukemic drug venetoclax. Therefore, all future work will be focused on optimizing and validating the compounds outlined previously towards creating an anti-leukemic agent that can be administered as either a single agent treatment or as a combination treatment with venetoclax. While the works presented thus far are promising, more work is needed to optimize and validate our covalent-based and protein degrading-based therapeutics to be safe and effective treatment options.

References:

(1) Gavrilescu, L. C.; Denkers, E. Y. Apoptosis and the Balance of Homeostatic and Pathologic Responses to Protozoan Infection. *Infection and Immunity* **2003**, 71 (11), 6109. https://doi.org/10.1128/IAI.71.11.6109-6115.2003.

(2) Lee, E.; Song, C.-H.; Bae, S.-J.; Ha, K.-T.; Karki, R. Regulated Cell Death Pathways and Their Roles in Homeostasis, Infection, Inflammation, and Tumorigenesis. *Exp Mol Med* **2023**, 55 (8), 1632–1643. https://doi.org/10.1038/s12276-023-01069-y.

(3) Youle, R. J.; Strasser, A. The BCL-2 Protein Family: Opposing Activities That Mediate Cell Death. *Nat Rev Mol Cell Biol* **2008**, 9 (1), 47–59. https://doi.org/10.1038/nrm2308.

(4) Elkholi, R.; Renault, T. T.; Serasinghe, M. N.; Chipuk, J. E. Putting the Pieces Together: How Is the Mitochondrial Pathway of Apoptosis Regulated in Cancer and Chemotherapy? *Cancer Metab* **2014**, 2, 16. https://doi.org/10.1186/2049-3002-2-16.

(5) Qian, S.; Wei, Z.; Yang, W.; Huang, J.; Yang, Y.; Wang, J. The Role of BCL-2 Family Proteins in Regulating Apoptosis and Cancer Therapy. *Front. Oncol.* **2022**, 12. https://doi.org/10.3389/fonc.2022.985363.

(6) Kale, J.; Osterlund, E. J.; Andrews, D. W. BCL-2 Family Proteins: Changing Partners in the Dance towards Death. *Cell Death Differ* **2018**, 25 (1), 65–80. https://doi.org/10.1038/cdd.2017.186.

(7) Kazi, A.; Sun, J.; Doi, K.; Sung, S.-S.; Takahashi, Y.; Yin, H.; Rodriguez, J. M.; Becerril, J.; Berndt, N.; Hamilton, A. D.; Wang, H.-G.; Sebti, S. M. The BH3 α-Helical Mimic BH3-M6 Disrupts Bcl-XL, Bcl-2, and MCL-1 Protein-Protein

Interactions with Bax, Bak, Bad, or Bim and Induces Apoptosis in a Bax- and Bim-Dependent Manner. *The Journal of Biological Chemistry* **2010**, 286 (11), 9382. https://doi.org/10.1074/jbc.M110.203638.

(8) Petros, A. M.; Olejniczak, E. T.; Fesik, S. W. Structural Biology of the Bcl-2 Family of Proteins. *Biochimica et Biophysica Acta (BBA) - Molecular Cell Research* **2004**, 1644 (2), 83–94. https://doi.org/10.1016/j.bbamcr.2003.08.012.

(9) Westphal, D.; Kluck, R. M.; Dewson, G. Building Blocks of the Apoptotic Pore: How Bax and Bak Are Activated and Oligomerize during Apoptosis. *Cell Death Differ* **2014**, 21 (2), 196–205. https://doi.org/10.1038/cdd.2013.139.

(10) Moldoveanu, T.; Czabotar, P. E. BAX, BAK, and BOK: A Coming of Age for the BCL-2 Family Effector Proteins. *Cold Spring Harbor Perspectives in Biology* **2020**, 12 (4), a036319. https://doi.org/10.1101/cshperspect.a036319.

(11) Peng, Y.; Croce, C. M. The Role of MicroRNAs in Human Cancer. *Sig Transduct Target Ther* **2016**, 1 (1), 1–9. https://doi.org/10.1038/sigtrans.2015.4.

(12) Wei, Y.; Cao, Y.; Sun, R.; Cheng, L.; Xiong, X.; Jin, X.; He, X.; Lu, W.; Zhao, M. Targeting Bcl-2 Proteins in Acute Myeloid Leukemia. *Frontiers in Oncology* **2020**, 10, 584974. https://doi.org/10.3389/fonc.2020.584974.

(13) Liu, L.; Cheng, X.; Yang, H.; Lian, S.; Jiang, Y.; Liang, J.; Chen, X.; Mo, S.; Shi, Y.; Zhao, S.; Li, J.; Jiang, R.; Yang, D.-H.; Wu, Y. BCL-2 Expression Promotes Immunosuppression in Chronic Lymphocytic Leukemia by Enhancing Regulatory T Cell Differentiation and Cytotoxic T Cell Exhaustion. *Molecular Cancer* **2022**, 21 (1), 59. https://doi.org/10.1186/s12943-022-01516-w.

(14) De Kouchkovsky, I.; Abdul-Hay, M. 'Acute Myeloid Leukemia: A Comprehensive Review and 2016 Update.' *Blood Cancer Journal* **2016**, 6 (7), e441–e441. https://doi.org/10.1038/bcj.2016.50.

(15) Kipps, T. J.; Stevenson, F. K.; Wu, C. J.; Croce, C. M.; Packham, G.; Wierda, W. G.; O'Brien, S.; Gribben, J.; Rai, K. Chronic Lymphocytic Leukaemia. *Nat Rev Dis Primers* **2017**, 3 (1), 1–22. https://doi.org/10.1038/nrdp.2016.96.

(16) *Acute Myeloid Leukemia - Cancer Stat Facts*. SEER. https://seer.cancer.gov/statfacts/html/amyl.html (accessed 2024-11-10).

(17) Pulte, D.; Castro, F. A.; Jansen, L.; Luttmann, S.; Holleczek, B.; Nennecke, A.; Ressing, M.; Katalinic, A.; Brenner, H.; GEKID Cancer Survival Working Group. Trends in Survival of Chronic Lymphocytic Leukemia Patients in Germany and the USA in the First Decade of the Twenty-First Century. *Journal of Hematology & Oncology* **2016**, 9 (1), 28. https://doi.org/10.1186/s13045-016-0257-2.

(18) *Chronic Lymphocytic Leukemia - Cancer Stat Fact*s. SEER. https://seer.cancer.gov/statfacts/html/clyl.html (accessed 2024-11-10).

(19) Hunger, S. P.; Teachey, D. T.; Grupp, S.; Aplenc, R. 93 - Childhood Leukemia. In *Abeloff's Clinical Oncology (Sixth Edition)*; Niederhuber, J. E., Armitage, J. O., Kastan, M. B., Doroshow, J. H., Tepper, J. E., Eds.; Elsevier: Philadelphia, **2020**; pp 1748-1764.e4. https://doi.org/10.1016/B978-0-323-47674-4.00093-1.

(20) Ashkenazi, A.; Fairbrother, W. J.; Leverson, J. D.; Souers, A. J. From Basic Apoptosis Discoveries to Advanced Selective BCL-2 Family Inhibitors. *Nat Rev Drug Discov* **2017**, 16 (4), 273–284. https://doi.org/10.1038/nrd.2016.253.

(21) Adams, J. M.; Cory, S. The BCL-2 Arbiters of Apoptosis and Their Growing Role as Cancer Targets. *Cell Death Differ* **2018**, 25 (1), 27–36. https://doi.org/10.1038/cdd.2017.161.

(22) Yap, J. L.; Chen, L.; Lanning, M. E.; Fletcher, S. Expanding the Cancer Arsenal with Targeted Therapies: Disarmament of the Antiapoptotic Bcl-2 Proteins by Small Molecules. *J. Med. Chem.* **2017**, 60 (3), 821–838. https://doi.org/10.1021/acs.jmedchem.5b01888.

(23) Tse, C.; Shoemaker, A. R.; Adickes, J.; Anderson, M. G.; Chen, J.; Jin, S.; Johnson, E. F.; Marsh, K. C.; Mitten, M. J.; Nimmer, P.; Roberts, L.; Tahir, S. K.; Xiao, Y.; Yang, X.; Zhang, H.; Fesik, S.; Rosenberg, S. H.; Elmore, S. W. ABT-263: A Potent and Orally Bioavailable Bcl-2 Family Inhibitor. *Cancer Research* **2008**, 68 (9), 3421–3428. https://doi.org/10.1158/0008-5472.CAN-07-5836.

(24) Rudin, C. M.; Hann, C. L.; Garon, E. B.; Oliveira, M. R. de; Bonomi, P. D.; Camidge, D. R.; Chu, Q.; Giaccone, G.; Khaira, D.; Ramalingam, S. S.; Ranson, M. R.; Dive, C.; McKeegan, E. M.; Chyla, B. J.; Dowell, B. L.; Chakravartty, A.; Nolan, C. E.; Rudersdorf, N.; Busman, T. A.; Mabry, M. H.; Krivoshik, A. P.; Humerickhouse, R. A.; Shapiro, G. I.; Gandhi, L. Phase II Study of Single-Agent Navitoclax (ABT-263) and Biomarker Correlates in Patients with Relapsed Small Cell Lung Cancer. *Clinical cancer research : an official journal of the American Association for Cancer Research* **2012**, 18 (11), 3163. https://doi.org/10.1158/1078-0432.CCR-11-3090.

(25) Santoshi, R. K.; Patel, R.; Patel, N. S.; Bansro, V.; Chhabra, G. A Comprehensive Review of Thrombocytopenia With a Spotlight on Intensive Care Patients. *Cureus* **2022**, 14 (8), e27718. https://doi.org/10.7759/cureus.27718.

(26) Afreen, S.; Bohler, S.; Müller, A.; Demmerath, E.-M.; Weiss, J. M.; Jutzi, J. S.; Schachtrup, K.; Kunze, M.; Erlacher, M. BCL-XL Expression Is Essential for Human Erythropoiesis and Engraftment of Hematopoietic Stem Cells. *Cell Death Dis* **2020**, 11 (1), 1–15. https://doi.org/10.1038/s41419-019-2203-z.

(27) Souers, A. J.; Leverson, J. D.; Boghaert, E. R.; Ackler, S. L.; Catron, N. D.; Chen, J.; Dayton, B. D.; Ding, H.; Enschede, S. H.; Fairbrother, W. J.; Huang, D. C. S.; Hymowitz, S. G.; Jin, S.; Khaw, S. L.; Kovar, P. J.; Lam, L. T.; Lee, J.; Maecker, H. L.; Marsh, K. C.; Mason, K. D.; Mitten, M. J.; Nimmer, P. M.; Oleksijew, A.; Park, C. H.; Park, C.-M.; Phillips, D. C.; Roberts, A. W.; Sampath, D.; Seymour, J. F.; Smith, M. L.; Sullivan, G. M.; Tahir, S. K.; Tse, C.; Wendt, M. D.; Xiao, Y.; Xue, J. C.; Zhang, H.; Humerickhouse, R. A.; Rosenberg, S. H.; Elmore, S. W. ABT-199, a Potent and Selective BCL-2 Inhibitor, Achieves Antitumor Activity While Sparing Platelets. *Nat Med* **2013**, 19 (2), 202–208. https://doi.org/10.1038/nm.3048.

(28) Commissioner, O. of the. *FDA approves new drug for chronic lymphocytic leukemia in patients with a specific chromosomal abnormality.* FDA. https://www.fda.gov/news-events/press-announcements/fda-approves-new-drug-chronic-lymphocytic-leukemia-patients-specific-chromosomal-abnormality (accessed 2024-11-10).

(29) Research, C. for D. E. and. *FDA Approves Venetoclax in Combination for AML in Adults*. FDA 2019.

(30) Wang, H.; Guo, M.; Wei, H.; Chen, Y. Targeting MCL-1 in Cancer: Current Status and Perspectives. *Journal of Hematology & Oncology* **2021**, 14 (1), 67. https://doi.org/10.1186/s13045-021-01079-1.

(31) Wei, A. H.; Roberts, A. W.; Spencer, A.; Rosenberg, A. S.; Siegel, D.; Walter, R. B.; Caenepeel, S.; Hughes, P.; McIver, Z.; Mezzi, K.; Morrow, P. K.; Stein, A. Targeting MCL-1 in Hematologic Malignancies: Rationale and Progress. *Blood reviews* **2020**, 44, 100672. https://doi.org/10.1016/j.blre.2020.100672.

(32) Liu, J.; Chen, Y.; Yu, L.; Yang, L. Mechanisms of Venetoclax Resistance and Solutions. *Frontiers in Oncology* **2022**, 12, 1005659. https://doi.org/10.3389/fonc.2022.1005659.

(33) Zhang, Q.; Riley-Gillis, B.; Han, L.; Jia, Y.; Lodi, A.; Zhang, H.; Ganesan, S.; Pan, R.; Konoplev, S. N.; Sweeney, S. R.; Ryan, J. A.; Jitkova, Y.; Dunner, K.; Grosskurth, S. E.; Vijay, P.; Ghosh, S.; Lu, C.; Ma, W.; Kurtz, S.; Ruvolo, V. R.; Ma, H.; Weng, C. C.; Ramage, C. L.; Baran, N.; Shi, C.; Cai, T.; Davis, R. E.; Battula, V. L.; Mi, Y.; Wang, J.; DiNardo, C. D.; Andreeff, M.; Tyner, J. W.; Schimmer, A.; Letai, A.; Padua, R. A.; Bueso-Ramos, C. E.; Tiziani, S.; Leverson, J.; Popovic, R.; Konopleva, M. Activation of RAS/MAPK Pathway Confers MCL-1 Mediated Acquired Resistance to BCL-2 Inhibitor Venetoclax in Acute Myeloid Leukemia. *Sig Transduct Target Ther* **2022**, 7 (1), 1–13. https://doi.org/10.1038/s41392-021-00870-3.

(34) Kotschy, A.; Szlavik, Z.; Murray, J.; Davidson, J.; Maragno, A. L.; Le Toumelin-Braizat, G.; Chanrion, M.; Kelly, G. L.; Gong, J.-N.; Moujalled, D. M.; Bruno, A.; Csekei, M.; Paczal, A.; Szabo, Z. B.; Sipos, S.; Radics, G.; Proszenyak, A.; Balint, B.; Ondi, L.; Blasko, G.; Robertson, A.; Surgenor, A.; Dokurno, P.; Chen, I.; Matassova, N.; Smith, J.; Pedder, C.; Graham, C.; Studeny, A.; Lysiak-Auvity, G.; Girard, A.-M.; Gravé, F.; Segal, D.; Riffkin, C. D.; Pomilio, G.; Galbraith, L. C. A.; Aubrey, B. J.; Brennan, M. S.; Herold, M. J.; Chang, C.; Guasconi, G.; Cauquil, N.; Melchiore, F.; Guigal-Stephan, N.; Lockhart, B.; Colland, F.; Hickman, J. A.; Roberts, A. W.; Huang, D. C. S.; Wei, A. H.; Strasser, A.; Lessene, G.; Geneste, O. The MCL1 Inhibitor S63845 Is Tolerable and Effective in Diverse Cancer Models. *Nature* **2016**, 538 (7626), 477–482. https://doi.org/10.1038/nature19830.

(35) Institut de Recherches Internationales Servier. *Phase I, International, Multicentre, Open-Label, Non-Randomised, Non-Comparative Study of Intravenously Administered S64315, a Mcl-1 Inhibitor, in Patients With Acute Myeloid Leukaemia (AML) or Myelodysplastic Syndrome (MDS)*; Clinical trial registration NCT02979366; clinicaltrials.gov, 2022. https://clinicaltrials.gov/study/NCT02979366 (accessed 2024-11-06).

(36) Institut de Recherches Internationales Servier. *An International Phase Ib Multicentre Study to Characterize the Safety and Tolerability of Intravenously Administered S64315, a Selective Mcl-1 Inhibitor, in Combination With Orally Administered Venetoclax, a Selective Bcl-2 Inhibitor in Patients With Acute Myeloid Leukaemia (AML).*; Clinical trial registration NCT03672695;

clinicaltrials.gov, 2024. https://clinicaltrials.gov/study/NCT03672695 (accessed 2024-11-06).

(37) Friberg, A.; Vigil, D.; Zhao, B.; Daniels, R. N.; Burke, J. P.; Garcia-Barrantes, P. M.; Camper, D.; Chauder, B. A.; Lee, T.; Olejniczak, E. T.; Fesik, S. W. Discovery of Potent Myeloid Cell Leukemia 1 (Mcl-1) Inhibitors Using Fragment-Based Methods and Structure-Based Design. *J. Med. Chem.* **2013**, 56 (1), 15–30. https://doi.org/10.1021/jm301448p.

(38) Lee, T.; Christov, P. P.; Shaw, S.; Tarr, J. C.; Zhao, B.; Veerasamy, N.; Jeon, K. O.; Mills, J. J.; Bian, Z.; Sensintaffar, J. L.; Arnold, A. L.; Fogarty, S. A.; Perry, E.; Ramsey, H. E.; Cook, R. S.; Hollingshead, M.; Davis Millin, M.; Lee, K.; Koss, B.; Budhraja, A.; Opferman, J. T.; Kim, K.; Arteaga, C. L.; Moore, W. J.; Olejniczak, E. T.; Savona, M. R.; Fesik, S. W. Discovery of Potent Myeloid Cell Leukemia-1 (Mcl-1) Inhibitors That Demonstrate in Vivo Activity in Mouse Xenograft Models of Human Cancer. *J. Med. Chem.* **2019**, 62 (8), 3971–3988. https://doi.org/10.1021/acs.jmedchem.8b01991.

(39) Pelz, N. F.; Bian, Z.; Zhao, B.; Shaw, S.; Tarr, J. C.; Belmar, J.; Gregg, C.; Camper, D. V.; Goodwin, C. M.; Arnold, A. L.; Sensintaffar, J. L.; Friberg, A.; Rossanese, O. W.; Lee, T.; Olejniczak, E. T.; Fesik, S. W. Discovery of 2-Indole-Acylsulfonamide Myeloid Cell Leukemia 1 (Mcl-1) Inhibitors Using Fragment-Based Methods. *J. Med. Chem.* **2016**, 59 (5), 2054–2066. https://doi.org/10.1021/acs.jmedchem.5b01660.

(40) Tron, A. E.; Belmonte, M. A.; Adam, A.; Aquila, B. M.; Boise, L. H.; Chiarparin, E.; Cidado, J.; Embrey, K. J.; Gangl, E.; Gibbons, F. D.; Gregory, G. P.;

Hargreaves, D.; Hendricks, J. A.; Johannes, J. W.; Johnstone, R. W.; Kazmirski, S. L.; Kettle, J. G.; Lamb, M. L.; Matulis, S. M.; Nooka, A. K.; Packer, M. J.; Peng, B.; Rawlins, P. B.; Robbins, D. W.; Schuller, A. G.; Su, N.; Yang, W.; Ye, Q.; Zheng, X.; Secrist, J. P.; Clark, E. A.; Wilson, D. M.; Fawell, S. E.; Hird, A. W. Discovery of Mcl-1-Specific Inhibitor AZD5991 and Preclinical Activity in Multiple Myeloma and Acute Myeloid Leukemia. *Nat Commun* **2018**, 9 (1), 5341. https://doi.org/10.1038/s41467-018-07551-w.

(41) Desai, P.; Lonial, S.; Cashen, A.; Kamdar, M.; Blachly, J. S.; Flinn, I. W.; O'brien, S.; Garcia, J.; Korde, N.; Moslehi, J.; Wey, M.; Cheung, P.; Sharma, S.; Olabode, D.; Chen, H.; Ali Syed, F.; Liu, M.; Saeh, J.; Tibes, R.; Andrade, M.; Kadia, T. P579: SAFETY, TOLERABILITY, PHARMACOKINETICS, AND PRELIMINARY ANTITUMOR ACTIVITY OF AZD5991 IN RELAPSED/ REFRACTORY HEMATOLOGIC MALIGNANCIES: A PHASE 1 FIRST-IN-HUMAN STUDY. *Hemasphere* **2023**, 7 (Suppl), e98838e7. https://doi.org/10.1097/01.HS9.0000969220.98838.e7.

(42) Lee, S.; Wales, T. E.; Escudero, S.; Cohen, D. T.; Luccarelli, J.; Gallagher, C.; Cohen, N. A.; Huhn, A. J.; Bird, G. H.; Engen, J. R.; Walensky, L. D. Allosteric Inhibition of Anti-Apoptotic MCL-1. *Nature structural & molecular biology* **2016**, 23 (6), 600. https://doi.org/10.1038/nsmb.3223.

(43) Flores-Romero, H.; Landeta, O.; Ugarte-Uribe, B.; Cosentino, K.; García-Porras, M.; García-Sáez, A. J.; Basañez, G. BFL1 Modulates Apoptosis at the Membrane Level through a Bifunctional and Multimodal Mechanism Showing Key

Differences with BCLXL. *Cell Death Differ* **2019**, 26 (10), 1880–1894. https://doi.org/10.1038/s41418-018-0258-5.

(44) Wang, G.; Diepstraten, S. T.; Herold, M. J. Last but Not Least: BFL-1 as an Emerging Target for Anti-Cancer Therapies. *Biochemical Society Transactions* **2022**, 50 (4), 1119. https://doi.org/10.1042/BST20220153.

(45) Huhn, A. J.; Guerra, R. M.; Harvey, E. P.; Bird, G. H.; Walensky, L. D. Selective Covalent Targeting of Anti-Apoptotic BFL-1 by Cysteine-Reactive Stapled Peptide Inhibitors. *Cell chemical biology* **2016**, 23 (9), 1123. https://doi.org/10.1016/j.chembiol.2016.07.022.

(46) Harvey, E. P.; Seo, H.-S.; Guerra, R. M.; Bird, G. H.; Dhe-Paganon, S.; Walensky, L. D. Crystal Structures of Anti-Apoptotic BFL-1 and Its Complex with a Covalent Stapled Peptide Inhibitor. *Structure* **2018**, 26 (1), 153-160.e4. https://doi.org/10.1016/j.str.2017.11.016.

(47) Kump, K. J.; Miao, L.; Mady, A. S.; Ansari, N. H.; Shrestha, U. K.; Yang, Y.; Pal, M.; Liao, C.; Perdih, A.; Abulwerdi, F. A.; Chinnaswamy, K.; Meagher, J. L.; Carlson, J. M.; Khanna, M.; Stuckey, J. A.; Nikolovska-Coleska, Z. Discovery and Characterization of 2,5-Substituted Benzoic Acid Dual Inhibitors of the Anti-Apoptotic Mcl-1 and Bfl-1 Proteins. *Journal of medicinal chemistry* **2020**, 63 (5), 2489. https://doi.org/10.1021/acs.jmedchem.9b01442.

(48) Feng, X.; Yan, Z.; Zhou, F.; Lou, J.; Lyu, X.; Ren, X.; Zeng, Z.; Liu, C.; Zhang, S.; Zhu, D.; Huang, H.; Yang, J.; Zhao, Y. Discovery of a Selective and Covalent Small-Molecule Inhibitor of BFL-1 Protein That Induces Robust Apoptosis in

Cancer Cells. *European Journal of Medicinal Chemistry* **2022**, 236, 114327. https://doi.org/10.1016/j.ejmech.2022.114327.

(49) Ku, B.; Liang, C.; Jung, J. U.; Oh, B.-H. Evidence That Inhibition of BAX Activation by BCL-2 Involves Its Tight and Preferential Interaction with the BH3 Domain of BAX. *Cell Research* **2010**, 21 (4), 627. https://doi.org/10.1038/cr.2010.149.

(50) Wang, X.; Bathina, M.; Lynch, J.; Koss, B.; Calabrese, C.; Frase, S.; Schuetz, J. D.; Rehg, J. E.; Opferman, J. T. Deletion of MCL-1 Causes Lethal Cardiac Failure and Mitochondrial Dysfunction. *Genes & Development* **2013**, 27 (12), 1351. https://doi.org/10.1101/gad.215855.113.

(51) Rasmussen, M. L.; Taneja, N.; Neininger, A. C.; Wang, L.; Robertson, G. L.; Riffle, S. N.; Shi, L.; Knollmann, B. C.; Burnette, D. T.; Gama, V. MCL-1 Inhibition by Selective BH3 Mimetics Disrupts Mitochondrial Dynamics Causing Loss of Viability and Functionality of Human Cardiomyocytes. *iScience* **2020**, 23 (4), 101015. https://doi.org/10.1016/j.isci.2020.101015.

(52) Negotei, C.; Colita, A.; Mitu, I.; Lupu, A. R.; Lapadat, M.-E.; Popovici, C. E.; Crainicu, M.; Stanca, O.; Berbec, N. M. A Review of FLT3 Kinase Inhibitors in AML. *Journal of Clinical Medicine* **2023**, 12 (20), 6429. https://doi.org/10.3390/jcm12206429.

(53) Boffo, S.; Damato, A.; Alfano, L.; Giordano, A. CDK9 Inhibitors in Acute Myeloid Leukemia. *J Exp Clin Cancer Res* **2018**, 37, 36. https://doi.org/10.1186/s13046-018-0704-8.

(54) (1) Gilliland, D. G.; Griffin, J. D. The Roles of FLT3 in Hematopoiesis and Leukemia. *Blood* **2002**, 100 (5), 1532–1542. https://doi.org/10.1182/blood-2002-02-0492.

(55) Nakao, M.; Yokota, S.; Iwai, T.; Kaneko, H.; Horiike, S.; Kashima, K.; Sonoda, Y.; Fujimoto, T.; Misawa, S. Internal Tandem Duplication of the Flt3 Gene Found in Acute Myeloid Leukemia. *Leukemia* **1996**, 10 (12), 1911–1918.

(56) Daver, N.; Venugopal, S.; Ravandi, F. FLT3 Mutated Acute Myeloid Leukemia: 2021 Treatment Algorithm. *Blood Cancer J.* **2021**, 11 (5), 1–9. https://doi.org/10.1038/s41408-021-00495-3.

(57) Daver, N.; Schlenk, R. F.; Russell, N. H.; Levis, M. J. Targeting FLT3 Mutations in AML: Review of Current Knowledge and Evidence. *Leukemia* **2019**, 33 (2), 299–312. https://doi.org/10.1038/s41375-018-0357-9.

(58) Research, C. for D. E. and. Midostaurin. *FDA* **2019**.

(59) Weisberg, E.; Boulton, C.; Kelly, L. M.; Manley, P.; Fabbro, D.; Meyer, T.; Gilliland, D. G.; Griffin, J. D. Inhibition of Mutant FLT3 Receptors in Leukemia Cells by the Small Molecule Tyrosine Kinase Inhibitor PKC412. *Cancer Cell* **2002**, 1 (5), 433–443. https://doi.org/10.1016/S1535-6108(02)00069-7.

(60) (1) Gallogly, M. M.; Lazarus, H. M.; Cooper, B. W. Midostaurin: A Novel Therapeutic Agent for Patients with FLT3-Mutated Acute Myeloid Leukemia and Systemic Mastocytosis. *Therapeutic Advances in Hematology* **2017**, 8 (9), 245. https://doi.org/10.1177/2040620717721459.

(61) Zarrinkar, P. P.; Gunawardane, R. N.; Cramer, M. D.; Gardner, M. F.; Brigham, D.; Belli, B.; Karaman, M. W.; Pratz, K. W.; Pallares, G.; Chao, Q.; Sprankle, K.

G.; Patel, H. K.; Levis, M.; Armstrong, R. C.; James, J.; Bhagwat, S. S. AC220 Is a Uniquely Potent and Selective Inhibitor of FLT3 for the Treatment of Acute Myeloid Leukemia (AML). *Blood* **2009**, 114 (14), 2984. https://doi.org/10.1182/blood-2009-05-222034.

(62) Research, C. for D. E. and. FDA Approves Quizartinib for Newly Diagnosed Acute Myeloid Leukemia. *FDA* **2024**.

(63) Smith, C. C.; Paguirigan, A.; Jeschke, G. R.; Lin, K. C.; Massi, E.; Tarver, T.; Chin, C.-S.; Asthana, S.; Olshen, A.; Travers, K. J.; Wang, S.; Levis, M. J.; Perl, A. E.; Radich, J. P.; Shah, N. P. Heterogeneous Resistance to Quizartinib in Acute Myeloid Leukemia Revealed by Single-Cell Analysis. *Blood* **2017**, 130 (1), 48. https://doi.org/10.1182/blood-2016-04-711820.

(64) Mori, M.; Kaneko, N.; Ueno, Y.; Yamada, M.; Tanaka, R.; Saito, R.; Shimada, I.; Mori, K.; Kuromitsu, S. Gilteritinib, a FLT3/AXL Inhibitor, Shows Antileukemic Activity in Mouse Models of FLT3 Mutated Acute Myeloid Leukemia. *Investigational New Drugs* **2017**, 35 (5), 556. https://doi.org/10.1007/s10637-017-0470-z.

(65) Dumas, P.-Y.; Villacreces, A.; Guitart, A. V.; El-habhab, A.; Massara, L.; Mansier, O.; Bidet, A.; Martineau, D.; Fernandez, S.; Leguay, T.; Pigneux, A.; Vigon, I.; Pasquet, J.-M.; Desplat, V. Dual Inhibition of FLT3 and AXL by Gilteritinib Overcomes Hematopoietic Niche-Driven Resistance Mechanisms in FLT3-ITD Acute Myeloid Leukemia. *Clinical Cancer Research* **2021**, 27 (21), 6012–6025. https://doi.org/10.1158/1078-0432.CCR-20-3114.

(66) Kawase, T.; Nakazawa, T.; Eguchi, T.; Tsuzuki, H.; Ueno, Y.; Amano, Y.; Suzuki, T.; Mori, M.; Yoshida, T. Effect of Fms-like Tyrosine Kinase 3 (FLT3) Ligand (FL) on Antitumor Activity of Gilteritinib, a FLT3 Inhibitor, in Mice Xenografted with FL-Overexpressing Cells. *Oncotarget* **2019**, 10 (58), 6111–6123. https://doi.org/10.18632/oncotarget.27222.

(67) Astellas Pharma Global Development, Inc. *A Phase 3 Open-Label, Multicenter, Randomized Study of ASP2215 Versus Salvage Chemotherapy in Patients With Relapsed or Refractory Acute Myeloid Leukemia (AML) With FLT3 Mutation*; Clinical trial registration NCT02421939; clinicaltrials.gov, **2024**. https://clinicaltrials.gov/study/NCT02421939 (accessed 2024-11-10).

(68) Research, C. for D. E. and. FDA Approves Gilteritinib for Relapsed or Refractory Acute Myeloid Leukemia (AML) with a FLT3 Mutation. *FDA* **2024**.

(69) Joshi, S. K.; Sharzehi, S.; Pittsenbarger, J.; Bottomly, D.; Tognon, C. E.; McWeeney, S. K.; Druker, B. J.; Traer, E. A Noncanonical FLT3 Gatekeeper Mutation Disrupts Gilteritinib Binding and Confers Resistance. *Am J Hematol* **2021**, 96 (7), E226–E229. https://doi.org/10.1002/ajh.26174.

(70) Ferng, T. T.; Terada, D.; Ando, M.; Tarver, T. C.; Chaudhary, F.; Lin, K. C.; Logan, A. C.; Smith, C. C. The Irreversible FLT3 Inhibitor FF-10101 Is Active against a Diversity of FLT3 Inhibitor Resistance Mechanisms. *Mol Cancer Ther* **2022**, 21 (5), 844–854. https://doi.org/10.1158/1535-7163.MCT-21-0317.

(71) Levis, M.; Perl, A.; Schiller, G.; Fathi, A. T.; Roboz, G.; Wang, E. S.; Altman, J.; Rajkhowa, T.; Ando, M.; Suzuki, T.; Subach, R. A.; Maier, G.; Madden, T.; Johansen, M.; Cheung, K.; Kurman, M.; Smith, C. A Phase 1 Study of the

Irreversible FLT3 Inhibitor FF-10101 in Relapsed or Refractory Acute Myeloid Leukemia. *Blood Advances* **2024**, 8 (10), 2527–2535. https://doi.org/10.1182/bloodadvances.2023010619.

(72) Toure, M. A.; Koehler, A. N. Addressing Transcriptional Dysregulation in Cancer through CDK9 Inhibition. *Biochemistry* **2023**, 62 (6), 1114–1123. https://doi.org/10.1021/acs.biochem.2c00609.

(73) Anshabo, A. T.; Milne, R.; Wang, S.; Albrecht, H. CDK9: A Comprehensive Review of Its Biology, and Its Role as a Potential Target for Anti-Cancer Agents. *Front. Oncol.* **2021**, 11. https://doi.org/10.3389/fonc.2021.678559.

(74) Boffo, S.; Damato, A.; Alfano, L.; Giordano, A. CDK9 Inhibitors in Acute Myeloid Leukemia. *J Exp Clin Cancer Res* **2018**, 37, 36. https://doi.org/10.1186/s13046-018-0704-8.

(75) Dhanasekaran, R.; Deutzmann, A.; Mahauad-Fernandez, W. D.; Hansen, A. S.; Gouw, A. M.; Felsher, D. W. The MYC Oncogene — the Grand Orchestrator of Cancer Growth and Immune Evasion. Nature reviews. *Clinical oncology* **2021**, 19 (1), 23. https://doi.org/10.1038/s41571-021-00549-2.

(76) Shapiro, G. I. Preclinical and Clinical Development of the Cyclin-Dependent Kinase Inhibitor Flavopiridol. *Clinical Cancer Research* **2004**, 10 (12), 4270s–4275s. https://doi.org/10.1158/1078-0432.CCR-040020.

(77) *FDA Grants Orphan Drug Status to TP-1287 for Ewing Sarcoma. Targeted Oncology.* https://www.targetedonc.com/view/fda-grants-orphan-drug-status-to-tp-1287-for-ewing-sarcoma (accessed 2024-11-07).

(78) Zhang, M.; Zhang, L.; Hei, R.; Li, X.; Cai, H.; Wu, X.; Zheng, Q.; Cai, C. CDK Inhibitors in Cancer Therapy, an Overview of Recent Development. *American Journal of Cancer Research* **2021**, 11 (5), 1913.

(79) Zhou, F.; Tang, L.; Le, S.; Ge, M.; Cicic, D.; Xie, F.; Ren, J.; Lan, J.; Lu, Q. The Pharmacodynamic and Mechanistic Foundation for the Antineoplastic Effects of GFH009, a Potent and Highly Selective CDK9 Inhibitor for the Treatment of Hematologic Malignancies. *Oncotarget* **2023**, 14, 997. https://doi.org/10.18632/oncotarget.28543.

(80) Rosa, K. *FDA Grants Fast Track Status to SLS009 for Relapsed/Refractory Acute Myeloid Leukemia.* **2024**, 1.

(81) Qi, J.; Zhou, K.; Qian, W.; Zang, A.; Kadia, T. M.; Lipsky, A. H.; Yang, Y.; Wang, Y.; Shen, H.; Zheng, B.; Zheng, C.; Cicic, D.; Wang, J. First in Human (FIH) Study of GFH009, a Highly Selective Cyclin-Dependent Kinase 9 (CDK9) Inhibitor, in Patients with Relapsed/Refractory (r/r) Hematologic Malignancies. *Blood* **2022**, 140 (Supplement 1), 9473–9474. https://doi.org/10.1182/blood-2022-159844.

(82) Tong, W.-G.; Chen, R.; Plunkett, W.; Siegel, D.; Sinha, R.; Harvey, R. D.; Badros, A. Z.; Popplewell, L.; Coutre, S.; Fox, J. A.; Mahadocon, K.; Chen, T.; Kegley, P.; Hoch, U.; Wierda, W. G. Phase I and Pharmacologic Study of SNS-032, a Potent and Selective Cdk2, 7, and 9 Inhibitor, in Patients With Advanced Chronic Lymphocytic Leukemia and Multiple Myeloma. *J Clin Oncol* **2010**, 28 (18), 3015–3022. https://doi.org/10.1200/JCO.2009.26.1347.

(83) Olson, C. M.; Jiang, B.; Erb, M. A.; Liang, Y.; Doctor, Z. M.; Zhang, Z.; Zhang, T.; Kwiatkowski, N.; Boukhali, M.; Green, J. L.; Haas, W.; Nomanbhoy, T.; Fischer, E. S.; Young, R. A.; Bradner, J. E.; Winter, G. E.; Gray, N. S. Pharmacological Perturbation of CDK9 Using Selective CDK9 Inhibition or Degradation. *Nat Chem Biol* **2018**, 14 (2), 163–170. https://doi.org/10.1038/nchembio.2538.

(84) Chen, R.; Wierda, W. G.; Chubb, S.; Hawtin, R. E.; Fox, J. A.; Keating, M. J.; Gandhi, V.; Plunkett, W. Mechanism of Action of SNS-032, a Novel Cyclin-Dependent Kinase Inhibitor, in Chronic Lymphocytic Leukemia. *Blood* **2009**, 113 (19), 4637–4645. https://doi.org/10.1182/blood-2008-12-190256.

(85) Squires, M. S.; Feltell, R. E.; Wallis, N. G.; Lewis, E. J.; Smith, D.-M.; Cross, D. M.; Lyons, J. F.; Thompson, N. T. Biological Characterization of AT7519, a Small-Molecule Inhibitor of Cyclin-Dependent Kinases, in Human Tumor Cell Lines. *Molecular Cancer Therapeutics* **2009**, 8 (2), 324–332. https://doi.org/10.1158/1535-7163.MCT-08-0890.

(86) Chen, E. X.; Hotte, S.; Hirte, H.; Siu, L. L.; Lyons, J.; Squires, M.; Lovell, S.; Turner, S.; McIntosh, L.; Seymour, L. A Phase I Study of Cyclin-Dependent Kinase Inhibitor, AT7519, in Patients with Advanced Cancer: NCIC Clinical Trials Group IND 177. *British Journal of Cancer* **2014**, 111 (12), 2262. https://doi.org/10.1038/bjc.2014.565.

(87) Zhao, W.; Zhang, L.; Zhang, Y.; Jiang, Z.; Lu, H.; Xie, Y.; Han, W.; Zhao, W.; He, J.; Shi, Z.; Yang, H.; Chen, J.; Chen, S.; Li, Z.; Mao, J.; Zhou, L.; Gao, X.; Li, W.; Tan, G.; Zhang, B.; Wang, Z. The CDK Inhibitor AT7519 Inhibits Human

Glioblastoma Cell Growth by Inducing Apoptosis, Pyroptosis and Cell Cycle Arrest. *Cell Death Dis* **2023**, 14 (1), 1–11. https://doi.org/10.1038/s41419-022-05528-8.

(88) National Cancer Institute (NCI). *A Phase 1 Trial of the Combination of the Heat Shock Protein-90 (HSP90) Inhibitor Onalespib (AT13387) and the Cyclin-Dependent Kinase (CDK) Inhibitor AT7519M in Patients With Advanced Solid Tumors*; Clinical trial registration NCT02503709; clinicaltrials.gov, **2024**. https://clinicaltrials.gov/study/NCT02503709 (accessed 2024-11-10).

(89) *Onalespib and CDKI AT7519 in Treating Patients with Solid Tumors That Are Metastatic or Cannot Be Removed by Surgery - NCI.* https://www.cancer.gov/about-cancer/treatment/clinical-trials/search/v?id=NCI-2015-01098 (accessed 2024-11-10).

(90) Reddy, A. S.; Zhang, S. Polypharmacology: Drug Discovery for the Future. *Expert review of clinical pharmacology* **2013**, 6 (1), 10.1586/ecp.12.74. https://doi.org/10.1586/ecp.12.74.

(91) Kabir, A.; Muth, A. Polypharmacology: The Science of Multi-Targeting Molecules. *Pharmacological Research* **2022**, 176, 106055. https://doi.org/10.1016/j.phrs.2021.106055.

(92) Heitel, P. Emerging TACnology: Heterobifunctional Small Molecule Inducers of Targeted Posttranslational Protein Modifications. *Molecules* **2023**, 28 (2), 690. https://doi.org/10.3390/molecules28020690.

(93) Mullard, A. Protein Degraders Push into Novel Target Space. *Nature Reviews Drug Discovery* **2024**, 23 (11), 799–802. https://doi.org/10.1038/d41573-024-00170-9.

(94) Zhang, W.; Bai, Y.; Wang, Y.; Xiao, W. Polypharmacology in Drug Discovery: A Review from Systems Pharmacology Perspective. *Curr Pharm Des* **2016**, 22 (21), 3171–3181. https://doi.org/10.2174/1381612822666160224142812.

(95) Ryszkiewicz, P.; Malinowska, B.; Schlicker, E. Polypharmacology: Promises and New Drugs in 2022. *Pharmacol. Rep* **2023**, 75 (4), 755–770. https://doi.org/10.1007/s43440-023-00501-4.

(96) Lipinski, C. A. Lead- and Drug-like Compounds: The Rule-of-Five Revolution. *Drug Discovery Today: Technologies* **2004**, 1 (4), 337–341. https://doi.org/10.1016/j.ddtec.2004.11.007.

(97) Troup, R. I.; Fallan, C.; Baud, M. G. J. Current Strategies for the Design of PROTAC Linkers: A Critical Review. *Exploration of Targeted Anti-tumor Therapy* **2020**, 1 (5), 273. https://doi.org/10.37349/etat.2020.00018.

(98) Meanwell, N. A. Fluorine and Fluorinated Motifs in the Design and Application of Bioisosteres for Drug Design. *J. Med. Chem.* **2018**, 61 (14), 5822–5880. https://doi.org/10.1021/acs.jmedchem.7b01788.

(99) Boike, L.; Henning, N. J.; Nomura, D. K. Advances in Covalent Drug Discovery. *Nat Rev Drug Discov* **2022**, 21 (12), 881–898. https://doi.org/10.1038/s41573-022-00542-z.

(100) Singh, J.; Petter, R. C.; Baillie, T. A.; Whitty, A. The Resurgence of Covalent Drugs. *Nat Rev Drug Discov* **2011**, 10 (4), 307–317. https://doi.org/10.1038/nrd3410.

(101) Paramore, A.; Frantz, S. Bortezomib. *Nature Reviews Drug Discovery* **2003**, 2 (8), 611–612. https://doi.org/10.1038/nrd1159.

(102) Péczka, N.; Orgován, Z.; Ábrányi-Balogh, P.; Keserű, G. M. Electrophilic Warheads in Covalent Drug Discovery: An Overview. *Expert Opin Drug Discov* **2022**, 17 (4), 413–422. https://doi.org/10.1080/17460441.2022.2034783.

(103) Mehta, N. V.; Degani, M. S. The Expanding Repertoire of Covalent Warheads for Drug Discovery. *Drug Discovery Today* **2023**, 28 (12), 103799. https://doi.org/10.1016/j.drudis.2023.103799.

(104) Wu, H.; Wang, W.; Liu, F.; Weisberg, E. L.; Tian, B.; Chen, Y.; Li, B.; Wang, A.; Wang, B.; Zhao, Z.; McMillin, D. W.; Hu, C.; Li, H.; Wang, J.; Liang, Y.; Buhrlage, S. J.; Liang, J.; Liu, J.; Yang, G.; Brown, J. R.; Treon, S. P.; Mitsiades, C. S.; Griffin, J. D.; Liu, Q.; Gray, N. S. Discovery of a Potent, Covalent BTK Inhibitor for B-Cell Lymphoma. *ACS Chemical Biology* **2014**, 9 (5), 1086. https://doi.org/10.1021/cb4008524.

(105) *FDA Approves Imbruvica (ibrutinib) for Mantle Cell Lymphoma.* Drugs.com. https://www.drugs.com/newdrugs/fda-approves-imbruvica-ibrutinib-mantle-cell-lymphoma-3960.html (accessed 2024-11-10).

(106) Chan, A. M.; Goodis, C. C.; Pommier, E. G.; Fletcher, S. Recent Applications of Covalent Chemistries in Protein–Protein Interaction Inhibitors. *RSC Med. Chem.* **2022**, 13 (8), 921–928. https://doi.org/10.1039/D2MD00112H.

(107) Mullard, A. Protein Degraders Push into Novel Target Space. Nature Reviews *Drug Discovery* **2024**, 23 (11), 799–802. https://doi.org/10.1038/d41573-024-00170-9.

(108) Békés, M.; Langley, D. R.; Crews, C. M. PROTAC Targeted Protein Degraders: The Past Is Prologue. *Nat Rev Drug Discov* **2022**, 21 (3), 181–200. https://doi.org/10.1038/s41573-021-00371-6.

(109) Yoon, H.; Rutter, J. C.; Li, Y.-D.; Ebert, B. L. Induced Protein Degradation for Therapeutics: Past, Present, and Future. *J Clin Invest* **2024**, 134 (1). https://doi.org/10.1172/JCI175265.

(110) Xie, S.; Zhu, J.; Li, J.; Zhan, F.; Yao, H.; Xu, J.; Xu, S. Small-Molecule Hydrophobic Tagging: A Promising Strategy of Druglike Technology for Targeted Protein Degradation. *J. Med. Chem.* **2023**, 66 (16), 10917–10933. https://doi.org/10.1021/acs.jmedchem.3c00736.

(111) Liu, Z.; Hu, M.; Yang, Y.; Du, C.; Zhou, H.; Liu, C.; Chen, Y.; Fan, L.; Ma, H.; Gong, Y.; Xie, Y. An Overview of PROTACs: A Promising Drug Discovery Paradigm. *Molecular Biomedicine* **2022**, 3, 46. https://doi.org/10.1186/s43556-022-00112-0.

(112) Sakamoto, K. M.; Kim, K. B.; Kumagai, A.; Mercurio, F.; Crews, C. M.; Deshaies, R. J. Protacs: Chimeric Molecules That Target Proteins to the Skp1–Cullin–F Box Complex for Ubiquitination and Degradation. *Proc Natl Acad Sci U S A* **2001**, 98 (15), 8554–8559. https://doi.org/10.1073/pnas.141230798.

(113) Wurz, R. P.; Rui, H.; Dellamaggiore, K.; Ghimire-Rijal, S.; Choi, K.; Smither, K.; Amegadzie, A.; Chen, N.; Li, X.; Banerjee, A.; Chen, Q.; Mohl, D.; Vaish, A.

Affinity and Cooperativity Modulate Ternary Complex Formation to Drive Targeted Protein Degradation. *Nat Commun* **2023**, 14 (1), 4177. https://doi.org/10.1038/s41467-023-39904-5.

(114) Han, B. A Suite of Mathematical Solutions to Describe Ternary Complex Formation and Their Application to Targeted Protein Degradation by Heterobifunctional Ligands. *The Journal of Biological Chemistry* **2020**, 295 (45), 15280. https://doi.org/10.1074/jbc.RA120.014715.

(115) Kostic, M.; Jones, L. H. Critical Assessment of Targeted Protein Degradation as a Research Tool and Pharmacological Modality. *Trends in pharmacological sciences* **2020**, 41 (5), 305. https://doi.org/10.1016/j.tips.2020.02.006.

(116) Zhang, N.-Y.; Hou, D.-Y.; Hu, X.-J.; Liang, J.-X.; Wang, M.-D.; Song, Z.-Z.; Yi, L.; Wang, Z.-J.; An, H.-W.; Xu, W.; Wang, H. Nano Proteolysis Targeting Chimeras (PROTACs) with Anti-Hook Effect for Tumor Therapy. *Angew Chem Int Ed Engl* **2023**, 62 (37), e202308049. https://doi.org/10.1002/anie.202308049.

(117) Cecchini, C.; Pannilunghi, S.; Tardy, S.; Scapozza, L. From Conception to Development: Investigating PROTACs Features for Improved Cell Permeability and Successful Protein Degradation. *Front. Chem.* **2021**, 9. https://doi.org/10.3389/fchem.2021.672267.

(118) Bedford, L.; Lowe, J.; Dick, L. R.; Mayer, R. J.; Brownell, J. E. Ubiquitin-like Protein Conjugation and the Ubiquitin–Proteasome System as Drug Targets. *Nat Rev Drug Discov* **2011**, 10 (1), 29–46. https://doi.org/10.1038/nrd3321.

(119) Cruz Walma, D. A.; Chen, Z.; Bullock, A. N.; Yamada, K. M. Ubiquitin Ligases: Guardians of Mammalian Development. *Nat Rev Mol Cell Biol* **2022**, 23 (5), 350–367. https://doi.org/10.1038/s41580-021-00448-5.

(120) Jeong, Y.; Oh, A.-R.; Jung, Y. H.; Gi, H.; Kim, Y. U.; Kim, K. Targeting E3 Ubiquitin Ligases and Their Adaptors as a Therapeutic Strategy for Metabolic Diseases. *Exp Mol Med* **2023**, 55 (10), 2097–2104. https://doi.org/10.1038/s12276-023-01087-w.

(121) Bricelj, A.; Steinebach, C.; Kuchta, R.; Gütschow, M.; Sosič, I. E3 Ligase Ligands in Successful PROTACs: An Overview of Syntheses and Linker Attachment Points. *Front. Chem.* **2021**, 9. https://doi.org/10.3389/fchem.2021.707317.

(122) Xu, S.; Huo, J.; Huang, Y.; Aw, M.; Chen, S.; Mak, S.; Yip, L. Y.; Ho, Y. S.; Ng, S. W.; Tan, A. H.-M.; Lee, A.; Ou, X.; Lam, K.-P. Von Hippel-Lindau Protein Maintains Metabolic Balance to Regulate the Survival of Naive B Lymphocytes. *iScience* **2019**, 17, 379–392. https://doi.org/10.1016/j.isci.2019.07.002.

(123) Diehl, C. J.; Ciulli, A. Discovery of Small Molecule Ligands for the von Hippel-Lindau (VHL) E3 Ligase and Their Use as Inhibitors and PROTAC Degraders. *Chemical Society Reviews* **2022**, 51 (19), 8216. https://doi.org/10.1039/d2cs00387b.

(124) Ito, T. Protein Degraders - from Thalidomide to New PROTACs. *The Journal of Biochemistry* **2024**, 175 (5), 507–519. https://doi.org/10.1093/jb/mvad113.

(125) Dong, Y.; Ma, T.; Xu, T.; Feng, Z.; Li, Y.; Song, L.; Yao, X.; Ashby, C. R.; Hao, G.-F. Characteristic Roadmap of Linker Governs the Rational Design of

PROTACs. *Acta Pharmaceutica Sinica B* **2024**, 14 (10), 4266–4295. https://doi.org/10.1016/j.apsb.2024.04.007.

(126) Sun, Y.; Zhao, X.; Ding, N.; Gao, H.; Wu, Y.; Yang, Y.; Zhao, M.; Hwang, J.; Song, Y.; Liu, W.; Rao, Y. PROTAC-Induced BTK Degradation as a Novel Therapy for Mutated BTK C481S Induced Ibrutinib-Resistant B-Cell Malignancies. *Cell Res* **2018**, 28 (7), 779–781. https://doi.org/10.1038/s41422-018-0055-1.

(127) Singh, R.; Shaik, S.; Negi, B. S.; Rajguru, J. P.; Patil, P. B.; Parihar, A. S.; Sharma, U. Non-Hodgkin's Lymphoma: A Review. *Journal of Family Medicine and Primary Care* **2020**, 9 (4), 1834. https://doi.org/10.4103/jfmpc.jfmpc_1037_19.

(128) DiNardo, C. D.; Pratz, K. W.; Letai, A.; Jonas, B. A.; Wei, A. H.; Thirman, M.; Arellano, M.; Frattini, M. G.; Kantarjian, H.; Popovic, R.; Chyla, B.; Xu, T.; Dunbar, M.; Agarwal, S. K.; Humerickhouse, R.; Mabry, M.; Potluri, J.; Konopleva, M.; Pollyea, D. A. Safety and Preliminary Efficacy of Venetoclax with Decitabine or Azacitidine in Elderly Patients with Previously Untreated Acute Myeloid Leukaemia: A Non-Randomised, Open-Label, Phase 1b Study. *Lancet Oncol* **2018**, 19 (2), 216–228. https://doi.org/10.1016/S1470-2045(18)30010-X.

(129) Lin, K. H.; Winter, P. S.; Xie, A.; Roth, C.; Martz, C. A.; Stein, E. M.; Anderson, G. R.; Tingley, J. P.; Wood, K. C. Targeting MCL-1/BCL-XL Forestalls the Acquisition of Resistance to ABT-199 in Acute Myeloid Leukemia. *Sci Rep* **2016**, 6 (1), 27696. https://doi.org/10.1038/srep27696.

(130) Perini, G. F.; Ribeiro, G. N.; Pinto Neto, J. V.; Campos, L. T.; Hamerschlak, N. BCL-2 as Therapeutic Target for Hematological Malignancies. *J Hematol Oncol* **2018**, 11 (1), 65. https://doi.org/10.1186/s13045-018-0608-2.

(131) Wang, Q.; Wan, J.; Zhang, W.; Hao, S. MCL-1 or BCL-xL-Dependent Resistance to the BCL-2 Antagonist (ABT-199) Can Be Overcome by Specific Inhibitor as Single Agents and in Combination with ABT-199 in Acute Myeloid Leukemia Cells. *Leuk Lymphoma* **2019**, 60 (9), 2170–2180. https://doi.org/10.1080/10428194.2018.1563694.

(132) Diepstraten, S. T.; Anderson, M. A.; Czabotar, P. E.; Lessene, G.; Strasser, A.; Kelly, G. L. The Manipulation of Apoptosis for Cancer Therapy Using BH3-Mimetic Drugs. *Nat Rev Cancer* **2022**, 22 (1), 45–64. https://doi.org/10.1038/s41568-021-00407-4.

(133) Wang, L.; Doherty, G. A.; Judd, A. S.; Tao, Z.-F.; Hansen, T. M.; Frey, R. R.; Song, X.; Bruncko, M.; Kunzer, A. R.; Wang, X.; Wendt, M. D.; Flygare, J. A.; Catron, N. D.; Judge, R. A.; Park, C. H.; Shekhar, S.; Phillips, D. C.; Nimmer, P.; Smith, M. L.; Tahir, S. K.; Xiao, Y.; Xue, J.; Zhang, H.; Le, P. N.; Mitten, M. J.; Boghaert, E. R.; Gao, W.; Kovar, P.; Choo, E. F.; Diaz, D.; Fairbrother, W. J.; Elmore, S. W.; Sampath, D.; Leverson, J. D.; Souers, A. J. Discovery of A-1331852, a First-in-Class, Potent, and Orally-Bioavailable BCL-XL Inhibitor. *ACS Med Chem Lett* **2020**, 11 (10), 1829–1836. https://doi.org/10.1021/acsmedchemlett.9b00568.

(134) Juárez-Salcedo, L. M.; Desai, V.; Dalia, S. Venetoclax: Evidence to Date and Clinical Potential. *Drugs Context* **2019**, 8, 212574. https://doi.org/10.7573/dic.212574.

(135) Konopleva, M.; Pollyea, D. A.; Potluri, J.; Chyla, B.; Hogdal, L.; Busman, T.; McKeegan, E.; Salem, A. H.; Zhu, M.; Ricker, J. L.; Blum, W.; DiNardo, C. D.; Kadia, T.; Dunbar, M.; Kirby, R.; Falotico, N.; Leverson, J.; Humerickhouse, R.; Mabry, M.; Stone, R.; Kantarjian, H.; Letai, A. Efficacy and Biological Correlates of Response in a Phase II Study of Venetoclax Monotherapy in Patients with Acute Myelogenous Leukemia. *Cancer Discov* **2016**, 6 (10), 1106–1117. https://doi.org/10.1158/2159-8290.CD-16-0313.

(136) Pollyea, D. A.; Pratz, K.; Letai, A.; Jonas, B. A.; Wei, A. H.; Pullarkat, V.; Konopleva, M.; Thirman, M. J.; Arellano, M.; Becker, P. S.; Chyla, B.; Hong, W.-J.; Jiang, Q.; Potluri, J.; DiNardo, C. D. Venetoclax with Azacitidine or Decitabine in Patients with Newly Diagnosed Acute Myeloid Leukemia: Long Term Follow-up from a Phase 1b Study. *Am J Hematol* **2021**, 96 (2), 208–217. https://doi.org/10.1002/ajh.26039.

(137) Kaufmann, S. H.; Karp, J. E.; Svingen, P. A.; Krajewski, S.; Burke, P. J.; Gore, S. D.; Reed, J. C. Elevated Expression of the Apoptotic Regulator Mcl-1 at the Time of Leukemic Relapse. *Blood* **1998**, 91 (3), 991–1000.

(138) Leverson, J. D.; Cojocari, D. Hematologic Tumor Cell Resistance to the BCL-2 Inhibitor Venetoclax: A Product of Its Microenvironment? *Front Oncol* **2018**, 8, 458. https://doi.org/10.3389/fonc.2018.00458.

(139) Luedtke, D. A.; Niu, X.; Pan, Y.; Zhao, J.; Liu, S.; Edwards, H.; Chen, K.; Lin, H.; Taub, J. W.; Ge, Y. Inhibition of Mcl-1 Enhances Cell Death Induced by the Bcl-2-Selective Inhibitor ABT-199 in Acute Myeloid Leukemia Cells. *Sig Transduct Target Ther* **2017**, 2 (1), 1–9. https://doi.org/10.1038/sigtrans.2017.12.

(140) Tahir, S. K.; Smith, M. L.; Hessler, P.; Rapp, L. R.; Idler, K. B.; Park, C. H.; Leverson, J. D.; Lam, L. T. Potential Mechanisms of Resistance to Venetoclax and Strategies to Circumvent It. *BMC Cancer* **2017**, 17 (1), 399. https://doi.org/10.1186/s12885-017-3383-5.

(141) Tausch, E.; Close, W.; Dolnik, A.; Bloehdorn, J.; Chyla, B.; Bullinger, L.; Döhner, H.; Mertens, D.; Stilgenbauer, S. Venetoclax Resistance and Acquired BCL2 Mutations in Chronic Lymphocytic Leukemia. *Haematologica* **2019**, 104 (9), e434–e437. https://doi.org/10.3324/haematol.2019.222588.

(142) Fletcher, S. *MCL-1 Inhibitors – Where Are We Now* (**2019**)? Expert Opinion on Therapeutic Patents 2019, 29 (11), 909–919. https://doi.org/10.1080/13543776.2019.1672661.

(143) Leverson, J. D.; Zhang, H.; Chen, J.; Tahir, S. K.; Phillips, D. C.; Xue, J.; Nimmer, P.; Jin, S.; Smith, M.; Xiao, Y.; Kovar, P.; Tanaka, A.; Bruncko, M.; Sheppard, G. S.; Wang, L.; Gierke, S.; Kategaya, L.; Anderson, D. J.; Wong, C.; Eastham-Anderson, J.; Ludlam, M. J. C.; Sampath, D.; Fairbrother, W. J.; Wertz, I.; Rosenberg, S. H.; Tse, C.; Elmore, S. W.; Souers, A. J. Potent and Selective Small-Molecule MCL-1 Inhibitors Demonstrate on-Target Cancer Cell Killing Activity as Single Agents and in Combination with ABT-263 (Navitoclax). *Cell Death Dis* **2015**, 6 (1), e1590. https://doi.org/10.1038/cddis.2014.561.

(144) Sancho, M.; Leiva, D.; Lucendo, E.; Orzáez, M. Understanding MCL1: From Cellular Function and Regulation to Pharmacological Inhibition. *The FEBS Journal* **2022**, 289 (20), 6209–6234. https://doi.org/10.1111/febs.16136.

(145) Opferman, J. T.; Iwasaki, H.; Ong, C. C.; Suh, H.; Mizuno, S.; Akashi, K.; Korsmeyer, S. J. Obligate Role of Anti-Apoptotic MCL-1 in the Survival of Hematopoietic Stem Cells. *Science* **2005**, 307 (5712), 1101–1104. https://doi.org/10.1126/science.1106114.

(146) Vick, B.; Weber, A.; Urbanik, T.; Maass, T.; Teufel, A.; Krammer, P. H.; Opferman, J. T.; Schuchmann, M.; Galle, P. R.; Schulze-Bergkamen, H. Knockout of Myeloid Cell Leukemia-1 Induces Liver Damage and Increases Apoptosis Susceptibility of Murine Hepatocytes. Hepatology 2009, 49 (2), 627–636. https://doi.org/10.1002/hep.22664.

(147) Thomas, R. L.; Roberts, D. J.; Kubli, D. A.; Lee, Y.; Quinsay, M. N.; Owens, J. B.; Fischer, K. M.; Sussman, M. A.; Miyamoto, S.; Gustafsson, Å. B. Loss of MCL-1 Leads to Impaired Autophagy and Rapid Development of Heart Failure. *Genes Dev* **2013**, 27 (12), 1365–1377. https://doi.org/10.1101/gad.215871.113.

(148) Moujalled, D. M.; Pomilio, G.; Ghiurau, C.; Ivey, A.; Salmon, J.; Rijal, S.; Macraild, S.; Zhang, L.; Teh, T.-C.; Tiong, I.-S.; Lan, P.; Chanrion, M.; Claperon, A.; Rocchetti, F.; Zichi, A.; Kraus-Berthier, L.; Wang, Y.; Halilovic, E.; Morris, E.; Colland, F.; Segal, D.; Huang, D.; Roberts, A. W.; Maragno, A. L.; Lessene, G.; Geneste, O.; Wei, A. H. Combining BH3-Mimetics to Target Both BCL-2 and MCL1 Has Potent Activity in Pre-Clinical Models of Acute Myeloid Leukemia. *Leukemia* **2019**, 33 (4), 905–917. https://doi.org/10.1038/s41375-018-0261-3.

(149) Langdon, S. R.; Ertl, P.; Brown, N. Bioisosteric Replacement and Scaffold Hopping in Lead Generation and Optimization. *Mol Inform* **2010**, 29 (5), 366–385. https://doi.org/10.1002/minf.201000019.

(150) Sun, H.; Tawa, G.; Wallqvist, A. Classification of Scaffold-Hopping Approaches. *Drug Discov Today* **2012**, 17 (7–8), 310–324. https://doi.org/10.1016/j.drudis.2011.10.024.

(151) Cao, X.; Yap, J. L.; Newell-Rogers, M. K.; Peddaboina, C.; Jiang, W.; Papaconstantinou, H. T.; Jupitor, D.; Rai, A.; Jung, K.-Y.; Tubin, R. P.; Yu, W.; Vanommeslaeghe, K.; Wilder, P. T.; MacKerell, A. D.; Fletcher, S.; Smythe, R. W. The Novel BH3 α-Helix Mimetic JY-1-106 Induces Apoptosis in a Subset of Cancer Cells (Lung Cancer, Colon Cancer and Mesothelioma) by Disrupting Bcl-xL and Mcl-1 Protein–Protein Interactions with Bak. *Molecular Cancer* **2013**, 12 (1), 42. https://doi.org/10.1186/1476-4598-12-42.

(152) Chen, L.; Wilder, P. T.; Drennen, B.; Tran, J.; Roth, B. M.; Chesko, K.; Shapiro, P.; Fletcher, S. Structure-Based Design of 3-Carboxy-Substituted 1,2,3,4-Tetrahydroquinolines as Inhibitors of Myeloid Cell Leukemia-1 (Mcl-1). *Org. Biomol. Chem.* **2016**, 14 (24), 5505–5510. https://doi.org/10.1039/C5OB02063H.

(153) Conlon, I. L.; Drennen, B.; Lanning, M. E.; Hughes, S.; Rothhaas, R.; Wilder, P. T.; MacKerell Jr., A. D.; Fletcher, S. Rationally Designed Polypharmacology: α-Helix Mimetics as Dual Inhibitors of the Oncoproteins Mcl-1 and HDM2. *ChemMedChem* **2020**, 15 (18), 1691–1698. https://doi.org/10.1002/cmdc.202000278.

(154) Drennen, B.; Scheenstra, J. A.; Yap, J. L.; Chen, L.; Lanning, M. E.; Roth, B. M.; Wilder, P. T.; Fletcher, S. Structural Re-Engineering of the α-Helix Mimetic JY-1-106 into Small Molecules: Disruption of the Mcl-1–Bak-BH3 Protein–Protein Interaction with 2,6-Di-Substituted Nicotinates. *ChemMedChem* **2016**, 11 (8), 827–833. https://doi.org/10.1002/cmdc.201500461.

(155) Jung, K.-Y.; Vanommeslaeghe, K.; Lanning, M. E.; Yap, J. L.; Gordon, C.; Wilder, P. T.; MacKerell, A. D. Jr.; Fletcher, S. Amphipathic α-Helix Mimetics Based on a 1,2-Diphenylacetylene Scaffold. *Org. Lett.* **2013**, 15 (13), 3234–3237. https://doi.org/10.1021/ol401197n.

(156) Towards more drug-like proteomimetics: two-faced, synthetic α-helix mimetics based on a purine scaffold - *Organic & Biomolecular Chemistry* (RSC Publishing). https://pubs.rsc.org/en/content/articlelanding/2015/ob/c5ob00478k/unauth (accessed 2024-11-10).

(157) Lanning, M. E.; Yu, W.; Yap, J. L.; Chauhan, J.; Chen, L.; Whiting, E.; Pidugu, L. S.; Atkinson, T.; Bailey, H.; Li, W.; Roth, B. M.; Hynicka, L.; Chesko, K.; Toth, E. A.; Shapiro, P.; MacKerell, A. D.; Wilder, P. T.; Fletcher, S. Structure-Based Design of N-Substituted 1-Hydroxy-4-Sulfamoyl-2-Naphthoates as Selective Inhibitors of the Mcl-1 Oncoprotein. *European Journal of Medicinal Chemistry* **2016**, 113, 273–292. https://doi.org/10.1016/j.ejmech.2016.02.006.

(158) Johnson, B. L.; Rodgers, J. D. Practical Synthesis of 3-Carboxyindazoles. *Synthetic Communications* **2005**, 35 (20), 2681–2684. https://doi.org/10.1080/00397910500214318.

(159) Longworth, M.; Banister, S. D.; Mack, J. B. C.; Glass, M.; Connor, M.; Kassiou, M. The 2-Alkyl-2H-Indazole Regioisomers of Synthetic Cannabinoids AB-CHMINACA, AB-FUBINACA, AB-PINACA, and 5F-AB-PINACA Are Possible Manufacturing Impurities with Cannabimimetic Activities. *Forensic Toxicol* **2016**, 34 (2), 286–303. https://doi.org/10.1007/s11419-016-0316-y.

(160) Chen, L.; Fletcher, S. O-Alkylation of 3-Hydroxyisoxazoles Predominates under Mitsunobu Conditions. *Tetrahedron Letters* **2014**, 55 (10), 1693–1696. https://doi.org/10.1016/j.tetlet.2014.01.065.

(161) Fletcher, S. The Mitsunobu Reaction in the 21 St Century. *Organic Chemistry Frontiers* **2015**, 2 (6), 739–752. https://doi.org/10.1039/C5QO00016E.

(162) Fletcher, S. Regioselective Alkylation of the Exocyclic Nitrogen of Adenine and Adenosine by the Mitsunobu Reaction. *Tetrahedron Letters* **2010**, 51 (22), 2948–2950. https://doi.org/10.1016/j.tetlet.2010.03.103.

(163) Li, P.; He, H.; Zhang, Y.; Yang, R.; Xu, L.; Chen, Z.; Huang, Y.; Bao, L.; Xiao, G. Glycosyl Ortho-(1-Phenylvinyl)Benzoates Versatile Glycosyl Donors for Highly Efficient Synthesis of Both O-Glycosides and Nucleosides. *Nature Communications* **2020**, 11, 405. https://doi.org/10.1038/s41467-020-14295-z.

(164) Wan, Y.; Li, Y.; Yan, C.; Wen, J.; Tang, Z. Discovery of Novel Indazole-Acylsulfonamide Hybrids as Selective Mcl-1 Inhibitors. *Bioorganic Chemistry* **2020**, 104, 104217. https://doi.org/10.1016/j.bioorg.2020.104217.

(165) Newell LF, Cook RJ. Advances in acute myeloid leukemia *BMJ.* **2021**;375:n2026. doi: 10.1136/bmj.n2026.

(166) Bhansali RS, Pratz KW, Lai C Recent advances in targeted therapies in acute myeloid leukemia. *J. Hematol. Oncol.* **2023**;16:29. doi: 10.1186/s13045-023-01424-6.

(167) Fletcher, S.; Hamilton, A. D. Protein Surface Recognition and Proteomimetics: Mimics of Protein Surface Structure and Function. *Curr Opin Chem Biol* **2005**, 9 (6), 632–638. https://doi.org/10.1016/j.cbpa.2005.10.006.

(168) Takahashi S. Downstream molecular pathways of FLT3 in the pathogenesis of acute myeloid leukemia: biology and therapeutic implications. *J. Hematol. Oncol.* **2011**;4:13. doi: 10.1186/1756-8722-4-13.

(169) Kiyoi H, Kawashima N, Ishikawa Y. FLT3 mutations in acute myeloid leukemia: Therapeutic paradigm beyond inhibitor development. *Cancer Sci.* **2020**;111:312–322. doi: 10.1111/cas.14274.

(170) Cohen P, Cross D, Jänne PA. Kinase drug discovery 20 years after imatinib: progress and future directions. *Nat. Rev. Drug Discov.* **2021**;20:551-569. doi: 10.1038/s41573-021-00195-4.

(171) Acharya B, Saha D, Armstrong D, Lakkaniga NR, Frett B. FLT3 inhibitors for acute myeloid leukemia: successes, defeats, and emerging paradigms. *RSC Med. Chem.* **2022**;13:798-816. doi: 10.1039/d2md00067a

(172) VEN therapy: https://www.fda.gov/drugs/resources-information-approved-drugs/fda-grants-regular-approval-venetoclax-combination-untreated-acute-myeloid-leukemia

(173) www.clinicaltrials.gov

(174) Zhu R, Li L, Nguyen B, Seo J, Wu M, Seale T, Levis M, Duffield A, Hu Y, Small D. FLT3 tyrosine kinase inhibitors synergize with BCL-2 inhibition to eliminate FLT3/ITD acute leukemia cells through BIM activation. *Signal Transduct. Target. Ther.* **2021**;6:186. doi: 10.1038/s41392-021-00578-4.

(175) Brinton LT, Zhang P, Williams K, Canfield D, Orwick S, Sher S, Wasmuth R, Beaver L, Cempre C, Skinner J, Cannon M, Govande M, Harrington B, Lehman A, Byrd JC, Lapalombella R, Blachly JS. Synergistic effect of BCL2 and FLT3 co-inhibition in acute myeloid leukemia.i **2020**;13:139. doi: 10.1186/s13045-020-00973-4.

(176) Anighoro A, Bajorath J, Rastelli G. Polypharmacology: challenges and opportunities in drug discovery. *J. Med. Chem.* **2014**;57:7874-87. doi: 10.1021/jm5006463.

(177) Chen L, Chauhan J, Yap JL, Goodis CC, Wilder PT, Fletcher S. Discovery of N-sulfonylated aminosalicylic acids as dual MCL-1/BCL-xL inhibitors. *RSC Med Chem.* **2022**;14:103-112. doi: 10.1039/d2md00277a.

(178) Whiting E, Raje MR, Chauhan J, Wilder PT, Van Eker D, Hughes SJ, Bowen NG, Vickers GEA, Fenimore IC, Fletcher S. Discovery of Mcl-1 inhibitors based on a thiazolidine-2,4-dione scaffold. *Bioorg Med Chem Lett.* **2018**;28:523-528. doi: 10.1016/j.bmcl.2017.11.023.

(179) Cao X, Yap JL, Newell-Rogers MK, Peddaboina C, Jiang W, Papaconstantinou HT, Jupitor D, Rai A, Jung KY, Tubin RP, Yu W, Vanommeslaeghe K, Wilder PT, MacKerell AD Jr, Fletcher S, Smythe RW. The novel BH3 alpha-helix mimetic JY-1-106 induces apoptosis in a subset of cancer cells (lung cancer, colon cancer

and mesothelioma) by disrupting Bcl-xL and Mcl-1 protein-protein interactions with Bak. *Mol Cancer.* **2013**;12:42. doi: 10.1186/1476-4598-12-42.

(180) Yap, J. L., Cao, X., Vanommeslaeghe, K., Jung, K.-Y., Peddaboina, C., Wilder, P. T., Nan, A., MacKerell, Jr., A. D., Smythe, W. R., Fletcher, S.. Relaxation of the rigid backbone of an oligoamide-foldamer-based α-helix mimetic: Identification of potent Bcl-x L inhibitors. *Org. Biomol. Chem.* **2012**;10;2928-2933. https://doi.org/10.1039/C2OB07125H

(181) Drennen B, Scheenstra JA, Yap JL, Chen L, Lanning ME, Roth BM, Wilder PT, Fletcher S. Structural Re-engineering of the alpha-Helix Mimetic JY-1-106 into Small Molecules: Disruption of the Mcl-1-Bak-BH3 Protein-Protein Interaction with 2,6-Di-Substituted Nicotinates. *ChemMedChem.* **2016**;11:827-33. doi: 10.1002/cmdc.201500461.

(182) Chen L, Lowe B, Fletcher S. Tetrazole and acylsulfonamide bioisosteric replacements of the carboxylic acid in a dual MCL-1/BCL-x(L) inhibitor are tolerated. *RSC Adv*. **2023**;13:34322-34334. doi: 10.1039/d3ra05711a.

(183) Chen L, Chan AM, Wilder PT, Fletcher S. 1-Sulfonylated 1,2,3,4-tetrahydroquinoline-6-carboxylic acids as simple, readily-accessible MCL-1 inhibitors. *Drug Dev Res.* **2022**;83:1879-1889. doi: 10.1002/ddr.22004.

(184) Chen L, Yap JL, Yoshioka M, Lanning ME, Fountain RN, Raje M, Scheenstra JA, Strovel JW, Fletcher S. BRD4 Structure-Activity Relationships of Dual PLK1 Kinase/BRD4 Bromodomain Inhibitor BI-2536. *ACS Med Chem Lett.* **2015**;6:764-9. doi: 10.1021/acsmedchemlett.5b00084.

(185) Chan AM, Mitchell A, Grogan L, Shapiro P, Fletcher S. Histone deacetylase (HDAC) inhibitor specificity determinants are preserved in a class of dual HDAC/non-covalent proteasome inhibitors. *Bioorg Med Chem.* **2024**;104:117680. doi: 10.1016/j.bmc.2024.117680.

(186) Drennen B, Goodis CC, Bowen N, Yu W, Vickers G, Wilder PT, MacKerell AD Jr, Fletcher S. Scaffold hopping from indoles to indazoles yields dual MCL-1/BCL-2 inhibitors from MCL-1 selective leads. *RSC Med Chem.* **2022**;13:963-969. doi: 10.1039/d2md00095d.

(187) Conlon IL, Drennen B, Lanning ME, Hughes S, Rothhaas R, Wilder PT, MacKerell AD Jr, Fletcher S. Rationally Designed Polypharmacology: alpha-Helix Mimetics as Dual Inhibitors of the Oncoproteins Mcl-1 and HDM2. *ChemMedChem* **2020**;15:1691-1698. doi: 10.1002/cmdc.202000278.

(188) Yuan T, Qi B, Jiang Z, Dong W, Zhong L, Bai L, Tong R, Yu J, Shi J. Dual FLT3 inhibitors: Against the drug resistance of acute myeloid leukemia in recent decade. *Eur. J. Med. Chem.* **2019**;178:468-483. doi: 10.1016/j.ejmech.2019.06.002.

(189) This PDB corresponds to VEN bound to the G101A mutation of BCL-2; the binding is the same as to WT BCL-2.

(190) Ku YY, Chan VS, Christesen A, Grieme T, Mulhern M, Pu YM, Wendt MD. Development of a Convergent Large-Scale Synthesis for Venetoclax, a First-in-Class BCL-2 Selective Inhibitor. *J. Org. Chem.* **2019**;84:4814-4829. doi: 10.1021/acs.joc.8b02750.

(191) Liang X, Yang Q, Wu P, He C, Yin L, Xu F, Yin Z, Yue G, Zou Y, Li L, Song X, Lv C, Zhang W, Jing B. The synthesis review of the approved tyrosine kinase inhibitors for anticancer therapy in 2015-2020. *Bioorg. Chem.* **2021**;113:105011. doi: 10.1016/j.bioorg.2021.105011.

(192) Rahmani, M, Nkwocha J, Hawkins E, Pei X, Parker RE, Kmieciak M, Leverson JD, Sampath D, Ferreira-Gonzalez A, Grant S. Cotargeting BCL-2 and PI3K Induces BAX-Dependent Mitochondrial Apoptosis in AML Cells. *Cancer Res* **2018**;78:3075-3086. doi: 10.1158/0008-5472.CAN-17-3024. Epub 2018 Mar 20.

(193) Lee LY, Hernandez D, Rajkhowa T, Smith SC, Raman JR, Nguyen B, Small D, Levis M. Preclinical studies of gilteritinib, a next-generation FLT3 inhibitor. *Blood.* **2017**;:257-260. doi: 10.1182/blood-2016-10-745133.

(194) Nordigården A, Kraft M, Eliasson P, Labi V, Lam EW, Villunger A, Jönsson JI. BH3-only protein Bim more critical than Puma in tyrosine kinase inhibitor-induced apoptosis of human leukemic cells and transduced hematopoietic progenitors carrying oncogenic FLT3. *Blood* 2009;113:2302-11. doi: 10.1182/blood-2008-07-167023.

(195) Creed M., Baldeosingh R., Eberly C.L., Schlee C.S., Kim M.J., Cutler J.A., Pandey A., Civin C.I., Fossett N.G., Kingsbury T.J. PAX-SIX-EYA-DACH Network modulates GATA-FOG function in fly hematopoiesis and human erythropoiesis. Development 147:dev177022, 2020. doi:10.1242/dev.177022.

(196) Bank, R. P. D. RCSB PDB - *6JQR: Crystal structure of FLT3 in complex with gilteritinib.* https://www.rcsb.org/structure/6jqr (accessed 2024-11-10).

(197) Faller, C. E.; Raman, E. P.; Alexander D MacKerell, J.; Guvench, O. Site Identification by Ligand Competitive Saturation (SILCS) Simulations for Fragment-Based Drug Design. *Methods in molecular biology* (Clifton, N.J.) **2015**, 1289, 75. https://doi.org/10.1007/978-1-4939-2486-8_7.

(198) Bank, R. P. D. RCSB PDB - *5X02: Crystal structure of the FLT3 kinase domain bound to the inhibitor FF-10101.* https://www.rcsb.org/structure/5x02 (accessed 2024-11-10).

(199) Lovly, C. M.; Shaw, A. T. Molecular Pathways: Resistance to Kinase Inhibitors and Implications for Therapeutic Strategies. *Clinical cancer research : an official journal of the American Association for Cancer Research* **2014**, 20 (9), 2249. https://doi.org/10.1158/1078-0432.CCR-13-1610.

(200) Burke, M. R.; Smith, A. R.; Zheng, G. Overcoming Cancer Drug Resistance Utilizing PROTAC Technology. Frontiers in Cell and Developmental Biology 2022, 10, 872729. https://doi.org/10.3389/fcell.2022.872729.

(201) Kattner, P.; Strobel, H.; Khoshnevis, N.; Grunert, M.; Bartholomae, S.; Pruss, M.; Fitzel, R.; Halatsch, M.-E.; Schilberg, K.; Siegelin, M. D.; Peraud, A.; Karpel-Massler, G.; Westhoff, M.-A.; Debatin, K.-M. Compare and Contrast: Pediatric Cancer versus Adult Malignancies. *Cancer Metastasis Rev* **2019**, 38 (4), 673–682. https://doi.org/10.1007/s10555-019-09836-y.

(202) Birkinshaw, R. W.; Gong, J.; Luo, C. S.; Lio, D.; White, C. A.; Anderson, M. A.; Blombery, P.; Lessene, G.; Majewski, I. J.; Thijssen, R.; Roberts, A. W.; Huang, D. C. S.; Colman, P. M.; Czabotar, P. E. Structures of BCL-2 in Complex with

Venetoclax Reveal the Molecular Basis of Resistance Mutations. *Nature Communications* **2019**, 10, 2385. https://doi.org/10.1038/s41467-019-10363-1.

(203) He, Y.; Zhang, X.; Chang, J.; Kim, H.-N.; Zhang, P.; Wang, Y.; Khan, S.; Liu, X.; Zhang, X.; Lv, D.; Song, L.; Li, W.; Thummuri, D.; Yuan, Y.; Wiegand, J. S.; Ortiz, Y. T.; Budamagunta, V.; Elisseeff, J. H.; Campisi, J.; Almeida, M.; Zheng, G.; Zhou, D. Using Proteolysis-Targeting Chimera Technology to Reduce Navitoclax Platelet Toxicity and Improve Its Senolytic Activity. *Nat Commun* **2020**, 11 (1), 1996. https://doi.org/10.1038/s41467-020-15838-0.

(204) Lv, D.; Pal, P.; Liu, X.; Jia, Y.; Thummuri, D.; Zhang, P.; Hu, W.; Pei, J.; Zhang, Q.; Zhou, S.; Khan, S.; Zhang, X.; Hua, N.; Yang, Q.; Arango, S.; Zhang, W.; Nayak, D.; Olsen, S. K.; Weintraub, S. T.; Hromas, R.; Konopleva, M.; Yuan, Y.; Zheng, G.; Zhou, D. Development of a BCL-xL and BCL-2 Dual Degrader with Improved Anti-Leukemic Activity,. *Nat Commun* **2021**, 12 (1), 6896. https://doi.org/10.1038/s41467-021-27210-x.

(205) Esteve-Arenys, A.; Roue, G. BFL-1 Expression Determines the Efficacy of Venetoclax in MYC+/BCL2+ Double Hit Lymphoma. *Oncoscience* **2018**, 5 (3–4), 59. https://doi.org/10.18632/oncoscience.402.